



Swansea University
Prifysgol Abertawe



Swansea University E-Theses

Development of novel coatings for dye-sensitized solar cell applications.

Vyas, Niladri

How to cite:

Vyas, Niladri (2015) *Development of novel coatings for dye-sensitized solar cell applications..* thesis, Swansea University.

<http://cronfa.swan.ac.uk/Record/cronfa42397>

Use policy:

This item is brought to you by Swansea University. Any person downloading material is agreeing to abide by the terms of the repository licence: copies of full text items may be used or reproduced in any format or medium, without prior permission for personal research or study, educational or non-commercial purposes only. The copyright for any work remains with the original author unless otherwise specified. The full-text must not be sold in any format or medium without the formal permission of the copyright holder. Permission for multiple reproductions should be obtained from the original author.

Authors are personally responsible for adhering to copyright and publisher restrictions when uploading content to the repository.

Please link to the metadata record in the Swansea University repository, Cronfa (link given in the citation reference above.)

<http://www.swansea.ac.uk/library/researchsupport/ris-support/>

Development of Novel Coatings for Dye- Sensitized Solar Cell Applications



**Swansea University
Prifysgol Abertawe**

Niladri Vyas

*Thesis Submitted to Swansea University in Fulfilment of the
Requirements for the Degree of Doctor of Philosophy*

Sustainable Product Engineering Centre for Innovative Functional
Coatings, College of Engineering, Swansea University, United Kingdom

2015

ProQuest Number: 10798105

All rights reserved

INFORMATION TO ALL USERS

The quality of this reproduction is dependent upon the quality of the copy submitted.

In the unlikely event that the author did not send a complete manuscript and there are missing pages, these will be noted. Also, if material had to be removed, a note will indicate the deletion.



ProQuest 10798105

Published by ProQuest LLC (2018). Copyright of the Dissertation is held by the Author.

All rights reserved.

This work is protected against unauthorized copying under Title 17, United States Code
Microform Edition © ProQuest LLC.

ProQuest LLC.
789 East Eisenhower Parkway
P.O. Box 1346
Ann Arbor, MI 48106 – 1346

DECLARATION

This work has not previously been accepted in substance for any degree and is not being concurrently submitted in candidature for any degree.

Signed (Candidate)

Date16.02.15.....

STATEMENT 1

This thesis is the result of my own investigations, except where otherwise stated. Where correction services have been used, the extent and nature of the correction is clearly marked in a footnote(s).

Other sources are acknowledged by footnotes giving explicit references. A bibliography is appended.

Signed (Candidate)

Date16.02.15.....

STATEMENT 2

I hereby give consent for my thesis, if accepted, to be available for photocopying and for inter-library loan, and for the title and summary to be made available to outside organisations.

Signed .. (Candidate)

Date16.02.15.....



SUMMARY

This research work was undertaken to solve an industrial problem related to roll-to-roll production of dye-sensitised solar cells (DSCs). It is possible to manufacture DSCs in a roll-to-roll production line on a sheet metal such as titanium. However, DSCs produced in such a way are not commercially viable due to the use of expensive titanium metal. Therefore, the intention behind this work was to utilize a cheap sheet metal such as ECCS (electro chrome coated steel) to manufacture DSCs in a roll-to-roll production facility of TATA steel Europe, as this project was funded by them.

Unfortunately, ECCS corrodes in the I^-/I_3^- redox electrolyte present in a DSC therefore, to protect ECCS from the corrosion whilst using it as a DSC substrate was the real challenging task in this research. In order to solve this problem high temperature resistant polyimide based coatings were developed which can be used to coat ECCS substrates whilst maintaining excellent dimensional stability at the DSC processing temperatures. Such coatings were electrically conducting which helped preserve the electrical conductivity of the underlying metallic substrate.

Electrically conductive polyimides were developed by simply blending conductive fillers such as carbon materials and titanium nitride. It was initially thought that carbon/polyimide based coatings would be suitable for this application. However, severe interfacial charge recombination and poor reflectivity made carbon/PI coatings inferior compared to the TiN/PI coatings. TiN/PI coatings performed well but poor reflectivity produced low current outputs. Moreover, TiN/PI was found to reduce the catalytic activity of thermally deposited platinum therefore it was not useful as a counter electrode material. As a solution to these problems, TiN and carbon materials based hybrid coatings were developed. Hybrid coatings did perform efficiently in terms of overall PV performance but due to poor reflectivity, such coatings also produced low J_{sc} values. However, counter electrodes prepared using hybrid coating demonstrated excellent PV performance with thermally deposited platinum.

Furthermore, TCO (transparent conducting oxide) free glass substrates can also be used to manufacture low-cost PV devices when coated with these conductive coatings.

ACKNOWLEDGEMENTS

First and foremost, I offer my earnest gratitude to my supervisor Prof. David Worsley who kindly offered me the opportunity to pursue this doctoral degree at Swansea University under his invaluable guidance. I am highly obliged to SPECIFIC, Swansea University and TATA steel for providing financial support and necessary resources to complete this research work in the most efficient manner. The greatest thanks go to my second supervisor Dr. Trystan Watson for his bountiful help and supervision without which this work would not have been possible. I am forever indebted to Trystan for his kindness.

I am sincerely thankful to Dr. Matthew Carnie for friendly discussions and advice that helped me write this thesis. In addition, I would like to thank Dr. Cecile Charbonneau and Dr. James McGettrick for helping me collect SEM and XPS data respectively.

I am so proud to be a part of SPECIFIC innovation centre, which is almost like a family full of helpful people. Therefore, I would like to extend my deepest gratitude to all the members of SPECIFIC family who helped me unconditionally at various stages of my research. I would specially like to appreciate the contributions from Katherine Hooper, David Wragg, Dr. Bruce Phillip, Jenny Baker, Joel Troughton, Peter Greenwood, Dr. Mathew Davies, Daniel Bryant and all the members of 'PV', 'Corrosion' and 'Battery' teams for their friendly support throughout my work.

There is no word that can describe my love and respect for my parents who fulfilled all my dreams and demands to the best of their abilities. I am so lucky to have such great parents that without them my whole life is meaningless. It is only because of them I could finish my Ph.D., as there were instances when I was completely broke and they helped me regain my confidence. Thus, this thesis is dedicated to the most wonderful parents in the world who I love so much. Last but not least, I would like to thank my sister and her family for the encouragement that I needed to achieve this. Finally, I would like to express my sincere gratitude to the members of Argyle and Rhyddings Park Presbyterian Church and all my friends for their best wishes and blessings.

Niladri Vyas

11/09/2014

LIST OF ABBREVIATIONS AND SYMBOLS

R_p	Average peak height
R_a	Average roughness
E_g	Band-gap
BE	Binding energy
BTU	British thermal units
BIPV	Building integrated photovoltaics
R_{ce}	Charge transfer resistance
C_μ	Chemical capacitance
CVD	Chemical vapour deposition
N719	Cis-bis(isothiocyanato)-bis(2,2'-bipyridyl-4,4'-dicarboxylato)-ruthenium(II) (deprotonated)
N3	Cis-bis(isothiocyanato)-bis(2,2'-bipyridyl-4,4'-dicarboxylato)-ruthenium(II) (protonated)
CIS	Copper indium di-selenide
CIGS	Copper indium gallium (di)selenide
DAQ	Data acquisition
C_{dl}	Double layer capacitance
DSC	Dye-sensitized solar cell
DIY	Do it yourself
EPFL	École polytechnique fédérale de Lausanne
OECD	Economic Cooperation and Development
ECCS	Electro chrome coated steel
EIS	Electrochemical impedance spectroscopy
τ_n	Electron recombination lifetime
eV	Electron volts
E	Energy
FF	Fill factor
FTO	Fluorine-doped tin oxide
FT	Fourier transform
ν	Frequency
Q	Heat energy
HOMO	Highest occupied molecular orbital
Z_{img}	Impedance imaginary (Z = impedance)
Z_{real}	Impedance real
IPCE	Incident photon to electron conversion efficiency
IUPAC	International Union for Pure and Applied Chemistry
KE	Kinetic energy

LHE	Light harvesting efficiency
LUMO	Lowest occupied molecular orbital
J_{\max}	Maximum current density
P_{\max}	Maximum power
V_{\max}	Maximum voltage
MLCT	Metal to ligand charge transfer
MoC	Molybdenum carbide
MWCNT	Multi-walled carbon nanotube
NMP	N-Methyl-2-pyrrolidone
NCG	Non-conductive glass
V_{oc}	Open circuit voltage
η	Photoconversion efficiency
PSC	Photoelectrochemical solar cell
S	Photosensitizer in ground state
PV	Photovoltaic
PVD	Physical vapour deposition
h	Plank's constant
PEDOT	Poly(3,4-ethylenedioxythiophene)
PSS	Poly(styrenesulfonate)
BYK 419	Polyether-modified polydimethylsiloxane in butyl glycol
PET	Polyethylene terephthalate
PI	Polyimide
R_{rc}	Recombination resistance
Redox	Reduction-oxidation
R	Resistance
SEM	Scanning electron microscopy
R_s	Series resistance
R_s	Sheet resistance
J_{sc}	Short-circuit current density
R_{sh}	Shunt resistance
\square	Square
DECC	The Department of Energy & Climate Change
TGA	Thermo gravimetric analysis
TCO	Transparent conductive oxide
UV-VIS	Ultraviolet-Visible
ϕ	Work function
XRD	X-ray diffraction
XPS	X-ray photoelectron spectroscopy

TABLE OF CONTENTS

Chapter 1: Introduction & Literature Review

1.1	Introduction	2
1.2	Solar energy	3
1.3	Photovoltaic technologies	3
1.4	Dye-sensitized solar cells (DSCs)	5
1.4.1	Operating principle	6
1.4.1.1	Charge transfer	6
1.4.1.2	Charge recombination	8
1.5	DSC components	9
1.5.1	Working electrodes	9
1.5.1.1	Transparent conductive oxide (TCO) coated glass	10
1.5.1.2	Titanium metal	11
1.5.1.3	Steels	12
1.5.2	Titanium dioxide (TiO ₂) photoanode	13
1.5.3	Dye-sensitizer	13
1.5.4	Redox electrolyte	14
1.5.5	Catalyst	15
1.5.6	Sealant	15
1.5.7	Counter electrode	16
1.6	DSC characterization techniques	16
1.6.1	Solar simulation technique	16
1.6.2	Optoelectronic transient technique	18
1.6.3	Electrochemical impedance spectroscopy (EIS)	19
1.7	High-temperature resistant polymers	22
1.7.1	Polyimide	22
1.7.2	Synthesis of polyimide	23
1.7.3	Properties of polyimide	24
1.8	Electrically conductive polyimide	25
1.8.1	Photovoltaic applications of polyimide	27
1.9	Fillers for conductive polyimide	28
1.9.1	Graphite	28
1.9.2	Carbon nanotubes	29
1.9.3	Carbon black	30
1.9.4	Application of carbon materials in DSCs	31
1.9.5	Titanium nitride (TiN)	32
1.9.5.1	Synthesis of TiN	33
1.9.5.2	Properties of TiN	33
1.9.5.3	Application of TiN in dye-sensitized solar cells	34
1.10	Characterization of conductive coatings	37
1.10.1	Electrical resistivity measurement	37
1.10.2	Thermogravimetric analysis (TGA)	38
1.10.3	Reflectance measurement	39
1.10.4	Scanning electron microscopy	39
1.10.5	Stylus profilometry	39
1.10.6	X-ray photoelectron spectroscopy (XPS)	39
1.11	Aims and objectives	41
1.12	References	42

Chapter 2: Experimental Methods

2.1	Materials	53
2.1.1	Glass and metal substrates	53
2.1.2	Materials for dye-sensitized solar cells	53
2.1.3	Organic polymers and surfactant	54
2.1.4	Conductive fillers	55
2.2	Development of polyimide (PI) coating	55
2.2.1	Modification of polyamic acid	56
2.2.2	Coated substrate preparation	56
2.2.3	Curing of polyamic acid into polyimide	58
2.3	Electrically conductive PI coating	58
2.3.1	Preparation of carbon/polyimide coatings	58
2.3.2	Preparation of TiN/polyimide coatings	60
2.3.3	Preparation of hybrid coatings	61
2.4	Characterization of conductive coatings	61
2.4.1	Electrical sheet resistance measurement	62
2.4.2	Surface profilometry	62
2.4.3	Reflectance measurement	63
2.4.4	Thermogravimetry	63
2.4.5	Scanning electron microscopy	64
2.4.6	X-ray photoelectron spectroscopy	64
2.5	Fabrication of dye-sensitized solar cells	65
2.5.1	TiO ₂ working electrode preparation	65
2.5.2	Dye treatment	68
2.5.3	Counter electrode preparation	69
2.5.4	Device construction	69
2.6	DSC characterization	70
2.6.1	Solar simulation	70
2.6.2	Electrochemical impedance spectroscopy	72
2.6.3	Optoelectronic transient technique	72
2.7	References	73

Chapter 3: Assessment of Characterization Techniques to Determine Performance of Dye-sensitized Solar cells

3.1	Introduction	75
3.2	Experimental	76
3.3	Results and discussion	77
3.3.1	Current-voltage (J-V) characteristics	77
3.3.2	Electrochemical impedance studies	80
3.3.3	Optoelectronic transients measurements	86
3.3.4	Photovoltage decay measurements	89
3.4	Conclusions	90
3.5	References	91

Chapter 4: Carbon/Polyimide Coatings for Dye-sensitized Solar Cell Applications

4.1	Introduction	93
-----	--------------	----

4.2	Experimental	95
4.3	Results and discussion	96
4.3.1	MWCNT/polyimide coatings	96
4.3.2	MWCNT and graphite containing polyimide coatings	102
4.3.3	Graphite added polyimide coatings	106
4.3.4	Photovoltaic characterization	110
4.3.4.1	J-V characteristics of 40wt%graphite/PI working electrodes	110
4.3.4.2	EIS of 40wt% graphite/PI working electrodes	112
4.3.4.3	Photovoltage decay analysis of 40wt% graphite/PI working electrodes	114
4.3.4.4	Reflectance measurements of 40wt%graphite/PI and FTO glass	115
4.3.4.5	J-V characteristics of 40wt%graphite/PI counter electrodes	116
4.3.4.6	EIS of 40wt% graphite/PI counter electrodes	119
4.4	Conclusions	120
4.5	References	121

Chapter 5: TiN/Polyimide Coatings for Dye-sensitized Solar Cell Applications

5.1	Introduction	124
5.2	Experimental	125
5.3	Results and discussion	126
5.3.1	Characterization of TiN/PI coatings	126
5.3.2	Selection of the best TiN/PI composition for DSC application	131
5.3.3	SEM analysis of 90wt% TiN/PI coating	134
5.3.4	XPS of heat-treated 90wt% TiN/PI coating	134
5.3.5	J-V characteristics of 90wt% TiN/PI working electrodes	137
5.3.6	EIS of 90wt% TiN/PI working electrodes	140
5.3.7	Transient measurements of 90wt% TiN/PI working electrodes	143
5.3.7.1	Photovoltage decay measurements	143
5.3.7.2	Electron lifetime measurements	144
5.3.7.3	Charge density measurements	145
5.3.8	Reflectance measurements of 90wt%TiN/PI and FTO glass	147
5.3.9	J-V characteristics of 90wt% TiN/PI counter electrodes	147
5.3.10	EIS of 90wt% TiN/PI counter electrodes	150
5.4	Conclusions	153
5.5	References	154

Chapter 6: Hybrid Coatings for Dye-sensitized Solar Cell Applications

6.1	Introduction	157
6.2	Experimental	158
6.3	Results and discussion	159
6.3.1	Characterization of hybrid coatings	159
6.3.2	Scanning electron microscopy	161
6.3.3	Photovoltaic characterization	162
6.3.3.1	J-V characteristics of hybrid working electrodes	162
6.3.3.2	EIS of hybrid working electrodes	165
6.3.3.3	Photovoltage decay measurements	166
6.3.3.4	Electron lifetime measurements	167

6.3.3.5	J-V characteristics of hybrid counter electrodes	167
6.3.3.6	EIS of hybrid counter electrodes	169
6.4	Conclusions	171
6.5	References	172
Chapter 7: Conclusions and Future Work		
7.1	Conclusions	174
7.2	Future work	176
List of Publications & Presentations		178

LIST OF FIGURES

[1.1]	Simplified Illustration of a forward illuminated DSC.	5
[1.2]	Schematic representation of electron transfer kinetics within a DSC.	6
[1.3]	Charge recombination kinetics within a DSC.	8
[1.4]	Various components of a dye-sensitized solar cell.	9
[1.5]	Schematic representation of a reverse illuminated dye-sensitized solar cell.	10
[1.6]	Chemical structure of the N719 Ruthenium complex sensitizer, N3 has the same structure when all carboxylate groups are protonated.	14
[1.7]	Effect of incident light on the I-V characteristics of a DSC.	17
[1.8]	AC current response in a linear system.	20
[1.9]	Nyquist curve of a standard glass-glass dye-sensitized solar cell.	21
[1.10]	Equivalent circuit model for Nyquist plots.	21
[1.11]	Poly-condensation reaction between pyromellitic dianhydride and a diamine.	24
[1.12]	Crystal structure of graphite.	28
[1.13]	Various functional groups on carbon surface.	31
[1.14]	Schematic representation of four-point probe measurement technique.	38
[1.15]	Simplified diagram of the X-ray photoelectron spectrophotometer.	40
[2.1]	Schematic of the effect of surfactant on coating properties.	56
[2.2]	Coating application technique.	57
[2.3]	Curing process of polyamic acid into polyimide.	58
[2.4]	(a) Cured TiN/PI coating on NCG (de-laminated) (b) Cured TiN/PI coating on ECCS substrate.	60
[2.5]	(a) non-conducting glass substrates with cured 5wt% TiN/PI coating (b) same substrates with cured top coating (no delamination observed).	61
[2.6]	Standard sample for sheet resistance measurement.	62
[2.7]	Schematic of a stylus profilometer and sample scanning technique.	62
[2.8]	Schematic representation of reflectance measurement using a UV-Vis spectrophotometer.	63
[2.9]	Schematic of a thermogravimetric analyser.	64
[2.10]	Schematic representation of TiO ₂ deposition on a clean substrate.	66
[2.11]	TiO ₂ deposition on a clean FTO glass substrate.	66
[2.12]	Dried and sintered TiO ₂ films on a FTO glass substrate.	67
[2.13]	Shaping of a TiO ₂ film on a FTO glass substrate.	67
[2.14]	TiO ₂ deposition technique on coated substrates.	68
[2.15]	FTO glass strips with dye-sensitized TiO ₂ films.	69
[2.16]	Assembled device (a) schematic (b) FTO based typical device.	70
[2.17]	Schematic of a solar simulator used for DSC testing.	71
[2.18]	Schematic of a test cell for solar simulation.	71
[2.19]	Simplified diagram of the equipment used for optoelectronic transient measurements.	72
[3.1]	Average J-V characteristics of optimized and un-optimized DSCs in forward illumination mode: based on two sets of six devices each.	78
[3.2]	Average J-V characteristics of optimized and un-optimized DSCs in reverse illumination mode: based on two sets of six devices each.	78
[3.3]	Nyquist plots of optimized and un-optimized devices based on their average values (data consist of the average of three best performing devices from	80

	each set).	
[3.4]	Average charge transfer resistance (R_{ct}) vs. applied potential (data consist of the average of three best performing devices from each set).	81
[3.5]	Average charge recombination resistance (R_{rc}) vs. applied potential (data consist of the average of three best performing devices from each set).	82
[3.6]	Average chemical capacitance (C_{μ}) vs. applied potential (data consist of the average of three best performing devices from each set).	83
[3.7]	Average electron lifetime vs. applied potential (data consist of the average of three best performing devices from each set).	84
[3.8]	Average Bode plots of optimized and un-optimized devices showing phase shift vs. frequency (data consist of the average of three best performing devices from each set).	85
[3.9]	Average recombination lifetime vs. voltage (data consist of the average of three best performing devices from each set).	86
[3.10]	Average charge density vs. voltage (data consist of the average of three best performing devices from each set).	87
[3.11]	Average current density vs. lifetime (data consist of the average of three best performing devices from each set).	88
[3.12]	Photovoltage decay vs. time (data consist of the average of three best performing devices from each set).	89
[4.1]	Carbon based coatings on metallic and non-metallic substrates as (a) working electrodes and (b) counter electrodes.	94
[4.2]	Surface profile of a typical MWCNT/PI coating cured at 350°C.	96
[4.3]	Surface profile of an un-pigmented PI coating cured at 350°C.	97
[4.4]	R_a and R_p of MWCNT/PI on non-conducting glass.	99
[4.5]	R_a and R_p of MWCNT/PI on ECCS.	99
[4.6]	TG analysis of polyimide precursor.	101
[4.7]	Average thickness of MWCNT/PI on (a) NCG and (b) ECCS.	101
[4.8]	Surface profile of a typical graphite/MWCNT/PI coating.	103
[4.9]	R_a and R_p of Graphite-MWCNT/PI on non-conducting glass.	104
[4.10]	R_a and R_p of Graphite-MWCNT/PI on ECCS.	104
[4.11]	Average R_a and R_p values of MWCNT/PI and graphite/MWCNT/PI coatings at 450°C.	105
[4.12]	Graphite/MWCNT/PI on (a) NCG and (b) ECCS: coating thickness vs. temperature.	105
[4.13]	Surface profile of a typical graphite/PI coating.	106
[4.14]	R_a and R_p of Graphite/PI on non-conducting glass.	109
[4.15]	R_a and R_p of Graphite/PI on ECCS.	109
[4.16]	Coating thickness vs. temperature of Graphite/PI on (a) NCG and (b) ECCS.	109
[4.17]	Average J-V characteristics of cells based on graphite/PI coated NCG, ECCS and their comparison with standard FTO glass devices.	111
[4.18]	Average charge recombination resistance vs. voltage: based on graphite/PI coated ECCS, NCG and standard FTO cells: based on 9 best performing devices.	113
[4.19]	Average chemical capacitance vs. voltage: based on graphite/PI coated ECCS, NCG and standard FTO cells: based on 9 best performing devices.	113
[4.20]	Photovoltage decay in DSCs based on graphite/PI coated working electrodes	115

	and their comparison with FTO glass based devices: based on 9 best performing devices.	
[4.21]	Comparison of “%Reflectance” between FTO glass and 40 wt% graphite/PI coatings after heat treatment at 450°C for 30 minutes.	115
[4.22]	Average current-voltage characteristics of graphite/PI coating on NCG and ECCS substrates as counter electrodes and their comparison with a standard FTO glass cell.	117
[4.23]	Average charge transfer resistance vs. voltage.	119
[4.24]	Average double layer capacitance vs. voltage.	120
[5.1]	Sheet resistance vs. wt% TiN in PI at 350°C.	126
[5.2]	TiN/PI coatings: sheet resistance vs. time at 450°C over 30 minutes.	128
[5.3]	Percentage increase in sheet resistance of TiN/PI coatings after heat-treatment at 450°C for 30 minutes.	129
[5.4]	R_a and R_p values of TiN/PI coatings after curing at 350°C and heat treatment at 450°C for 30 minutes.	130
[5.5.a]	90 wt% TiN/PI on ECCS substrates heat -treated at 350°C and 450°C.	132
[5.5.b]	One year old ECCS based DSC substrate coated with 90% TiN/PI coating without any significant signs of corrosion (Right) Uncoated ECCS substrate exposed to DSC electrolyte (Left)	132
[5.6]	SEM images 90 wt% TiN/PI coating: (a) cured at 350°C for 5 minutes and (b) heat-treated at 450°C for 30 minutes.	134
[5.7]	Quantification of elements present in the heat-treated 90 wt% TiN/PI coating.	135
[5.8]	XPS analysis of heat-treated 90 wt% TiN Coating: (a) Carbon 1S, (b) Titanium 2p, (c) Oxygen 1s and (d) Nitrogen 1s.	136
[5.9]	Average J-V curves of 90 wt% TiN/PI coated ECCS and non-conducting glass based DSCs and their comparison with standard FTO glass and titanium metal cells.	137
[5.10]	Delaminated TiO_2 on 90 wt% TiN/PI during its $TiCl_4$ treatment.	140
[5.11]	Average charge transfer resistance in the coated ECCS, coated NCG, FTO glass and titanium metal working electrodes based cells: average data based on 12 best devices.	141
[5.12]	Average Bode plots of DSCs based on 90 wt% TiN/PI coated ECCS and glass cells and their comparison with FTO glass, Ti metal cells and uncoated ECCS cells at an applied potential of 0.7V: average data based on 12 best devices.	142
[5.13]	Average photovoltage decay measurements of 90 wt% TiN/PI coated working electrodes and their comparison with FTO and Ti based cells: average data based on 12 best devices.	144
[5.14]	Average transient electron lifetime vs. voltage in 90 wt% TiN/PI coated substrates and their comparison with FTO and Ti based cells: average data based on 12 best devices.	145
[5.15]	Average charge density vs. voltage in 90 wt% TiN/PI coated substrates and their comparison with FTO and Ti based cells: average data based on 12 best devices.	146
[5.16]	% Reflectance vs. wavelength of FTO glass and 90 wt% TiN/PI at 450°C.	147
[5.17]	Average J-V characteristics of 90 wt% TiN/PI coated counter electrodes with thermally decomposed and sputter platinum vs. typical FTO cells with	148

	thermally deposited and sputter platinum: average data based on 24 devices.	
[5.18]	Average charge transfer resistance at the counter electrodes of the 90 wt% TiN/PI coated ECCS and non-conducting glass electrodes and FTO based cells (with thermally deposited and sputter platinum): average data based on 18 devices.	151
[5.19]	Average electrical double layer capacitance in platinized counter electrodes/electrolyte interface of 90 wt% TiN/PI coated ECCS and non-conducting glass electrodes and FTO based cells (with thermally deposited and sputter platinum): average data based on 18 devices.	152
[6.1]	Hybrid coatings and their comparison with best performing graphite/PI and TiN/PI coatings on non-conductive glass substrate: sheet resistance vs. composition.	159
[6.2]	Hybrid coatings and their comparison with best performing graphite/PI and TiN/PI coatings on non-conductive glass substrate: R_a and R_p vs. composition.	160
[6.3]	Hybrid coating cured at 350°C/5 mins.	161
[6.4]	Hybrid coating heated at 450°C/30 mins.	161
[6.5]	Average J-V curves of TiN-graphite hybrid coating based working electrodes and their comparison with standard FTO devices.	162
[6.6]	Average J_{sc} and η values: a comparison between graphite/PI, hybrid/PI and TiN/PI based devices.	163
[6.7]	%reflectance vs. wavelength in TiN-graphite hybrid coating based working electrodes and their comparison with standard FTO coated substrate.	164
[6.8]	Average charge recombination resistance in hybrid coating based working electrodes and their comparison with standard FTO devices: average based on 9 best performing cells.	165
[6.9]	Average photovoltage decay curves of TiN-graphite hybrid coating based working electrodes and their comparison with standard FTO cells: average based on 9 best performing devices.	166
[6.10]	Average recombination lifetime vs. voltage in TiN-graphite hybrid coating based working electrodes and their comparison with standard FTO cells: average based on 9 best performing devices.	167
[6.11]	Average J-V characteristics of TiN-graphite hybrid coating based counter electrodes and their comparison with standard FTO cells: average based on 9 best performing devices.	168
[6.12]	Average charge transfer resistance vs. voltage in TiN-graphite hybrid coating based counter electrodes and their comparison with standard FTO cells: average based on 9 best performing devices.	170
[6.13]	Average double layer capacitance vs. voltage in TiN-graphite hybrid coating based counter electrodes and their comparison with standard FTO cells: average based on 9 best performing devices.	171

LIST OF TABLES

[1.1]	Best performing photovoltaic devices tested under global AM1.5 spectrum (1000 W/m ²) at 25 °C.	4
[1.2]	Quantities obtained from the current-voltage characteristics.	18
[1.3]	Polyimide properties.	24
[1.4]	Properties of TiN.	34
[2.1]	Materials used for DSC manufacturing.	54
[2.2]	Properties of the polyimide precursor.	55
[2.3]	Properties of conductive fillers.	55
[2.4]	Experimental setup for XPS analysis.	65
[2.5]	Settings used for solar simulation.	70
[3.1]	Average TiO ₂ film thickness of the cells chosen for characterization.	77
[3.2]	Average current-voltage data of optimized and un-optimized cells: based on total 12 devices.	79
[4.1]	Sheet resistance of MWCNT/PI coatings on NCG and ECCS substrates.	98
[4.2]	R _s and R _p values of uncoated substrates and un-pigmented PI films.	100
[4.3]	Sheet resistance values of graphite/MWCNT/PI coatings on NCG and ECCS substrates.	103
[4.4]	Sheet resistance values of graphite/PI based coatings on NCG and ECCS substrates.	107
[4.5]	Average current-voltage data obtained from the solar simulation experiment.	111
[4.6]	J-V characteristics of Graphite/PI coated ECCS and non-conducting glass counter electrodes with platinum catalyst.	118
[4.7]	Average J-V characteristics of graphite/PI coated ECCS and non-conducting glass counter electrodes without platinum catalyst.	118
[5.1]	R _s and R _p values of cured TiN/PI coatings at 350°C for 5 minutes.	127
[5.2]	90 wt% TiN/PI on ECCS substrates: at 350°C and at 450°C.	132
[5.3]	DSCs based on 90 wt% TiN/PI coated working electrodes and their comparison with FTO glass and Ti-metal based devices.	138
[5.4]	Electron lifetimes of DSCs based on 90 wt% TiN/PI coated working electrodes and their comparison with FTO and titanium metal based cells: average data based on 12 best cells.	142
[5.5]	Average J-V data of 90 wt% TiN/PI coated counter electrodes (with thermally deposited and sputter platinum) and their comparison with FTO glass based typical devices.	149
[6.1]	Average current-voltage characteristics of TiN-graphite hybrid coating based working electrodes.	163
[6.2]	TiN-graphite hybrid coating based counter electrodes and their comparison with standard FTO cells.	169

CHAPTER 1

INTRODUCTION & LITERATURE REVIEW

1.1 Introduction

A dye-sensitized solar cell (DSC) is a special type of excitonic device ^[1] that contains a thin layer of mesoporous TiO₂ sensitized with a metal- complex dye. DSCs with reasonable efficiency were first reported by Michael Grätzel and Brian O'Regan in their pioneering paper published in 1991^[1]. One aspect of DSCs that make them particularly attractive is the relatively inexpensive and readily available nature of their major components, in contrast with the traditional 1st and 2nd generations' homo and hetero junction photovoltaic devices ^[2] where the manufacturing cost is still primarily dependant on the raw materials.

In a classical DSC architecture, the working electrode consists of a mesoporous film of TiO₂ nanoparticles deposited on a conductive substrate and sensitized with an organometallic ruthenium-based dye ^[1]. Optimum properties for the oxide film are obtained by high temperature sintering (at 450-500 °C) of a titania paste, hence limiting the range of materials qualifying as electrode substrate. Typically, the working electrode is prepared on a TCO (transparent conducting oxide) coated glass, which is transparent, electrically conductive and high-temperature stable ^[3]. However, TCO coated glass sheets are not flexible in nature thus large scale industrial manufacturing of TCO based DSCs in a roll-to-roll operation line could be a difficult task to achieve ^[4].

Metal-mounted reverse-illuminated DSCs ^[5, 6] on the other hand are becoming popular due to their flexibility and superior electrical conductivity, which allow their roll-to-roll processing. For instance, titanium metal foil ^[7] has already been successfully introduced as a working electrode material in commercialised DSC products ^[8, 9]. However, for obvious economic reasons, it would be preferable to use lower cost metal materials such as steel. An inherent difficulty in this case relates to controlling or inhibiting the corrosion of the metal sheet when in contact with the aggressive I⁻/I₃⁻ electrolyte ^[10] used in a DSC. This issue may be solved by applying a protective coating (with good electrical conductivity and high temperature stability) to prevent any contact between the electrolyte and the underlying metal. Hence, this thesis is based on formulation of protective coatings for low-cost steel (e.g. ECCS) mounted dye-sensitized solar cells followed by their photovoltaic (PV) characterization using optical and electrochemical techniques.

1.2 Solar energy

The sun is an unparalleled source of energy, which is cost-free, clean and abundant. Nuclear fusion of hydrogen atoms is mainly responsible for the enormous amount of energy that is being produced by the sun ^[11]. The energy from the sun reaches the earth in the form of electromagnetic radiation, which can be converted into electricity to fulfil earth's energy requirements. It has been calculated that the earth's annual energy demand is approximately 1.3×10^5 TWh, which is equivalent to the energy we get from the sun in just 6 hours ^[12]. Therefore, efforts have been made in order to harness the sun's energy in different ways among which solar photovoltaics is a reliable method of electricity generation ^[13].

1.3 Photovoltaic technologies

A photovoltaic cell or most commonly known as a 'solar cell' converts sun's energy into electricity. The discovery of photovoltaic effect in 1839 pioneered this technology, which led to a breakthrough in 1954, when a group of scientists at Bell laboratories manufactured the first ever silicon based solar cell with merely 6% photoconversion efficiency ^[14]. Ever since this discovery, a great deal of technological advancement has been achieved in this field and almost sixty years later, the efficiency of the traditional silicon based solar cells has now reached beyond 20% ^[15]. However, the silicon based first generation solar cells are an expensive means of energy conversion, as they require high purity crystalline silicon ^[15]. Details about these first generation solar cells can be found in Table 1.1, which also provides information about different types of photovoltaic cells (lab-scale) with accredited record efficiency values.

Investigations on low-cost device manufacturing started several decades ago with the development of a thin film photovoltaic device made of copper sulphide and cadmium sulphide arranged in a bi-layer fashion. This device was first reported in 1972 directing the PV technology towards the next level, which is often referred to as the 'second generation' or 2G ^[16]. Today's improved versions of 2G solar cells are mainly based on CIGS (copper-indium-gallium-selenide) and GaInP (gallium-indium-phosphide) based thin film materials ^[17, 18] capable of converting over 20% of the sun's energy into electricity. Thin film technology has the potential to become a low-cost alternative in the future that can replace existing 1G solar cells however,

there are several technological issues that need to be addressed before it becomes a reality.

TABLE 1.1: Best performing photovoltaic devices tested under global AM1.5 spectrum (1000 W/m²) at 25 °C – reproduced from ^[19, 22].

Classification	Efficiency (%)	Area (cm ²)	V _{oc} (V)	J _{sc} (mA/cm ²)	Fill factor (%)	Test centre (date)
<i>Si-Wafer based</i>						
Si (large crystalline)	24.7	101.8	0.75	39.5	83.2	AIST (12/12)
Si (large crystalline)	24.2	155.1	0.72	40.5	82.9	NREL (5/10)
Si (large crystalline)	19.5	242.7	0.65	39.0	76.7	FhG ISE (3/11)
<i>Inorganic thin film</i>						
GaInP	20.8	0.24	1.45	16.04	89.3	NREL (5/13)
CIGS (thin film)	20.8	0.5	0.75	34.77	79.2	FhG-ISE (10/13)
CIGSS (Cd free)	19.7	0.49	0.68	37.06	77.8	AIST (11/12)
CZTSS (thin film)	12	0.43	0.49	34.8	69.4	Newport (7/13)
CZTS (thin film)	8.5	0.23	0.7	16.83	70.9	AIST (1/13)
<i>Excitonic</i>						
Dye sensitised	11.9	1	0.74	22.47	71.2	AIST (9/12)
Dye-sensitised	12.3	1	0.92	17.05	77.9	IMT, Switzerland
Dye sensitised	9.9	17.11	0.71	19.4	71.4	AIST (8/10)
Perovskite	14.1	0.2	1	21.34	65.7	Newport (5/13)
Organic	11.1	0.15	0.86	17.81	72.2	AIST (10/12)

The original research into excitonic or ‘third generation’ (3G) solar cell devices began prior to 2G. The photovoltaic nature of a single crystal of anthracene was first discovered by Kallmann and Pope in 1959 ^[20]. However, they could not clearly explain the phenomenon of exciton separation in the anthracene molecule when illuminated under sunlight ^[20]. Years after this discovery, a research by Tang *et al.* in 1986 first proposed a donor/acceptor based excitonic PV device based on organic semiconductors with 1% photoconversion efficiency (PCE) ^[21]. Five years later came the discovery of the dye-sensitized solar cell by Grätzel and O’Regan ^[1]. PCEs of various excitonic devices have improved steadily in subsequent years, and include the cobalt electrolyte based dye-sensitized cells with over 12% photoconversion

efficiency to date^[22]. Due to simple manufacturing techniques and lower cost, 3G solar cells could emerge as a low cost means of electricity generation in the near future.

1.4 Dye-sensitized solar cells

According to Michael Grätzel, dye-sensitized solar cells mimic the charge separation process in photosynthesis^[23]. This type of typical excitonic cell contains a high surface area TiO_2 photoanode sensitized with a metal complex dye.^[24] The photosensitive component of this device is the dye-sensitized TiO_2 , which is normally sandwiched between two TCO-glass electrodes accompanied by a redox electrolyte (ideally I^-/I_3^- couple) and a Pt-based catalyst. DSCs with transparent glass electrodes can be illuminated from both the forward (working electrode side) and reverse (counter electrode side) as illustrated in Figure 1.1 and subsequently in Figure 1.5. Some important features of this device include simple manufacturing processes, inexpensive raw materials and impressive photovoltaic performance^[1].

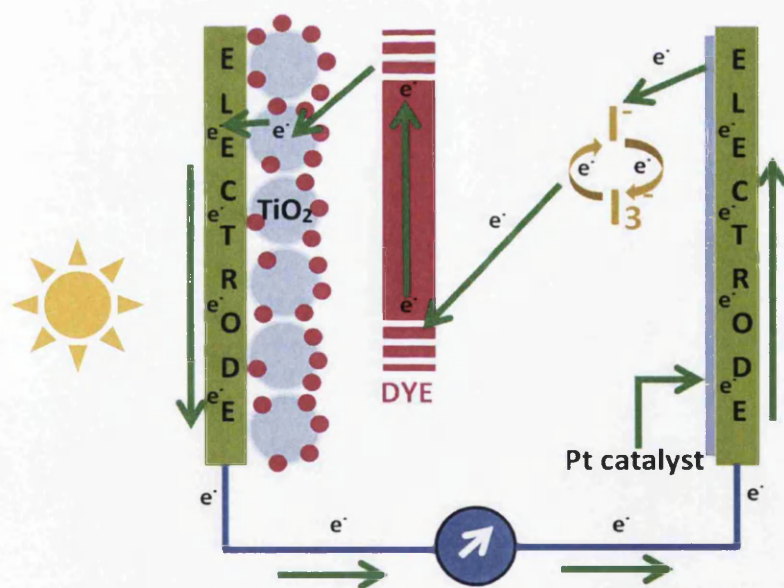


FIGURE 1.1: Simplified Illustration of a forward illuminated DSC.

For instance, most of its components are easily available from local suppliers, which can be used to manufacture a fully functional device for recreational purpose. Some DIY experts have used TiO_2 extracted from donut icing and red-wine (or tea) to manufacture homemade devices^[25-26]. Therefore, it is possible to manufacture DSCs at lower cost with respect to other contemporary technologies. In addition, DSCs can

be fabricated on transparent glass as well as flexible metallic and non-metallic substrates [18, 27], which is suitable for aesthetic and BIPV (building integrated photovoltaics) applications respectively [28]. Thus, there is a strong possibility of global industrialization of this technology in the near future as it has already attracted the attention of several multinational companies including TATA steel [29], Sony [30], Samsung [31] and Merck [32]. Furthermore, DSCs have a growing market in consumer electronics due to their outstanding low-light performance [33].

1.4.1 Operating principle

1.4.1.1 Charge transfer

A standard DSC is a photoelectrochemical device, which functions in the presence of any source of visible light obeying the principles of oxidation and reduction. The photon to current conversion within a DSC takes place through a combination of several charge transfer steps shown in Figure 1.2.

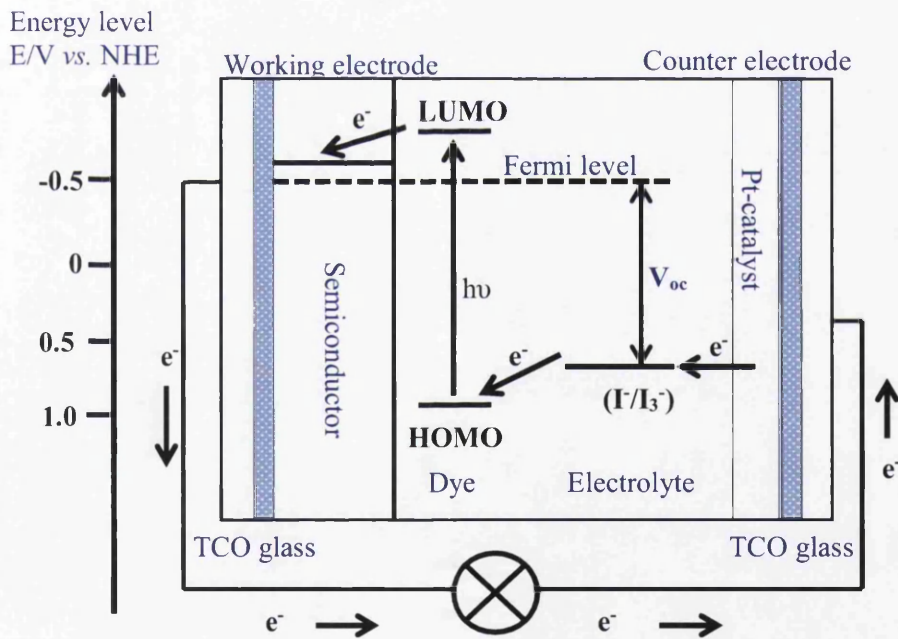
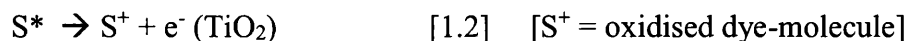


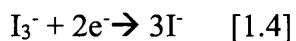
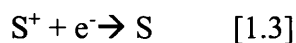
FIGURE 1.2: Schematic representation of electron transfer kinetics within a DSC.

The first stage involves photoexcitation of the dye-sensitizer (preferably, Ru-metal based) adsorbed onto the porous TiO_2 photoanode. This promotes the charge carriers from the ground state (S) to the excited state (S^*) of the dye molecule. The excited electrons are then injection into the TiO_2 conduction band causing oxidation of the photosensitive dye [34] as shown below in equations 1.1 and 1.2.



The injected electrons in the TiO_2 conduction band travel through the porous structure towards the electrically conductive working electrode (e.g. TCO glass) and finally reach the counter electrode through an external circuit connected between the working and the counter electrodes of a DSC [35].

Finally, reduction of the oxidized photosensitizer (S^+) takes place by the iodide ion (I^-) which itself oxidizes to the triiodide ion (I_3^-). The oxidised I_3^- ion is then diffuses towards the counter electrode where in presence of the platinum catalyst it reduces back to the I^- state [34, 35].



Some limiting factors that may affect the DSC operation include [34]:

1. The HOMO-LUMO gap of the dye-sensitizer must be small enough to facilitate absorption of visible light at longer wavelengths. In addition, a negative energy gap between the LUMO and the TiO_2 conduction band enhances the rate of electron injection to the semiconductor film.
2. On the other hand, the HOMO of the dye-sensitizer should be more positive than the redox potential of the electrolyte. This results in faster reduction of the dye-molecule by the redox couple.
3. V_{oc} acts as a driving force for the electron transfer process occurring in a DSC, which is normally governed by the energy gap between the Fermi level of the semiconductor and the redox potential of the electrolyte.

1.4.1.2 Charge recombination

The photovoltaic performance of a DSC can be severely affected by recombination of the photogenerated electrons with the dye and the redox electrolyte ^[34]. However, compared to fast charge injection from the photosensitizer into the conduction band of the TiO_2 , charge recombination between the oxidised dye and the injected electrons takes place at much slower rate, between micro and milliseconds. In addition, faster electron transfer (~ 100 ps) from the I^- species into the oxidised dye also helps suppress the recombination between the injected electrons and the dye ground state. Faster re-generation of the dye ground state also reduces the possibility of electron recombination from the S^* to S state, which is relatively slower than the re-generation process ^[34, 36].

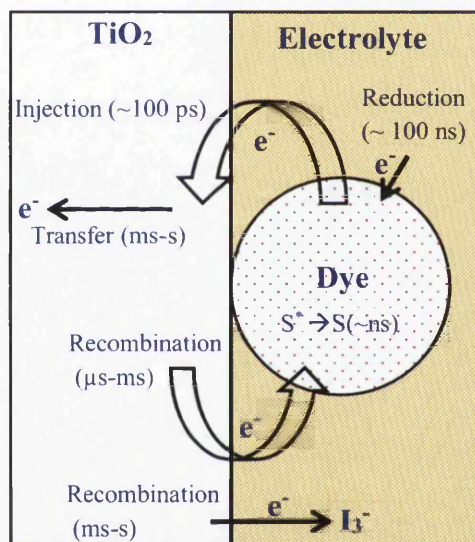


FIGURE 1.3: Charge recombination kinetics within a DSC.

The electrons injected into the conduction band of the TiO_2 film can also recombine with the tri-iodide (I_3^-) ions. This type of charge recombination mostly occurs at the TiO_2 /electrolyte interface due to high surface area of the mesoporous semiconductor film. However, charge recombination at the TCO glass/electrolyte interface may also occur if it is not fully covered by the TiO_2 film. This primary recombination process could significantly reduce the PV performance of a DSC, which is very similar to the recombination in atypical p-n junction device. Thus, the current obtained due to this type of recombination is often referred to as the 'dark current' ^[34, 37].

1.5 DSC components

In the standard DSC designed by Grätzel and co-workers, the dye-sensitized TiO_2 film was sandwiched between two TCO coated glass electrodes (Figure 1.4). A redox electrolyte containing I^-/I_3^- couple was then injected through a tiny hole present in the platinum (Pt) deposited counter electrode. A detailed schematic of a device has already been presented in Figure 1.1. Thus, this section will focus on the individual DSC components with recent literature examples.

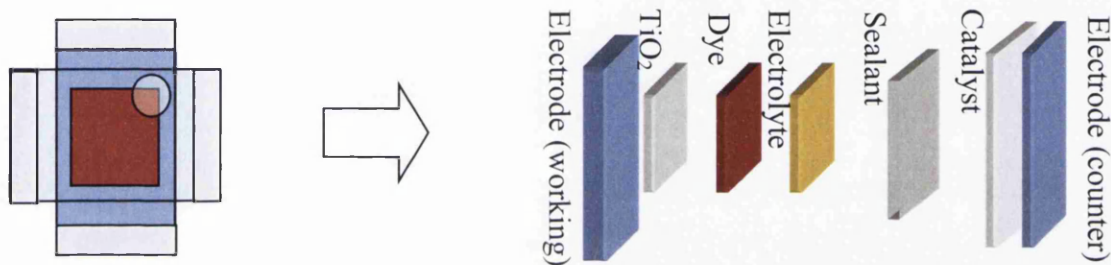


FIGURE 1.4: Various components of a dye-sensitized solar cell.

1.5.1 Working electrodes

The working electrode (WE) of a dye-sensitized solar cell is an electrically conductive (with low electrical resistance) substrate, which provides physical support to the mesoporous TiO_2 photoanode. Due to its conductive nature, the WE also helps extract electrons from the TiO_2 conduction band to the external circuit [1]. In a traditional DSC architecture, transparent WEs are preferred over opaque ones to construct a forward illuminated device where the incident photons directly interact with the photosensitive component to yield maximum photon-to-current conversion efficiency (Figure 1.1) [38]. However, the transparent WE can also be replaced by an opaque metal substrate in case of metal-mounted DSCs. In this case a transparent counter electrode (CE) is required in combination with the opaque WE to construct the device [38]. The transparent CE should also conduct electricity in order to collect electrons from the external circuit. A DSC with an opaque WE is termed as a 'reverse illuminated' device (Figure 1.5), which can lead to lower photoconversion

efficiencies due to absorption of the visible light at around 430 nm by the triiodide species of the redox electrolyte^[39].

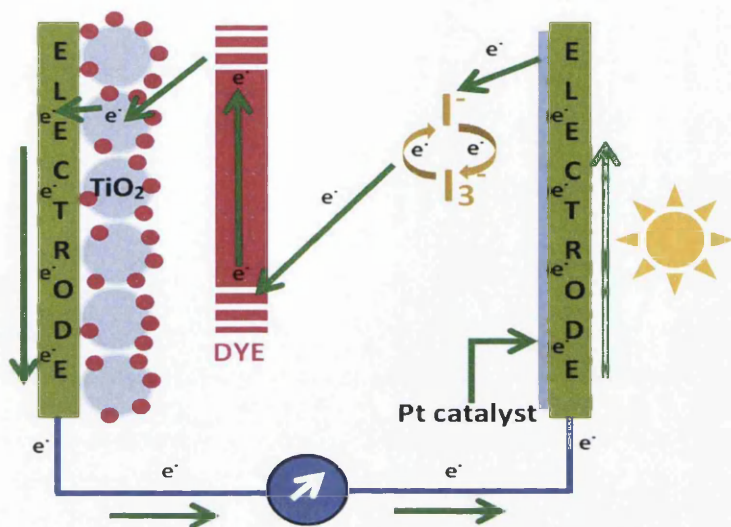


FIGURE 1.5: Schematic representation of a reverse illuminated dye-sensitized solar cell.

In contrast to glass based devices, the metal mounted DSCs are easy to handle and flexible in nature thus suitable for the large-scale production in a roll-to-roll manufacturing facility. However, it has been reported that the redox electrolyte present in the device could corrode the metallic working electrode^[10]. Therefore, WE selection for a metal mounted DSC is a key part of the fabrication process.

Thus, in this section, the merits of existing working electrode materials are discussed in accordance with the goals of this thesis (as outlined in section 1.1 and 1.11).

1.5.1.1 Transparent conductive oxide (TCO) coated glass

Transparent conductive oxides or TCOs are high temperature resistant ceramic materials used in optoelectronic applications due to their high temperature stability and low electrical resistivity. TCOs were first produced by Badeker in 1907 followed by their large-scale production during World War II for aerospace applications^[40, 41].

Fluorine doped tin oxide (FTO) and tin-doped indium oxides (ITO) are the most commonly used TCOs for various electronic applications including dye-sensitized solar cells. TCOs for DSC working electrode require low sheet resistance and high thermal stability due to the requirement for TiO₂ sintering at 450°C. It was observed

that at room temperature ITO demonstrates low electrical resistance, which gradually increases with temperature. Thus, ITO based WEs are not recommended for DSC application. On the other hand, resistance of FTO remains nearly the same at least up to 450°C – 500°C making it a credible choice for DSC fabrication [34]. The sheet resistance of an FTO coated glass varies between 8-15 Ω/\square whereas for ITO it is in the order of 6-7 Ω/\square [34, 42].

TCO coated glass WEs for DSC application can be developed in a number of ways including, spray pyrolysis [43], sol-gel techniques [44], chemical vapour deposition [45], chemical bath deposition [46] and sputtering [47]. The TCO film thickness in this case is usually maintained around 300 nm – 1000 nm [42, 48]. Despite several advantages, TCO coated glass WEs are fragile and inappropriate as DSC substrates for roll-to-roll manufacturing due to their rigidity.

1.5.1.2 Titanium metal

Titanium is an earth abundant material that consists 0.6% of the earth's crust [49]. Titanium demonstrates outstanding strength to weight ratio. Thus, the origin of its name is associated with the 'Titans' of Greek mythology [49]. It is flexible and corrosion resistant metal therefore it is a preferred WE material for roll-to-roll DSC manufacturing [7]. In addition, upon heat treatment Ti develops a compact layer of TiO₂ on its surface which is beneficial for preventing recombination reactions (effects of TiO₂ protective layer is discussed in detail in the results sections) occurring at the WE/electrolyte interface [50].

Dye-sensitized solar cells manufactured in a conventional way on Ti metal substrates with screen-printed TiO₂ films sintered at 500°C have already displayed over 7% photoconversion efficiencies [8]. Furthermore, as a step forward towards roll-to-roll manufacturing, Watson *et al.* used NIR heating technique to fast-sinter the mesoporous TiO₂ layer on Ti metal substrates achieving a sinter in only 12.5 seconds with comparable performance to devices sintered in a convection oven [6].

However, titanium extraction is an expensive and time-consuming process, which is why titanium metal is more expensive than the easily available ferrous alloys [51]. Thus, considering the aims of this project titanium based WEs will not be suitable as low-cost substrates for roll-to-roll production of metal mounted DSCs.

1.5.1.3 Steel

In order to avoid the use of expensive titanium metal, the industrial sponsor of this project (TATA steel) was more inclined towards the use of low-cost steels in this project as the company itself is one of the biggest producers of architectural steels in the Europe. Suitability of low-cost steels as DSC substrates had already been investigated by Dr. Bruce Phillip of Swansea University, during his doctoral project. A substantial portion of his research involved electrochemical investigations of coated (e.g. Aludip, Zalutite etc.) and uncoated (e.g. ECCS, stainless steel etc.) steel substrates in contact with the DSC electrolyte. From the first set of experiments, it was reported that most steel-based substrates failed to demonstrate corrosion resistant properties when exposed to the DSC electrolyte. However, stainless steel appeared to be very promising for DSC application, as it did not exhibit any signs of corrosion during the initial study. Hence, it was believed at that time that stainless steel could be a possible alternative to expensive Ti as a contemporary study also reported the same fact presenting device efficiencies over 4% in general [52, 53].

Subsequent studies showed that stainless steel exhibited pitting corrosion after prolonged exposure in the I^-/I_3^- electrolyte solution rendering it unsuitable under long-term exposure. The same trend was observed by Kanta and Decroly when they used stainless steel electrodes in their study and immersed them in the electrolyte solution for few days [54].

Thus, it is clear that steel-based substrates including stainless steel are unfavourable for DSC application in spite of their lower cost. However, steel-based substrates could be protected by applying a protective layer, which will prevent electrolyte exposure to the underlying metal. On the basis of this principal TATA steel launched this research project where the primary aim was to develop a high-temperature resistant (due to the requirement for TiO_2 sintering) and electrically conductive organic coating that could protect low-cost steel substrates from the electrolyte corrosion.

A TATA product ECCS was proposed as a low-cost substrate for DSC application. A high-temperature resistant polymer was chosen as a matrix for the conductive organic coatings, which are discussed in section 1.7 and 1.8.

1.5.2 Titanium dioxide photoanode

The photoanode of a DSC consists of a dye-sensitized TiO₂ film, which is mesoporous in nature. Titanium dioxide is the most commonly used wide band-gap semiconductor material for this application due to its low-cost, easy availability and non-toxic nature. In addition, TiO₂ is an n-type semiconductor material with three naturally occurring polymorphs, anatase, rutile and brookite. The anatase TiO₂ ($E_g = 3.23$ eV) is preferred for DSC application [55].

The TiO₂ photoanode for DSC application is normally prepared from a colloidal paste of TiO₂ nanoparticles of 10 – 30 nm size. Bigger nanoparticles (250 – 300 nm) can also be added in the same paste to scatter the incident photons leading to improvement in the device performance [34]. For low-cost device manufacturing, this TiO₂ paste can be deposited onto the working electrode using either a doctor blade or screen-printing technique followed by a high-temperature (450°C – 500°C) sintering step, which results in a mesoporous TiO₂ film with interconnected particles [34].

The thickness of a mesoporous TiO₂ film prepared in this way using a scotch tape can vary between 7-10 μm with an actual surface area of approximately 1000 cm²/g. High surface area in this case promotes increased dye-adsorption in the mesoporous TiO₂ [34].

1.5.3 Dye sensitizer

The most commonly used dye in a typical dye-sensitized solar cell is a ruthenium (II) based complex, which absorbs between 400 – 800 nm. This dye is known as di-tetrabutylammoniumcis-bis(isothiocyanato)bis(2,2'-bipyridyl-4,4'-dicarboxylato)ruthenium(II) or N719 in short. The N719 dye (Figure 1.6) can exist in both protonated and de-protonated states. The protonated version is known as N3 that can absorb up to 700 nm in the visible region [56]. The sensitization of the mesoporous TiO₂ takes place through the attachment of functional groups present in the Ru-dye with the surface of the semiconductor film. Thus, in case of N719 dye, the adsorption of the dye molecules onto the TiO₂ surface could occur via the carboxylate bidentate coordination as supported by FT-IR studies [58-62]. The anchoring of the Ru-complex dye onto the semiconductor surface increases the

interaction between the ligand and the TiO₂ conduction band facilitating better electron injection from the dye molecule into the mesoporous TiO₂ [34].

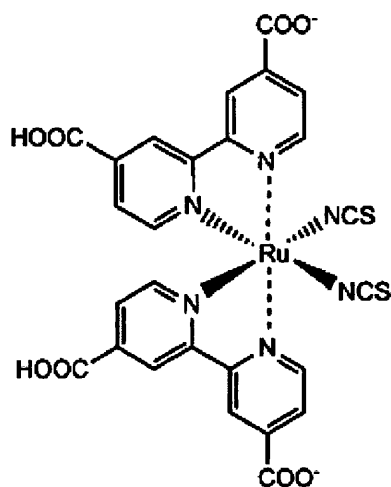


FIGURE 1.6: Chemical structure of the N719 Ruthenium, N3 has the same structure when all carboxylate groups are protonated [57].

1.5.4 Redox electrolyte

Reduction (re-generation) of the photosensitive Ru-dye in a typical DSC takes place via the electrolyte present in the device. This type of electrolyte can deliver electrons from the counter electrode to the oxidised dye molecule via a reduction-oxidation cycle, which is why it is most commonly known as a redox electrolyte. A redox electrolyte in a typical DSC is made of I/I₃⁻ ions that are initially reduced (e.g. I₃⁻ + 2e⁻ → 3I⁻ couple) by the incoming electrons at the platinised counter electrode followed by its oxidation (e.g. I₂ + I⁻ → I₃⁻) by the photosensitive dye. This electrolyte can frequently alter itself between reduced/oxidised and oxidised/reduced states, thus it can perform numerous redox cycles when used in a DSC [63].

The I/I₃⁻ (iodide/tri-iodide) redox couple is a mixture of iodine and an iodide salt which can be prepared using lithium iodide, sodium iodide, potassium iodide, tetraalkylammonium iodide (R₄NI) or imidazolium-derivative of iodides (concentrations of 0.1 – 0.5 M) along with (0.05 – 0.1M) I₂ solution. A non-protonic solvent (e.g. acetonitrile, propionitrile, methoxyacetonitrile, propylene carbonate, and their mixture) is mainly used to prepare the electrolyte solution in this case. It has been reported that the low viscosity electrolyte solvents give better performing cells due to faster ionic movement. Therefore, methoxyacetonitrile is chosen as a

solvent for the I/I_3^- redox couple as it gives the best performing cells (due to higher diffusion coefficient of I_3^- , which is in the order of $5.4 - 6.2 \times 10^{-6} \text{ cm}^2 \text{ s}^{-1}$). The mesoporous TiO_2 adsorbs the cations (e.g. Li^+ , K^+ , Na^+ and R_4N^+) liberated by the dissociation of iodide salts which in turn affects the device performance by shifting the conduction band level of the semiconductor film [34, 64, 65].

1.5.5 Catalyst

The counter electrode of a dye-sensitised solar cell is normally coated with a catalyst which catalyses the I_3^- reduction kinetics at the counter electrode helping the cell perform better. The catalyst is applied as a thin coating on the surface of the counter electrode. Platinum (Pt) and carbon (C) are commonly used catalyst materials for DSC application [75].

The platinum catalyst is always preferred to fabricate DSCs because of its superior catalytic activity. The catalytic performance of the platinum catalyst depends on the deposition method on the surface of the counter electrode. Normally, a solution of chloroplatinic acid hydrate ($\text{H}_2\text{PtCl}_6 \cdot x\text{H}_2\text{O}$) in isopropanol is used as a platinum precursor for pyrolytic deposition of Pt catalyst (at 400°C for 30 minutes in air) onto the counter electrode surface [66]. However, there are other methods that can be used for Pt deposition; such methods include electrochemical deposition [67], sputtering [68], and spin coating [69]. It has been found that electrochemically and vapour deposited Pt-catalyst are unstable in electrolyte solution [70, 71, 72]. The platinum catalyst is expensive and therefore efforts have been made towards the development of cheaper catalysts based on WC (tungsten carbide) and MoC (molybdenum carbide) [73].

The use of a carbon catalyst for DSCs was first proposed by Kay and Grätzel in 1996 where allotropes of carbon such as, carbon black and graphite were used to coat the counter electrodes of the dye-sensitized solar cells [74]. In addition, carbon nanotubes can also serve as a counter electrode catalyst [75]. Nevertheless, platinum is the ultimate choice for DSCs.

1.5.6 Sealant

A DSC should be sealed perfectly to prevent electrolyte leakage and solvent evaporation. Therefore, a sealant material is required to perform this task. This

sealant material should have chemical inertness towards the electrolyte and the other components of a dye-sensitized solar cell with good photochemical stability. In addition, sealant material should be durable without showing any signs of degradation.

Several types of sealant have been proposed by various researchers such as epoxy glue [76], water glass (sodium silicate) [74] and a vacuum sealant Torr Seal [77]. However, a copolymer of ethylene and acrylic acid, commercially known as Surlyn (Du Pont) acts as the best sealing material for DSCs which is chemically stable and relatively long lasting [34].

1.5.7 Counter electrode

The counter electrode (CE) is typically also made of same material as the working electrode. FTO coated glass is the most widely used counter electrode material. In addition, different types of steels (including stainless and ECCS) and titanium metal can also be used as a counter electrode material for DSC application. The materials stated above have already been discussed in section 1.5.1. The counter electrode in a dye-sensitized solar cell acts as a substrate for the deposited catalyst and it must be electrically conductive to harvest electrons from the external circuit.

1.6 DSC characterization techniques

A dye-sensitized solar cell displays the characteristics of a photosensitive diode, which works according to the principals of electrochemistry. Thus, characterization of a typical DSC often includes the solar simulation and electrochemical impedance spectroscopy (EIS) to assess the device performance accurately. Therefore, in this thesis both the solar simulation and EIS have been included for PV characterization along with optoelectronic transient measurements. This will help extract precise information about interfacial charge transfer and recombination reactions occurring in the fabricated devices.

1.6.1 Solar simulation technique

Unlike conventional diodes, DSCs are special type photosensitive diodes, which require sunlight to produce electricity under forward bias condition. The photoconversion efficiency of a dye-sensitized solar cell can be calculated from the

current (I) produced within the device plotted against the applied voltage (V)^[78]. The I-V characteristic of a DSC is normally measured under a standard solar spectrum of 1.5 air-mass (AM). This standard solar spectrum is simulated using a light source (preferably a xenon arc lamp) that provides artificial sun light with an intensity equivalent to 1000 W/m^2 or 1 Sun. The AM 1.5 in this case represents a standard condition when the sunlight travels in the atmosphere 1.5 times longer than when the sun is at the zenith^[79].

Important quantities such as short-circuit current, I_{sc} (when, $V=0$) and open-circuit voltage, V_{oc} (when, $I=0$) can be determined from a typical I-V curve (Figure 1.7) obtained from the solar simulation technique.

Other important parameters such as, maximum power point P_{max} and fill factor can also be derived from the I-V characteristics of a DSC. A brief description about each parameter can be found in Table 1.2^[80].

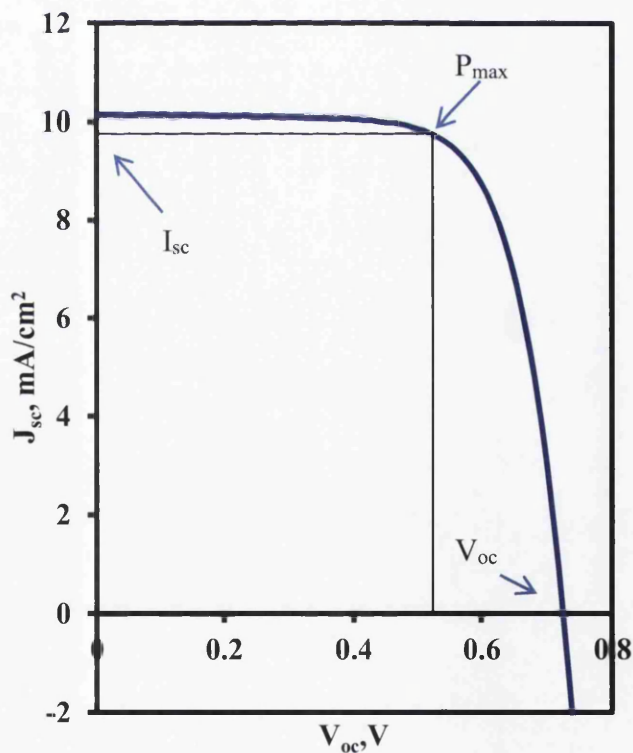


FIGURE 1.7: Effect of incident light on the I-V characteristics of a DSC (taken from one of the experiments shown in Chapter 3).

TABLE 1.2: Quantities obtained from the current-voltage characteristics ^[80].

Quantity	Definition
V_{oc}	refers to the voltage between the terminals of the cell when I (current) = 0
I_{sc}	can be defined as the short circuit current generated across the cell at voltage (V) = 0
J_{sc}	is the short circuit current generated per unit area (I/Area) i.e. short circuit current density
J_{max}	is the maximum current density obtained from the J -V curve
V_{max}	is the maximum voltage obtained at the J_{max} in the J-V curve
P_{max}	is the product of $J_{max} \times V_{max}$, which is the maximum power
FF	is the ratio of the theoretically obtained power and the measured power. $FF = (J_{max} \times V_{max}) / J_{sc} \times V_{oc}$
η	refers to the efficiency of the cell = $J_{sc} \times V_{oc} \times FF / P_{max}$

1.6.2 Optoelectronic transient technique

In optoelectronic transient measurement, a dye-sensitised solar cell is optically perturbed using a light source followed by the measurement of transient signals either in the form of current or voltage obtained after the perturbation process. This technique provides useful information about electron transport, recombination, and concentration within a dye-sensitized solar cell. This technique is similar to the electrochemical impedance spectroscopy but instead of AC potential, optical perturbation is used. Furthermore, transient analysis may be performed at a faster rate than the corresponding EIS measurement depending on the number of conditions applied during the scan. This facilitates capturing the device characteristics as a ‘snap-shot’ during each applied condition ^[81].

Optoelectronic transients are mainly divided into two categories such as, (a) photocurrent transients and (b) photovoltage transients.

(a) Photocurrent transients

Photocurrent transients mainly provide information regarding electron diffusion coefficients within a device. Photocurrent transients are obtained by determining the change in the photocurrent within a DSC (kept under short-circuit conditions) caused by an optical excitation pulse. This process generates additional charge carriers that help determine the nature of photocurrent transients within a cell. In a standard

device with minimum recombination, photocurrent transients can be used to estimate electron diffusion coefficient or D_n through the equation given below ^[81]:

$$D_n = \frac{d^2}{6t_{\text{peak}}} \quad [1.5]$$

[Where d = TiO_2 film thickness and t_{peak} = maximum photocurrent peak after the optical excitation, measured by software]

(a) Photovoltage transients

Photovoltage transient measurements help estimate charge recombination and transport lifetimes within a dye-sensitized solar cell. Photovoltage transients are measured in the same manner as photocurrent transients. However, it is essential to perform all the measurements under open-circuit conditions. Both the electron recombination and transport lifetimes are estimated indirectly from the charge extraction data obtained under open circuit conditions. Charge extraction data obtained by photovoltage transient measurement gives concentration of excess charge carriers within a device, which in turn can be used to calculate electron recombination and transport lifetimes in a DSC. This is a complex calculation, which is performed by software specially programmed for this study. Photovoltage transient measurements can also be used to determine photovoltage decay in a device in absence of illumination ^[81].

The major advantage of this technique is it can be even used to study unstable devices that degrade with time. However, it is a time consuming process to assemble the equipment for transient measurements. It normally requires a data acquisition board, few LEDs and some transistors. Thus, a low-cost instrument can be customised according to the nature of the analysis ^[81].

1.6.3 Electrochemical impedance spectroscopy (EIS)

Similar to the Ohmic resistance, impedance also demonstrates an electrical circuit's ability to resist the flow of current ^[82]. However, electrochemical impedance does not follow 'Ohm's law' as the signals obtained from an electrochemical cell are in the form of a sinusoidal AC current.

As DSCs are a special type of electrochemical cell, the electrochemical impedance occurring within a DSC is measured by applying an AC potential to the cell followed by measuring its AC current response. Unlike ideal electrical circuits (where applied voltage and current would be in phase in case of a wire of infinitely low resistance), AC current signals obtained from a DSC do not match with the applied sinusoidal AC potential and a phase shift is observed in this case (Figure 1.8) ^[82].

Therefore, impedance of an electrochemical cell is represented by 'Z', which is divided into real and imaginary components (Z_{real} and Z_{img}) in the form of complex numbers. Therefore, when Z_{real} and Z_{img} are plotted on X and Y axes respectively we get a Nyquist curve (Figure 1.9) of impedance at a specific frequency. Nyquist plot of a DSC is composed of generally three semicircles, which represents various interfacial electron transfer processes at a given frequency. The semicircle corresponding to the high frequency region refers to the charge transfer process occurring at the counter electrode of the device followed by the semicircle at the mid-frequency region, which represents electron recombination at the mesoporous TiO_2 /electrolyte and the substrate/electrolyte interfaces of the cell. Finally, the third semicircle at the low frequency region displays electron diffusion in the redox electrolyte of the cell (Figure 1.9) ^[83].

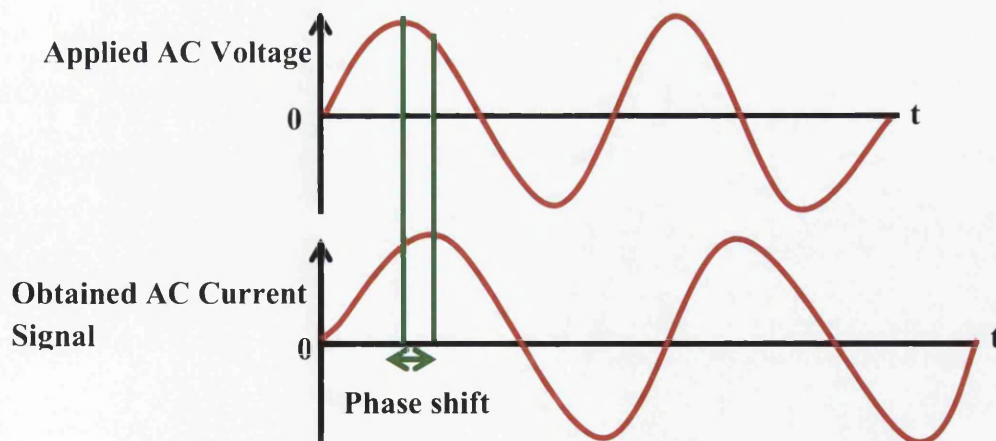


FIGURE 1.8: AC current response in a linear system.

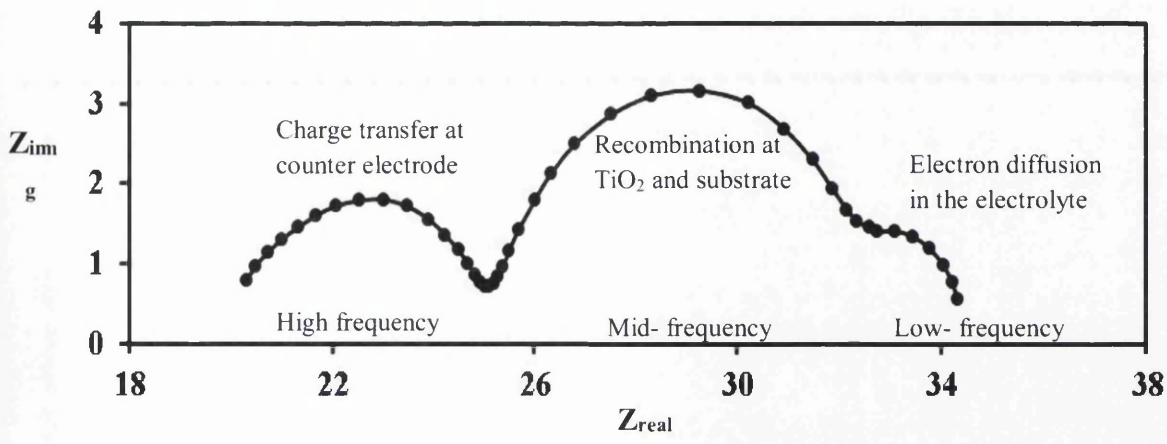


FIGURE 1.9: Nyquist curve of a standard glass-glass dye-sensitised solar cell.

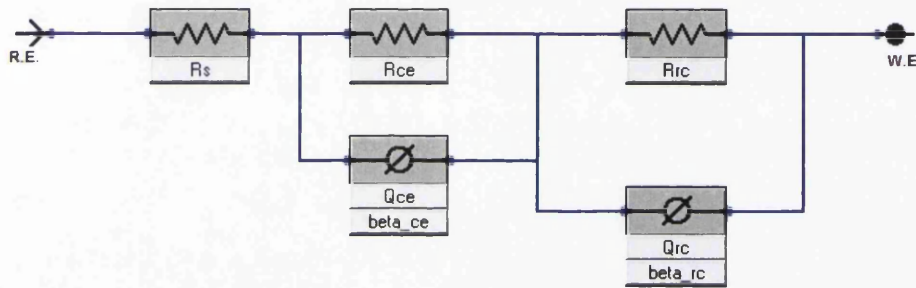


FIGURE 1.10: Equivalent circuit model for Nyquist plots.

Modelling of the Nyquist plot of a DSC provides quantitative information about the charge transfer kinetics occurring within the cell. Quantities such as R_{rc} (recombination resistance), R_{ce} (charge transfer resistance), and the chemical capacitance (obtained by inserting a constant phase element in the equivalent circuit, which models the behaviour of an imperfect capacitor in this case) can be obtained by simply fitting a model to the Nyquist plot. The model most widely used for this purpose is given in Figure 1.10.

1.7 High-temperature resistant polymers

It has already been mentioned in section 1.5.1.3 that the corrosion of low-cost steels such as ECCS can be prevented by using an organic coating, which is conductive and high-temperature resistant in nature. The heat-resistant property of this coating will play a pivotal role in this case, as the polymer should demonstrate good dimensional stability during the TiO₂ sintering step. Thus, engineering polymers with high service temperatures are proposed.

It was initially believed that engineering polymers such as, polyamidimides (PAI), polyetheretherketone (PEEK), polyethersulphone (PES), polytetrafluoroethylene (PTFE) and polyimide (PI) could be ideal for this application. However, it was later discovered that most of these (PAI, PEEK and PES) have service temperatures below 300°C whilst the others (PTFE and PI) could remain stable even at 300°C. In addition, both PTFE and PI demonstrate outstanding resistance to chemical attacks^[84]. Nevertheless, PTFE was not suitable for DSC application as it is a thermoplastic polymer, which cannot be used beyond 300°C. On the other hand polyimide is a thermosetting resin that remains stable beyond 300°C due to its high glass transition temperature (>400°C)^[84-85]. Furthermore, there is an evidence in favour of high-temperature application of polyimide during the manufacturing of CIGS solar cells where it has been reported that the CIGS crystals were grown on a polyimide substrates at ~ 450°C^[86].

Hence, polyimide based organic coatings could be very useful for the protection of low-cost metal substrates whilst maintaining the structural integrity during the high-temperature processing of DSC electrodes. However, polyimide is a non-conductive polymer, which requires modification in order to conduct electricity. Therefore, various methods for the development of conductive polyimides are discussed in section 1.8.

1.7.1 Polyimide (PI)

Polyimides find a wide range of applications in electronics, automotive and in the aerospace industries due to their excellent mechanical and thermal properties^[87]. Polyimides act as insulators and hence are suitable for manufacturing circuit boards, resistors and adhesives for the electronic applications. On the other hand, polyimide

based lightweight composites are being extensively used in the aerospace as well as in the automotive industries^[87].

The reaction between di-anhydrides and diamines produces polyimides of different molecular weight and characteristics. Depending on the nature of the precursor, polyimides are mainly divided into two parts, aromatic polyimides and aliphatic polyimides. Unlike the aliphatic ones, aromatic polyimides possess ring structure in the backbone of the polymer chain, which incorporates high temperature stability (250°C - 300°C) and high softening point in the polymer molecule. In addition, the properties such as toughness and chemical stability are governed by the degree of cross linking and chain extension. Most of the polyimides are thermosetting in nature; however, thermoplastic polyimides are also possible, if a partly cured polyimide composition contains residual plasticizing solvents^[88-90].

1.7.2 Synthesis of polyimide

High performance polyimides are synthesised through the poly-condensation reaction between an aromatic dianhydride such as, pyromellitic dianhydride and an aromatic diamine (Figure 1.11). The physical properties of such polyimides majorly depend on the nature of the diamine precursors. Hence, it has been discovered that the high thermal and oxidative stabilities of the polyimides rely on diamine selection e.g., m-phenylenediamine, benzidine, and di-(4-aminophenyl) ether give polyimides with best performance in terms of heat resistivity and oxidative stability. The well-known high performance polyimide, commercially available as 'Kapton' (DuPont) needs di-(4-aminophenyl) ether in its synthesis. Polyimides are produced in a two stage synthetic process where a poly (amic acid) intermediate is obtained in the first stage by the amidation reaction of the precursors in a polar solvent (preferably, dimethylformamide or dimethylacetamide). Poly (amic acid) is soluble, fusible and transformable into desired shapes (e.g. coatings, film, fibre, laminate etc.) followed by its curing in the second stage. The curing of poly (amic acid) involves cross-linking between the polymer chains at a temperature over 150°C to produce a rigid polyimide structure at the end of the process^[89].

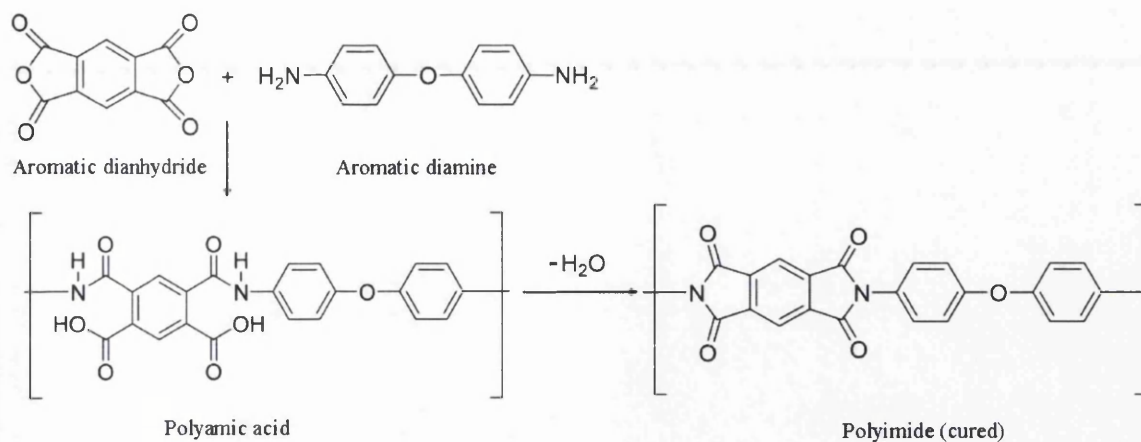


FIGURE 1.11: Poly-condensation reaction between pyromellitic dianhydride and a diamine^[91].

1.7.3 Properties of polyimides

Various properties of polyimide are given in Table 1.3, which mainly include mechanical, thermal, and physical properties. It can be seen from Table 1.3 that PI exhibits excellent physical as well as thermal properties. It is evident from the table that PI absorbs less amount of water, which is beneficial for the PI based coatings in terms of their durability. On the other hand, PI has a high processing temperature, which is why it is suitable for various high-temperature applications. In addition, PI is flexible in nature due to high flexural modulus, thus ideal as coatings on flexible metallic substrates.

TABLE 1.3: Polyimide properties^[92].

Mechanical Properties		State	Test method (ASTM)
Elastic Modulus (MPa)	2905	compressive	D638
	3174 - 32085	tensile	D638
Flexural Modulus (MPa)	2912 - 20700	23 °C	D790
	7107 - 18561	149 °C	D790
Tensile Strength (MPa)	30 - 158	at break	D638
	30 - 158	at yield	D638
Compressive Strength (MPa) at yield or break	133 - 227	---	D695
Flexural Strength (MPa) at yield or break	45 - 345	---	D790
Elongation at break (%)	1	---	D638
Hardness	110 - 120	Rockwell M	D638

Izod Impact (J/cm of notch) 1/8" thick specimen unless noted	0.3 - 8.0	---	D256A
Thermal Properties		State	Test method (ASTM)
Coef of Thermal Expansion ($10^{-6}/^{\circ}\text{C}$)	15 - 50	---	D696
Thermal Conductivity ($\text{W/m}^{\circ}\text{C}$)	0.230 - 0.502	---	C177
Melting Temperature ($^{\circ}\text{C}$)	thermoset	T_m , crystalline	---
Processing Temperature ($^{\circ}\text{C}$)	238 - 252	general	---
Physical Properties		State	Test method (ASTM)
Specific Gravity	1.41 - 1.9	---	D792
Water Absorption (% weight increase)	0.45 - 1.25	after 24 hours	D570

1.8 Electrically conductive polyimides

After having discussed other engineering polymers in section 1.7, it is now evident that polyimide could withstand high processing temperatures required during the fabrication of low-cost steel mounted dye-sensitized solar cells. However, this protective layer of polyimide should be electrically conductive in nature to facilitate the electron transfer process from the mesoporous TiO_2 to the underlying metal substrate. Therefore, in this section different methods of development of conductive polyimides have been discussed briefly.

Electrically conductive polyimides find applications in electronics due to their excellent thermal and mechanical properties^[93]. Being an insulator polyimide does not conduct electricity. However, it is possible to develop electrically conductive polyimides via different synthetic approaches. One such approach involves addition of electrically conductive fillers into the polymer matrix followed by homogeneous mixing of the constituents. In this manner, various conductive particles such as metals (e.g. silver) and ceramics (e.g. carbon) can be blended with the polymer in order to develop an electrically conductive formulation.

Silver added polyimide pastes are mainly used to form electrical contacts in circuit boards. This type of metal filled polyimide demonstrates very low volume resistivity ($1 \times 10^{-4} \Omega\text{-cm}$) due to high concentration of filler materials ($>81 \text{ wt\% Ag}$)^[94]. Silver ion based metallised polyimide film can also demonstrate significantly low sheet resistance of $0.09 \Omega/\square$, which is due to the formation of silver nanoparticles within the polymer matrix followed by the reduction of the Ag-ions^[95].

On the other hand, carbon added polyimides are also very popular for other electronic applications including conductive inks and anti-static coatings. For instance, graphite/carbon black added polyimide based conductive inks could demonstrate sheet resistance from $130 - 2000 \Omega/\square$ when the amount of fillers was adjusted between 15-85 weight% for carbon black and 85 - 15 weight % for graphite^[96]. In addition, carbon nanotube blended polyimide films for anti-static application demonstrate sheet resistance values ranging from $50 - 1 \times 10^{15} \Omega/\square$ ^[97]. Another anti-static coating with 16.7 wt% carbon nanofiber dispersed in a polyimide matrix exhibits a sheet resistance of around $70 \Omega/\square$ ^[98].

Solution blending of polyamic acid (PI precursor) with an electrically conductive polymer such as polyaniline also results in a conductive polymer blend with volume resistivity in the order of $10^2 - 10^3 \Omega\text{-cm}$ ^[99].

Thus, it can be seen in this case that only metal powder pigmented polyimide films demonstrate sufficiently low resistance values for application into DSC. However, the metallic fillers present in this type of coating could eventually be exposed to the corrosive DSC electrolyte. This can substantially degrade both the electrical and physical properties of metal-powder loaded PI coatings. Therefore, chemically inert fillers such as carbon could be used for DSC application despite the high sheet resistance values of the reported PI based coatings compared to the typical FTO coated ($7-15 \Omega/\square$) glass electrodes. However, it may be possible to obtain lower resistance values from the carbon/polyimide coatings through some modifications in the existing formulation techniques.

A more detailed description of potential fillers materials is given in section 1.9

1.8.1 Photovoltaic applications of polyimide

Different generations of photovoltaic cells use polyimides as an alternative to transparent conducting oxide (TCO) coated glass substrates to fabricate cheap and flexible solar cells. Polyimide films are being widely used in polycrystalline thin film solar cells where they act as low cost flexible substrates resulting in a huge amount of reduction in weight compared to the glass based cells. Use of polyimides in thin film solar cell technology offers a possibility of roll-to-roll production on a large scale. Polyimides are non-conducting in nature therefore it is necessary to have a very thin coating of indium tin-oxide (ITO) or Al doped zinc oxide (AZO) on them in order to achieve desired electrical conductivity for PV applications. On the other hand, surface metallised (coated with Ni/Pt and Mo respectively) polyimides can also be used for PV application as in case of dye-sensitised solar cells and amorphous Si-based cells ^[100, 103].

Flexible CIGS solar cells can be manufactured on thin polyimide sheets. An industrial version of polyimide named UPILEX-25S is normally kept at $\sim 480^{\circ}\text{C}$ to grow CIGS crystals via the molecular beam epitaxy or MBE method. This results in flexible CIGS devices with 15.7% photoconversion efficiency ^[101].

Another class of solar cells based on cadmium telluride/cadmium sulphide (CdTe/CdS) semiconductor materials also use polyimide films as an alternative to TCO coated glass substrates to develop flexible thin film solar cells. Introduction of polyimide substrates in thin film solar cells have reduced both the weight and thickness to a significant amount. Normally, a $5\mu\text{m}$ thin film of the semiconductor compound is deposited onto a $10\text{-}\mu\text{m}$ thin polyimide film to construct a flexible solar cell with photoconversion efficiency over 11% ^[102].

A recent study has reported the development of DSC counter electrodes by metalizing polyimide films with $10\text{-}\mu\text{m}$ thin nickel (Ni) layer followed by deposition of Pt-catalyst on the top. It is important to mention that chemical metallization process was followed in this experiment where NiCl_2 solution was reduced using NaBH_4 (sodium borohydride) in order to produce Ni-coated polyimide films. The photoconversion efficiency of such device was reported around 5.83% ^[103].

1.9 Fillers for conductive polyimide

It has already been mentioned in section 1.8 that electrically conductive polyimides for DSC application can be prepared by adding conductive fillers such as graphite, carbon black and carbon nanotubes. On the other hand, titanium nitride (TiN) can also act as potential filler for the preparation of conductive polyimide. These fillers are corrosion resistant and electrically conductive in nature thus could be used to formulate conductive PI-coatings with corrosion resistant properties to facilitate DSC manufacturing on low-cost steel substrates. Therefore, a brief description of the chosen fillers has been given in this section for better understanding of the subject.

1.9.1 Graphite

Graphite is one of the naturally occurring allotropes of carbon, which displays slightly opposite characteristics to that of diamond. Unlike diamond, graphite is sp^2 hybridised and all carbon atoms in graphite are bonded in such a way so that they form a sheet like hexagonal crystal system (Figure 1.12). All graphite sheets are stacked over each other giving rise to excellent lubrication property. In addition, graphite is an outstanding conductor of both heat and electricity. Delocalized electrons of π -molecular orbitals in graphite results in metal like electrical conductivity which can be as low as 3×10^4 S/cm and on the other hand thermal conductivity of graphite at room temperature was found to be around 2 W/cm/K ^[104].

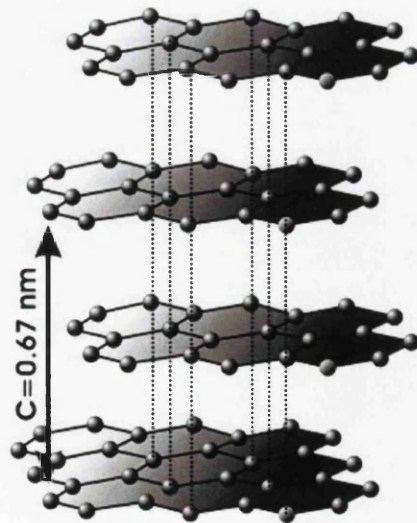


FIGURE 1.12: Crystal structure of graphite ^[105].

The versatile nature of graphite makes it an attractive candidate for various applications extending from automotive to electronics. Graphite based refractories are widely used in various industries as they are thermally stable up to 2000°C without any dimensional deformation and demonstrate excellent resistance against various chemical attacks.

The only shortcoming of graphite-based refractories is they can only be used in a reducing environment as they are highly sensitive to oxygen and oxidise easily at elevated temperatures ^[106]. Moreover, due to high electrical conductivity, graphite based electrodes are widely used in arc furnaces for steel making ^[107]. In addition, various graphite-based composites play a significant role in automotive as well as aerospace application, for instance, graphite-aluminium composites can remarkably reduce the weight of an internal combustion engine. Graphite fibre reinforced epoxy composites are well known for their application in automotive and aircraft components ^[108-109]. Graphite also finds application in photovoltaic cells where traditional silicon based solar cells are sometimes fabricated on silicon carbide (SiC) coated graphite substrates in order to facilitate high temperature deposition of crystalline silicon, which substantially improves both microstructural as well as photovoltaic properties of the crystalline silicon ^[110].

Due to catalytic nature, graphite based counter electrodes are sometimes used as a cheap alternative to platinum in dye-sensitized solar cells ^[111].

1.9.2 Carbon nanotubes

Nanotubes of carbon have tubular structure, which is responsible for their excellent electrical as well as mechanical properties. Carbon nanotubes (CNTs) were discovered in 1991. Due to extraordinary physical properties, CNTs have countless applications in numerous fields such as construction, aerospace, automotive, and electronics. A single walled carbon nanotube or SWCNT is considered as a “rolled up” graphene sheet; whereas a multi walled carbon nanotube (MWCNT) consists of several concentric tubes of graphene fitted one in the other ^[112].

Carbon nanotubes are normally synthesised at higher temperatures using two popular techniques known as arc discharge and laser ablation. However, at present CNTs are being synthesized using chemical vapour deposition (CVD) technique, at much lower temperature (<800°C) in presence of different catalysts such as Fe, Co, Mo,

Pd, Ni etc. In the CVD technique, CNTs can be grown in a controlled manner maintaining specific length, diameter and orientation [113].

Carbon nanotubes possess conjugated and highly anisotropic structure, which gives rise to excellent electrical properties and as a result, CNTs can be used in various electronic devices. The electrical resistivity of a single walled carbon nanotube was recorded around 10^{-6} Ω .cm under ballistic conduction (i.e. when the medium has negligible resistivity), whereas, resistivity of the MWCNT remains around 3×10^{-5} Ω .cm under the same conditions. Hence, CNTs are often considered as the best, in terms of their electrical conductivities compared to metals such as copper at room temperature. However, the presence of any defect in the CNT structure may significantly diminish their electrical conductivity [114].

Furthermore, carbon nanotubes are also catalytic in nature and hence could be used in dye-sensitized solar cells. CNT based counter electrodes are sometime preferred over expensive platinum catalyst as they demonstrate attractive photovoltaic performance which is nearly the same as the DSCs with platinum based counter electrodes. However, catalytic activity of CNTs greatly depends upon the technique used for counter electrode preparation [115].

1.9.3 Carbon black

Carbon black is a carbon rich (>99% carbon) filler material with outstanding electrical and thermal properties. Submicron carbon particles of 10 – 500 nm particle sizes are the key constituents of this material. However, trace amounts of hydrogen and oxygen could be present in the black due to carboxylic and hydroxyl surface functional groups [116, 117].

Gas phase pyrolysis of hydrocarbons is the most widely used technique for carbon black production through five major processes, namely lampblack process, channel process, acetylene process, thermal process and oil furnace process. However, most commercially available carbon blacks are of the ‘furnace black’ grade (particle size 120 – 500 nm) obtained from the oil-furnace process [116, 117].

Carbon black is mainly used in rubber processing and tyre-manufacturing industries as addition of carbon black in the rubber matrix significantly enhances the tensile

strength and abrasion resistant properties of the resulting product. Carbon black is also used as a pigment in the paint industry and as a stabilizer for many plastic materials. In addition, due to the excellent electrical conductivity, carbon black is also used in manufacturing low cost conductive inks for various electronic applications [117, 118].

1.9.4 Application of carbon materials in dye-sensitized solar cells

In the current scenario, carbon materials such as graphite and carbon nanotubes find their application in some electrical and optoelectronic devices due to their attractive physical and electrical properties. One such application involves incorporation of carbon materials in the counter electrode of a dye-sensitized solar cell as an alternative to the expensive platinum. Similar to the platinum catalyst, carbon also helps accelerate the tri-iodide reduction process at the CE of a device due its catalytic nature. Therefore, carbon materials are not usually preferred as a DSC working electrode as they may catalyse charge recombination (section 1.4.1.2) within the cell. The catalytic activity of carbon depends on the surface functional groups (Figure 1.13) which act as active sites for the catalysis [119].

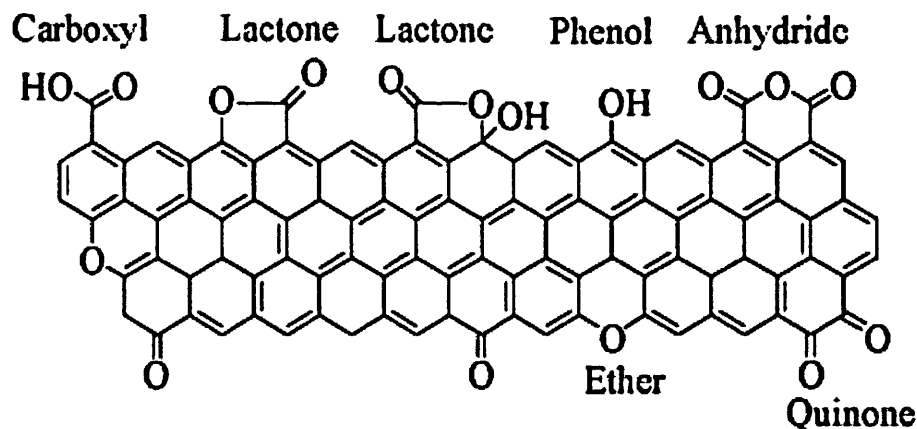


FIGURE 1.13: Various functional groups on carbon surface [121].

These groups or active sites are normally located at the crystal edges of a defect free crystal, which leads to an increase in the catalytic activity of such materials depending on the number of available reactive sites [120]. Therefore, instead of working electrodes, graphite and carbon nanotubes are preferably used as catalysts in the counter electrode of a device. A typical DSC counter electrode is made of an

FTO glass sheet as a conductive substrate and a catalyst (normally Pt) coated onto it. A study carried out by Sun *et al.* demonstrated that a composite made of Polyaniline (PANI) and flexible graphite (FG) can be used as a platinum and FTO free substrate material for DSC application with a photoconversion efficiency of 7.36% [122]. In addition, DSCs with solid polymer electrolyte can also be fabricated in the same manner; however, the composite counter electrode in this case was made of poly (3, 4-ethylene dioxythiophene) (PEDOT) and exfoliated graphite (EFG) that can act as both the catalyst and the conducting substrate material. The photoconversion efficiency obtained in this case was ~ 5.78% [123].

On the other hand, carbon nanotube based catalyst can also provide high efficiency devices. For instance, a composite film containing PEDOT: PSS (polystyrenesulfonate)/carbon nanotube demonstrated over 6% photoconversion efficiency. The composite film in this case was spin-coated onto an FTO glass substrate for optimised performance [124]. CNTs can be deposited directly onto the FTO glass substrate using CVD technique. It has been reported that, vertically aligned (CVD grown) CNTs onto an FTO glass substrate may perform even better than the traditional Pt- catalyst as the DSCs obtained in this case exhibited over 10% photoconversion efficiency [125]. In addition, spray coated carbon nanotubes on FTO glass can also serve as an efficient catalyst for DSC application giving cells over 7% efficiency. However, the photoconversion efficiency obtained in this case was highly dependent on the thickness of the catalyst layer [126].

1.9.5 Titanium nitride (TiN)

Titanium nitride is an extremely hard and abrasion resistant ceramic material, which can withstand high temperature up to 2930°C. Due to high hardness and abrasion resistance properties, TiN is widely used to coat various substrates such as, steels, aluminium, titanium and carbides. In addition, TiN is electrically conductive with electrical resistivity of $1.3 \times 10^{-6} \Omega.m$. Therefore, TiN is being largely used in microelectronics as a conducting diffusive barrier between the active device and the metal contacts [127]. TiN is also available as a powder and will be discussed in this context as a potential pigment for polyimide. This is because the industrial sponsor of this research was specifically interested in exploring TiN based organic coatings and their suitability for DSC applications.

1.9.6 Synthesis of TiN

Nitration of the titanium metal or the TiO_2 in a nitrogen rich environment produces TiN. Various synthetic routes such as electrochemical synthesis ^[128], 2 stage aerosol synthesis ^[129], thermal plasma reactor synthesis ^[130], and carbothermal reduction synthesis ^[131], have been employed to synthesise TiN.

In the electrochemical synthesis process, the titanium metal electrodes were electrochemically oxidised in presence of potassium amide in liquid ammonia to deposit TiN nanoparticles onto the electrode surface ^[128]. Whereas, in a two-stage aerosol process, titanium and titania (TiO_2) particle containing aerosols were prepared in the aqueous as well as in the methanol solutions followed by their pyrolysis at 1000 – 1200°C in ammonia environment to obtain TiN nanoparticles of 30 - 38 nm size ^[129].

An ore of titanium, known as ilmenite (FeTiO_3) was used in synthesis of TiN. Methane and ammonia gases were used to create the reactive atmosphere within the reactor ^[130].

In the carbothermal reduction process, carbon acts as a reducing agent for the TiO_2 in presence of nitrogen to yield TiN. However, high reaction temperature (~ 1000°C) is required for this reaction to take place ^[131].

1.9.7 Properties of TiN

Mechanical, electrical and thermal properties of TiN are given below in Table 1.4. It is evident from the table that TiN is highly conductive in nature. Due to low electrical resistivity value, TiN could be an ideal filler material for PI based conductive coatings for DSC application. In addition, Knoop hardness data show that TiN is a hard material, which can improve scratch resistance behaviour of the TiN /PI composite coatings. TiN is a good conductor of heat that may help in the curing process of the composite coating.

TABLE 1.4: Properties of TiN ^[132].

Property	Value	Conditions	References
Compressive strength	0.9724 GPa	Ceramic	CRC Materials Science and Engineering Handbook, p.419
Density	5.43 kg/m ³	Ceramic	CRC Materials Science and Engineering Handbook, p.50-52
Electrical resistivity	1.3 x 10 ⁻⁶ Ω.m	Ceramic, at room temperature	CRC Materials Science and Engineering Handbook, p.565
Electrical resistivity	3.4 x 10 ⁻⁶ Ω.m	Ceramic, at melting temperature	CRC Materials Science and Engineering Handbook, p.565
Electrical resistivity	81300 Ω.m	Ceramic, at liquid air temperature	CRC Materials Science and Engineering Handbook, p.565
Hardness, Knoop(KH)	2160 kg/mm/mm	30g, Ceramic	CRC Materials Science and Engineering Handbook, p.472
Hardness, Knoop(KH)	1770 kg/mm/mm	100g, Ceramic	CRC Materials Science and Engineering Handbook, p.472
Modulus of Rupture	4930 GPa	Ceramic	CRC Materials Science and Engineering Handbook, p.534
Thermal conductivity	28.84 W/m-K	Ceramic, at 25°C.	CRC Materials Science and Engineering Handbook, p.281
Young's Modulus	250.37 GPa	Ceramic	CRC Materials Science and Engineering Handbook, p.509

1.9.8 Application of TiN in dye-sensitized solar cells

Titanium nitride is an electrically conductive material that displays some catalytic behaviour. It has been found that the catalytic activity of TiN is inversely proportional with the particle size. This means nano-TiN is more catalytic whereas micron sized TiN or bigger particles are non-catalytic in nature. This is due to the higher surface area of nano-sized TiN particles than their micron-sized counterparts ^[133]. It is needless to mention that the electrical conductivity of TiN remains unaffected in this case. Thus considering the aims of this research project, it is possible to use micron-sized TiN powder as novel filler in a polyimide based high-temperature resistant conductive coating. This type of coating is specially proposed for WE application therefore presence of non-catalytic micron sized TiN will not

cause charge recombination in the manufactured cells (recombination related issues have already been discussed in sections 1.4.1.2 and 1.9.2). In addition, both the TiN and the PI are chemically inert materials [84, 134]. Thus; the composite coating could protect the low-cost steel substrate from the corrosive electrolyte whilst serving as a working electrode material in a metal mounted DSC. This is a novel approach, which for the first time combines the electrical properties of TiN with the outstanding physical properties of PI in the form of a composite coating for DSC application. The composite coating prepared in such a way will be lower in cost and easy to apply.

Following examples contain current trends in DSC research particularly focused on the TiN based components.

At present there has been only one report of the use of TiN coated working electrodes (TCO-less glass in this case) for DSC fabrication. A radio frequency magnetron sputtering technique was used to produce thin TiN layers of thickness ~ 66 to 167 nm onto the non-conducting glass (NCG) substrates. The electrical sheet resistance of the TiN coated glass electrodes was found to increase with the thickness of the coating (around $4.4 \Omega / \square$ for a 167 nm thick coating). Consequently, the efficiency of the fabricated devices varied with the TiN coating thickness. It has been found that a DSC fabricated on a 136 nm thick TiN coating was the most efficient one with a photoconversion efficiency of 7.4% whereas, the others with 66 and 86 nm thick TiN coatings gave 3.3 and 6.8% cells respectively [135]. It is noteworthy in this case, that sputtered thin films of TiN were non-catalytic as in general films display relatively lower surface area than the nanosized particles [136, 137].

There is a great deal of information available on nano-TiN based counter electrodes as nano-TiN can be used as a catalyst, alternative to the expensive platinum. Due to high surface area, nano-TiN helps accelerate charge transfer process at the CE of a device followed by an increase in the photovoltaic performance.

Highly ordered TiN nanotubes grown on a Ti foil performs almost identical to the Pt deposited FTO glass based counter electrodes. Highly ordered TiN nanotubes were obtained by nitridation of electrodeposited TiO₂ nanotubes on Ti foil at 800°C in presence of ammonia. The photoconversion efficiency in this case was recorded

around 7.73%, which was slightly higher than 7.45% as displayed by a device with typical Pt-deposited FTO counter electrode [138].

In a similar study, Li *et al.* demonstrated that a mixture of nano-TiN and conductive carbon black can lead to even higher efficiency devices. In this study, an ethanol based paste containing TiO₂/carbon black was first doctor bladed onto a Ti foil followed by its nitridation at around 800°C in ammonia atmosphere. In this manner, a Ti foil based counter electrode was obtained containing the nano-TiN/carbon black film. Dye-sensitised solar cells fabricated using such a counter electrode demonstrated over 7.9% photoconversion efficiencies [139].

Titanium nitride can also serve as an excellent counter electrode material when it is blended with other electrically conductive materials such as PEDOT: PSS and carbon nanotubes. TiN nanoparticles ranging from 10 -50 nm were mechanically blended with poly (3, 4-ethylene-dioxythiophene) PEDOT: PSS, an electrically conducting polymer to obtain a composite film of both. This composite film was then applied onto the FTO substrate using doctor blade technique followed by DSC construction. The device with TiN / PEDOT: PSS counter electrode performed better than the FTO/Pt one with efficiency 7.06% higher than the 6.57% of FTO/Pt device [140].

On the other hand, DSC with nano-TiN / carbon nanotubes based counter electrode display slightly lower photo conversion efficiency than the ideal FTO/Pt based DSC. Only 10 wt% addition of nano-TiN within the carbon nanotube matrix leads to 5.46% photo conversion efficiency whereas the efficiency of FTO/Pt based DSC was found around 5.68%, which was slightly higher than the TiN/CNT based DSC. However, the V_{oc} of TiN/CNT device was higher than the FTO/Pt one [141].

Furthermore, TiN finds application in other DSC components such as, in I⁻/I₃⁻ electrolyte and TiO₂ photoanode. It has been found in a study that, when TiN and its thermally treated version (TiN heated at 500°C for 30 minutes) was added into a quasi-solid gel electrolyte made up of poly (vinylidene fluoride-co - hexafluoropropylene) PVDF-HFP, then the efficiency of the DSC was found to be increased from 4.15% to 5.33 %. The efficiency enhancement of the DSC was due to the partial conversion of the TiN into the TiO₂, which had been confirmed by the XRD [142].

Not only in the electrolyte but TiN can also be used in TiO₂ photoanode in order to improve DSC efficiency. Addition of 0.125% thermally treated TiN into 5.5 μm

thick TiO₂ film can improve the efficiency of a DSC from 2.38% to 3.40%. The efficiency of the DSC continued to increase up to 1% addition of TiN in the TiO₂ photoanode, which resulted in an increase in efficiency from 3.40% to 3.77%. The increase in DSC efficiency was due the higher electron conductivity and longer electron lifetime in the TiO₂ photoanode, which was due to the addition of TiN [143].

1.10 Characterization of conductive coatings

1.10.1 Electrical resistivity measurement

The electrical sheet resistance (R_s) values of the developed coatings were measured using a four point-probe technique (Figure 1.14). In this method, current is passed through the coating using the outer points of the probe and the voltage is measured across the coating using two inner points of the probe. Ideally, the points are equidistant from each other with a spacing of 1 mm.

Measurement of R_s using the four-point probe technique depends upon the coating thickness and a correction factor related to the sample geometry. Two conditions have to be fulfilled in order to obtain the sheet resistance values of the conductive coatings. The first condition is, the coating thickness should be less than 40% of the point spacing (e.g. a four point probe with 1 mm probe spacing can only measure R_s of a coating thinner than 400 μm), otherwise it will not be considered as a thin film. The second condition is that the edges of the coatings should locate at least 4 times the point spacing from the measurement area, which means the probing area should be 4 mm (in case of 1 mm point spacing) away from each side of the sample. This avoids consideration of the correction factor whilst calculating the sheet resistance of the coatings [144]. Thus, sheet resistance (R_s) of a coating is given by [144]:

$$R_s = 4.53 \times V/I \Omega/\square \quad [1.6]$$

The sheet resistance values are often expressed in 'Ohm'/'square' or simply (Ω/\square). The term ohm/square is equivalent to the resistance between two electrodes placed on the opposite sides of a theoretically assumed square.

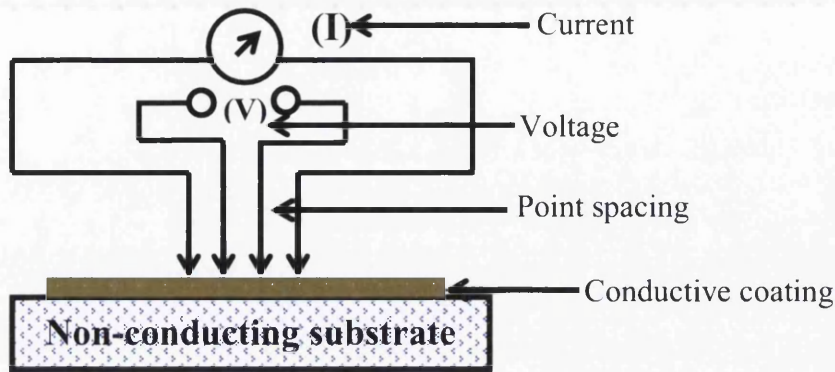


FIGURE 1.14: Schematic representation of four-point probe measurement technique.

Volume resistivity or simply resistivity of a coating can also be calculated from its sheet resistance value if the thickness of the coating is already known ^[144]. Hence, the equation for resistivity calculation is given by:

$$\text{Volume resistivity } (R_p) = R_s \times t \text{ } \Omega\text{-cm} \quad (t = \text{thickness of the coating}) \quad [1.7]$$

It is noteworthy in this case that the four-point probe technique is unable to provide R_s values for the coatings (conductive) prepared on an already electrically conducting substrate. In such a case instead of sheet resistance, Z-axis conductivity is obtained due to the conducting nature of the underlying substrate material.

1.10.2 Thermogravimetric analysis (TGA)

Thermogravimetric analysis or TGA is a quantitative technique where change in mass of a substance is recorded as a function of temperature. In isothermal TGA, change in mass of a substance is recorded as a function of time ^[145]. TGA provides an idea about the thermal stability of materials. A typical TGA plot consists of % weight loss vs. temperature, which can be used to determine the thermal characteristics of a material.

1.10.3 Reflectance measurement using UV-VIS spectrometer

Light reflectance property of a coated working electrode can be recorded using a UV-Vis spectrophotometer. As in some cases the photoconversion efficiency of a DSC could depend upon reflectivity of the working electrode, therefore determination of substrate reflectance was an essential part of this research. It has been reported in literatures that DSCs based on highly reflective working electrodes demonstrated higher photoconversion efficiency. This is because more light is absorbed by the photosensitive dye due to highly reflective working electrode surface ^[146].

1.10.4 Scanning electron microscopy (SEM)

Scanning electron microscopy was used in this research to determine surface morphology of the developed coatings. A standard SEM operates between 1-30 KV, which provides image resolution down to ~ 1 nm. In this research, a scanning electron microscope with resolution 1.5 nm was used to study the distribution of conductive fillers in the polymer matrix. Furthermore, characteristics of heat-treated coatings were also studied using this method to ensure whether any visible polymer degradation occurred during the high temperature heat-treatment ^[147, 148].

1.10.5 Stylus Profilometry

Stylus profilometry is a 'contact' type technique, which uses a probe (stylus) which scans across the surface to measure the height variation as a function of distance. The technique was used to study the surface topography of the developed coatings ^[149]. Surface properties such as, average roughness (R_a), average peak height (R_p) and the thickness of a coating can be determined using this technique.

1.10.6 X-ray photoelectron spectroscopy (XPS)

X-ray photoelectron spectroscopy (XPS) is a most widely used quantitative method for studying chemical compositions of various surfaces. This technique is also known as electron spectroscopy for chemical analysis or ESCA, which is entirely based on the principles of photoelectric effect. Prof. Kai Siegbahn (Nobel Prize 1981) from Uppsala University, Sweden has been given the credit for the development of this technique in the 1960's ^[150, 151].

The spectral lines in XPS are obtained when electrons within an atom are ejected from their respective orbitals (1s, 2s, 2p etc.) by the incident radiation. Most elements in XPS are identified by determining their corresponding binding energies (BE) in electron volts (eV). The BE is calculated by measuring the energy of the photoexcited electrons ejected from the first shell, which contains discrete chemical information regarding individual elements present in the test sample. Thus, the binding energy or BE is expressed through the following equation ^[151, 152]:

$$BE = h\nu - KE - \phi$$

Where, h = Plank's constant, ν = frequency,
 KE = kinetic energy and ϕ = work function

In an ideal XPS spectra, BE is plotted against the intensity of the radiation which gives information about elements present on the surface, chemical environments on the surface, oxidation states of transition metals and the valence band electronic structure of the elements ^[150]. Figure 1.15 shows a simplified diagram of an XPS instrument.

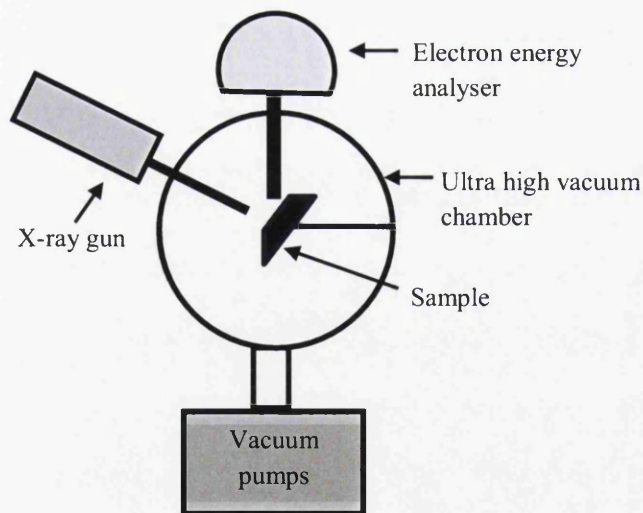


FIGURE 1.15: Simplified diagram of the X-ray photoelectron spectrophotometer ^[150].

1.11 Aims and objectives

In the beginning of this research, a thorough assessment of different characterization techniques will be carried out to study the photovoltaic performance of typical dye-sensitized solar cells. These results are key, as they will be used as a benchmark in subsequent studies to compare the PV performance of novel coating based devices with the standard glass mounted cells.

Novel coatings for DSC application will be formulated in the next stage of this research using a polyimide matrix and electrically conductive fillers such as carbon and titanium nitride. Thus, three sets of conductive coatings are presented, carbon/polyimide, TiN/polyimide and C-TiN/polyimide. Electrical, optical, thermal and surface properties of each formulation will be studied precisely at this point to identify an optimum composition from each set. The optimum composition for DSC application will have a relatively smooth surface with lower sheet resistance (equivalent to the TCO coated glass, 7- 15 Ω/\square). In addition, assessment of high temperature stability (up to 450°C) of this composition will also be an essential task at this stage.

The third phase of this research will involve photovoltaic characterization of devices fabricated using the coatings described above. Results obtained from the PV characterization will be analysed rigorously and compared with the typical glass mounted reverse illuminated devices. In addition, data obtained from the PV characterization will also help identify the best performing coatings for use in ECCS mounted devices that can further be compared with Ti-metal and uncoated-ECCS based cells.

Finally, in order to determine the charge transfer characteristics of coated ECCS substrates as counter electrodes, glass mounted forward illuminated hybrid devices will be constructed using platinised CEs based on coated ECCS. PV performance demonstrated by such devices will be compared with the DSCs made of typical glass counter electrodes. Furthermore, developed coatings can also act as an alternative to the TCO coated glass. Despite the opacity, such coatings can still be used on non-conductive glass (NCG) to manufacture dye-sensitized solar cells. Thus, in the final stage of this research PV performance of DSCs with coated NCG electrodes (for

both WE and CE applications) will be determined and compared with the standard cells.

1.12 References

- [1] B. O'Regan and M. Grätzel, "A low-cost, high-efficiency solar-cell based on dye-sensitized colloidal TiO₂ films", *Nature*, vol. 353, pp. 737-740, 1991.
- [2] M. Grätzel, "Dye-sensitized solar cells", *Journal of Photochemistry and Photobiology C-Photochemistry Reviews*, vol. 4, pp. 145-153, 2003.
- [3] C. J. Barbe, F. Arendse, P. Comte, M. Jirousek, F. Lenzmann, V. Shklover, M. Grätzel, "Nanocrystalline titanium oxide electrodes for photovoltaic applications", *Journal of the American Ceramic Society*, vol. 80, pp. 3157-3171, 1997.
- [4] F. Kong, S. Yuan Dai, and K. J. Wang, "Review of recent progress in dye-sensitized solar cells," *Advances in Optoelectronics*, vol. 2007, pp. 1-13, 2007.
- [5] K. Miettunen, X. Ruan, T. Saukkonen, J. Halme, M. Toivola, G. Huang, P. Lund, "Stability of dye solar cells with photoelectrode on metal substrates", *Journal of the Electrochemical Society*, vol. 157, pp. B814-B819, 2010.
- [6] T. M. Watson, I. Mabbett, and D. A. Worsley, "Ultrafast TiO₂ sintering of metal mounted dye-sensitized solar cells", *Photovoltaics for the 21st Century 6, ECS transactions*, vol. 33, pp. 151-158, 2011.
- [7] T. Watson, G. Reynolds, D. Wragg, G. Williams, D. Worsley, "Corrosion monitoring of flexible metallic substrates for dye-sensitized solar cells", *Int. J. Photoenergy*, pp 1-8 ,2013.
- [8] S. Ito, N.-L.C. Ha, G. Rothenberger, P. Liska, P. Comte, S. M. Zakeeruddin, P Péchy, M. K. Nazeeruddin and M. Grätzel, "High-efficiency (7.2%) flexible dye-sensitized solar cells with Ti-metal substrate for nanocrystalline-TiO₂ photoanode", *Chemical Communications*, pp. 4004-4006, 2006.
- [9] G24innovations: <http://www.g24i.com/pages,technology,73.html>
- [10] G. J. Reynolds, T. M. Watson, G. Williams, and D. A. Worsley, "Corrosion resistance of metallic substrates for the fabrication dye-sensitized solar cells", *Photovoltaics for the 21st Century 6, ECS transactions*, vol. 33, pp. 129-138, 2011.
- [11] <http://telstar.ote.cmu.edu/environ/m3/s2/02sun.shtml>
- [12] <http://www.helpsavetheclimate.com/solar.html>
- [13] http://www.eia.gov/kids/energy.cfm?page=solar_home-basics-k.cfm
- [14] http://www.nrel.gov/education/pdfs/educational_resources/high_school/solar_cell_history.pdf
- [15] Meng Tao, "Inorganic photovoltaic solar cells: silicon and beyond", http://www.electrochem.org/dl/interface/wtr/wtr08/wtr08_p30-35.pdf
- [16] University of Delaware, IEC history, <http://www.udel.edu/iec/history.html>
- [17] P. Jackson, D. Hariskos, E. Lotter, S. Paetel, R. Wuerz, R. Menner, W. Wischmann and M. Powalla., "New world record efficiency for Cu(In,Ga)Se-2 thin-film solar cells beyond 20%", *Progress in Photovoltaics*, vol. 19, pp. 894-897, 2011.

- [18] J. F. Geisz, M. A. Steiner, I. Garcia, S. R. Kurtz, and D. J. Friedman, "Enhanced external radiative efficiency for 20.8% efficient single-junction GaInP solar cells", *Applied Physics Letters*, vol. 103, 2013.
- [19] M. A. Green, K. Emery, Y. Hishikawa, W. Warta, and E. D. Dunlop, "Solar cell efficiency tables (version 43)", *Progress in Photovoltaics*, vol. 22, pp. 1-9, 2014.
- [20] T. L. Benanti and D. Venkataraman, "Organic solar cells: An overview focusing on active layer morphology", *Photosynthesis Research*, vol. 87, pp. 73-81, 2006.
- [21] H. Spanggaard and F. C. Krebs, "A brief history of the development of organic and polymeric photovoltaics", *Solar Energy Materials and Solar Cells*, vol. 83, pp. 125-146, 2004.
- [22] A. Yella, H.W. Lee, H. N. Tsao, C. Yi, A. K. Chandiran, M. K. Nazeeruddin, E. W. Guang Diao, C.Y. Yeh, S. M. Zakeeruddin, M. Grätzel, "Porphyrin-sensitized solar cells with cobalt (II/III)-based redox electrolyte exceed 12 percent efficiency", *Science*, vol. 334, pp. 629-634, 2011.
- [23] Michael Grätzel interview, <http://www.youtube.com/watch?v=LYVwJyQBxcM>
- [24] T. Horiuchi, H. Miura, and S. Uchida, "Highly-efficient metal-free organic dyes for dye-sensitized solar cells", *Chemical Communications*, pp. 3036-3037, 2003.
- [25] How To Make a Solar Cell with Donuts and Tea,
<http://www.wired.com/wiredscience/2009/03/donutsolar/>
- [26] RashmiNanjundaswamy, Dye-sensitized solar cells,
http://www.nisenet.org/sites/default/files/catalog/uploads/5553/solarcell_facilitator_guide_0.pdf
- [27] A. F. Nogueira, C. Longo, and M. A. De Paoli, "Polymers in dye sensitized solar cells: overview and perspectives", *Coordination Chemistry Reviews*, vol. 248, pp. 1455-1468, 2004.
- [28] <http://www.photovoltaic-production.com/5318/ideal-match-for-bipv/>
- [29] http://www.pv-tech.org/news/tata_steel_dyesol_produce_worlds_largest_dye_sensitized_photovoltaic_module
- [30] http://www.sony.net/SonyInfo/csr/SonyEnvironment/technology/solar_cells.html
- [31] <http://www.samsungdi.com/nextenergy/dssc-solar-cell-battery.jsp>
- [32] http://www.merck-performance-materials.com/en/solar_and_energy/photovoltaics/dssc/dssc.html
- [33] <http://exeger.com/consumer-electronics>
- [34] Antonio Luque, Steven Hegedus, in *Handbook of Photovoltaic Science and Engineering*, John Wiley & Sons Ltd., 2003.
- [35] Khalil EbrahimJasim, *Dye Sensitized Solar Cells - Working Principles, Challenges and Opportunities*,
<http://www.intechopen.com/download/get/type/pdfs/id/23333>
- [36] S. A. Haque, E. Palomares, B. M. Cho, A. N. M. Green, N. Hirata, D. R. Klug, J. R. Durrant, "Charge separation versus recombination in dye-sensitized nanocrystalline solar cells: the minimization of kinetic redundancy", *Journal of the American Chemical Society*, vol. 127, pp. 3456-3462, 2005.

- [37] <http://pveducation.org/pvcdrom/pn-junction/bias-of-pn-junction>
- [38] G. K. Mor, K. Shankar, M. Paulose, O. K. Varghese, and C. A. Grimes, "Use of highly-ordered TiO₂ nanotube arrays in dye-sensitized solar cells", *Nano Letters*, vol. 6, pp. 215-218, 2006.
- [39] M. Wang, N. Chamberland, L. Breau, J.-E. Moser, R. Humphry-Baker, B. Marsan, S.M. Zakeeruddin, M. Grätzel, "An organic redox electrolyte to rival triiodide/iodide in dye-sensitized solar cells", *Nature Chemistry*, vol. 2, pp. 385-389, 2010.
- [40] J. U. Brehm, M. Winterer, and H. Hahn, "Synthesis and local structure of doped nanocrystalline zinc oxides", *Journal of Applied Physics*, vol. 100, 2006.
- [41] Arsenault E., Three-dimensional transparent conducting oxide based dye sensitized solar cells, Master of Science Thesis, University of Toronto, 2011, https://tspace.library.utoronto.ca/bitstream/1807/29468/4/Arsenault_Eric_20116_MSc_thesis.pdf
- [42] Suzuki A, Transparent Conductive ZnO Films: New light for Indium-free solar cells, Osaka Sangyo University, Japan, 2004.
- [43] E. Shanthi, V. Dutta, A. Banerjee, and K. L. Chopra, "Electrical and optical properties of undoped and antimony doped tin oxide films", *Journal of Applied Physics*, vol. 51, pp. 6243-6251, 1980.
- [44] C. Terrier, J. P. Chatelon, and J. A. Roger, "Electrical and optical properties of Sb:SnO₂ thin films obtained by the sol-gel method", *Thin Solid Films*, vol. 295, pp. 95-100, 1997.
- [45] K. S. Kim, S. Y. Yoon, W. J. Lee, and K. H. Kim, "Surface morphologies and electrical properties of antimony-doped tin oxide films deposited by plasma-enhanced chemical vapor deposition", *Surface & Coatings Technology*, vol. 138, pp. 229-236, 2001.
- [46] W.-H. Luo, T.-K. Tsai, J.-C. Yang, W.-M. Hsieh, C.-H. Hsu, and J.-S. Fang, "Enhancement in conductivity and transmittance of zinc oxide prepared by chemical bath deposition", *Journal of Electronic Materials*, vol. 38, pp. 2264-2269, 2009.
- [47] A. Klein, C. Koerber, A. Wachau, F. Saeuberlich, Y. Gassenbauer, R. Schafranek, S.P. Harveyb, T.O. Mason, "Surface potentials of magnetron sputtered transparent conducting oxides", *Thin Solid Films*, vol. 518, pp. 1197-1203, 2009.
- [48] Solaronix SA, Switzerland, TCO22-15 Glass, <http://www.solaronix.com/products/tcolayers/tco2215/>
- [49] Titanium, <http://www.makermends.com/metals.html>
- [50] M. Toivola, J. Halme, K. Miettunen, K. Aitola, and P. D. Lund, "Nanostructured dye solar cells on flexible substrates-review", *International Journal of Energy Research*, vol. 33, pp. 1145-1160, 2009.
- [51] Titanium metal, <http://www.squireswatches.com/Question%20in%20Time/TITANIUM.htm>
- [52] Bruce Phillip, "Investigation of Metal Substrates for Photovoltaic Applications", EngD thesis, Swansea University, UK, 2010.
- [53] K. Miettunen, J. Halme, M. Toivola, and P. Lund, "Initial performance of dye solar cells on stainless steel substrates", *Journal of Physical Chemistry C*, vol. 112, pp. 4011-4017, 2008.

- [54] A. F. Kanta and A. Decroly, "An investigation of the electrolytic solution effects on stainless steel electrode for dye-sensitized solar cells", *Materials Chemistry and Physics*, vol. 130, pp. 843-846, 2011.
- [55] J. J. Lee, Md. M. Rahman, S. Sarker, N.C. Deb Nath, A.J. Saleh Ahammad and J. K. Lee, "Metal oxides and their composites for the photoelectrode of dye sensitized solar cells", Konkuk University, Korea, <http://www.intechopen.com/books/advances-in-composite-materials-for-medicine-and-nanotechnology/metal-oxides-and-their-composites-for-the-photoelectrode-of-dye-sensitized-solar-cells>
- [56] T. Watson, C. Charbonneau, D. Bryant, and D. Worsley, "Acid treatment of titania pastes to create scattering layers in dye-sensitized solar cells", *International Journal of Photoenergy*, 2012.
- [57] J. M. Cole, "A new form of analytical chemistry: distinguishing the molecular structure of photo-induced states from ground-states", *Analyst*, vol. 136, pp. 448-455, 2011.
- [58] R. Argazzi, C. A. Bignozzi, T. A. Heimer, F. N. Castellano, and G. J. Meyer, "Enhanced spectral sensitivity from ruthenium(II) polypyridyl based photovoltaic Devices", *Inorganic Chemistry*, vol. 33, pp. 5741-5749, 1994.
- [59] K. S. Finnie, J. R. Bartlett, and J. L. Woolfrey, "Vibrational spectroscopic study of the coordination of (2,2'-bipyridyl-4,4'-dicarboxylic acid)ruthenium(II) complexes to the surface of nanocrystalline titania", *Langmuir*, vol. 14, pp. 2744-2749, 1998.
- [60] M. K. Nazeeruddin, M. Amirasr, P. Comte, J. R. Mackay, A. J. McQuillan, R. Houriet, M. Grätzel, "Adsorption studies of counterions carried by the sensitizer cis-dithiocyanato (2,2'-bipyridyl-4,4'-dicarboxylate) ruthenium(II) on nanocrystalline TiO₂ films", *Langmuir*, vol. 16, pp. 8525-8528, 2000.
- [61] K. Murakoshi, G. Kano, Y. Wada, S. Yanagida, H. Miyazaki, M. Matsumoto, Sadao Murasawa, "Importance of binding states between photosensitizing molecules and the TiO₂ surface for efficiency in a dye-sensitized solar-cell", *Journal of Electroanalytical Chemistry*, vol. 396, pp. 27-34, 1995.
- [62] K. Sayama, H. Sugihara, and H. Arakawa, "Photoelectrochemical properties of a porous Nb₂O₅ electrode sensitized by a ruthenium dye", *Chemistry of Materials*, vol. 10, pp. 3825-3832, 1998.
- [63] D. Cahen, G. Hodes, M. Grätzel, J. F. Guillemoles, and I. Riess, "Nature of photovoltaic action in dye-sensitized solar cells", *Journal of Physical Chemistry B*, vol. 104, pp. 2053-2059, 2000.
- [64] Y. Liu, A. Hagfeldt, X. R. Xiao, and S. E. Lindquist, "Investigation of influence of redox species on the interfacial energetics of a dye-sensitized nanoporous TiO₂ solar cell", *Solar Energy Materials and Solar Cells*, vol. 55, pp. 267-281, 1998.
- [65] K. Hara, T. Horiguchi, T. Kinoshita, K. Sayama, and H. Arakawa, "Influence of electrolytes on the photovoltaic performance of organic dye-sensitized nanocrystalline TiO₂ solar cells", *Solar Energy Materials and Solar Cells*, vol. 70, pp. 151-161, 2001.
- [66] Chmiel, G, Dye sensitized solar cells (DSC): Progress towards application, 2nd World Conference and Exhibition on Photovoltaic Solar Energy Conversion, 6-10 July, Vienna Austria, 1998.

- [67] A. Hagfeldt, B. Didriksson, T. Palmqvist, H. Lindstrom, S. Sodergren, H. Rensmo, Sten-Eric Lindquist, "Verification of high efficiencies for the Grätzel-cell - a 7% efficient solar cell based on dye-sensitized colloidal TiO₂ films", *Solar Energy Materials and Solar Cells*, vol. 31, pp. 481-488, 1994.
- [68] M. K. Nazeeruddin, A. Kay, I. Rodicio, R. Humphrybaker, E. Muller, P. Liska, N. Vlachopoulos, M. Grätzel, "Conversion of light to electricity by cis-X₂bis(2,2'-bipyridyl-4,4'-dicarboxylate)ruthenium(II) charge-transfer sensitizers (X = Cl-, Br-, I-, CN-, And SCN-) on nanocrystalline TiO₂ electrodes", *Journal of the American Chemical Society*, vol. 115, pp. 6382-6390, 1993.
- [69] S. H. Kim and C. W. Park, "Novel application of platinum ink for counter electrode preparation in dye sensitized solar cells", *Bulletin of the Korean Chemical Society*, vol. 34, pp. 831-836, 2013.
- [70] N. Papageorgiou, W. F. Maier, and M. Grätzel, "An iodine/triiodide reduction electrocatalyst for aqueous and organic media", *Journal of the Electrochemical Society*, vol. 144, pp. 876-884, 1997.
- [71] E. Olsen, G. Hagen, and S. E. Lindquist, "Dissolution of platinum in methoxypropionitrile containing LiI/I²⁻", *Solar Energy Materials and Solar Cells*, vol. 63, pp. 267-273, 2000.
- [72] Janne Halme, Dye-sensitized nanostructured and organic photovoltaic cells: technical review and preliminary tests, Department of Engineering Physics and Mathematics, Helsinki University of technology, Finland 2002.
- [73] M. Wu, X. Lin, A. Hagfeldt, and T. Ma, "Low-cost molybdenum carbide and tungsten carbide counter electrodes for dye-sensitized solar cells", *Angewandte Chemie-International Edition*, vol. 50, pp. 3520-3524, 2011.
- [74] A. Kay and M. Grätzel, "Low cost photovoltaic modules based on dye sensitized nanocrystalline titanium dioxide and carbon powder", *Solar Energy Materials and Solar Cells*, vol. 44, pp. 99-117, 1996.
- [75] W. J. Lee, E. Ramasamy, D. Y. Lee, and J. S. Song, "Efficient dye-sensitized cells with catalytic multiwall carbon nanotube counter electrodes", *ACS Applied Materials & Interfaces*, vol. 1, pp. 1145-1149, 2009.
- [76] O. Kohle, M. Grätzel, A. F. Meyer, and T. B. Meyer, "The photovoltaic stability of bis(isothiocyanato)ruthenium(II)-bis-2,2'-bipyridine-4,4'-dicarboxylic acid and related sensitizers", *Advanced Materials*, vol. 9, pp. 904-&, 1997.
- [77] J. Kruger, R. Plass, L. Cevey, M. Piccirelli, M. Grätzel, and U. Bach, "High efficiency solid-state photovoltaic device due to inhibition of interface charge recombination", *Applied Physics Letters*, vol. 79, pp. 2085-2087, 2001.
- [78] Photovoltaic cell I-V characterization theory, National Instruments, <http://www.ni.com/white-paper/7230/en/>
- [79] Tannia Marinado, Photoelectrochemical studies of dye-sensitized solar cells using organic dyes, Doctoral Thesis, School of Chemical Science and Engineering, Kungliga Tekniska Högskolan, Stockholm, 2009.
- [80] Solar cell parameters, <http://pveducation.org/pvcdrom/design/solar-cell-parameters>

- [81] P. R. F. Barnes, K. Miettunen, X. Li, A. Y. Anderson, T. Bessho, M. Grätzel, Brian C. O'Regan, "Interpretation of optoelectronic transient and charge extraction measurements in dye-sensitized solar cells", *Advanced Materials*, vol. 25, pp. 1881-1922, 2013.
- [82] Application note, Basics of electrochemical impedance spectroscopy, Gamry instruments, <http://www.gamry.com/assets/Application-Notes/Basics-of-EIS.pdf>
- [83] Q. Wang, J. E. Moser, and M. Grätzel, "Electrochemical impedance spectroscopic analysis of dye-sensitized solar cells", *Journal of Physical Chemistry B*, vol. 109, pp. 14945-14953, 2005.
- [84] Ensinger, <http://www.ensinger-online.com/en/materials/high-temperature-plastics/polyarylsulfones-psu-ppsu/>
- [85] Jeffrey D. Zahn, *Methods in bioengineering: biomicrofabrication and biomicrofluidics*, Artech House, 2009.
- [86] R. Caballero, C. A. Kaufmann, T. Eisenbarth, T. Unold, S. Schorr, R. Hesse, R. Klenk, H. W. Schock, "The effect of NaF precursors on low temperature growth of CIGS thin film solar cells on polyimide substrates", *Physica Status Solidi a-Applications and Materials Science*, vol. 206, pp. 1049-1053, 2009.
- [87] K. L. Mittal, *Polyimides and Other High-temperature Polymers: Synthesis, Characterization, and Applications*, BRILL NV, The Netherlands, Volume 5, 2009.
- [88] U.S. Department of Defence, *Composite Materials Hand Book, Polymer matrix composites: materials usage, design and analysis*, Volume 3, 2002, ISBN 978-1-59124-508-7.
- [89] Manas Chanda, Salil K. Roy, *Plastics Technology Handbook*, Fourth Edition, CRC Press, FL 2007.
- [90] S. M. Ataei, N. B. Laleh, "Synthesis and Properties of Polyimides and Copolyimides Containing Pyridine Units: A Review", *Iranian Polymer Journal*, vol. 17 (2), pp. 95-124, 2008.
- [91] A. Ghosh, S. K. Sen, S. Banerjee, and B. Voit, "Solubility improvements in aromatic polyimides by macromolecular engineering", *RSC Advances*, vol. 2, pp. 5900-5926, 2012.
- [92] Polyimide properties, http://www.efunda.com/Materials/polymers/properties/polymer_datasheet.cfm?MajorID=PI&MinorID=7
- [93] Electrically Conducting Adhesives, <http://www.epdtonthenet.net/article/8610/Electrically-Conducting-Adhesives.aspx>
- [94] Creative materials, https://server.creativematerials.com/datasheets/DS_110_19.pdf
- [95] Z. P. Wu, D. Z. Wu, W. T. Yang, and R. G. Jin, "Preparation of highly reflective and conductive metalized polyimide films through surface modification: processing, morphology and properties", *Journal of Materials Chemistry*, vol. 16, pp. 310-316, 2006.
- [96] Morton Katz, Darrell J. Parish, "Conductive polyimide containing carbon black and graphite and preparation thereof", United States patent- US 5075036 A, 1991.

- [97] H. Moriyama, K. Uhara, “Electrically conductive polyimide compositions having a carbon nanotube filler component and methods relating thereto”, United States patent: US 7273661 B2, 2007.
- [98] Ronald L. Jacobsen, “Carbon nanofiber filled materials for charge dissipation”, Applied Sciences, Inc., OH, USA.
- [99] G. Min, “Conducting polymers and their applications in the film industry - Polyaniline polyimide blended films”, *Synthetic Metals*, vol. 102, pp. 1163-1166, 1999.
- [100] A. Vijh, X. Yang, W. Du, X. Deng, and IEEE, “Film adhesion in triple junction a-Si solar cells on polyimide substrates”, in *31st IEEE Photovoltaic Specialists Conference*, Lake Buena Vista, pp. 611-613, FL, 2005.
- [101] T. Nakada, T. Kuraishi, T. Inoue, T. Mise, and IEEE, “CIGS thin film solar cells on polyimide foils”, in *35th IEEE Photovoltaic Specialists Conference*, Honolulu, HI, pp. 330-334, 2010.
- [102] X. Mathew, J. P. Enriquez, A. Romeo, and A. N. Tiwari, “CdTe/CdS solar cells on flexible substrates”, *Solar Energy*, vol. 77, pp. 831-838, 2004.
- [103] S. J. Cherng, C. M. Chen, “Thermal treatment of a Ni/Pt bi-layer deposited on a polyimide film for dye-sensitized solar cells”, Department of Chemical Engineering, National Chung Hsing University, Taiwan,
http://research.nchu.edu.tw/upfiles/ADUupload/oc_downmul2373107128.pdf
- [104] Susumu Yoshimura, R.P.H. Chang, *Supercarbon: Synthesis, Properties and Applications*, Springer, 1998.
- [105] V. M. Klein, The application of carbon materials in advanced technologies, International Conference on Economic Engineering and Manufacturing Systems, Brasov, 25 – 26 October 2007, http://www.recentonline.ro/021/Marascu-Klein_VI_01a-R21.pdf
- [106] B.K. Sharma, *Industrial Chemistry (including Chemical Engineering)*, GOEL Publishing House, 1997.
- [107] A. F. Holleman, E. Wibler, N. Wiberg, *Inorganic Chemistry*, Academic Press, 2001.
- [108] S. M. Lee, *Handbook of Composite Reinforcements*, John Wiley & Sons, 1992.
- [109] K. L. Reifsnider, *Damage in composite materials: basic mechanisms, accumulation, tolerance, and characterization: a symposium*, ASTM International, 1982.
- [110] A. Goetzberger, V. U. Hoffmann, *Photovoltaic Solar Energy Generation*, Springer, 2005.
- [111] C. K. Dyer, P. K. T. Moseley, Z. Ogumi, D. A. J. Rand, B. Scrosati, *Encyclopedia of electrochemical power sources*, Newnes, 2009.
- [112] Nanocyl, <http://www.nanocyl.com/en/CNT-Expertise-Centre/Carbon-Nanotubes>
- [113] J. Prasek, J. Drbohlavova, J. Chomoucka, J. Hubalek, O. Jasek, V. Adam, R. Kizek, “Methods for carbon nanotubes synthesis—review”, *Journal of Materials Chemistry*, vol 21, pp 15872–15884, 2011.
- [114] Q. Li, Y. Li, X. F. Zhang, S. B. Chikkannavar, Y. H. Zhao, A. M. Dangelewicz, L. X. Zheng, S. K. Doorn, Q. X. Jia, D. E. Peterson, P. N. Arendt, Y. T. Zhu, “Structure dependent electrical properties of carbon nanotube fibers”, *Advanced Materials*, vol 19, 3358–3363, 2007.

- [115] K. Aitola, Doctoral Dissertation, “Carbon nanomaterials as counter electrodes for dye solar cells”, Department of Applied Physics, Aalto University publication series 62/2012, Finland 2012, ISSN 1799-4942.
- [116] G. E. Totten, S. R. Westbrook, R. J. Shah, “Fuels and lubricants handbook: technology, properties, performance, and testing”, ASTM International, vol. 1, 2003.
- [117] T. Whelan, *Polymer Technology Dictionary*, Springer, 1994.
- [118] J. C. Huang, “Carbon black filled conducting polymers and polymer blends”, *Advances in Polymer Technology*, vol. 21, pp. 299-313, 2002.
- [119] P. Serp, J. L. Figueiredo, *Carbon Materials for Catalysis*, John Wiley & Sons, 2009.
- [120] T. N. Murakami, S. Ito, Q. Wang, Md. K. Nazeeruddin, T. Bessho, I. Cesar, P. Liska, R. H. Baker, P. Comte, P. Péchy, M. Grätzel, “Highly efficient dye-sensitized solar cells based on carbon black counter electrodes”, *Journal of The Electrochemical Society*, vol 153, pp A2255- A2261, 2006.
- [121] L. N. ZHU, J. ZHA, Q. Fang, “Quantitative and qualitative analyses of oxygen-containing surface functional groups on activated carbon”, *Chemical Journal of Chinese Universities*, vol. 33(03), pp. 548-554, 2012.
- [122] H. Sun, Y. Luo, Y. Zhang, D. Li, Z. Yu, K. Li, Q. Meng, “In Situ Preparation of a flexible polyaniline/carbon composite counter electrode and its application in dye-sensitized solar cells”, *J. Phys. Chem. C*, vol 114, pp 11673–11679, 2010.
- [123] S. Nagarajan, P. Sudhagar, V. Raman, W. Cho, K. S. Dhathathreyan, Y. S. Kang, “A PEDOT-reinforced exfoliated graphite composite as a Pt- and TCO-free flexible counter electrode for polymer electrolyte dye-sensitized solar cells”, *J. Mater. Chem A*, vol 1, pp 1048–1054, 2013.
- [124] B. Fan, X. Mei, K. Sun, J. Ouyang, “Conducting polymer/carbon nanotube composite as counter electrode of dye-sensitized solar cells”, *Applied Physics Letters*, vol 93, pp 143103, 2008.
- [125] J. G. Nama, Y. J. Park, B. S. Kim, J. S. Lee, “Enhancement of the efficiency of dye-sensitized solar cell by utilizing carbon nanotube counter electrode”, *Scripta Materialia*, Vol 62, Issue 3, pp 148–150, 2010.
- [126] E. Ramasamy, W. J. Lee, D. Y. Lee, J. S. Song, “Spray coated multi-wall carbon nanotube counter electrode for tri-iodide (I_3^-) reduction in dye-sensitized solar cells”, *Electrochemistry Communications*, Vol 10, Issue 7, pp 1087–1089, 2008.
- [127] Titanium Nitride, http://en.wikipedia.org/wiki/Titanium_nitride
- [128] L. E. Griffiths, M. R. Lee, A. R. Mount, H. Kondoh, T. Ohta, and C. R. Pulham, “Low temperature electrochemical synthesis of titanium nitride”, *Chemical Communications*, pp. 579-580, 2001.
- [129] M. Drygas, C. Czosnek, R. T. Paine, and J. F. Janik, “Two-stage aerosol synthesis of titanium nitride TiN and titanium oxynitride TiO_xN_y nanopowders of spherical particle morphology”, *Chemistry of Materials*, vol. 18, pp. 3122-3129, 2006.
- [130] P. V. Ananthapadmanabhan, P. R. Taylor, W. X. Zhu, “Synthesis of titanium nitride in a thermal plasma reactor”, *Journal of Alloys and Compounds*, vol. 287, pp. 126-129, 1999.

- [131] A. Ortega, M. A. Roldan, C. Real, "Carbothermal synthesis of titanium nitride (TiN): Kinetics and mechanism", *International Journal of Chemical Kinetics*, vol. 37, pp. 566-571, 2005.
- [132] Titanium Nitride properties, <http://www.memstnet.org/material/titaniumnitridetinbulk/#>
- [133] J. W. Kim, J.-H. Shim, S. C. Kim, A. Remhof, A. Borgschulte, O. Friedrichs, R. Gremaud, F. Pendolino, A. Züttel, Y. W. Cho, K. H. Oh, "Catalytic effect of titanium nitride nanopowder on hydrogen desorption properties of NaAlH₄ and its stability in NaAlH₄", *Journal of Power Sources*, vol. 192, pp. 582-587, 2009.
- [134] Brycoat, <http://www.brycoat.com/coating-services/pvd-coatings/titanium-nitride-tin.html>
- [135] B. Yoo, K.-J. Kim, Y. H. Kim, K. Kim, M. J. Ko, W. M. Kim, N. G. Park, "Titanium nitride thin film as a novel charge collector in TCO-less dye-sensitized solar cell," *Journal of Materials Chemistry*, vol. 21, pp. 3077-3084, 2011.
- [136] D. A. H. Hanaor, G. Triani, and C. C. Sorrell, "Morphology and photocatalytic activity of highly oriented mixed phase titanium dioxide thin films", *Surface & Coatings Technology*, vol. 205, pp. 3658-3664, 2011.
- [137] R. A. Aziz and I. Sopyan, "Synthesis of TiO₂-SiO₂ powder and thin film photocatalysts by sol-gel method", *Indian Journal of Chemistry Section a-Inorganic Bio-Inorganic Physical Theoretical & Analytical Chemistry*, vol. 48, pp. 951-957, 2009.
- [138] Q. W. Jiang, G. R. Li, and X. P. Gao, "Highly ordered TiN nanotube arrays as counter electrodes for dye-sensitized solar cells", *Chemical Communications*, pp. 6720-6722, 2009.
- [139] G. R. Li, F. Wang, J. Song, F. Y. Xiong, and X. P. Gao, "TiN-conductive carbon black composite as counter electrode for dye-sensitized solar cells", *Electrochimica Acta*, vol. 65, pp. 216-220, 2012.
- [140] H. Xu, X. Zhang, C. Zhang, Z. Liu, X. Zhou, S. Pang, X. Chen, S. Dong, Z. Zhang, L. Zhang, P. Han, X. Wang, G. Cui, "Nanostructured titanium nitride/PEDOT:PSS composite films as counter electrodes of dye-sensitized solar cells", *ACS Applied Materials & Interfaces*, vol. 4, pp. 1087-1092, 2012.
- [141] G.R. Li, F. Wang, Q.W. Jiang, X. P. Gao, P.W. Shen, "Carbon nanotubes with titanium nitride as a low-cost counter-electrode material for dye-sensitized solar cells", *Angewandte Chemie-International Edition*, vol. 49, pp. 3653-3656, 2010.
- [142] C. P. Lee, L. Y. Lin, R. Vittal, K. C. Ho, "Favorable effects of titanium nitride or its thermally treated version in a gel electrolyte for a quasi-solid-state dye-sensitized solar cell", *Journal of Power Sources*, vol. 196, pp. 1665-1670, 2011.
- [143] C. P. Lee, L. Y. Lin, K. W. Tsai, R. Vittal, K. C. Ho, "Enhanced performance of dye-sensitized solar cell with thermally-treated TiN in its TiO₂ film prepared at low temperature", *Journal of Power Sources*, vol. 196, pp. 1632-1638, 2011.
- [144] Bridge Technology, Four point probe technique, <http://four-point-probes.com/sheet-resistance-and-the-calculation-of-resistivity-or-thickness-relative-to-semiconductor-applications/>

- [145] A beginner's guide to TGA, Perkin Elmer,
http://www.perkinelmer.co.uk/CMSResources/Images/4474556GDE_TGABeginnersGuide.pdf
- [146] Y. Liu, H. Shen, X. R. Huang, and Y. J. Deng, "A new improved structure of dye-sensitized solar cells with reflection film", *Chinese Science Bulletin*, vol. 51, pp. 369-373, 2006.
- [147] Micro and nanotechnology laboratory, Hitachi S4800 FE-SEM, Illinois University,
<http://mntl.illinois.edu/equipment/hitachi4800.htm>
- [148] Connexions, SEM and its application for polymer science,
<http://cnx.org/content/m38344/latest/?collection=col110699/latest>
- [149] Application note, Roughness measurement with a stylus profiler, <http://www.tri-statetech.com/pdf/roughmeas.pdf>
- [150] NSF partnership for international research and education, Introduction to X-ray photoelectron spectroscopy, power point presentation, <http://pire-ecci.ucsb.edu/pire-ecci-old/summerschool/papers/vohs1.pdf>, 2013
- [151] Helmholtz Zentrum Berlin für Materialien und Energie, Introduction into X-ray and UV Photoelectron Spectroscopy (XPS/UPS), power point presentation, http://staff.mbi-berlin.de/hertel/ProMINT/MPSch/WS2010-11/Vollmer_WS_2010_02.pdf, 2013
- [152] Handbook of X-ray photoelectron spectroscopy, J.F Moulder, W.F. Stickle, P.E. Sobol, K.D. Bomben, Physical Electronics Inc., USA, 1995.

CHAPTER 2

EXPERIMENTAL METHODS

2.1 Materials

This research deals with low cost dye-sensitised solar cell fabrication on coated metallic and glass substrates. Therefore, a wide range of materials has been used in this case to develop different types of conductive coatings and dye-sensitised solar cells followed by their qualitative and quantitative analysis. Materials used in this research are normally divided into two categories, i) materials for dye-sensitised solar cells and ii) materials for conductive coatings. However, some materials e.g. metal and glass substrates were commonly used for both purposes. This section will provide detailed information about the materials used in this research with a focus on their physical and chemical properties.

2.1.1 Glass and metal substrates

Glass: Both electrically conductive and non-conductive glass (NCG) substrates were used in this research. Electrically conductive glass sheets with sheet resistance values of $15 \Omega/\square$ and $7 \Omega/\square$ were purchased from Solaronix, Switzerland coated with 500 and 700 nm thick coatings of fluorine doped tin oxide (F: SnO₂) respectively. The thickness of the glass substrates was approximately 2.2 mm.

Plain soda lime glass sheets were used as NCG substrates with a thickness the same as conductive glass sheets. These glass sheets were purchased from a local supplier.

Metals: Electro-chromium coated steel (ECCS) substrates were supplied by TATA steel Europe and titanium metal foils were purchased from Goodfellow, UK. The said metal substrates were 0.21 and 1.5 mm thick respectively.

2.1.2 Materials for dye-sensitised solar cells

Materials used for the manufacturing of dye-sensitized solar cells are listed in Table 2.1.

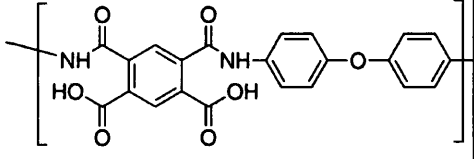
TABLE 2.1: Materials used for DSC manufacturing.

<i>Name</i>	<i>Supplier</i>	<i>Purity/grade</i>	<i>Purpose</i>
Titania pastes (TiO ₂) DSL 18NR-AO	Dyesol, UK	AO (Anatase TiO ₂ with 20 and 450 nm particle size),	DSC photoanode preparation
N719 Dye	Dyesol, Australia	Industry grade	Sensitization of the photoanode
Titanium(IV) chloride tetrahydrofuran complex	Sigma-Aldrich, UK	97%	For TiCl ₄ treatment
<i>Anhy.</i> Iodine	Sigma-Aldrich, UK	99.99%	Electrolyte
Guanidine thiocyanate	Sigma-Aldrich, UK	>99%	Electrolyte
1- Methylbenzimidazole	Sigma-Aldrich, UK	99%	Electrolyte
1-methyl-3- propylimidazolium iodide	Solaronix, Switzerland	DSC grade	Electrolyte
3- Methoxypropionitrile	Sigma-Aldrich, UK	>98%	Electrolyte solvent
Chloroplatinic acid, hexahydrate	Sigma-Aldrich, UK	99.99%	Catalyst
Isopropanol	Fisher Scientific, UK	99.90%	Catalyst solvent
Ethanol	Sigma-Aldrich, UK	99.50%	Dye solvent
Silver paint	Electrolube, UK	Paint	Silver contacts
Surlyn (25µm, 50µm)	Solaronix, Switzerland	Gaskets	Sealant
Additional Solvents			
Acetone	Fisher Scientific, UK	99.6%	Solvent

2.1.3 Organic polymer and surfactant

Organic coatings with electrically conductive fillers were developed using a polyimide precursor, Poly (pyromellitic dianhydride-co-4, 4'-oxydianiline), amic acid, which had been purchased from Sigma-Aldrich, UK. Various properties of this precursor have been given in Table 2.2. A surfactant based on polyether-modified polydimethylsiloxane in butyl glycol was used in the organic coatings to prevent de-wetting of the coatings on metallic and non-metallic substrates. This surfactant was supplied by TATA steel Europe under the trade name of BYK 419.

TABLE 2.2: Properties of the polyimide precursor.

Polyimide precursor	Concentration	Refractive Index	Viscosity (poise)	Density, g/cm ³
	15.0 wt. %±5 wt. % in NMP/aromatic hydrocarbons	n _{20/D} 1.5	50-70	1.09

2.1.4 Conductive fillers

Three types of electrically conductive fillers were used in this research, purchased from Sigma-Aldrich, UK. Properties of each type of filler are described in Table 2.3.

TABLE 2.3: Properties of conductive fillers^[1-3].

Name of the filler	Form	Melting point, °C	Density, g/cm ³	Electrical resistivity (Ω.cm)
Titanium nitride (TiN)	< 3 μm particles	2930	~5.24	25-30 μΩ.cm
Graphite (C)	1-2 μm particles	3652	~2.09	8.0 x10 ⁻⁴
Multiwalled Carbon Nanotubes (MWCNT)	Powder, > 95%C	3652	~2.10	5.40 x10 ⁻⁴

2.2 Development of polyimide (PI) coating

A significant amount of experimental work in this research was based on preparation of different types of polyimide-based coatings for DSC application. As already discussed in section 1.7, polyimide is a chemically inert material with outstanding thermal stability. Therefore, it was chosen to coat corrosion prone low cost metal substrates such as ECCS for their application as DSC substrates. However, polyimide itself cannot be used to coat such substrates as it is electrically insulating in nature. Therefore, coatings based on pigmented polyimide were developed. In addition, this type of electrically conductive coatings can also be used to coat NCG sheets for their application as TCO free substrates for low cost DSC manufacturing.

2.2.1 Modification of polyamic acid

Organic polymers normally demonstrate de-wetted spots when coated onto a substrate. De-wetting is a process when a thin film of polymer ruptures to form small islands of the polymer film onto the substrate surface. Mismatch of surface tension between the polymer and the substrate results in de-wetting of the polymer onto the substrates^[4]. This can be avoided by the addition of a surfactant into the polymer solution, which will prevent the polymer film from delaminating. Hence, a surfactant commercially known as BYK 419 (polyether-modified polydimethylsiloxane in butyl glycol) was added (0.3 wt%) into the polyimide precursor (Poly (pyromellitic dianhydride-co-4, 4'-oxydianiline), amic acid) before its application as a coating. Both the precursor and the surfactant were mixed thoroughly using a glass rod for approximately 15 minutes and kept in a glass jar as a stock.

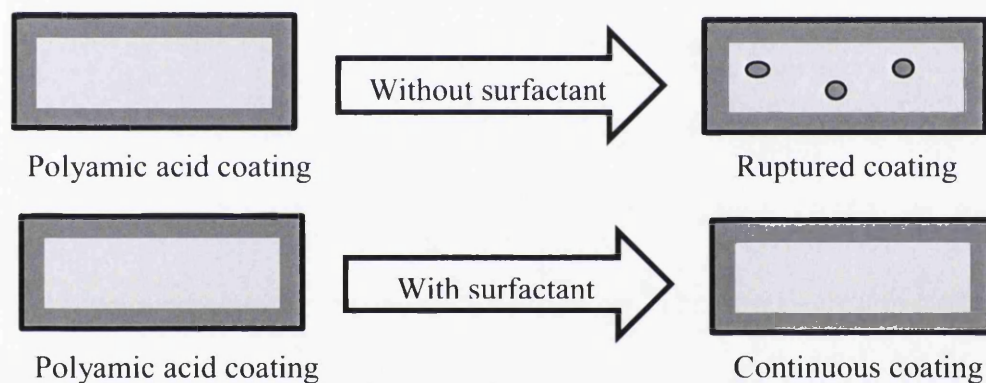


FIGURE 2.1: Schematic of the effect of surfactant on coating properties.

2.2.2 Coated substrate preparation

The modified polyimide precursor i.e. the surfactant added polyamic acid was then applied onto the NCG and ECCS substrates (15 mm x 25 mm) using doctor blade technique with scotch tapes as height guides. Therefore, thickness of the coating can be controlled by altering the number of tapes used. A typical thickness for one scotch tape is 50 μm (Figure 2.2).

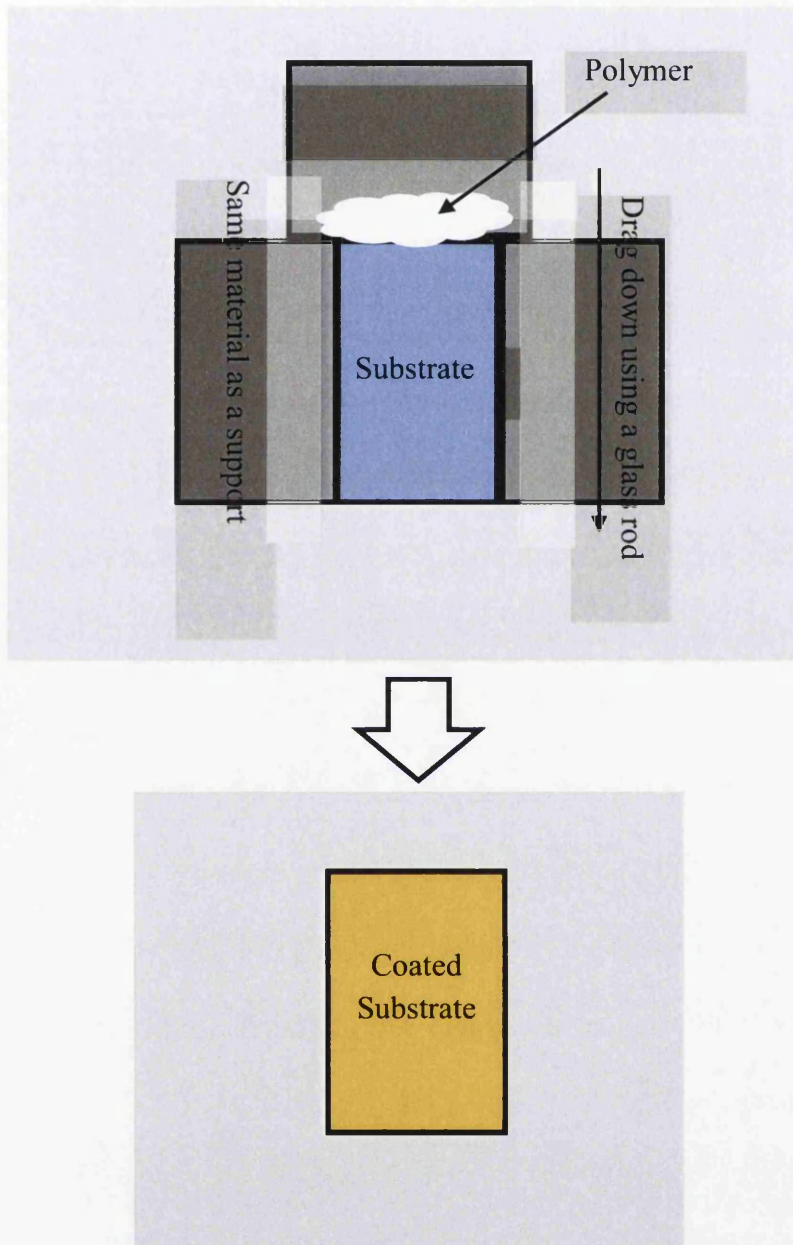


FIGURE 2.2: Coating application technique on NCG and ECCS substrates.

2.2.3 Curing of polyamic acid into polyimide

Temperature dependant imidization of the polyamic acid (see section 1.7.2) results in a cross-linked polyimide structure (Figure 2.3). Therefore, substrates coated with polyamic acid were cured in two easy steps. The first step involved drying of the wet coating at 150°C for 150 seconds in a convection oven followed by the imidization step carried out at 350°C for 300 seconds. Cured polyimide coatings containing the wetting agent outlined above were stable and adhered well onto both the NCG and ECCS substrates.

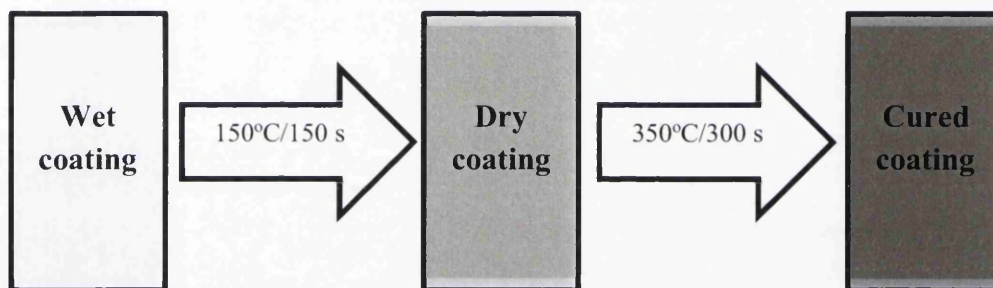


FIGURE 2.3: Curing process of polyamic acid into polyimide.

2.3 Electrically conductive PI coatings

After having understood the process of coating formation and curing of unpigmented PI, electrically conductive polyimide coatings were developed by incorporating pigments such as MWCNT, graphite and TiN into the polyamic acid precursor.

2.3.1 Preparation of carbon/polyimide coatings

Multi-walled carbon nanotubes (MWCNTs), graphite (particle size 1-2 μm) and graphite/MWCNT based electrically conductive composite coatings were developed by incorporating MWCNT, graphite/MWCNT and graphite particles separately into the polyimide precursor, poly (pyromellitic dianhydride-co-4, 4'-oxydianiline) amic acid. The wettability of the polymer precursor on the substrate was improved prior to

carbon materials addition by mixing 0.3 wt% wetting agent (polyether-modified polydimethylsiloxane in butyl glycol by weight) with the precursor.

The conducting additions were mixed uniformly with the polymer precursor in a glass jar for 30 minutes (divided into three 10 minutes steps) using a simple hand blending method. Prolonged mixing of carbon materials into the polymeric matrix results in a homogeneous mix of evenly distributed carbon particles. It is however important to mention that the amount of carbon particles in the polymer matrix was determined with respect to the weight of wet polymer precursor. For instance, a 10 wt% carbon/polyimide composition contains 10g carbon in 100g liquid precursor. In other words, this can also be expressed as 10 PHR, where 'PHR' stands for 'parts (of filler) per hundred parts of resin' [5, 6].

Substrates were then coated with these formulations (according to the method described in section 2.2.2) using a doctor blade technique followed by their heat treatment in a convection oven preheated at 150°C for 150 seconds. This is required in order to evaporate the NMP (N-Methyl-2-pyrrolidone) solvent base of the polyimide precursor. Subsequently the coatings were heat treated in a preheated furnace at 350°C for 300 seconds to cure the polyimide precursor into polyimide through imidization process. Carbon based coatings with high filler content tended to delaminate on a smooth substrate such as glass upon their curing but on ECCS; they adhered well due to the pre-existing micro roughness. A 2 wt% graphite/polyimide coating was applied as an interlayer onto the glass substrates and cured at 350°C for 300 minutes (after drying at 150°C for 150 seconds) to enhance the adhesion between the glass substrates and the carbon rich top coatings. Examples regarding the role of interlayer in coating adhesion can be found in Figures 2.4 and 2.5 of this section.

Cured carbon based polyimide coatings were then further heat-treated up to 450°C for 30 minutes to assess their suitability for DSC application (see section 1.7). Key properties such as electrical resistance, average surface roughness (R_a), and average coating thickness were determined following this high temperature treatment. Depending on thermal, electrical, and surface morphological characterization, the best composition was then identified from this experiment and used to coat NCG and

ECCS substrates to prepare DSC electrodes, for use as either a working or counter electrode in a device.

2.3.2 Preparation of TiN/polyimide coatings

Titanium nitride added polyimide coatings had been developed according to the method already described in the previous section (2.3.1).

TiN particles of $< 3 \mu\text{m}$ size were then added into the polymeric precursor matrix at various weight percentages (30% - 90% by the precursor weight) to obtain compositions with different TiN concentrations. Blending of TiN particles into the precursor was carried out manually in small pots using glass rods for approximately 30 minutes (divided into three 10 minutes steps). Uniform blending of TiN particles into the polymer precursor gave rise to homogenized mixtures with evenly distributed titanium nitride particles. Developed compositions were then applied onto the ECCS and NCG substrates using a doctor blade technique (see section 2.2.2) with Scotch tapes as a height guide. Coated substrates were then heat-treated in a preheated convection oven at 150°C for 150 seconds to eliminate the NMP solvent base from the polymer precursor, which resulted in solvent-free dry coatings onto the ECCS and NCG substrates. Dry coatings were then further heat-treated at 350°C for 5 minutes in a preheated furnace to cure the polymer precursor into a cross-linked polyimide structure. Cured coatings were taken out and cooled down in a normal atmosphere. It was observed that, cured coatings on glass suffered from severe delamination, as highly pigmented TiN coatings do not stick well on smooth NCG substrates (Figure 2.4-a). In contrast, the presence of micro roughness on ECCS promotes adhesion between the coatings and the metallic substrates (Figure 2.4- b).

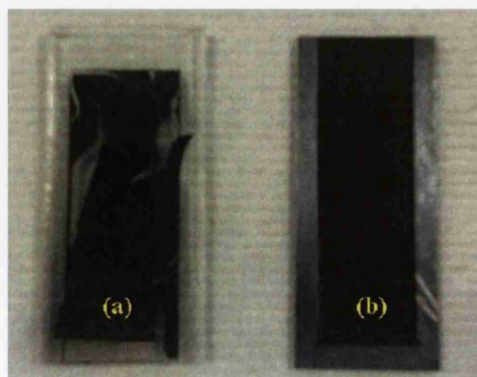


FIGURE 2.4: (a) Cured TiN/PI coating on NCG (de-laminated) (b) Cured TiN/PI coating on ECCS substrate.

Similar to the previous section (2.3.1), the problem of delamination was solved by applying an interlayer of 5 wt% TiN/PI onto the NCG substrates, which was cured in the same manner prior to the application of highly concentrated top coatings (Figure 2.5). The micro level asperities present on to the ECCS surface act as adhesion promoter thus application of 5 wt% TiN/PI interlayer was not necessary in this case.

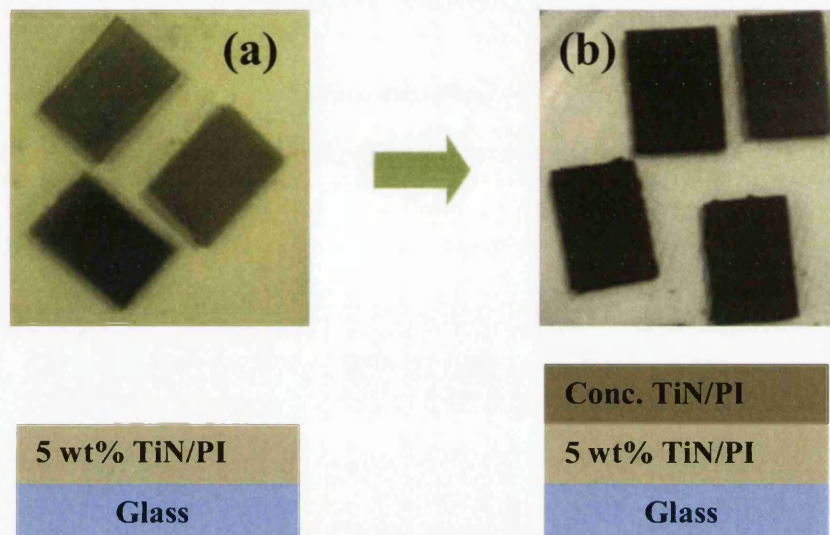


FIGURE 2.5: (a) non-conducting glass substrates with cured 5 wt% TiN/PI coating (b) same substrates with cured top coating (no delamination observed).

2.3.3 Preparation of hybrid coatings

Titanium nitride and graphite hybrid coatings were developed using the same method already described in the sections 2.3.1 and 2.3.2. Different proportions of graphite and titanium nitride were added into the polyamic acid solution to develop such coatings. Like other coatings, highly pigmented hybrid coatings also delaminated on NCG substrates in this case but it was again easily solved by applying a 5 wt% TiN/PI under layer.

2.4 Characterization of conductive coatings

This section provides a brief outline of testing methods used for the characterisation of electrically conductive coatings. The working principles associated with each technique have already been discussed in the literature review chapter (Chapter 1) of this thesis.

2.4.1 Electrical sheet resistance measurement

The sheet resistance (see section 1.10.1) of the cured coatings was measured on non-conducting glass substrates of dimension 40 mm x 40 mm (Figure 2.6). Developed coatings were simply doctor bladed onto the glass substrates followed by their drying at 150°C for 150 seconds and curing at 350°C for 5 minutes. Jandel RM 3000 probe station was used to carry out all the measurements in this case.

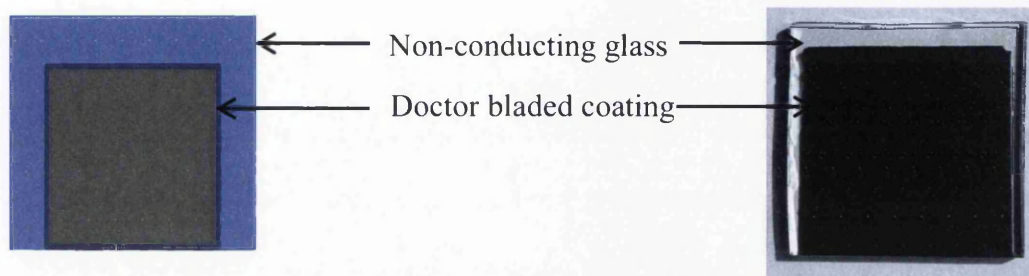


FIGURE 2.6: Standard sample for sheet resistance measurement.

2.4.2 Surface profilometry

The samples for profilometry (see section 1.10.5) were prepared on NCG and ECCS substrates using the doctor blade technique. As shown in Figure 2.7, portions of the film were removed at two different locations to allow the stylus to rest on the bare substrate before and after the scan. In this way, coating thickness was calculated from the step height between the coated and uncoated area. All surface scans in this research were performed using a fully automated stylus profilometer, Veeco Dektak 150.

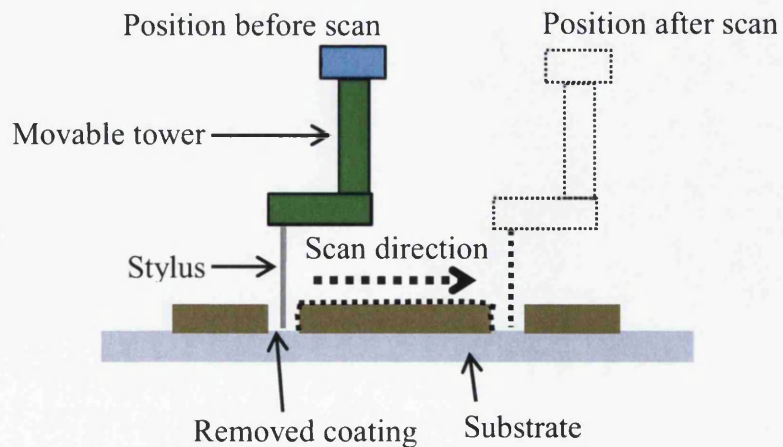


FIGURE 2.7: Schematic of a stylus profilometer and sample scanning technique.

2.4.3 Reflectance measurement

A UV-Vis spectrophotometer (Perkin Elmer, Lambda 650) was used to determine reflectance properties (see section 1.10.3) of the developed coatings, which were doctor bladed onto 40 mm x 40 mm glass substrates prior to their insertion in the reflectance port shown in Figure 2.8. In addition, reflectance of un-coated FTO glass substrate (40 mm x 40 mm) was also recorded for comparison purposes^[7].

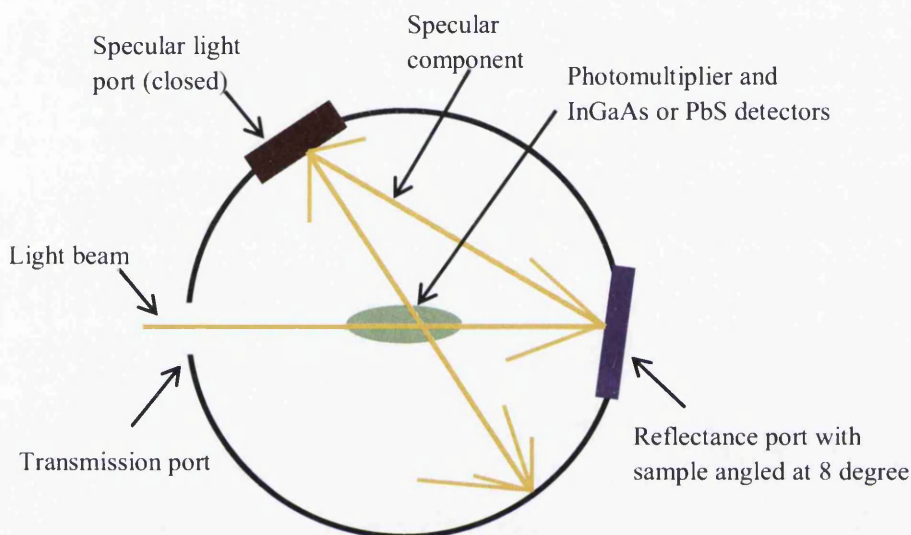


FIGURE 2.8: Schematic representation of reflectance measurement using a UV-Vis spectrophotometer^[7].

2.4.4 Thermogravimetry

Perkin Elmer Pyris 1 thermogravimetric analyser was used to determine the thermal stability of small quantities of polymer samples, see section 1.10.2 for brief theoretical information about TGA.

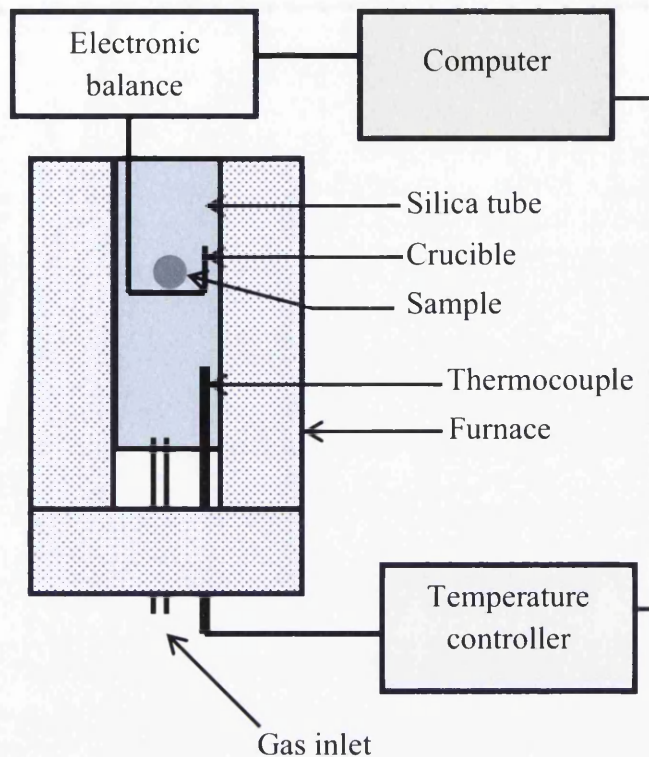


FIGURE 2.9: Schematic of a thermogravimetric analyser.

2.4.5 Scanning electron microscopy

A scanning electron microscope (Hitachi S-4800) was used to study the surface topography of developed coatings on NCG substrates after curing at 350°C and sintering at 450°C.

2.4.6 X-ray photoelectron spectroscopy

Surface characteristics of the developed coatings were studied using XPS technique. A theoretical background of the technique has already been provided in section 1.10.6. A VG ESCALAB XPS instrument operating at a base pressure of 10^{-10} mbar was used in this case with following settings (Table 2.4) to analyse the samples. All photoelectron peaks are referenced to the C (1s) hydrocarbon peak at 284.8 eV.

TABLE 2.4: Experimental setup for XPS analysis.

X-ray source	Achromatic-Aluminium K α
Source energy	1486.6 eV
Survey scan pass energy	50 eV
Core level scan pass energy	10 eV
Number of scans	10
Dwell time	0.05 s

2.5 Fabrication of dye-sensitized solar cells

This research work was focused on liquid state DSC fabrication and their characterization. The term liquid state in this case suggests that the fabricated DSCs contains a liquid I⁻/I₃⁻ redox electrolyte. Liquid state DSCs are relatively straightforward to manufacture but require a significant amount of time and involve a series of manufacturing steps. A wide range of substrate materials such as FTO glass, metals, and coated metallic and non-metallic materials were used in this research to fabricate different types of dye-sensitized solar cells without affecting the other vital components. This means, no change had been made in the TiO₂ paste, dye, electrolyte and the catalyst during the device fabrication steps. Such components were commercially purchased and used throughout the research. The purpose of this section is to explain the entire DSC manufacturing process that was followed in this research.

2.5.1 TiO₂ working electrode preparation

The TiO₂ working electrode was prepared through the steps described below.

Step 1: Substrate cleaning

The substrate for TiO₂ deposition was thoroughly cleaned using a soap solution (Triton X) followed by rinsing with ethanol.

Step 2: TiO₂ deposition

The cleaned substrate was then mounted on a working mat using 3M Scotch™ tapes as height guides followed by deposition of the TiO₂ paste using doctor blade technique (Figures 2.10 and 2.11).

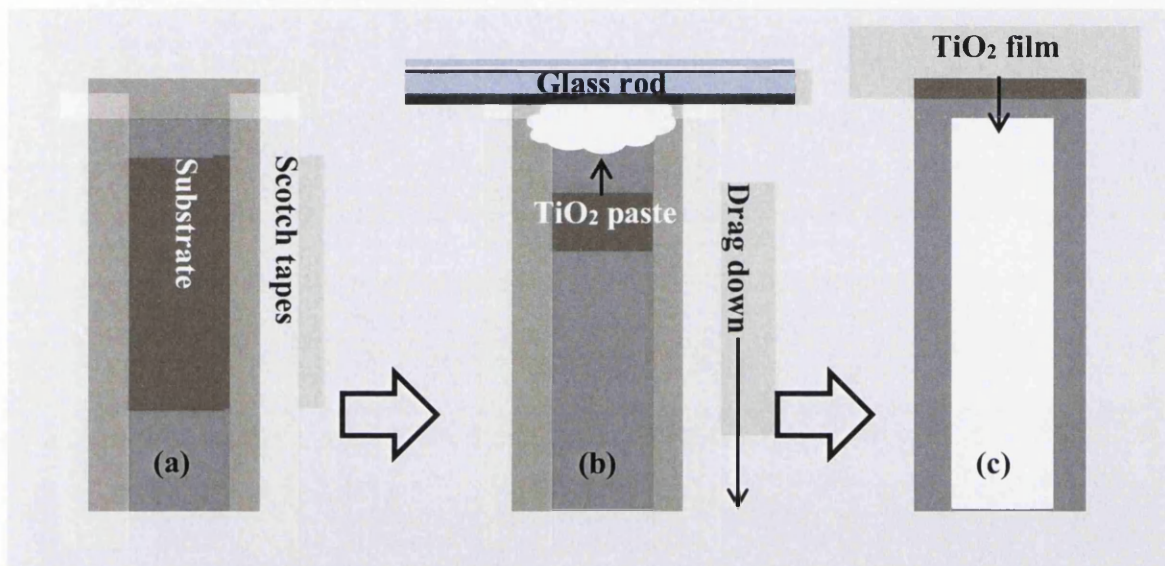


FIGURE 2.10: Schematic representation of TiO₂ deposition on a clean substrate.

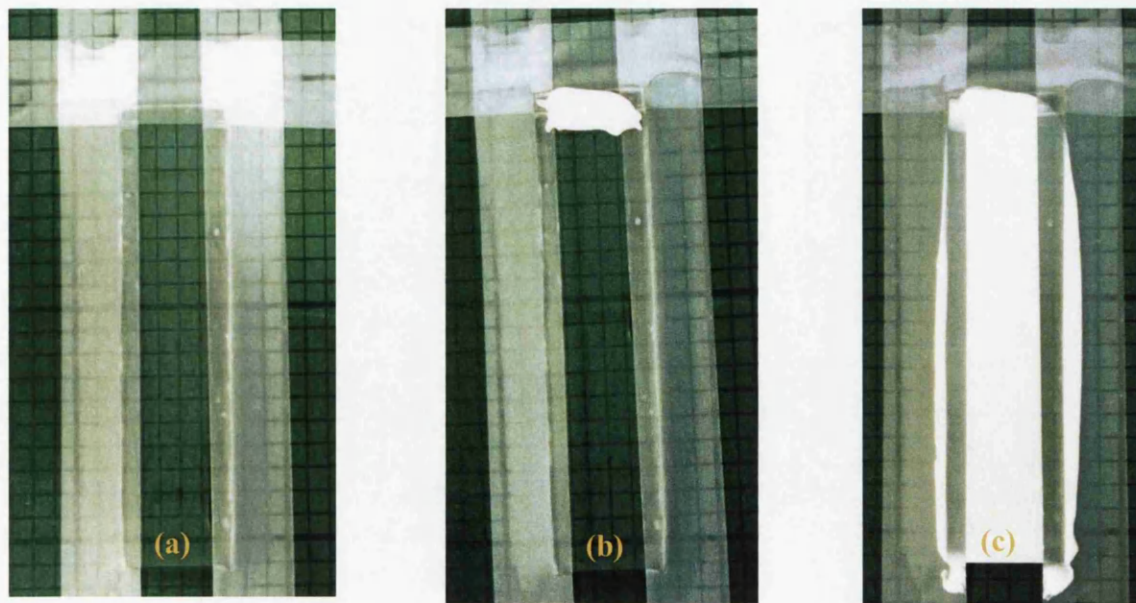


FIGURE 2.11: TiO₂ deposition on a clean FTO glass substrate.

Step 3: Sintering of TiO₂ film

The doctor bladed TiO₂ film was then dried at 150°C for 20 minutes in a convection oven to evaporate the solvent base. The dried TiO₂ film was then sintered at 450°C in a preheated oven to obtain the mesoporous TiO₂ film (Figure 2.12). The TiO₂ sintering time may vary from 10 to 30 minutes depending upon the nature of application.

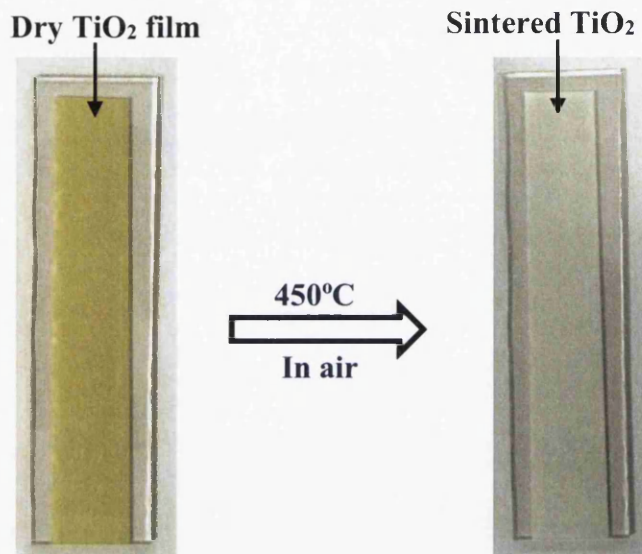


FIGURE 2.12: Dried and sintered TiO₂ films on a FTO glass substrate.

Step 4: Shaping of TiO₂ films

The substrate with a sintered TiO₂ film was cut into small strips of 15 mm x 25 mm dimensions (Figure 2.13) using a glasscutter followed by the creation of a 1 cm² active area in the middle of each strip by trimming down the TiO₂ film using a cover slip.

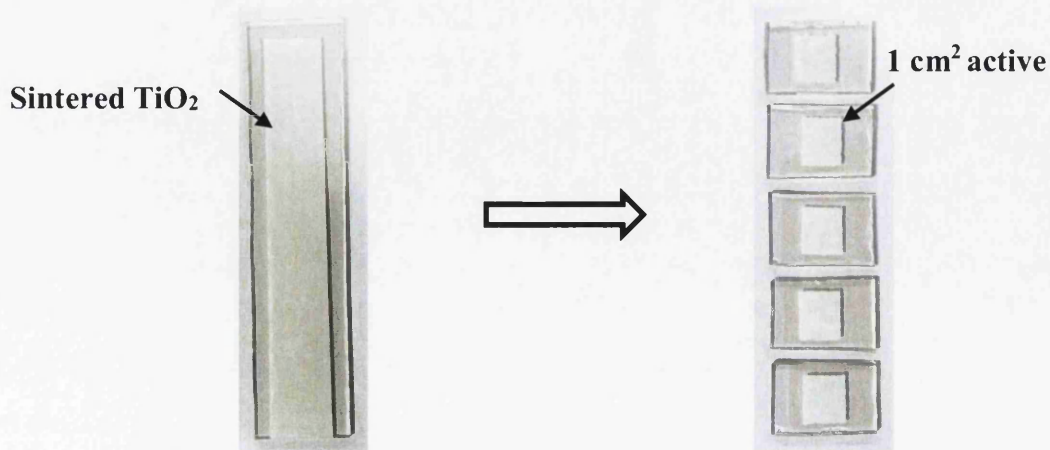


FIGURE 2.13: Shaping of a TiO₂ film on a FTO glass substrate.

For coated substrates, instead of a long strip (Figure 2.13) pre-cut substrates (15 mm x 25 mm) were used. A 1cm² active area was created in such a way (Figure 2.14) on each substrate using scotch tapes as height guide, that TiO₂ shaping was not required after the sintering step. Shaping of TiO₂ onto the coated substrates might result in coating damage therefore this unconventional TiO₂ deposition technique was used.

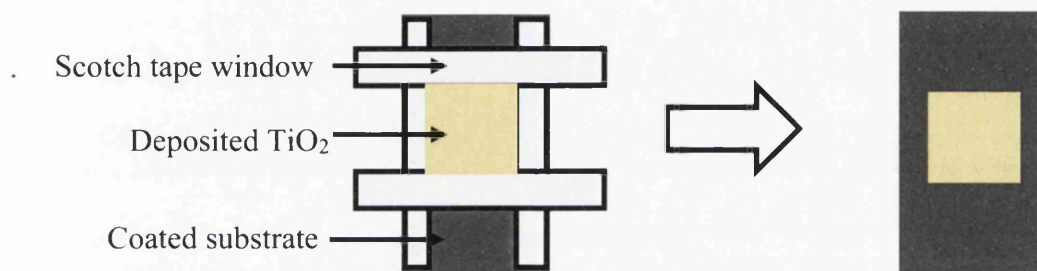


FIGURE 2.14: TiO₂ deposition technique on coated substrates.

Step 5: TiCl₄ treatment of TiO₂ films

TiCl₄ treatment of the TiO₂ films is an optional step during DSC fabrication. A water-based solution of 0.5 mM Titanium (IV) chloride tetrahydrofuran complex was used to deposit a thin layer of TiO₂ crystallites on the mesoporous TiO₂ film and the exposed FTO glass. This thin layer of TiO₂ may prevent electron recombination (see section 1.4.1.2) at the substrate/electrolyte and the mesoporous TiO₂/electrolyte interfaces resulting in significant enhancement in the average photoconversion efficiency of the fabricated cells. This type of thin TiO₂ layer can be applied just by immersing the mesoporous TiO₂ film into the TiCl₄ solution for 30 minutes at 80°C followed by an additional sintering step of 30 minutes at 450°C^[8].

2.5.2 Dye treatment

The small strips were immersed into a dye bath containing an ethanol-based 0.3 mM solution of N719 dye. Dye-sensitization is an 18-20 hours long process after which dye-sensitized TiO₂ films were obtained (Figure 2.15). Dye adsorbed TiO₂ films were then rinsed with ethanol to remove the excess dye followed by their assembly with the counter electrodes.

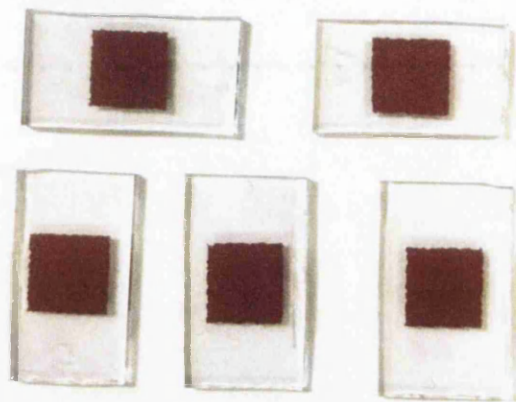


FIGURE 2.15: FTO glass strips with dye-sensitized TiO₂ films.

2.5.3 Counter electrode preparation

The cathode of a DSC is most commonly known as a counter electrode (CE). Counter electrodes are electrically conductive in nature with a catalyst deposited on the functional side, which facilitates the electron transfer process from the external load to the redox electrolyte. Substrates for counter electrodes were first cut into small strips of 15 mm x 25 mm dimensions followed by drilling a 0.5 mm hole in each strip (including coated pre-cut substrates) from the non-conducting/non-functional side. All the strips with drilled holes were rinsed with ethanol followed by drying using a hair drier. A catalyst solution, which had been prepared by dissolving 5mM H₂PtCl₆, 6H₂O (chloroplatinic acid hexahydrate) in isopropanol was then, deposited using a capillary onto the dried substrates. Thermally decomposed platinum catalyst was obtained by heating the substrates to 385°C for 15 minutes.

2.5.4 Device construction

Dye-sensitised solar cells were constructed by placing the counter electrodes over the working electrodes separated by Surlyn™ gaskets at a specific thickness (usually 25 and 50 μm). Assembled electrodes were sealed using a hot press pre-heated at 108°C. Sealed devices were then taken out of the press and allowed to cool. A redox electrolyte solution (0.8 M 1-propyl-3-methylimidazolium iodide, 0.3 M 1Methylbenzimidazole, 0.1 M I₂ and 0.05 M guanidinium thiocyanate dissolved in N-methoxypropionitrile) was then vacuum injected within the sealed devices through the holes present in the counter electrodes. The open holes were immediately sealed

after filling by melting a Surlyn™ strip placed under a circular cover glass. Finally, a silver ink was used to deposit conductive silver contacts on the terminals of the cells as shown in Figure 2.16.

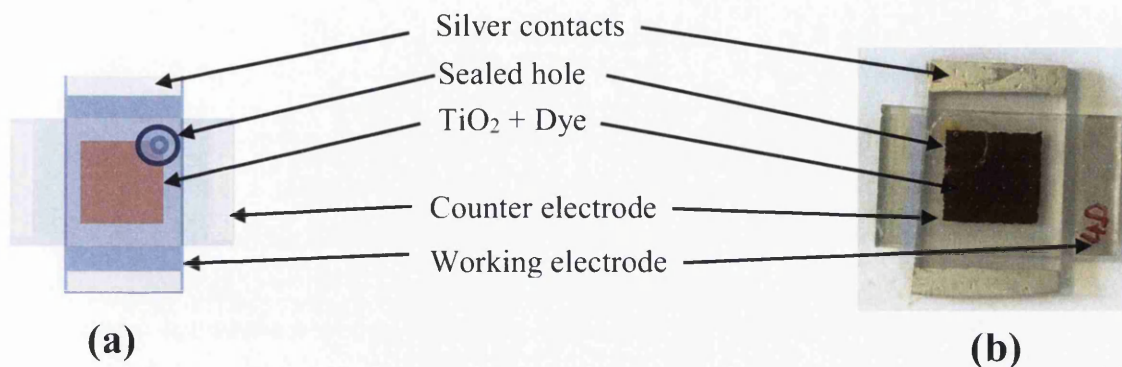


FIGURE 2.16: Assembled device (a) schematic (b) FTO based typical device.

2.6 DSC characterization

This section provides a brief outline of testing methods used for the characterisation of dye-sensitized solar cells. The working principles associated with each technique have already been discussed in the literature review chapter of this thesis.

2.6.1 Solar simulation

The I-V characteristics of fabricated DSCs were measured using a class AAA solar simulator (Oriel Sol 3A) with a 450-watt xenon arc lamp, which provides power output equivalent to 1 sun (100 mW/cm^2) to carry out simulation experiments at 1.5 air-mass. All simulation experiments were carried out by applying the following settings (Table 2.5) to the software that controls the simulator. It is needless to mention that the same settings were used to measure the dark current in the absence of light.

TABLE 2.5: Settings used for solar simulation.

Sample area	1 cm ²
Irradiance	1 Sun
Pre sweep delay	1
Max reverse bias	-0.1V
Max forward bias	0.8 V
No. of sweep points	200
Current limit	20 mA

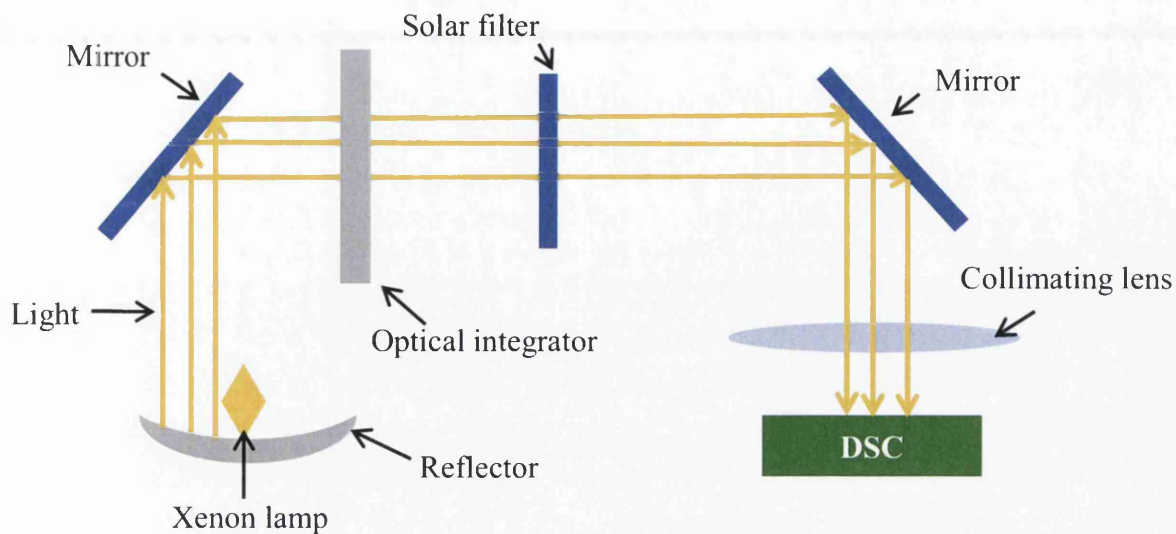


FIGURE 2.17: Schematic of a solar simulator used for DSC testing ^[9].

In the beginning of the experiment, the intensity of the light was adjusted to 1 Sun using an NREL certified crystalline silicon reference cell. A source meter (Keithley 2400) was then connected to the cell using crocodile clips (Figure 2.18) to record the current – voltage characteristics of the cell. A forward bias was applied during the simulation experiments, which remained unchanged whilst studying the I-V characteristics under light and dark conditions. The theory associated with this technique has been discussed briefly in section 1.6.1.

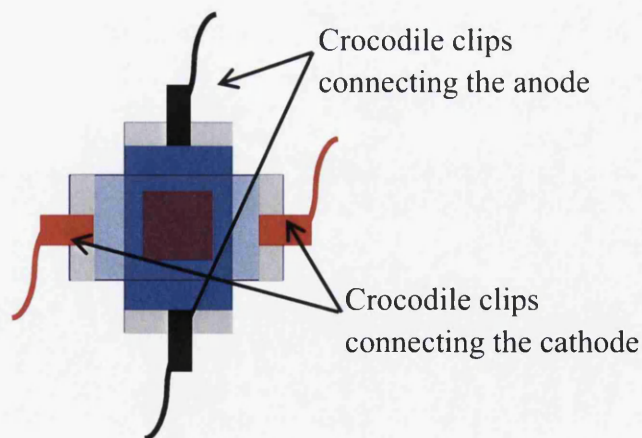


FIGURE 2.18: Schematic of a test cell for solar simulation.

2.6.2 Electrochemical impedance spectroscopy

A Gamry reference 600 three-electrode potentiostat was used to measure the electrochemical impedance of fabricated dye-sensitised solar cells. All the impedance measurements were carried out under dark governed by specialised software. A DC potential range between -0.5 V to -0.85 V was used to collect the impedance data whilst the AC potential was kept at 10 mV with a frequency range between 10^5 – 0.1 hertz. Further information regarding EIS can be found in 1.6.3.

2.6.3 Optoelectronic transient technique

A custom-built instrument (schematic representation, Figure 2.19) was used to collect transient data from the optically perturbed DSCs. A DSC is first connected to a DAQ (data acquisition) system through its working and counter electrodes followed by the optical perturbation process. Signals collected by the DAQ system are then supplied to the attached computer, which then converts the signals into presentable plots. The thickness of a TiO_2 photoanode is an important parameter in this experiment, which has to be entered correctly before running the scan. A brief outline describing the principle behind this technique can be found in section 1.6.2.

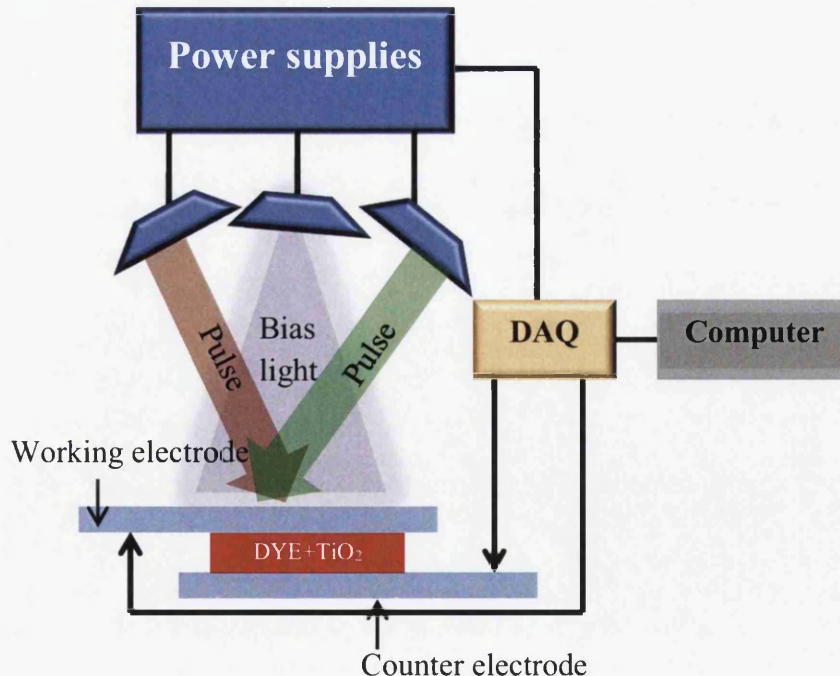


FIGURE 2.19: Simplified diagram of the equipment used for optoelectronic transient measurements ^[10].

2.7 References

- [1] Titanium Nitride, Wikipedia, http://en.wikipedia.org/wiki/Titanium_nitride#cite_note-6
- [2] Resistivity, Conductivity and Temperature Coefficients for some Common Materials, http://www.engineeringtoolbox.com/resistivity-conductivity-d_418.html
- [3] Y. Ando, X. Zhao, H. Shimoyama, G. Sakai, K. Kaneto, "Physical properties of multiwalled carbon nanotubes", *International Journal of Inorganic Materials*, vol. 1, pp. 77-82, 1999
- [4] L. Xue, Y. Han, "Inhibition of dewetting of thin polymer films", *Progress in Materials Science*, vol. 57, pp. 947-979, Jul 2012
- [5] P. Kadam, B. Pawar, S. Mhaske, "Studies in Effect of Low Concentration of Cenosphere on Mechanical, Thermal, Electrical, Crystallinity, Colorimetric and Morphological Properties of Epoxy Cured with Triethylenetetramine" *Journal of Minerals and Materials Characterization and Engineering*, vol. 1, pp. 117-123, 2013
- [6] PHR definition, <http://composite.about.com/library/glossary/p/bldef-p3938.htm>
- [7] Perkin Elmer, LAMBDA 650/750/850/950/1050, http://www.perkinelmer.com/CMSResources/Images/44-135972BRO_009201B_0LambdaAccessories.pdf
- [8] S. W. Lee, K. S. Ahn, K. Zhu, N. R. Neale, A. J. Frank, "Effects of $TiCl_4$ Treatment of Nanoporous TiO_2 Films on Morphology, Light Harvesting, and Charge-Carrier Dynamics in Dye-Sensitized Solar Cells", *Journal of Physical Chemistry C*, vol. 116, pp. 21285-21290, 2012.
- [9] Solar Simulator schematic, <http://www.opticsbalzers.com/pictures/2000/2136.jpg>
- [10] P. R. F. Barnes, K. Miettunen, X. Li, A. Y. Anderson, T. Bessho, M. Gratzel, B.C.O'Regan, "Interpretation of Optoelectronic Transient and Charge Extraction Measurements in Dye-Sensitized Solar Cells", *Advanced Materials*, vol. 25, pp. 1881-1922, 2013

CHAPTER 3

ASSESSMENT OF CHARACTERIZATION TECHNIQUES TO DETERMINE PERFORMANCE OF DSC

3.1 Introduction

The aim of this chapter is to assess various techniques used for photovoltaic characterization of dye-sensitized solar cells in order to provide an analytical foundation for the subsequent materials development. Traditional glass-based DSCs containing I^-/I_3^- redox electrolyte will be used for this purpose. In order to create measurable variation in device performance, two device fabrication methodologies were used. These will help quantify the variation in the device performance and various trends obtained from the PV characterization, which could act as a reference whilst interpreting the data presented in the following chapters. The following device types were constructed:

- (a) Un-optimised – conventional DSC with FTO glass electrodes of $15 \Omega/\square$ sheet resistance
- (b) Optimised – as above but with $7 \Omega/\square$ FTO glass electrodes and $TiCl_4$ treated mesoporous TiO_2 film

In addition, optimization of devices will help understand the significance of substrate sheet resistance and $TiCl_4$ treatment on the device performance compared to its un-optimized counterpart. This could be beneficial whilst planning manufacturing steps for the novel substrate based DSCs followed by their characterization. This study provides specific information corresponding to each technique used for DSC characterization, which in turn will be helpful for understanding fundamental PV characteristics of a typical device (glass mounted DSC in this case). In addition, results obtained from this experiment will provide information on what experimental techniques can be used to determine the efficacy of particular optimisation. Finally, this investigation will provide the foundations for a subsequent comparative study between glass, titanium metal and substrates with novel coating based dye-sensitized solar cells that feature in the following chapters.

3.2 Experimental

In this chapter, photovoltaic performances of dye-sensitized solar cells have been discussed in light of various DSC characterization techniques. DSCs were fabricated using conventional FTO glass substrates using the materials already listed in sections 2.1.1 and 2.1.2 and the method already described in section 2.5. In order to create variation in the electrochemical properties, optimized cells were constructed using FTO glass electrodes (working and counter) of $7 \Omega/\square$ sheet resistance with enhanced charge collection efficiency due to low internal resistances^[1] of the electrodes and additional TiCl_4 treatment of the mesoporous TiO_2 film. In contrast, un-optimized cells were fabricated using most widely used $15 \Omega/\square$ glass electrodes without any TiCl_4 treatment of the mesoporous TiO_2 film.

Different characterization techniques were employed to perform photovoltaic as well as electrochemical characterization of the fabricated cells. Such techniques involve solar simulation (see sections 1.6.1 and 2.6.1) using Oriel Sol 3A solar simulator to determine current density – voltage (J-V) characteristics followed by the electrochemical characterization under dark using electrochemical impedance spectroscopy (see sections 1.6.3 and 2.6.2). Finally, transient photocurrent and photovoltage analysis (see sections 1.6.2 and 2.6.3) were carried out to quantify transport, recombination, and lifetime of the charge carriers within the fabricated cells.

3.3 Results & Discussion

Two sets containing six devices each were analysed in this study. The first set contained optimized cells followed by the second one dedicated to un-optimized devices. The optimized devices were based on $7 \Omega/\square$ FTO coated glass electrodes and treated with TiCl_4 solution whereas the un-optimized cells were fabricated without the TiCl_4 treatment and were based on commonly used $15 \Omega/\square$ FTO glass electrodes. It has been reported by Sommeling *et al.* that DSCs fabricated using FTO glass with low sheet resistance ($\sim 8 \Omega/\square$) and TiCl_4 treatment exhibit higher J_{sc} and photoconversion efficiency values [2]. Thus, optimized devices were fabricated using similar experimental conditions to compare their overall PV performance with the un-optimised cells.

The PV performance of dye-sensitized solar cells may vary depending upon the thickness of the TiO_2 photoanode. Hence, a stylus profilometer (Veeco Dektak 150) was used to determine the average TiO_2 film thickness values of optimized and un-optimized cells given in Table 3.1 [3]. It is noteworthy in this case that the photoanodes for optimized and un-optimized cells came from different batches, which means they were prepared separately using a doctor blade technique.

TABLE 3.1: Average TiO_2 film thickness of the cells chosen for characterization.

<i>Cells</i>	<i>TiO₂ film thickness (μm)</i>
Optimized	7.91 (± 0.41)
Un-optimized	8.94 (± 0.78)

3.3.1 Current – voltage (*J-V*) characteristics

Current-voltage measurements using a solar simulator show that the optimized cells (Figure 3.1, Table 3.2) are $\sim 17\%$ more efficient than the un-optimized ones under forward illumination mode (Figure 3.1). Augmented PV performance of optimized cells was expected due to the TiCl_4 treatment of the mesoporous TiO_2 photoanode, which resulted in higher J_{sc} values ($\sim 11\%$ increase) probably due to the conduction

band edge shift of the TiO_2 photoanode, which is mainly attributed to the TiCl_4 treatment [2].

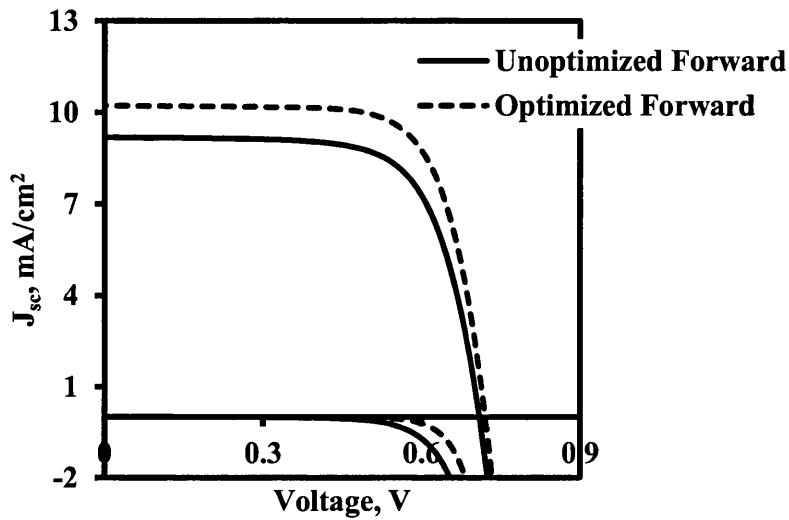


FIGURE 3.1: Average J-V characteristics of optimized and un-optimized DSCs in forward illumination mode: based on two sets of six devices each.

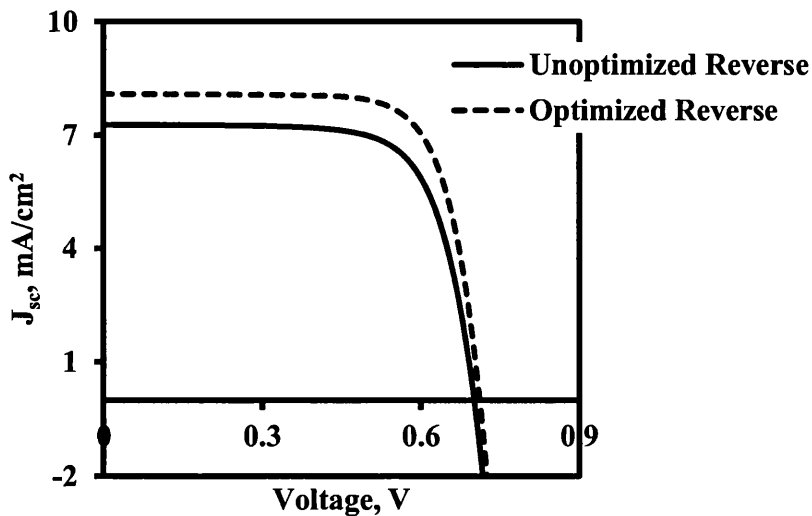


FIGURE 3.2: Average J-V characteristics of optimized and un-optimized DSCs in reverse illumination mode: based on two sets of six devices each.

However, the open circuit voltage (V_{oc}) remained similar in both type of cells (Table 3.2) without any significant deviation. In addition, the difference between average fill factors in both cases was substantially low. Nevertheless, the optimized cells exhibited slightly higher average fill factor, which could be due to the better catalytic performance of the platinum catalyst on counter electrodes made of $7 \Omega/\square$ FTO glass.

It is also evident from Figure 3.1 that the rate of charge recombination in un-optimized cells could be faster than the optimized set. Dark current curves obtained from the solar simulation study seem to support this fact. It can be seen that the onset of dark current in case of un-optimized cells is around 0.45 V whereas; the onset is shifted towards 0.6 V in case of optimized devices.

TABLE 3.2: Average current-voltage data of optimized and un-optimized cells: based on total 12 devices.

Optimized	V_{oc} (V)	J_{sc} (mA/cm²)	Fill factor (%)	Efficiency (%)
Forward	0.71 (±0.00)	10.21 (±0.32)	72.51 (±0.88)	5.32 (±0.17)
Reverse	0.7 (±0.00)	8.09 (±0.18)	74.41 (±0.79)	4.28 (±0.08)
Un-optimized	V_{oc} (V)	J_{sc} (mA/cm²)	Fill factor (%)	Efficiency (%)
Forward	0.7 (±0.00)	9.17 (±0.21)	70.26 (±2.07)	4.56 (±0.13)
Reverse	0.69 (±0.00)	7.27 (±0.48)	72.23 (±1.87)	3.67 (±0.2)

Thus, it can be seen from this section that the initial device performance can be obtained in terms of current-voltage characteristics obtained from solar simulation technique, which gives vital information regarding V_{oc}, J_{sc}, fill factor and the efficiency of a dye-sensitised solar cell. This technique can be sensitive to minor alteration in the device fabrication technique, which is evident from the results demonstrated by optimized and un-optimized sets. In addition, a hint regarding interfacial charge recombination can also be obtained from this study. The dark current curves obtained in this case can be very useful in predicting the charge recombination in the first place. Thus, solar simulation technique will be extensively used in the following chapters to understand the fundamental difference between the PV characteristics of a typical FTO glass based device and the one based on a different substrate material.

3.3.2 Electrochemical impedance spectroscopy

Electrochemical impedance spectroscopy (EIS) is an extremely useful technique, which is being used to understand charge transfer kinetics associated with different interfaces within a dye-sensitised solar cell. An AC output response of different cells over a large frequency region (0.1 to 10^5 Hz) was studied under low to high bias (0.5 V to 0.85 V) conditions, although impedance data close to the open circuit voltage at one sun (V_{oc} of device) were given preference in this case (see section 2.6.2 for further information on the measurement technique). Figure 3.3 represents Nyquist plots obtained from the EIS study of optimized and un-optimized cells respectively. Informally, Nyquist plots consist of semicircles. However, number and nature of semicircles depend specifically on the type of the electrochemical system that is being analysed. Therefore, in this case only two types of semicircles (A and B in Figure 3.3) are noticed in each plot, which represent electrochemical impedance at different interfaces (see section 1.6.3) within the fabricated dye-sensitised solar cells.

In Figure 3.3 the semicircles smaller in sizes (denoted by type “A”) represent the charge transfer resistance (R_{ce}) at the counter electrode (Pt coated) / electrolyte interface, which largely rely upon the catalytic activity of the platinum catalyst. There is a possibility that higher catalytic activity of the Pt catalyst could result in smaller semicircle in a Nyquist plot. Thus, it can be seen from Figure 3.3 that the semicircle representing average R_{ce} for optimized devices is smaller than the one corresponding to un-optimized cells.

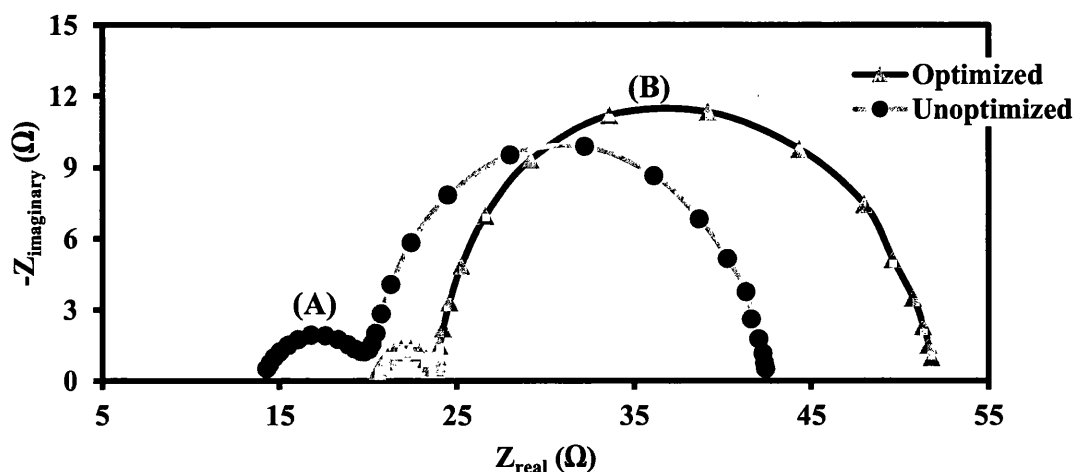


FIGURE 3.3: Nyquist plots of optimized and un-optimized devices based on their average values (data consist of the average of three best performing devices from each set).

This could be due to better catalytic performance of the catalyst on low sheet resistance counter electrodes ($7 \Omega/\square$) facilitating faster charge transfer at the counter electrode/electrolyte interface of optimized devices. Higher average fill-factor demonstrated by optimized devices also suggests the same possibility. This is a good example where both the current-voltage characteristics and EIS investigation indicate towards the same fact establishing the reliability of these techniques for DSC characterization. However, quantification of R_{ce} values (for both optimized and un-optimized cells) from the equivalent circuit modelling will reveal more information in the following results.

Equivalent circuit modelling of EIS data based on a model with constant phase elements (see section 1.6.3) gives a clear idea about different interfaces present within a DSC and their corresponding resistance and capacitance values at different applied potentials. A typical J-V characteristic is normally unable to provide such information, which is why EIS is preferred to extract this kind of information from a DSC.

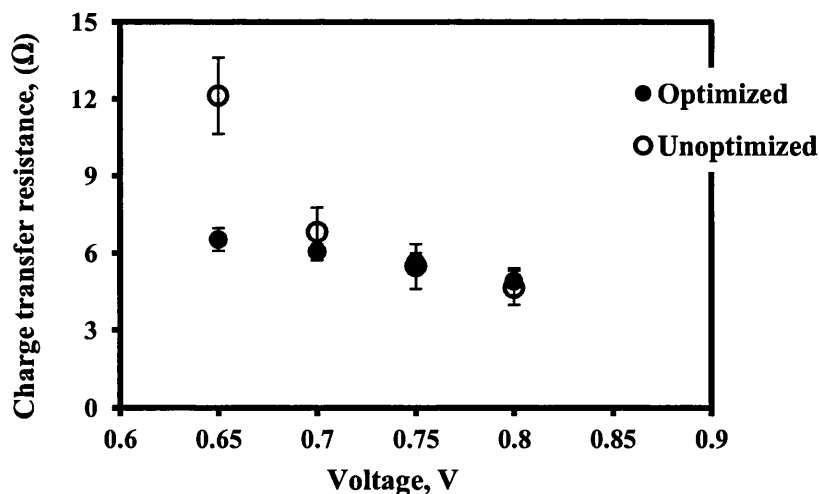


FIGURE 3.4: Average charge transfer resistance (R_{ce}) vs. applied potential (data consist of the average of three best performing devices from each set).

It is obvious from Figure 3.4 that the charge transfer resistances (R_{ce}) in both sets of cells decrease with increasing bias potential. Therefore, it can be concluded that higher bias potential enhances the charge transfer rate at the CE/electrolyte interface due to increase in the driving force of the charge transfer process ^[4]. However, it can be seen from Figure 3.4 that average R_{ce} of optimized cells remained significantly

low even at a potential around 0.65 V, which could be due to the better catalytic performance of the Pt-catalyst deposited on the counter electrodes of such cells.

The Nyquist plot also provides generalized information regarding charge recombination kinetics occurring within a dye-sensitized solar cell. The bigger semicircles (belonging to the mid frequency region, represented by type “B” in Figure 3.3) in the Nyquist plots obtained in this case mostly represent recombination resistance (R_{rc}) at the TiO_2 /electrolyte interface of a DSC. In addition, the bigger the semicircle the higher is the charge recombination resistance, which in turn reduces the charge recombination rate within a DSC. However, R_{rc} decreases with increasing applied potential leading to faster recombination of charges at the TiO_2 /electrolyte interface of a DSC [5].

R_{rc} vs. voltage plot (Figure 3.5) obtained from the equivalent circuit modelling show steady decrease in the recombination resistance with increasing bias potential in both optimized and un-optimized cells. Both set of cells show nearly same recombination resistance values close to the open circuit voltage, which apparently suggests that the charge recombination in both cases is almost same.

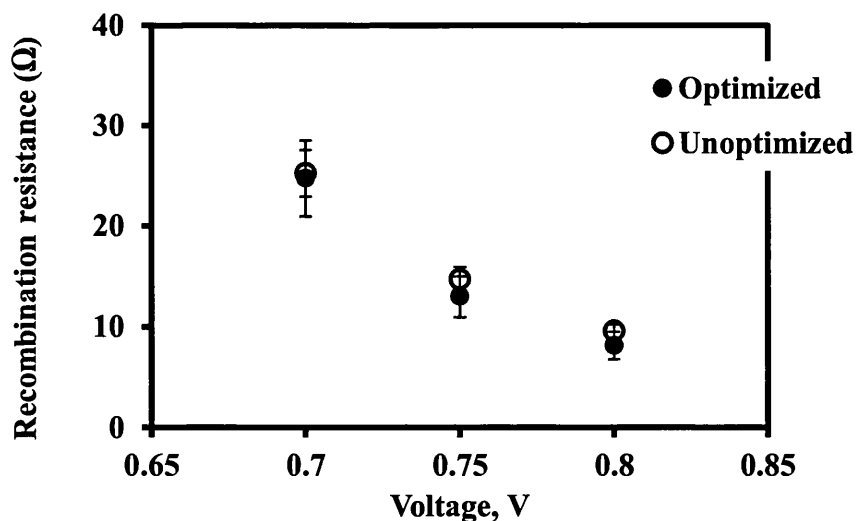


FIGURE 3.5: Average charge recombination resistance (R_{rc}) vs. applied potential (data consist of the average of three best performing devices from each set).

This feature of EIS could be considered as a limitation of this technique as it fails to provide clear information regarding the charge recombination sites and the type of

recombination reaction occurring within the fabricated devices. A DSC is said to consist of several interfaces among which substrate/electrolyte and the TiO₂/electrolyte interfaces are the most important. It has been reported that the photogenerated electrons are most likely to recombine with the electrolyte at these two interfaces but specific information regarding recombination sites cannot be extracted from EIS. Therefore, in order to obtain a clear idea about the interfacial charge recombination, transient and photovoltage decay measurements have been introduced in the following sections. Recombination resistance (R_{rc}) in a DSC is also related to the chemical capacitance (C_{μ}) at the TiO₂/electrolyte interface, which increases with increasing V_{oc} values. This means higher chemical capacitance results in increase in the charge accumulation at the TiO₂ /electrolyte interface.

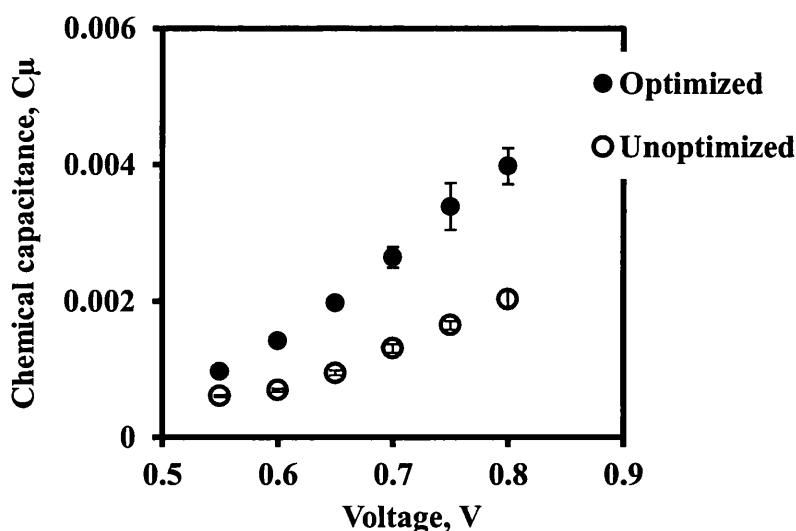


FIGURE 3.6: Average chemical capacitance (C_{μ}) vs. applied potential (data consist of the average of three best performing devices from each set).

Cells belonging to the optimized set (Figure 3.6) show higher chemical capacitance values near the open circuit voltage at 1 Sun. This suggests that TiCl₄ treatment in the optimized cells could be responsible for higher chemical capacitance in such devices. An increase in the chemical capacitance of TiCl₄ treated devices was already reported by Sommeling *et al.* which was due to increased number of density of states or DOS (in this context DOS means sites available in the Fermi level of the TiO₂ film for the photogenerated electrons to occupy) in the TiCl₄ treated TiO₂ film. This could also result in higher J_{sc} values due to downward shift of the conduction band edge of the mesoporous TiO₂ films [2].

The electron recombination lifetime (τ_n) at open circuit is the average residence time in seconds spent by an electron in the TiO_2 conduction band; before its recombination with the redox electrolyte or an oxidised dye molecule. The product of R_{rc} and C_μ gives electron lifetime τ_n , which decreases exponentially with increasing voltage. Lower electron lifetime is an indication of higher charge recombination within a device. This has a detrimental effect on the PV performance of a dye-sensitized solar cell due to reduction in the open circuit voltage. Thus, electron lifetimes calculated for un-optimized and optimized cells (Figure 3.7) suggest that the un-optimized devices have significantly lower electron lifetimes, which in turn related to their substandard PV performance compared to the optimized set.

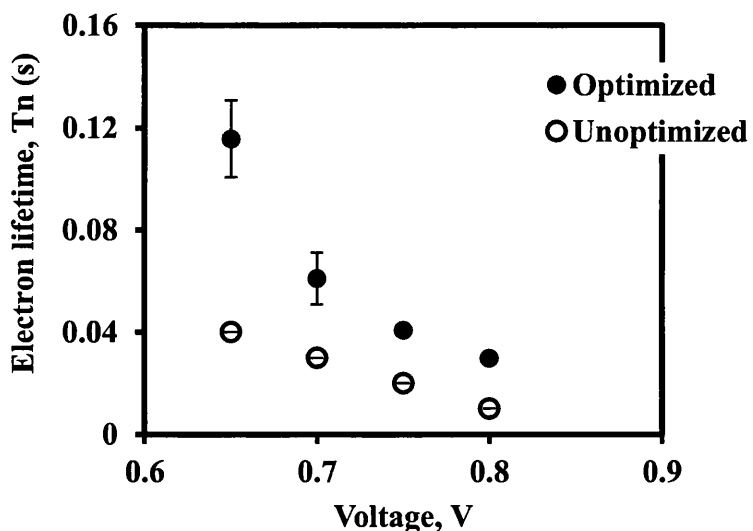


FIGURE 3.7: Average electron lifetime vs. applied potential (data consist of the average of three best performing devices from each set).

After the Nyquist plot, the Bode plot is another very essential tool for understanding interfacial electrochemical processes taking place in a dye-sensitized solar cell. Unlike the semi-circular nature of the Nyquist plot, Bode plot provides peaks associated with AC phase shift due to an applied potential, the amplitude of the peaks decreases with increasing voltage [4].

Figure 3.8 shows a comparison between Bode plots obtained from the EIS analysis of optimized and un-optimized devices. The peak with apex in the low frequency region (~4 Hz) is related to the optimized cells whereas the peak belong to the un-

optimized set has an apex at around 10 Hz. It is usually common in DSC Bode plots that if an apex of a peak shifts towards the higher frequency region then it is due to the higher rate of charge recombination taking place at the TiO_2 /electrolyte interface of the cell ¹⁶. The same scenario was observed in case of un-optimized cells where the apex of the peak shifted towards the high frequency region (Figure 3.8) indicating rapid interfacial charge recombination. In contrast, the peak associated with the optimized set stayed in the low frequency region suggesting relatively slower rate of charge recombination compared to the un-optimized set.

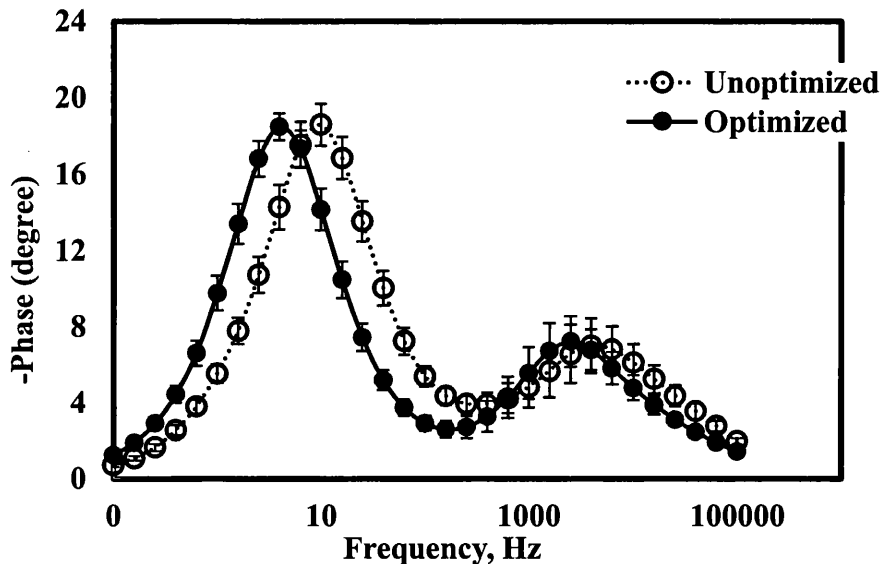


FIGURE 3.8: Average Bode plots of optimized and un-optimized devices showing phase shift vs. frequency (data consist of the average of three best performing devices from each set).

In case of DSCs, EIS is mainly used to reinforce the data obtained from the current-voltage characteristics. This is because current-voltage characteristics do not provide any information regarding the interfacial charge transfer mechanisms taking place within a device. Due to this reason, EIS comes into play to describe such mechanisms that are actively involved in controlling the PV performance of a DSC. It can be seen from this section that EIS plays a central role in describing the charge transfer and recombination mechanisms in optimized and un-optimized devices. Results presented in this section clearly show that the two types of cells (optimized and un-optimized) are different from each other in terms of their electrochemical characteristics. Hence, the biggest advantage of using EIS technique is, it helps

identify electrochemically distinct devices in a precise manner. Therefore, utilization of this technique in subsequent chapters will be beneficial for reporting the difference between the charge transfer mechanisms in DSCs based on novel substrates and the one consist of typical FTO glass electrodes. However, a clear idea regarding charge recombination and transport characteristics can be obtained from transient measurements that are described in the following section.

3.3.3 Optoelectronic transient measurements

As already mentioned in the previous section, that the data obtained from EIS analysis under dark can be extended further with the help of transient photovoltage and photocurrent studies. Transient studies were performed on optimized as well as un-optimized cells to determine charge transport and recombination characteristics of the cells. All transient studies in this case were carried out under illumination equivalent to the 1 sun.

Electron lifetime data obtained from the transient studies (Figure 3.9) shows that the optimized cells possess slightly higher electron lifetimes than the un-optimized ones due to the formation of a thin TiO_2 compact layer formed by the TiCl_4 treatment. This thin layer of TiO_2 appears to be acting as a blocking layer at the FTO /electrolyte interface by reducing the extent of recombination reaction in the high efficiency cells. In contrast, such a blocking layer is absent in case of un-optimized cells and thus could give rise to lower efficiencies due to higher charge recombination.

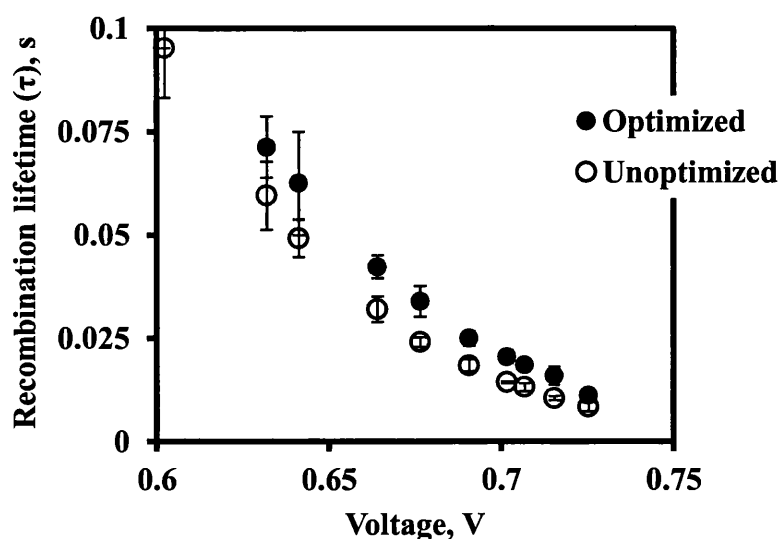


FIGURE 3.9: Average recombination lifetime vs. voltage (data consist of the average of three best performing devices from each set).

Charge density or carrier density within a dye-sensitized solar cell represents the density of the photoexcited electrons injected into the conduction band of the TiO₂ photoanode by the photosensitive dye molecule. Charge densities of the fabricated devices display directly proportional relationship with the voltage in Figure 3.10. Therefore, carrier densities in such cells increase with increasing voltage, which in turn can also enhance the current output of the cells. However, in the event of significant charge recombination the current output of a cell may also decrease. The higher charge density obtained in optimized cells could be due to the TiCl₄ treatment, which can dramatically increase the trap states in the Fermi level of the meso-porous TiO₂ film. This is because formation of an additional TiO₂ layer by the TiCl₄ treatment changes the surface charge on the porous TiO₂ photoanode, which in turn changes the electrical field responsible for controlling the potential of the energy states in the mesoporous TiO₂ (conduction band and trap states) at the TiO₂/electrolyte interface [7].

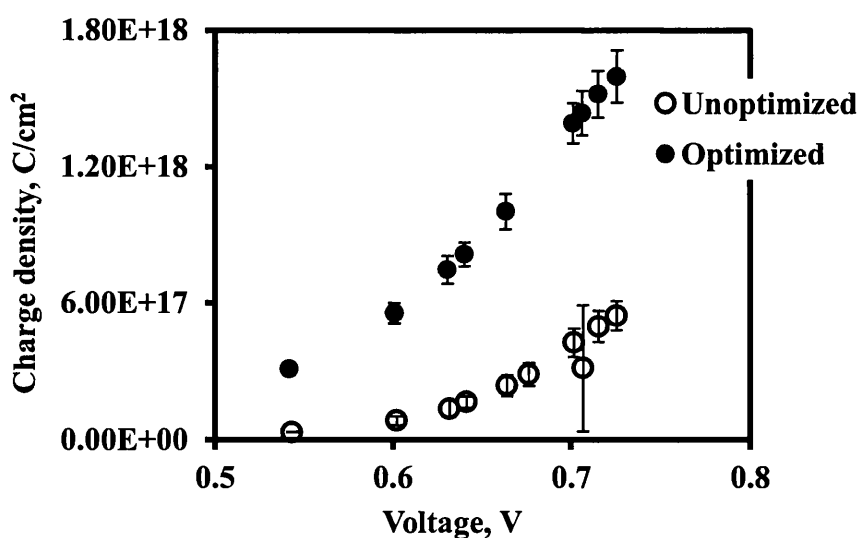


FIGURE 3.10: Average charge density vs. voltage (data consist of the average of three best performing devices from each set).

In order to investigate the effect of TiCl₄ treatment on the performance of optimized cells, electron transport lifetimes of both cell types are compared in Figure 3.11.

It can be seen from Figure 3.11 that TiCl₄ treatment has no remarkable influence on the transport lifetimes of the optimized and un-optimized cells. Therefore, it can be

concluded in this case that faster electron transport could not be one of the reasons behind higher J_{sc} values observed in the optimized cells. Thus, increase in the average J_{sc} value by 11% in optimized cells could be due to greater dye loading and the downward shift of the conduction band edge of the TiO_2 film [2].

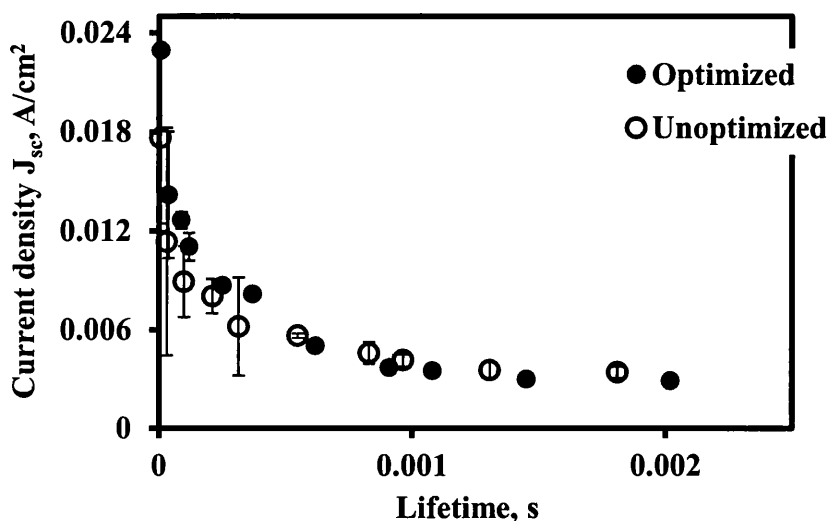


FIGURE 3.11: Average current density vs. lifetime (data consist of the average of three best performing devices from each set).

Electrochemical impedance spectroscopy is a very useful technique that helps analyse electrochemical behaviour of a dye-sensitised solar cell. Vital information regarding charge recombination, chemical capacitance and charge transport can be extracted from this technique. However, results obtained from this study may contain some errors if an inappropriate equivalent circuit model is chosen for the analysis of an EIS spectrum. In addition, it is possible that an important feature such as charge transport characteristics within the TiO_2 film could be suppressed by another e.g. charge transfer resistance in the EIS spectrum [8]. Therefore, in order to obtain accurate results and to validate EIS data, optoelectronic transient technique has been introduced in this section. This technique is mainly useful in determining carrier lifetime, transport and density within a dye-sensitized solar cell as described in section 3.3.3. Thus, optoelectronic transient technique will play a significant role in the following chapters for studying electron lifetime, transport and concentration within novel substrate based DSCs.

3.3.4 Photovoltage decay measurements

Photovoltage (PV) decay measurement (see section 1.6.2) provides information about charge recombination at the substrate/electrolyte interface of a dye-sensitised solar cell. Therefore, a clear evidence of charge recombination occurring at the FTO substrate/electrolyte interfaces of fabricated cells can be obtained from this experiment. Figure 3.12 shows that the photovoltage decay rate corresponding to the optimized cells treated with TiCl_4 is much slower than the un-optimized cells without such a treatment. It is now evident from Figure 3.12 that the untreated cells suffered from severe recombination at the FTO/electrolyte interface as indicated by the sudden drop in the photovoltage as a function of time ^[9]. TiCl_4 treatment results in a thin compact layer of TiO_2 film on the mesoporous TiO_2 as well as on the bare FTO glass. This compact TiO_2 film appears to be preventing recombination at the FTO/electrolyte interface as the cells (un-optimized) without such a layer displayed rapid voltage drop when the bias light was turned off.

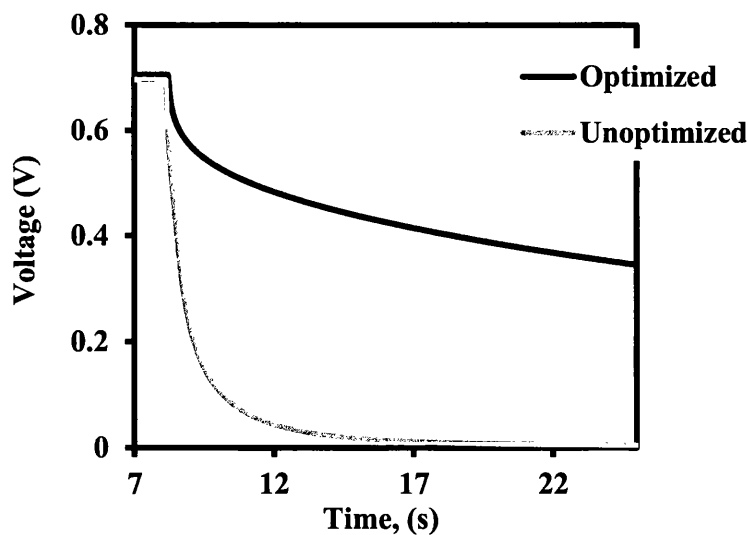


FIGURE 3.12: Photovoltage decay vs. time (data consist of the average of three best performing devices from each set).

It is evident in this case that PV decay measurement helps identify the difference between the optimized and un-optimized devices in a distinctive manner. This could be helpful whilst assessing the interfacial charge recombination at the coated substrate/electrolyte interfaces of the devices based on novel substrate materials. Information obtained from this technique is as credible as other characterization

techniques such as EIS and solar simulation. In addition, interpretation of results obtained from this technique is relatively straight forward, which would be helpful whilst comparing the charge recombination characteristics of novel substrate based DSCs and their FTO glass based counterparts (standard DSCs).

3.4 Conclusions

The most widely used characterization techniques such as solar simulation, EIS and optoelectronic transient measurements have been discussed in this chapter in the context of optimized and un-optimized DSCs. Each of the characterization technique was assessed carefully whilst analysing the data obtained from the PV characterization of the manufactured devices (optimized and un-optimized). The devices (optimized and un-optimized) manufactured in this case were different from each other in terms of their photovoltaic characteristics thus helping identify the dissimilarities using the characterization techniques mentioned earlier. Findings associated with this study could act as a reference in subsequent chapters whilst discussing the photovoltaic characteristics of novel substrate based devices in a precise manner. This chapter also tries to explain various advantages and disadvantages associated with each characterization technique that may be useful whilst selecting a technique to perform a specific analysis. On the other hand, this chapter emphasises the effects of TiCl_4 treatment and substrate conductivity on device performance as optimized devices with TiCl_4 treatment demonstrated approximately 17% increase in the average photoconversion efficiency. This also led to 11% increase in the average J_{sc} value of the said devices due to conduction band-edge shift in the mesoporous TiO_2 film. It also appears from this study that TiCl_4 treated optimized devices were capable of minimising charge carrier recombination at the substrate/electrolyte interface which is similar to the characteristics of a compact TiO_2 blocking layer, which minimises electron recombination with the redox electrolyte present in a DSC. In addition, optimized devices with low sheet resistance ($7 \Omega/\square$) substrates demonstrated higher charge collection efficiency than their un-optimized counterparts with substrates of higher sheet resistance ($15 \Omega/\square$).

3.5 References

- [1] T. Hoshikawa, M. Yamada, R. Kikuchi and K. Eguchi, "Impedance analysis of internal resistance affecting the photoelectrochemical performance of dye-sensitized solar cells," *Journal of the Electrochemical Society*, vol. 152, pp. E68-E73, 2005.
- [2] P. M. Sommeling, B. C. O'Regan, R. R. Haswell, H. J. P. Smit, N. J. Bakker, J. J. T. Smits, J. M. Kroon, and J. A. M. van Roosmalen, "Influence of a $TiCl_4$ post-treatment on nanocrystalline TiO_2 films in dye-sensitized solar cells," *Journal of Physical Chemistry B*, vol. 110, pp. 19191-19197, Oct 5 2006.
- [3] C.-P. Hsu, K.-M. Lee, J. T.-W. Huang, C.-Y. Lin, C.-H. Lee, L.-P. Wang, Song-Yeu Tsaic, Kuo-Chuan Ho, "EIS analysis on low temperature fabrication of TiO_2 porous films for dye-sensitized solar cells," *Electrochimica Acta*, vol. 53, pp. 7514-7522, Oct 30 2008.
- [4] C. J. Raj, S. N. Karthick, A. D. Savariraj, K. V. Hemalatha, P. Song-Ki, H.-J. Kim, K. Prabakar, "Electrochemical properties of TiO_2 encapsulated ZnO nanorod aggregates dye sensitized solar cells," *Journal of Alloys and Compounds*, vol. 537, pp. 159-164, Oct 5 2012.
- [5] F. Fabregat-Santiago, J. Bisquert, G. Garcia-Belmonte, G. Boschloo, and A. Hagfeldt, "Influence of electrolyte in transport and recombination in dye-sensitized solar cells studied by impedance spectroscopy," *Solar Energy Materials and Solar Cells*, vol. 87, pp. 117-131, May 2005.
- [6] P. Zhu, Y. Wu, M. V. Reddy, A. S. Nair, S. Peng, N. Sharma, V. K. Peterson, B. V. R. Chowdari and S. Ramakrishna, " TiO_2 nanoparticles synthesized by the molten salt method as a dual functional material for dye-sensitized solar cells," *RSC Advances*, vol. 2, pp. 5123-5126, 2012.
- [7] B. C. O'Regan, J. R. Durrant, P. M. Sommeling, and N. J. Bakker, "Influence of the $TiCl_4$ treatment on nanocrystalline TiO_2 films in dye-sensitized solar cells. 2. Charge density, band edge shifts, and quantification of recombination losses at short circuit", *Journal of Physical Chemistry C*, vol. 111, pp. 14001-14010, Sep 20 2007.
- [8] P. R. F. Barnes, K. Miettunen, X. Li, A. Y. Anderson, T. Bessho, M. Gratzel, Brian C. O'Regan, "Interpretation of Optoelectronic Transient and Charge Extraction Measurements in Dye-Sensitized Solar Cells", *Advanced Materials*, vol. 25, pp. 1881-1922, Apr 4 2013.
- [9] H. Choi, C. Nahm, J. Kim, J. Moon, S. Nam, D.-R. Jung, Byungwoo Park, "The effect of $TiCl_4$ -treated TiO_2 compact layer on the performance of dye-sensitized solar cell", *Current Applied Physics*, vol. 12, pp. 737-741, May 2012.

CHAPTER 4

CARBON/POLYIMIDE COATINGS FOR DYE-SENSITIZED SOLAR CELL APPLICATIONS

4.1 Introduction

One of the expensive components of a commercially available flexible DSC is the titanium substrate. Therefore, this chapter deals with potential replacements to the titanium based on lower cost alternatives. ECCS (electrolytic chromium coated steel) is a commercially available mass-produced low cost sheet metal manufactured by TATA steel, which could potentially act as a flexible DSC substrate replacing the expensive titanium metal in metal mounted DSCs [1-3]. However, ECCS is corroded by the commonly used I^-/I_3^- redox electrolyte in a dye-sensitized solar cell [4]. Therefore, utilization of bare ECCS in DSC manufacturing is not recommended when it comes to commercialization of this technology [4].

Corrosion of ECCS could be prevented by applying a chemically inert but electrically conductive protective coating, which would form a barrier between the electrolyte and the metal substrate without compromising the electrical conductivity of the metal. A key requirement for an organic coating under these circumstances is the ability to withstand the high processing temperatures (as outlined in section 1.7).

As a possible solution, carbon loaded polyimide based protective coatings are presented in this chapter. Carbon is an electrically conductive material therefore by controlling carbon concentration in the polyimide matrix, it may be possible to generate the desired electrical conductivity in the developed coatings. In addition, both carbon and polyimide are chemically inert and high temperature resistant materials [5-8]. The coatings must be able to withstand the high temperature heating steps (TiO_2 coated photoelectrode preparation at $450^\circ C$ and Pt-deposition on counter electrode at $385^\circ C$) involved in processing of the DSC electrodes. Thus, coated ECCS substrates could function as both working and counter electrodes (CE) in reverse and forward illuminated DSCs respectively (Figure 4.1). Especially in case of CE application, coated ECCS based CE could be useful in manufacturing low-cost glass-metal hybrid (forward illuminated) devices with higher photoconversion efficiencies.

Furthermore, the potentially enhanced electrically conducting nature of this coating (it is a Z-axis conductor on ECCS substrates) would also enable us to fabricate DSCs using TCO free glass substrates in the same fashion (Figure 4.1). However, coatings on NCG (non-conducting glass) substrates should demonstrate sheet resistances

equivalent to the typical TCO coated glass electrodes for DSC application. Hence, highly conductive carbon fillers such as multi-walled carbon nanotubes (MWCNTs) and graphite were used in the following experiments as fillers for carbon/polyimide coatings. Most carbon materials are cheap, abundant and highly conductive in nature, hence a carbon based protective coating could be an ideal candidate for this application.

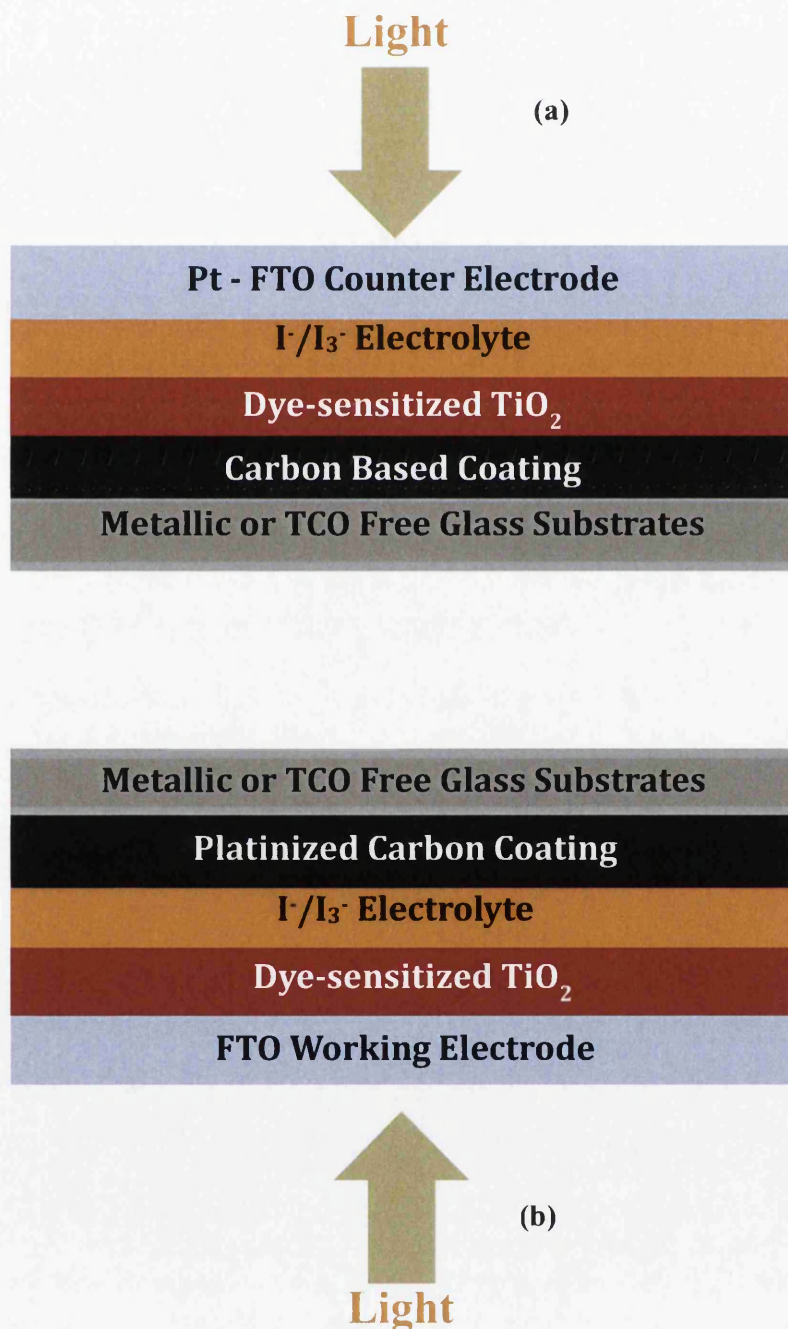


FIGURE 4.1: Device architecture of DSCs with carbon based coatings on metallic and non-metallic substrates as (a) working electrodes and (b) counter electrodes.

4.2 Experimental

Carbon/polyimide based conductive coatings were formulated using materials purchased from Sigma Aldrich, UK. The coating formulation and application techniques have already been discussed in section 2.3.1. Thus, MWCNT, MWCNT/graphite and graphite based conductive coatings were prepared and coated onto the ECCS and NCG substrates of approximately 0.21 and 2.2 mm thickness respectively. In case of NCG substrates, a 2 wt% graphite/PI under layer was used as adhesion promoter (section 2.3.1). ECCS substrates were supplied by TATA steel, UK whereas NCG substrates were purchased from a local supplier.

Applied wet coatings on both the substrates were cured (after drying at 150°C for 120 mins) using a specified curing profile (see section 2.2.3) followed by their characterization to determine surface, electrical and thermal properties. A stylus profilometer was employed to record the surface characteristics that include calculation of average roughness (R_a), average peak height (R_p) and coating thickness. On the other hand, a four-point probe equipment was used to determine electrical sheet resistance values of the coatings. Detailed information on both the techniques can be found in section 2.4.1 and 2.4.2. Finally, the thermal stability was evaluated as a function of time using a convection oven.

The photovoltaic characterization of dye-sensitised solar cells based on coated ECCS and NCG substrates was carried out using solar simulation and EIS techniques. More details on these techniques can be found in section 2.6.1 and 2.6.2.

4.3 Results & Discussion

4.3.1 MWCNT/polyimide coatings

MWCNT/polyimide coatings were developed initially as it was believed that MWCNT would perform extremely well for this specific application due to its higher electrical conductivity^[9]. It was observed in this case that MWCNT/PI formulation becomes difficult to process when the amount of MWCNT exceeds 4 wt% in the polyimide precursor causing a dramatic increase in the viscosity of the resulting formulation. Hence, compositions with MWCNT content only up to 4 wt% in the polyimide matrix were possible in this case.

An initial observation of the deposited material was an extremely rough surface morphology of MWCNT/PI coatings. A typical surface profile of cured MWCNT/PI coatings demonstrated very rough surfaces compared to the cured un-pigmented polyimide (Figures 4.2 and 4.3). The extremely rough surface in this case was produced due to the formation of big MWCNT agglomerates in the polyimide precursor, which were clearly visible to the naked eye and difficult to break. This is shown by the presence of sharp peaks in Figure 4.2. The sharp peaks are denoted by R_p in general that gives the average peak height. R_p mostly depends on the particle size thus a coating with fine particles may lead to lower R_p values which in turn reduces the average roughness (R_a) of the coating.

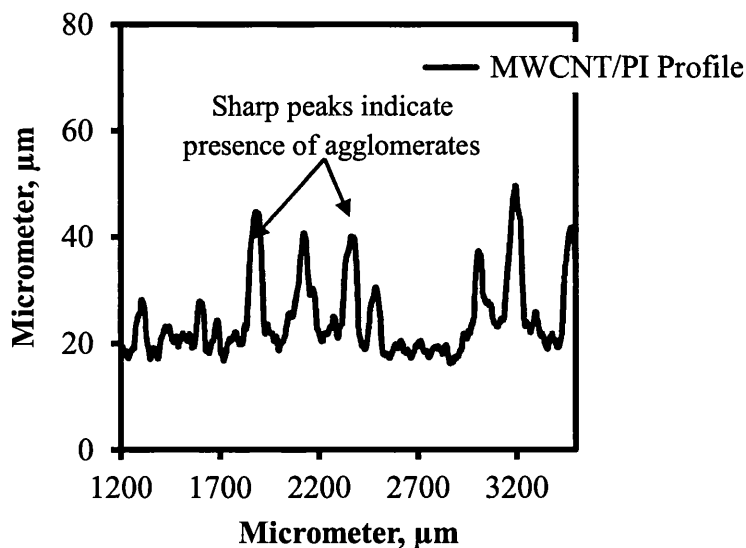


FIGURE 4.2: Surface profile of a typical MWCNT/PI coating cured at 350°C.

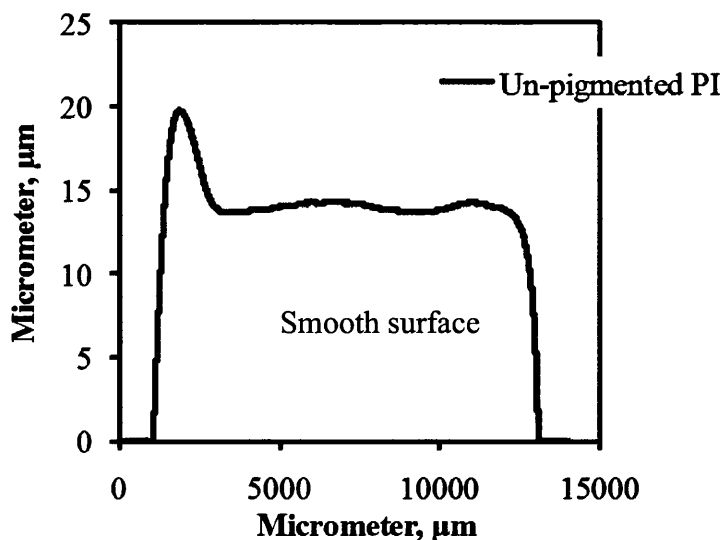


FIGURE 4.3: Surface profile of an un-pigmented PI coating cured at 350°C.

Strong Van der Waal forces are responsible for the MWCNT agglomeration, which eventually led to coarse surface morphology in this case ^[10]. Roughness is a critical factor here as coated substrates with high surface roughness may cause short-circuiting of the fabricated devices. Therefore, coatings with lowest possible roughness are always preferable for DSC application. This problem may have been solved easily by breaking the MWCNT agglomerates using an ultrasonic technique. However, it has been reported that the ultrasonic technique can degrade the physical properties (e.g. electrical conductivity which is very important in this case) of CNTs by damaging their tubular structure to a large extent ^[11]. Thus, the electrical conductivity of MWCNTs was preserved by adopting the manual mixing technique in this case.

Substrate conductivity is another critical issue in DSC fabrication as PV performance of a device can also depend on the charge collection efficiency of the substrate material. A typical substrate is an FTO coated glass with 15 Ω/\square sheet resistance that is often recommended for DSC application. Thus, any similar substrate material (excluding metals or Z-axis conductors) exceeding the sheet resistance limit (15 Ω/\square) will not be considered for this application. Table 4.1 shows sheet resistance values of various compositions of MWCNT added to polyimide cured at 350°C as well as heat treated at 450°C (to replicate the sintering process) coated onto both NCG and ECCS substrates. It was promising that all the coatings

prepared in this case could withstand 450°C for 30 minutes without any loss in the structural integrity, which was clearly visible to the naked eye. However, electrical sheet resistance values of the cured and heat-treated coatings (450°C for 30 minutes) remained very high on NCG substrates (not favourable for TCO less DSC manufacturing on NCG, see section 4.1) due to inadequate lateral percolation of MWCNTs because of their agglomeration in the PI matrix. In contrast, coated ECCS substrates demonstrated Z-axis electrical conductivity due to the underlying metallic substrates, which may be favourable for DSC application if it meets the roughness requirements.

TABLE 4.1: Sheet resistance of MWCNT/PI coatings on NCG and ECCS substrates.

NCG Substrate	Sheet resistance, Ω/\square		ECCS	Sheet resistance, Ω/\square	
	350°C	450°C		% MWCNT in PI	350°C
% MWCNT in PI					
1%	---	---	1%	826.31	47.56
2%	59.44K	59.88K	2%	Z-axis*	Z-axis
3%	1.11K	1.90K	3%	Z-axis	Z-axis
4%	60.6	65.34	4%	Z-axis	Z-axis

*Z-axis resistance of ECCS: $6.7 \times 10^{-3} \Omega$

Apart from the electrical conductivity, surface characteristics may also affect the device performance. Materials with high surface roughness may cause device short-circuiting as already mentioned in the beginning of this section. Thus, to be able to qualify as a potential substrate material for DSC application, these MWCNT/PI coatings should also demonstrate a smooth surface morphology suitable for device fabrication.

Figures 4.4 and 4.5 represent average roughness (R_a) and average peak height (R_p) of MWCNT/PI coatings on NCG and ECCS substrates at various temperatures. Despite the extremely high R_a and R_p values demonstrated by the MWCNT/PI coatings it was evident from the figures, that in most cases R_a and R_p values of cured coatings (at 350°C) on both the substrates remained almost same. Even after their high temperature heat treatment at 450°C up to 30 minutes. This suggests a good structural integrity and uniform pigment distribution in the polymer matrix.

However, in some cases significant variation in the R_a and R_p values was observed. For instance, R_a and R_p values of 2 wt% MWCNT/PI coating on NCG substrate appear to have significant variation before and after heat treatment (Figure 4.4). This could be due to the presence of bigger MWCNT agglomerates in the coating. A similar trend was observed in case of 1 wt% MWCNT/PI on ECCS exhibiting a substantial deviation in the R_p values before and after high temperature heat treatment (Figure 4.5).

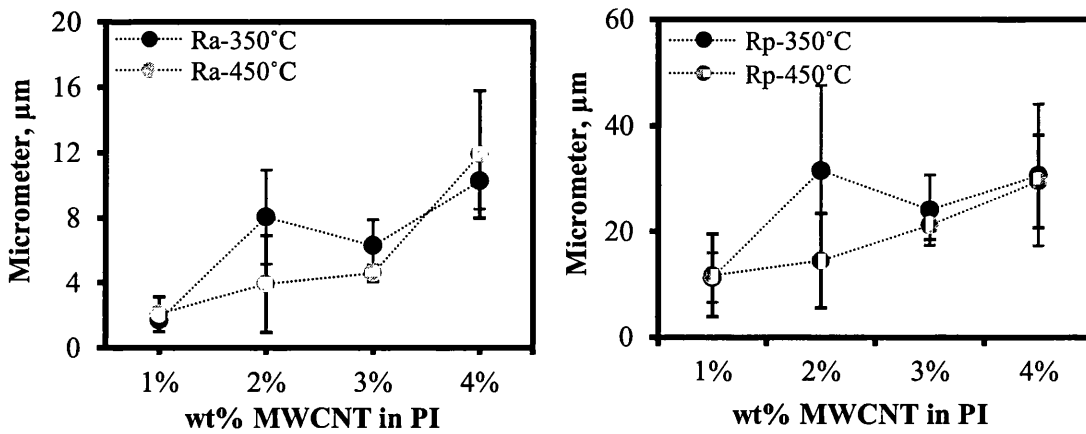


FIGURE 4.4: R_a and R_p of MWCNT/PI on non-conducting glass.

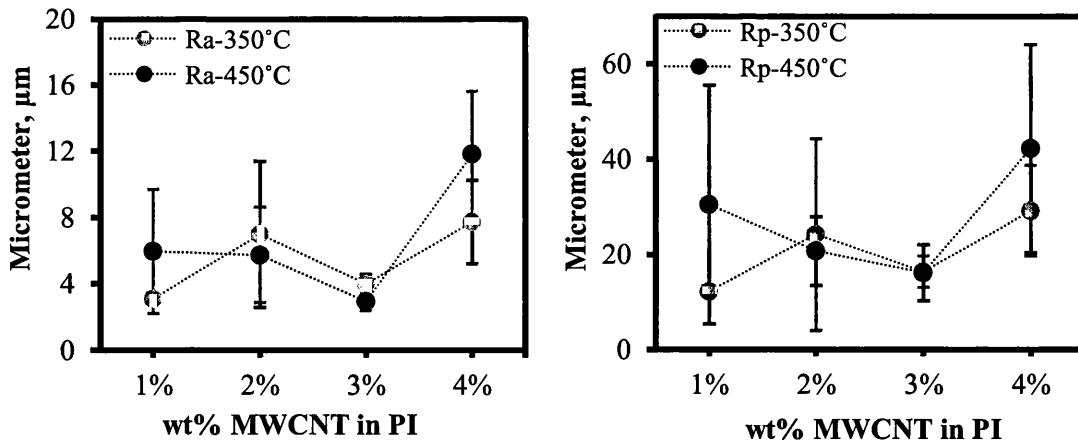


FIGURE 4.5: R_a and R_p of MWCNT/PI on ECCS.

It is important to mention in this case that the R_a and R_p values of developed MWCNT/PI based coatings (Figures 4.4 and 4.5) were also higher than the uncoated substrate materials and the un-pigmented polyimide films. It can be seen from Table 4.2 that the R_a and R_p values of glass and un-pigmented PI (cured and heat-treated films on NCG) were $\leq 0.1 \mu\text{m}$. This means both the glass and 0 wt% PI demonstrate an even surface morphology. In contrast, the R_a value of un-coated ECCS (Table 4.2) was approximately $1 \mu\text{m}$. This means the surface of ECCS is rougher than the non-conductive glass or un-pigmented PI films. In addition, the R_p ($2.96 \mu\text{m}$) value obtained from the ECCS surface scan was also higher than the glass and un-pigmented PI. Therefore, it may appear in this case that a substrate with ECCS like surface characteristics might not be suitable for DSC application. However, in reality it could be possible to construct a device on such a substrate as the gasket used for device sealing is sufficiently thick ($25\text{-}50 \mu\text{m}$ for a typical gasket) to prevent device short-circuiting.

TABLE 4.2: R_a and R_p values of uncoated substrates and un-pigmented PI films.

Quantities (μm)	ECCS	NCG	0% PI 350°C	0% PI 450°C
R_a	0.96	0.01	0.04	0.02
R_p	2.96	0.03	0.08	0.08

Changes in coating thickness with temperature may appear irrelevant in this context but it provides important information regarding the thermal stability of the coatings. Most polymers shrink because of high-temperature heat treatment but certain engineering polymers such as PI are said to be stable up to 500°C . Figure 4.6 shows a thermogravimetric (TG) analysis curve of polyimide (PI) used in this research. It can be seen from the figure that polyimide possesses excellent thermal stability up to 500°C . However, significant amount of weight loss was observed in the beginning of the TG analysis, which was due to the evaporation of the NMP (N-methyl-2 pyrrolidone) solvent base of the polyamic acid.

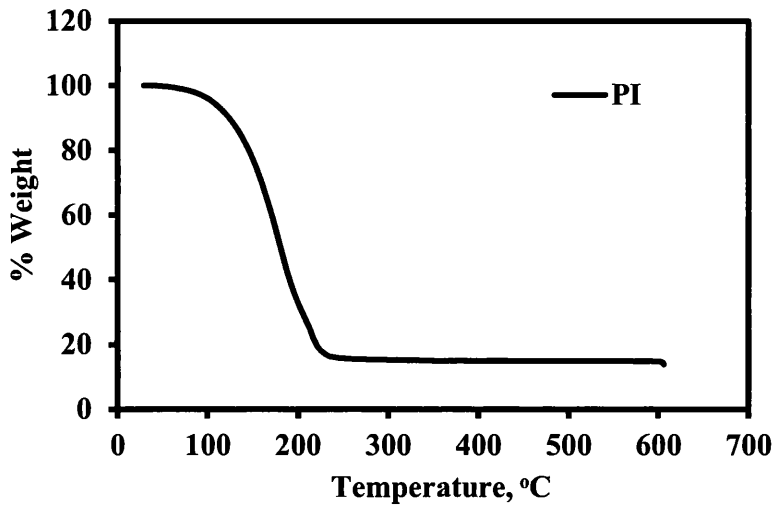


FIGURE 4.6: TG analysis of polyimide precursor.

Hence, it is evident from the TG analysis that the outstanding thermal stability of PI will also be translated into the pigmented PI coatings making them to withstand high temperature heat treatments involved in DSC processing. This is evident from the thickness measurements of MWCNT/PI coatings using a stylus profilometer before and after high-temperature (450°C) heating steps. Figure 4.7 shows the effect of high temperature heat treatment on the thickness of MWCNT/PI coatings. Profilometry data obtained in this case were based on both coated NCG (Figure 4.7, a) and ECCS (Figure 4.7, b) substrates. It can be seen from Figure 4.7 that MWCNT/PI coatings may withstand high temperature heat treatment up to 450°C for 30 minutes.

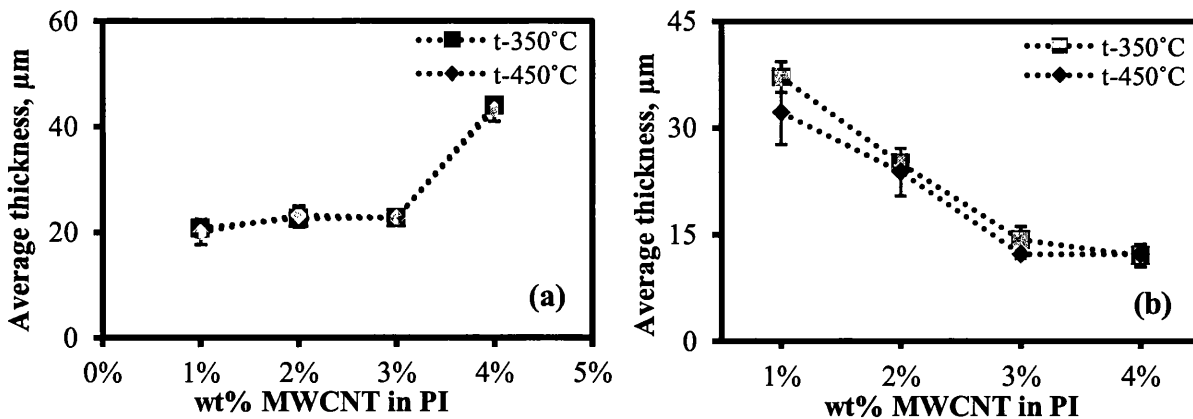


FIGURE 4.7: Average thickness of MWCNT/PI on (a) NCG and (b) ECCS.

It is evident from the figure that the thickness of cured coatings (at 350°C) did not change substantially after the high temperature (at 450°C) heating step. This suggests that the pigmented PI coatings do not shrink as a result of high temperature heat treatments and thus can be used as a protective layer for metal mounted DSCs.

However, it is evident from Figures 4.4 and 4.5 that successful device fabrication on MWCNT/PI coatings is highly unlikely in this case due to extremely coarse surface roughness with R_p values over 25 μm . This exceeds the thickness of an ideal gasket and due to this reason even coated ECCS with Z-axis conductivity will not qualify as a potential substrate for DSC application.

4.3.2 MWCNT and graphite containing PI coatings

It has already been seen in Table 4.1 and Figures 4.4 and 4.5 that MWCNT added polyimide coatings were non-ideal for DSC application due to their high surface roughness and high sheet resistance values. In order to address this issue, graphite particles were added to the MWCNT in the polyimide matrix. Graphite is a soft material and well known for its lubrication properties therefore it was hoped that the addition of graphite could possibly lead to lower R_a and R_p values. Moreover, graphite is a good conductor of electricity. Therefore; addition of graphite could support MWCNT in terms of overall improvement in the electrical conductivity of the developed coatings. This can be observed from Table 4.3 where sheet resistance of graphite/MWCNT/PI coatings on NCG substrates tend to decrease with an increase in the amount of graphite added. In this manner, 35 wt% graphite and 1 wt% MWCNT added PI demonstrated the lowest possible sheet resistance values (8.95 and 7.48 Ω/\square respectively) on NCG substrate (lower than a typical FTO coating). On the other hand, Z-axis conductivity was demonstrated by coated ECCS substrates. It is also evident from Table 4.3 that high temperature heat treatment at 450°C caused an increase in the electrical conductivity of the coatings due to improved interconnection between graphite and MWCNT particles.

Better interconnection between the carbon particles was possible in this case as fine graphite particles ($\sim 1\text{-}2 \mu\text{m}$) might occupy the gaps between large MWCNT agglomerates (see section 4.3.1) forming a more continuous conductive network. Table 4.3 further shows that graphite/MWCNT/PI coatings possess lower sheet

resistance than MWCNT/PI coatings (Table 4.1) thus could be useful for DSC application if, in addition, they possess low surface roughness.

It was observed that graphite addition does affect the average roughness of the cured coatings by reducing it to some extent. However, the presence of scattered MWCNT agglomerates within the coating continued to demonstrate significantly high roughness values, which could lead to short-circuiting of the fabricated DSCs. A typical surface profile (Figure 4.8) of graphite/MWCNT/PI shows a relatively smooth surface compared to MWCNT/PI coatings, however MWCNT agglomerates can easily be spotted from the sharp peaks present in the profile that represent R_p of the coating.

TABLE 4.3: Sheet resistance values of graphite/MWCNT/PI coatings on NCG and ECCS substrates.

NCG Substrate	Sheet resistance, Ω/\square		ECCS	Sheet resistance, Ω/\square	
	350°C	450°C		% Graphite/MWCNT in PI	350°C
25%G/1%CNT	28.54	24.5	25%G/1%CNT	Z-axis	Z-axis
30%G/1%CNT	15.52	13.37	30%G/1%CNT	Z-axis	Z-axis
30%G/2%CNT	12.38	10.04	30%G/2%CNT	Z-axis	Z-axis
35%G/1%CNT	8.95	7.48	35%G/1%CNT	Z-axis	Z-axis
35%G/0.5%CNT	12.94	11.28	35%G/0.5%CNT	Z-axis	Z-axis

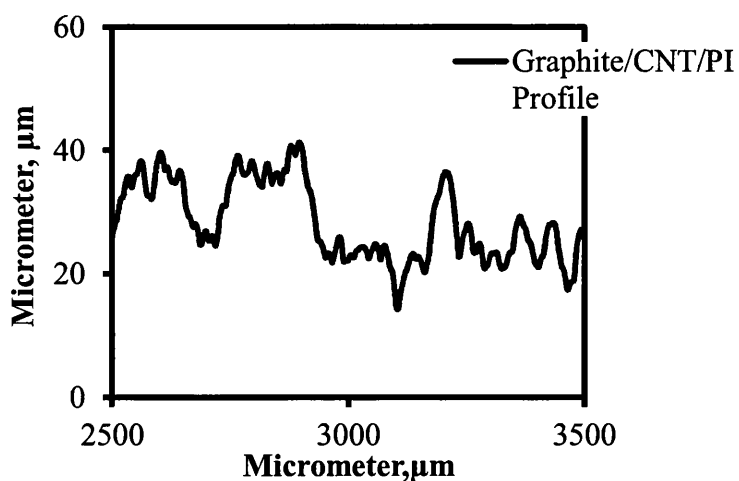


FIGURE 4.8: Surface profile of a typical graphite/MWCNT/PI coating.

To further investigate, the surface characteristics of graphite/MWCNT/PI, surface profiles of all the developed compositions (Table 4.3) were recorded before and after high temperature heat treatment. The R_a and R_p values obtained in this case are graphically presented in Figures 4.9 and 4.10. Figure 4.9 corresponds to the coated NCG followed by Figure 4.10 dedicated for coated ECCS substrates.

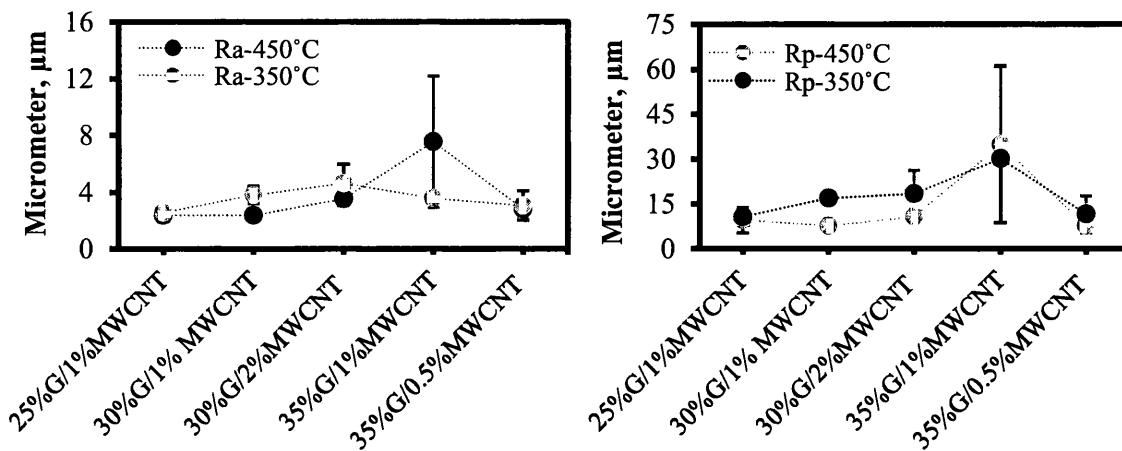


FIGURE 4.9: R_a and R_p of Graphite-MWCNT/PI on non-conducting glass.

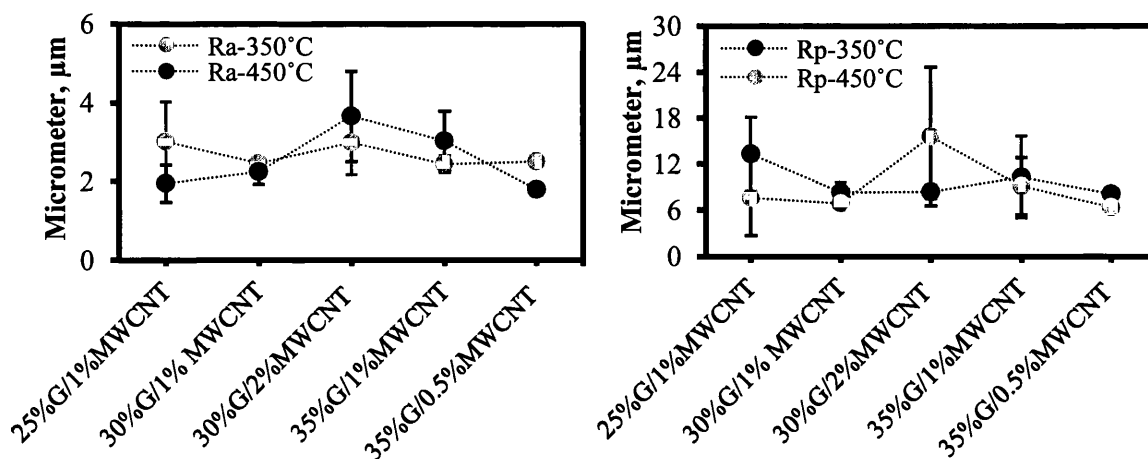


FIGURE 4.10: R_a and R_p of Graphite-MWCNT/PI on ECCS.

It is evident (Figures 4.9 and 4.10) that graphite/MWCNT /PI coatings displayed slightly lower R_a and R_p values (in average) than MWCNT/PI based coatings. For instance, Figure 4.11 shows a direct comparison between the average R_a and R_p values of MWCNT/PI and graphite/MWCNT/PI coatings after the high temperature heat treatment at 450°C for 30 minutes. Lower R_a and R_p values demonstrated by graphite/MWCNT/PI coatings were due to the presence of soft graphite particles, which helped reduce the R_a and R_p values of the coatings by mixing homogeneously

with the MWCNT agglomerates. However, some scattered MWCNT agglomerates remain and display higher R_p values in some cases. Scattered MWCNT also caused a substantial variation in the measured R_p values of some compositions. For example, significant variation in R_p values was observed (Figures 4.9 and 4.10) in case of 35 wt% graphite/1 wt% MWCNT/PI (on NCG) and 30 wt% graphite/2 wt% MWCNT/PI (on ECCS) coatings before and after the high temperature heating step.

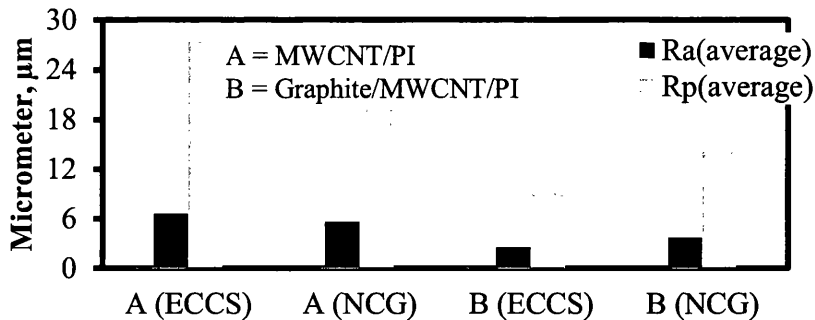


FIGURE 4.11: Average R_a and R_p values of MWCNT/PI and graphite/MWCNT/PI coatings at 450°C.

It is evident from Figure 4.11 and Table 4.3 that graphite additions in this case do have some positive effects on the surface roughness and the electrical properties of the developed coatings. However, the average R_a and R_p values of such coatings are still high ($R_a > 3\mu\text{m}$ and $R_p > 11\mu\text{m}$ at 450°C) and fluctuate significantly depending on the distribution of MWCNT agglomerates in the matrix.

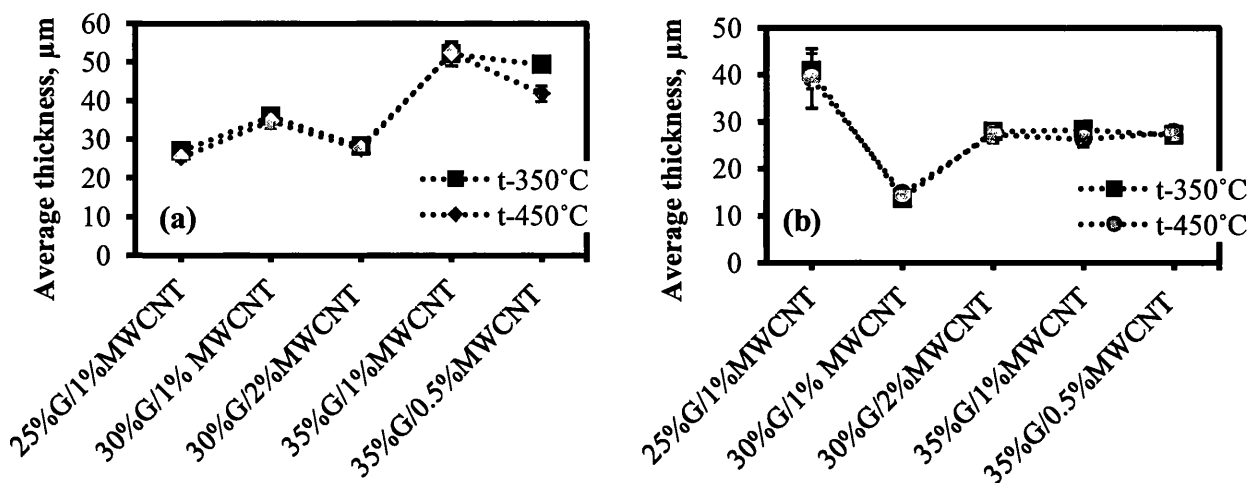


FIGURE 4.12: Graphite/MWCNT/PI on (a) NCG and (b) ECCS: coating thickness vs. temperature.

Thus, presence of MWCNT gives rise to an inhomogeneous surface characteristic that is not ideal for DSC fabrication although the coatings appear to display high temperature stability up to 450°C for approximately 30 minutes, as Figure 4.12 shows no significant variation in the coating thickness on both NCG and ECCS substrates.

4.3.3 Graphite added polyimide coatings

The MWCNT based coatings were initially developed because of its excellent electrical properties that have been previously reported. It was believed that coatings with MWCNT might perform better in terms of their electrical conductivity and hence could be utilized for DSC application. However, experimental results in sections 4.3.1 and 4.3.2 suggest that MWCNT/PI and graphite/MWCNT/PI coatings demonstrate uneven surface characteristics and due to this reason they may not be suitable for DSC application. Thus, in order to overcome this problem graphite/PI based coatings were studied. Graphite is soft and electrically conductive material, which is used as filler for a number of applications such as in adhesives and paints [12]. Therefore, it could be possible to formulate graphite added polyimide coatings that may demonstrate comparatively low surface roughness and high electrical sheet resistance values favourable for DSC application.

A typical graphite/PI coating represented in Figure 4.13 exhibits relatively smooth surface profile compared to its MWCNT based counterparts. Unlike MWCNT based coatings, peaks responsible for high R_p values are less prominent in this case (see Figures 4.2 and 4.8).

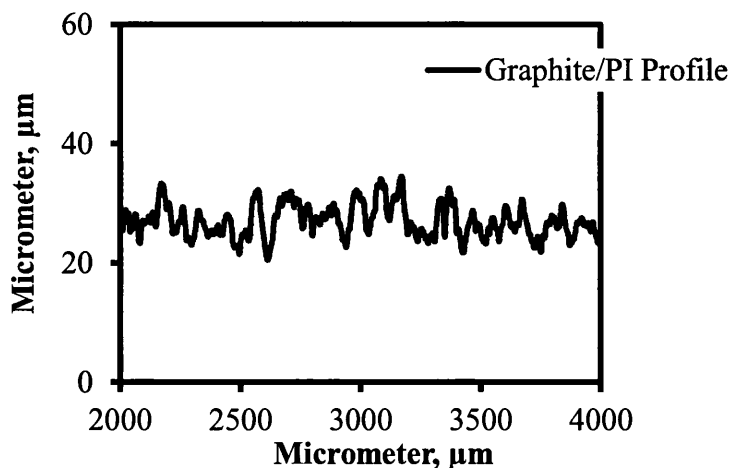


FIGURE 4.13: Surface profile of a typical graphite/PI coating.

This gives an indication that graphite/PI coatings might fulfil the requirement of an even surface needed for DSC manufacturing. However, they must also meet the substrate conductivity requirement (see section 4.3.1) for DSC application.

Table 4.4 shows that gradual addition of graphite particles in the PI matrix results in reduction in the electrical sheet resistance of the cured coatings (350°C treated) on NCG substrates. Heat treatment at 450°C for 30 minutes further reduces the sheet resistance to a significant amount. For instance, sheet resistance of 40 wt% graphite added polyimide coating was reduced from 21.36 Ω/\square to 13.41 Ω/\square after its heat treatment at 450°C for 30 minutes. Reduction in the sheet resistance followed by high temperature heat treatment could be due to better interconnection between small graphite particles ($\sim 2 \mu\text{m}$) present in the organic matrix. It is however, important to mention in this case that the formulation becomes highly viscous beyond 40 wt% graphite concentration in the polymer matrix; hence, it will no longer be suitable as a coating if graphite concentration exceeds 40% by the weight of the polymeric precursor. It can be seen from Table 4.4 that in most cases graphite/PI coatings on ECCS and NCG substrates demonstrate Z-axis conductivity and low sheet resistance values respectively apart from the 10 wt% graphite. This was due to inadequate percolation of graphite particles present in such a coating. The percolation between graphite particles was found to increase with graphite loading (in case of coated NCG substrates). In this manner a sudden drop in sheet resistance was observed (initiation of Z-axis conduction in case of coated ECCS, changes in sheet resistance could not be observed due to the underlying metal) when the concentration of graphite particles was increased to 20 wt%.

TABLE 4.4: Sheet resistance values of graphite/PI based coatings on ECCS and NCG substrates.

ECCS	Sheet resistance, Ω/\square		NCG Substrate	Sheet resistance, Ω/\square	
	350°C	450°C		% Graphite in PI	350°C
10%	78.41	76.51	10%	2.84K	1.91K
20%	Z-axis	Z-axis	20%	151.26	105.63
30%	Z-axis	Z-axis	30%	71.91	61.58
40%	Z-axis	Z-axis	40%	21.36	13.41

This point is known as percolation threshold after which the sheet resistance started to decrease steadily with increasing graphite concentration in the PI. Thus, a highly interconnected network of graphite particles was formed in case of 40 wt% graphite/PI coating which demonstrated comparatively low sheet resistance values. This type of coating with highly interconnected network maybe beneficial for DSC applications as it demonstrates desirable sheet resistance (see section 4.3.1).

The R_a and R_p values of cured and heat-treated coatings on NCG and ECCS substrates are shown in Figures 4.14 and 4.15 respectively. Unlike previous sections, (see sections 4.3.1 and 4.3.2) the R_a and R_p values of graphite/PI based coatings on both the substrates were significantly lower due to the absence of MWCNT agglomerates. Consequently, consistent R_a values ($< 2 \mu\text{m}$) were observed in most cases. For instance, R_a values of 20 wt%, 30 wt% and 40 wt% graphite/PI (at 450°C) on NCG were around 1.73, 1.81 and 1.88 μm respectively (Figure 4.14). On the other hand, R_p values obtained in this case were also very consistent and relatively lower than those displayed by MWCNT based coatings (see sections 4.3.1 and 4.3.2). The average R_p value of graphite/PI coatings (on NCG and ECCS) remained between 6-7 μm , which might be acceptable for DSC application as there will be less chances of device short-circuiting due to the even surface. This is in agreement with Figure 4.13 where a typical graphite/PI coating demonstrates relatively smooth surface compared to its MWCNT based counterparts. Graphite/PI coatings also demonstrate thermal stability parallel to other MWCNT based coating (see sections 4.3.1 and 4.3.2). Figure 4.16 suggests that graphite added PI matrix could also withstand high temperature heat treatment at 450°C for a prolonged time without exhibiting any signs of coating shrinkage. The coating thickness remained almost same before and after the high temperature heat treatment. For instance, the thickness of heat-treated (450°C) 20 wt% graphite/PI (on both NCG and ECCS) remained almost identical to its cured version at 350°C (Figure 4.16). Considering the thickness trends obtained in sections 4.3.1 and 4.3.2, it is evident that the thermal stability of PI matrix is independent of the type of filler used and their physical properties. It is evident from this section that graphite/PI coatings have better electrical as well as surface properties than MWCNT based PI coatings. In addition, such coatings appear to demonstrate some thermal stability at 450°C, which is one of the essential requirements for DSC fabrication in this case.

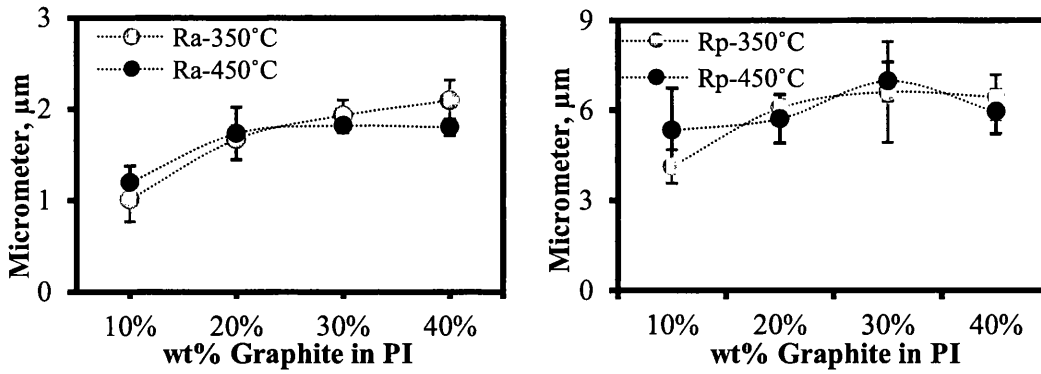


FIGURE 4.14: R_a and R_p of Graphite/PI on non-conducting glass.

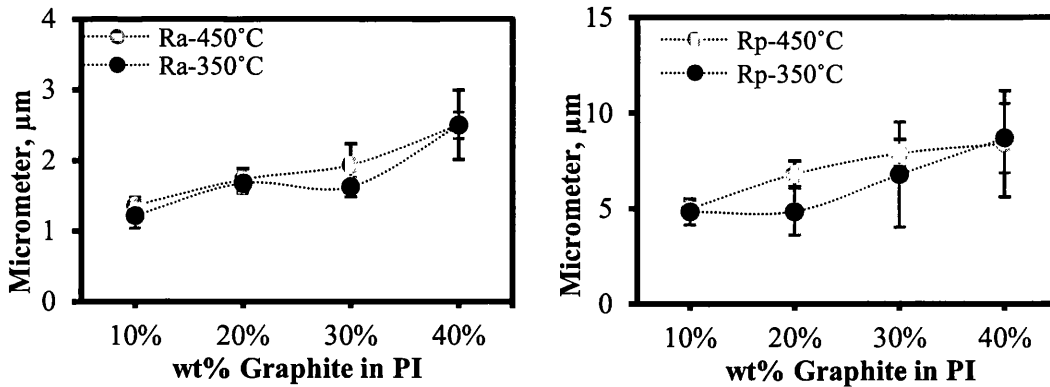


FIGURE 4.15: R_a and R_p of Graphite/PI on ECCS.

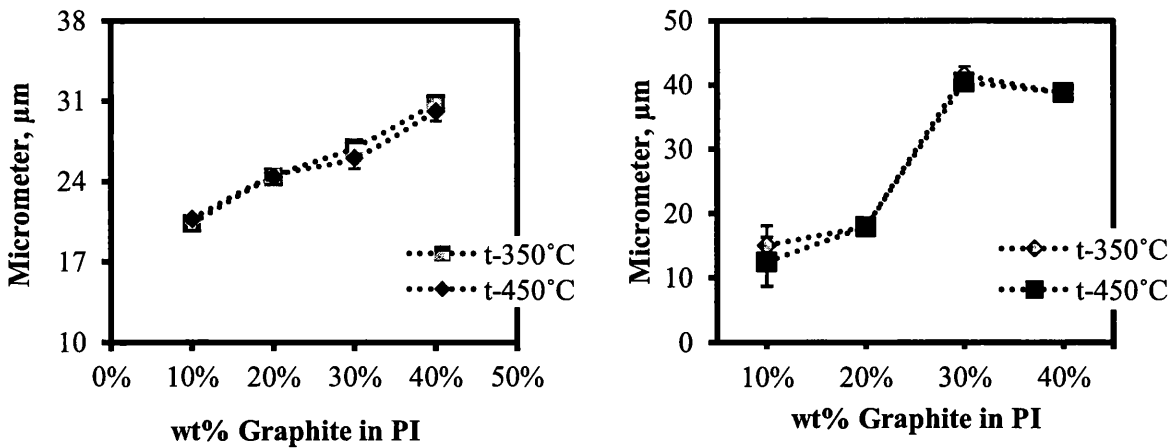


FIGURE 4.16: Coating thickness vs. temperature of graphite/PI on (a) NCG and (b) ECCS.

Therefore, the composition with 40 wt% graphite/PI will be used for DSC application due to its lower sheet resistance ($\sim 13.41 \Omega/\square$) and optimum surface characteristics ($R_a \sim 2 \mu\text{m}$ and $R_p \sim 7 \mu\text{m}$).

4.3.4 Photovoltaic Characterization

Based on electrical resistivity and surface morphology data the 40 wt% graphite added to polyimide coating was used to coat ECCS and NCG substrates in order to use them as DSC working and counter electrodes.

4.3.4.1 J-V characteristics of 40 wt% graphite/polyimide working electrodes

Figure 4.17 illustrates current voltage characteristics of DSCs based on 40 wt% graphite/polyimide coated ECCS and NCG working electrodes. Fourteen devices were constructed and their average current-voltage characteristics have been discussed in this section. It can be seen from Figure 4.17 that the average short-circuit current density (J_{sc}) obtained in case of FTO glass based cell is much higher than the cells with graphite/PI coated working electrodes. Consequently, it has been seen in Table 4.5 that FTO glass based cells demonstrated higher average photoconversion efficiency than the graphite/PI based devices. The poor photovoltaic performance of graphite/PI cells could be due to several reasons such as the catalytic nature of graphite inducing charge recombination at working electrode/electrolyte interface of graphite/PI cells; non-reflective nature of black graphite/PI coating could also be responsible for the substandard PV performance in this case. Therefore, the reason for the reduced performance will be investigated in the remainder of this chapter.

It was also alleged that variation in the TiO_2 film thickness could be one of the reasons (as an unconventional deposition technique was used, see section 2.5.1) behind poor PV performance demonstrated by graphite/PI cells. However, data presented in Table 4.5 reveal that the average TiO_2 film thickness in graphite/PI based cells is comparable to the cells with FTO glass as working electrode. Hence, the TiO_2 film thickness may not be responsible for lowering the J_{sc} values in graphite/PI cells. In addition, if there is no significant variation in the TiO_2 film thickness then there should not be any issues regarding the dye uptake by the cells as all of them were dyed in the same fashion. Considering these facts, a question may arise as to whether interfacial charge recombination in the cells is mainly responsible for such an anomalous behaviour due to the catalytic nature of graphite [13].

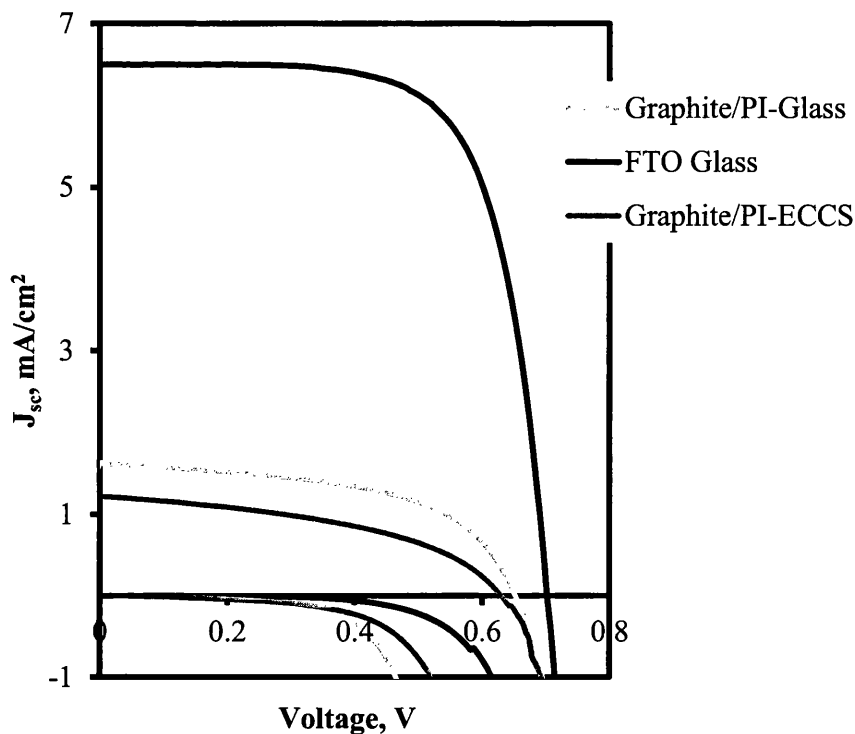


FIGURE 4.17: Average J-V characteristics of cells based on graphite/PI coated NCG, ECCS and their comparison with standard FTO glass devices.

TABLE 4.5: Average current-voltage data obtained from the solar simulation experiment.

Average current-voltage data based on 14 devices							
Cells	V_{oc} , (V)	J_{sc} , (mA/cm^2)	FF, %	η , %	R_s , Ω	R_{sh} , Ω	TiO ₂ thickness, μm
Graphite /PI- ECCS	0.61 (± 0.03)	1.2 (± 0.23)	45.74 (± 6.67)	0.35 (± 0.12)	123.83 (± 70.24)	1924.34 (± 494.82)	10.52 (± 3.21)
Graphite /PI-NCG	0.64 (± 0.01)	1.61 (± 0.51)	54.07 (± 1.57)	0.57 (± 0.2)	67.15 (± 29.38)	2225.59 (± 614.38)	11.80 (± 3.52)
FTO Glass	0.70 (± 0.00)	6.49 (± 0.32)	69.56 (± 0.08)	3.16 (± 0.15)	11.42 (± 0.49)	19983.99 (± 7566.22)	10.08 (± 2.65)

Therefore, referring back to the dark current (see sections 1.4.1.2 and 3.3.1) curves (Figure 4.17) it can be seen that graphite/PI based cells demonstrate higher average dark current than standard FTO devices. The onset of dark current in case of coated ECCS and NCG cells was around 0.3V whereas in case of FTO based devices the onset was slightly shifted towards a higher potential $> 0.3\text{V}$. The higher dark current demonstrated by graphite/PI based cell could be due to the catalytic nature of

graphite that may induce charge recombination at the substrate /electrolyte and TiO₂/electrolyte interfaces as the possibility of charge recombination at these two sites is often found to be higher in a DSC [14]. In addition, low average V_{oc} in both graphite/PI coated ECCS and NCG cells (Table 4.5) indicates faster charge recombination but this needs to be confirmed by electrochemical impedance spectroscopy.

Table 4.5 also demonstrates comparatively high series (R_s) and very low shunt (R_{sh}) resistances in both graphite/PI – ECCS and NCG cells that is likely responsible for diminishing the average fill factors in both cases. Dissimilarity in device electrodes (counter electrode was FTO glass based) could be the possible reason behind high series resistance values in this case. On the other hand, low R_{sh} could be due to the unconventional device architecture and the errors associated with it. It is needless to mention that the R_s and R_{sh} values were obtained automatically from the software dedicated for J-V measurements.

4.3.4.2 EIS of 40 wt% graphite/PI working electrodes

Dark current curves and low V_{oc} values obtained from the J-V characteristics provide a hint to the interfacial charge recombination in graphite/PI cells due to the catalytic nature of graphite. EIS is a reliable technique to obtain a generalized idea about interfacial charge recombination (see sections 1.4.1.2, 1.6.3 and 3.3.2) kinetics within a dye-sensitized solar cell. This technique is however unable to provide separate information corresponding to each interfacial recombination process taking place in a DSC. Nevertheless, EIS is a very useful tool to detect interfacial recombination in the first place. In EIS interfacial charge recombination at the substrate/electrolyte and the TiO₂/electrolyte interfaces are represented through the Nyquist plot (see sections 1.6.3 and 3.3.2) where the second semicircle (usually the bigger one) in the mid frequency region shows a combined impedance associated with both the interfacial recombination processes occurring in a DSC. Figure 4.18 shows charge recombination resistance (R_{rc}) vs. applied potential in graphite/PI and FTO glass based cells. Higher recombination resistance values displayed by standard FTO glass cells make it obvious in this figure that interfacial charge transfer kinetics in the FTO glass based cell is much slower than the graphite/PI coated cells. In addition, chemical capacitance data displayed in Figure 4.19 also suggests that the

rate of charge recombination in case of FTO based devices is slower than the graphite/PI based cells.

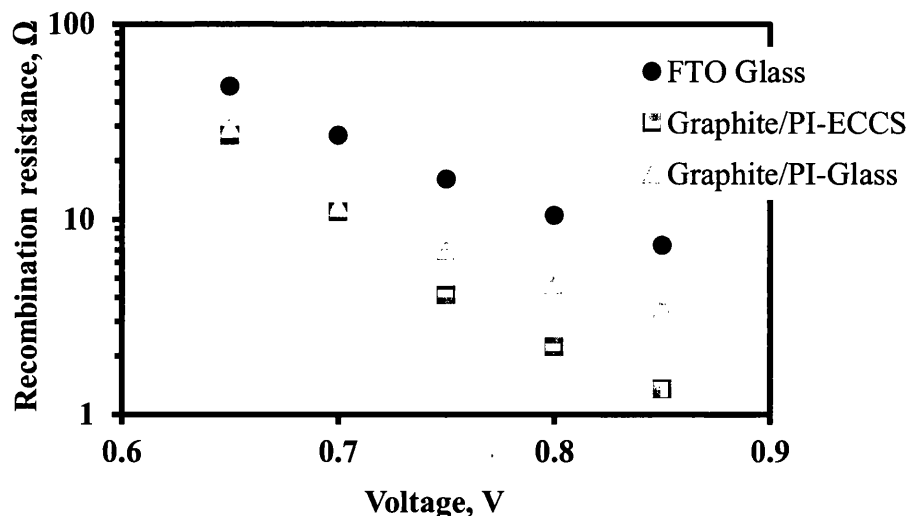


FIGURE 4.18: Average charge recombination resistance vs. voltage: based on graphite/PI coated ECCS, NCG and standard FTO cells: based on 9 best performing devices.

Lower average chemical capacitance displayed by FTO based devices supports this fact. This is vital information, which confirms that poor PV performance demonstrated by graphite/PI cells was actually due to interfacial charge recombination taking place at faster rates. This is likely due to the catalytic nature of graphite, which results in recombination via the substrate at a faster rate alongside the recombination via the TiO_2 film.

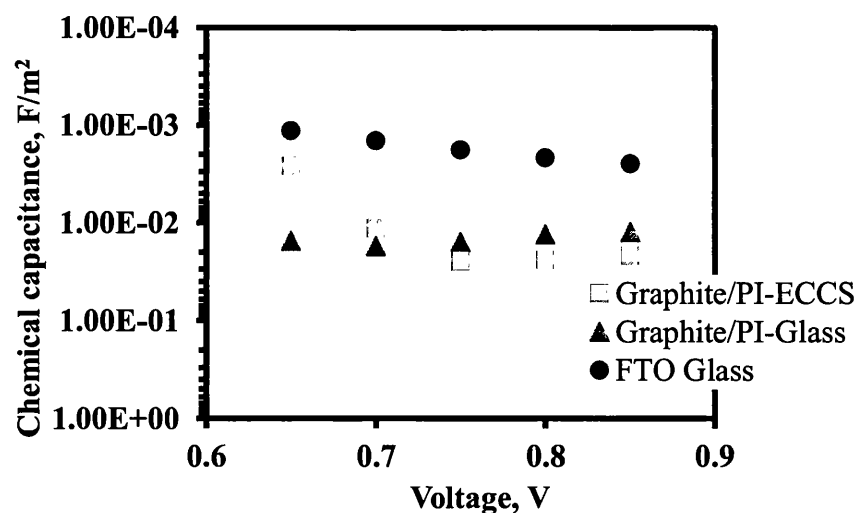


FIGURE 4.19: Average chemical capacitance vs. voltage: based on graphite/PI coated ECCS, NCG and standard FTO cells: based on 9 best performing devices.

However, photovoltage decay (PV) measurement will help collect more specific information about the type of recombination reaction occurring within a device. Results obtained from PV decay measurement have been discussed in the following subsection.

4.3.4.3 Photovoltage decay analysis of 40 wt% graphite/polyimide working electrodes

EIS analysis has already made it clear that interfacial charge recombination could be the reason behind poor PV performance displayed by the graphite/PI based cells, as it has already been seen in Figure 4.18 that interfacial charge recombination in graphite/PI cells is occurring at a faster rate. However, in addition to EIS other characterization technique is required to support this fact. Therefore, PV decay analysis was introduced to pinpoint the location of charge recombination in this case. PV decay could provide information regarding whether the recombination in graphite/PI cells is occurring at the substrate/electrolyte interface or not, as it has been assumed that the catalytic nature of graphite is responsible for catalysing the back reaction via the substrates in this case.

PV decay is an optoelectronic technique that measures V_{oc} decay over a specified time when the bias light is turned off (see sections 1.6.2 and 3.3.4). Thus, Figure 4.20 in this case shows average V_{oc} decay curves of graphite/PI based cells and their comparison with standard FTO glass devices.

It is evident from this figure that PV decay in FTO glass devices is much slower than graphite/PI based cells. This means, charge recombination at graphite/PI/electrolyte interface is taking place at a faster rate than at the FTO glass/electrolyte interface. Now it is clear in this case, that catalytic nature of graphite (Table 4.7) could be primarily responsible for interfacial charge recombination at the coated working electrode/electrolyte interface, which is vital information to explain the low J_{sc} values observed in this case. However, besides back reaction, the black colour of graphite/PI coating may also affect the J_{sc} values to a significant amount. Black coloured substrates could absorb substantial amount of visible light, which reduces the amount of reflected light interacting the photosensitive dye.

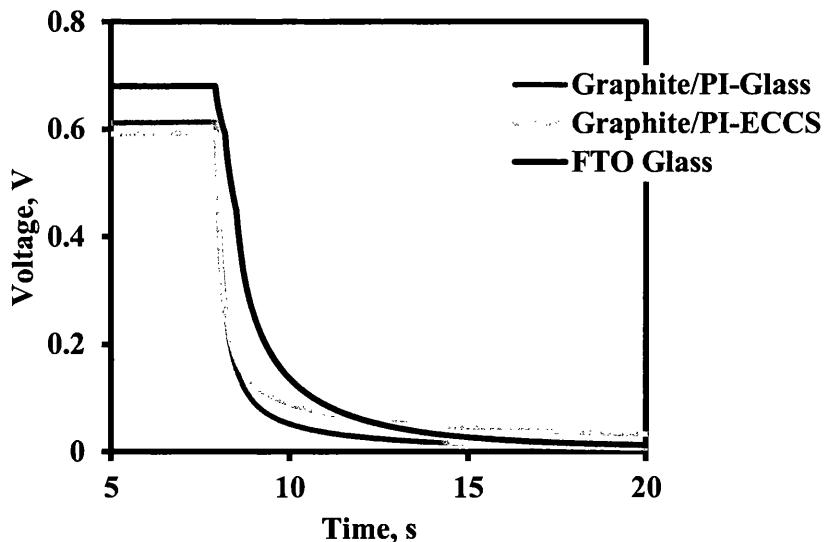


FIGURE 4.20: Photovoltage decay in DSCs based on graphite/PI coated working electrodes and their comparison with FTO glass based devices: based on 9 best performing devices.

Therefore, reflectance measurement was performed on graphite/PI coated substrates to compare their reflectance with 15 Ω/\square FTO glass substrates used to construct standard DSCs.

4.3.4.4 Reflectance measurements of 40 wt % graphite/PI and FTO glass

A spectrophotometer was used to carry out “% Reflectance” measurement on 40 wt% graphite added polyimide coatings after heat treatment at 450°C for 30 minutes.

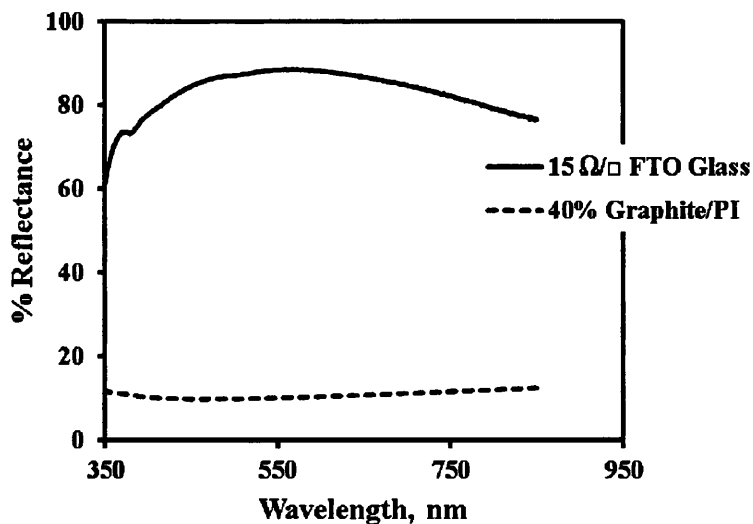


FIGURE 4.21: Comparison of “%Reflectance” between FTO glass and 40 wt% graphite/PI coatings after heat treatment at 450°C for 30 minutes.

Substrate reflectivity can significantly increase the efficiency of a dye-sensitised solar cell. Reflective substrates increase the optical path length of the light travelling through the device by returning it back to the photosensitive dye adsorbed onto the mesoporous TiO₂. Thus, more light is absorbed by the dye, which results in substantial increase in photocurrent and efficiency of the cell. It has already been seen that efficiency of a DSC with transparent electrodes is lower than the device with a reflective electrode [15]. On the other hand, if one of the electrodes is not reflective enough then it absorbs the incident light causing the photoconversion efficiency to decrease dramatically.

Figure 4.21 suggests that 40 wt% carbon added polyimide coating is significantly less reflective than fluorine doped tin oxide (FTO) coated glass in the visible region. Black colour of the coating is responsible for maximum light absorption onto its surface. Whereas, FTO coating on a transparent glass is more reflective with approximately 85% maximum reflectance at around 600 nm. Data obtained from the reflectance study concludes this experiment, as it is evident that, in addition to the back reaction at the substrate/electrolyte interface, black colour of graphite/PI coating is also responsible for diminishing the PV performance of graphite/PI based cells.

4.3.4.5 J-V characteristics of 40 wt% graphite/polyimide counter electrodes

Current voltage characteristics of graphite/polyimide coated counter electrodes (thermally platinised) has been discussed in this section. It was believed that 40 wt% graphite/PI coating could also serve as a counter electrode material in a DSC due to its conductive nature and hence could replace the expensive FTO glass CE from a typical DSC or could be used to manufacture forward illuminated glass-metal hybrid devices at lower cost. Figure 4.22 represents average J-V characteristics of 11 devices, which include platinised graphite/PI coated ECCS and NCG counter electrodes, and their comparison with standard FTO based CEs. Table 4.6 provides detailed information regarding the overall PV performance of cells fabricated under the same experimental conditions.

Current – voltage characteristics data in Table 4.6 clearly show that the average J_{sc} values obtained from the cells with graphite/PI (platinized) coated counter electrodes (6.65 mA/cm² for ECCS and 6.98 mA/cm² for non-conducting glass) were

comparable to the one displayed by standard cells with platinized FTO glass counter electrodes (average $J_{sc} = 8.19 \text{ mA/cm}^2$). However, a slight variation in their average photoconversion efficiencies was observed (Table 4.6). Emergence of high J_{sc} values in this case was associated with FTO glass working electrodes, which had been used to fabricate all the cells. However, the average J_{sc} values of graphite/PI counter electrode based devices were slightly lower than the standard FTO glass cells. This could be due to different counter electrode materials (graphite/PI and FTO) and the catalytic activity of Pt, which may also vary with the material characteristics. On the other hand, V_{oc} of the cells with graphite/PI coated counter electrodes remained relatively high without any visible anomalies. However, presence of low shunt resistance and slightly high series resistance in graphite/PI counter electrode based cells did affect the average fill factor of the cells by reducing it to a significant amount compared to the cells with FTO glass counter electrodes.

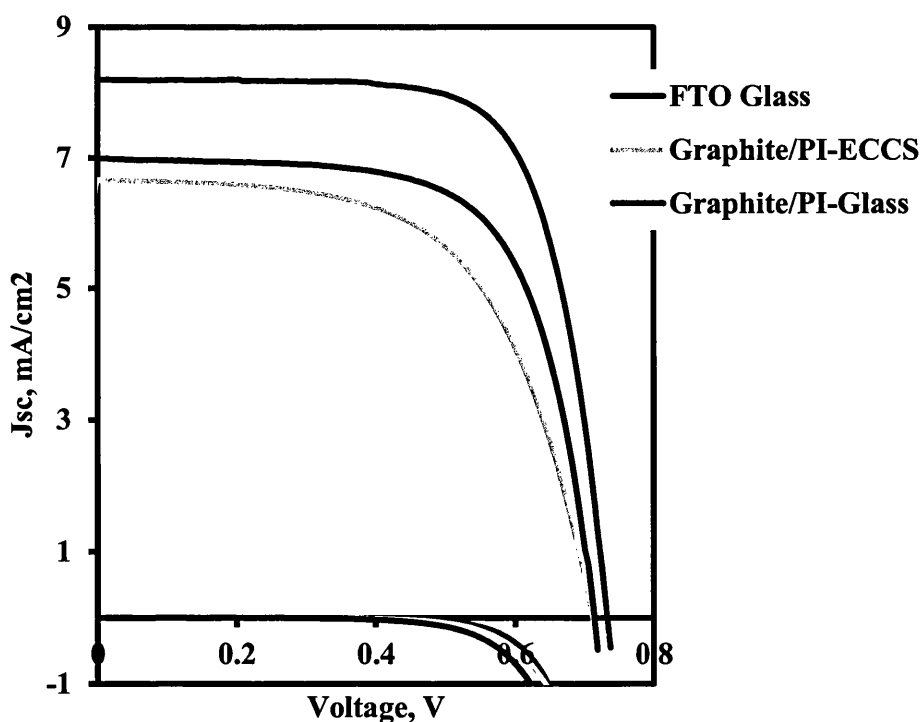


FIGURE 4.22: Average current-voltage characteristics of graphite/PI coating on NCG and ECCS substrates as counter electrodes and their comparison with a standard FTO glass cell.

TABLE 4.6: J-V characteristics of graphite/PI coated ECCS and non-conducting glass counter electrodes with platinum catalyst.

Average J-V Characteristics of Graphite/PI Coated Counter Electrodes: Based on 11 devices						
<i>Cells</i>	$V_{oc}, (V)$	$J_{sc}, (mA/cm^2)$	$FF, \%$	$\eta, \%$	R_s, Ω	$R_{sh} \Omega$
Graphite/PI -ECCS	0.70 (±0.00)	6.65 (±0.88)	59.44 (±5.60)	2.83 (±0.56)	21.29 (±6.82)	4482.08 (±1801.17)
Graphite/PI -Glass	0.71 (±0.00)	6.98 (±1.29)	67.19 (±1.55)	3.35 (±0.69)	12.48 (±3.49)	4085.34 (±191.41)
FTO Glass	0.73 (±0.00)	8.19 (±0.15)	71.68 (±1.20)	4.29 (±0.14)	10.19 (±1.16)	24393.37 (±18427.15)

Catalytic performance of the platinum present in the counter electrodes can also affect the photovoltaic performance of the fabricated cells. Table 4.7 clearly shows that the cells without platinum catalyst demonstrated extremely poor PV performance. V_{oc} , J_{sc} , and fill factor were severely affected by the extremely high series and substantially low shunt resistance values in this case. However, it can be seen from Table 4.7 that graphite/PI coating does have some catalytic activity but it is insufficient to catalyse triiodide reduction to any great extent although it is better than a simple FTO surface but certainly not as good as a platinized surface.

TABLE 4.7: Average J-V characteristics of graphite/PI coated ECCS and non-conducting glass counter electrodes without platinum catalyst.

Counter Electrodes Without Pt-catalyst: Average J-V characteristics based on 9 best performing cells						
<i>Cells</i>	$V_{oc}, (V)$	$J_{sc}, (mA/cm^2)$	$FF, \%$	$\eta, \%$	R_s, Ω	$R_{sh} \Omega$
Graphite/ PI-ECCS	0.63 (±0.07)	3.40 (± 1.34)	7.30 (± 2.07)	0.14 (±0.01)	3176.63 (± 802.53)	62.85 (± 46.42)
Graphite/ PI-Glass	0.38 (± 0.06)	2.54 (± 2.74)	14.54 (± 0.86)	0.12 (±0.11)	716.16 (± 289.34)	159.25 (±122.8)
FTO Glass	0.56 (± 0.04)	1.81 (± 0.38)	4.44 (± 0.42)	0.04 (±0.01)	140476.21 (±59765.32)	39.63 (± 9.44)

4.3.4.6 EIS of 40 wt% graphite/polyimide counter electrodes

Electrochemical impedance studies were performed on 9 best performing devices out of 11 already discussed in subsection 4.3.4.5. DSCs based on platinized graphite/PI coated counter electrodes show similar characteristics to the platinized FTO glass based counter electrodes. Figure 4.23 illustrates the average charge-transfer resistance at the counter electrode/electrolyte interface of the fabricated DSCs based on coated ECCS and non-conducting glass counter electrodes. It is clearly visible in this cases; that all coated counter electrodes with thermally decomposed platinum perform similarly to the platinized FTO glass counter electrodes. At voltage close to V_{oc} , (in this case V_{oc} of the device) the charge transfer resistance was found to be low in all cells indicating fast electron transfer from the counter electrodes to the triiodide species of the redox couple. High electron transfer rates displayed by the graphite/PI coated counter electrodes suggest that the decomposition of chloroplatinic acid on the rough graphite/PI surface is successfully completed.

Electrical double layer capacitance (C_{dl}), commonly known to represents the amount of charge stored at the interface between a conductive electrode and a liquid electrolyte) [16] between the platinised graphite/PI based counter electrodes and the electrolyte depends on the catalytic activity and the surface area of the platinized counter electrodes. Double layer capacitance is normally proportional to the surface area and the catalytic activity of the platinum catalyst, which means higher C_{dl} values correspond to greater catalytic activity and faster triiodide reduction at the counter electrode/electrolyte interface of a device.

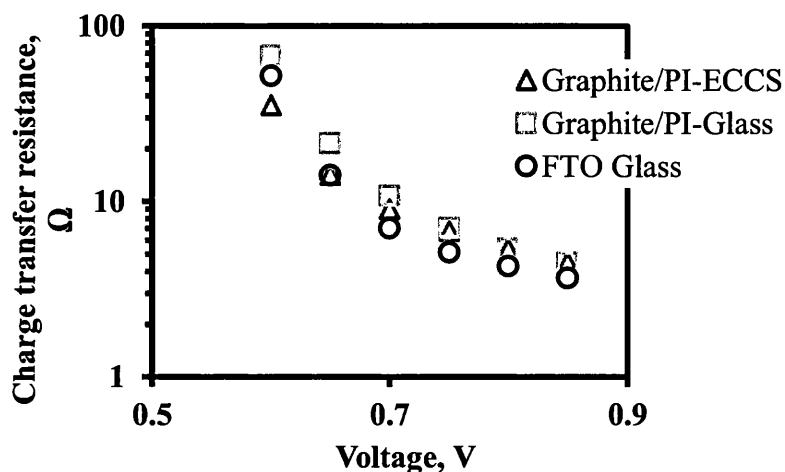


FIGURE 4.23: Average charge transfer resistance vs. voltage.

Figure 4.24 illustrates a comparison between the electrical double layer capacitance at the platinized FTO counter electrode/electrolyte interface and the platinized graphite/PI electrodes/electrolyte interface. It is clearly visible in this case that the average C_{dl} values of devices with graphite/PI coated NCG counter electrodes are almost identical to the cells with FTO glass CEs. However, the average C_{dl} values of cells with graphite/PI coated ECCS counter electrodes were slightly lower in this case. This could be due to the poor catalytic performance of the Pt catalyst.

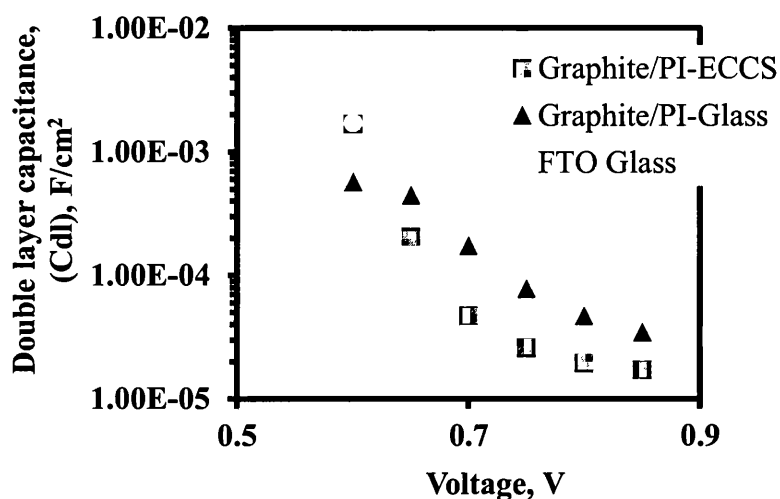


FIGURE 4.24: Average double layer capacitance vs. voltage.

4.4 Conclusions

The high roughness of carbon filled polyimide coatings could have been controlled using various methods such as functionalization of MWCNTs or sonication of the prepared formulations. However, such methods were not tried because it was already evident from preliminary experiments that carbon based polyimide coatings (graphite/PI, see section 4.3) were not suitable for DSC application due to their involvement in faster charge recombination kinetics in the fabricated DSCs. In addition, functionalization of MWCNTs is an entirely different field of study in terms of materials selection and optimization of physical properties of functionalized MWCNTs. This could be a time consuming approach therefore it was irrelevant to this study. Sonication on the other hand could lead to structural distortion of

MWCNTs affecting vital physical properties such as electrical conductivity (see section 4.3). Therefore, sonication was not an appropriate choice in this case.

As a result, Multiwalled carbon nanotubes added polyimide coatings displayed very high R_a and R_p values therefore were deemed unsuitable for DSC application. Thus, 40 wt% graphite added polyimide coating was used to manufacture DSCs due to its comparatively smooth surface and high temperature resistant properties. Furthermore, due to high electrical conductivity, this coating can also be used to coat non-conducting soda glass substrates as a replacement for the transparent conductive oxide coated glass. Dye-sensitized solar cells based on 40 wt% graphite/PI coated ECCS and NCG working electrodes exhibited signs of charge recombination at the coating/electrolyte interface that led to very poor PV performance. In addition, the black colour of the graphite/PI coating absorbed significant amount of incident light resulting in a substantial reduction in the J_{sc} values. However, DSCs with 40 wt% graphite/PI coated ECCS and NCG counter electrodes with thermally decomposed platinum demonstrated comparable PV performance to the platinized FTO based standard device.

Hence, it can be concluded from this study that 40 wt% graphite/PI based composite coating is not suitable for DSC working electrode application but it could be useful in manufacturing TCO less counter electrodes at a lower cost.

4.5 References

- [1] Steels for packaging, Arcelor Mittal, <http://fce.arcelormittal.com/packaging/493>
- [2] Packaging steels, TATA Steel, http://www.tatasteeleurope.com/en/products_and_services/products/flat/packaging_steels/
- [3] G24 Innovations, Commercial dye-sensitized solar cells, <http://www.g24i.com/pages,energy-harvesting,66.html>
- [4] Trystan Martyn Watson, Ian Mabbett, David Anthony Worsley, "Method for the Manufacturing of a Photovoltaic device", Patent No. WO 2010115584 A3, Tata Steel UK Limited, July 2011.
- [5] Dirk M. Guldi, Nazario Martin, in "Carbon Nanotubes and Related Structures: Synthesis, Characterization, Functionalization, and Applications", John Wiley & Sons, Jan 2010.
- [6] Bruce C. Gates, Helmut Knoezinger, Friederike C. Jentoft, in "Advances in

- Catalysis”, Academic Press, Feb 2009.
- [7] Geological Survey (U.S), in “Minerals Yearbook, 2008, V. 1, Metals and Minerals”, Government Printing Office, 2011.
- [8] K. L. Mittal, in “Polyimides and Other High-temperature Polymers: Synthesis, Characterization, and Applications”, vol. 5, BRILL, Apr 2009.
- [9] Y. Ando, X. Zhao, H. Shimoyama, G. Sakai, and K. Kaneto, “Physical properties of multiwalled carbon nanotubes”, *International Journal of Inorganic Materials*, vol. 1, pp. 77-82, Apr 1999.
- [10] Henry Kuo Feng, Nanda Gopal Sahoo, Lin Li, Siew Hwa Chan, Jianhong Zhao “An Innovative Approach for the Fabrication of Highly Conductive Nanocomposites with Different Carbon” *Proceedings of the 36th international MATADOR conference*, Springer, 2010.
- [11] Y. Y. Huang and E. M. Terentjev, “Dispersion of Carbon Nanotubes: Mixing, Sonication, Stabilization, and Composite Properties”, *Polymers*, vol. 4, pp. 275-295, Mar 2012
- [12] <http://www.masterbond.com/properties/graphite-filled-electrically-conductive-adhesives>.
- [13] Y.-S. Wei, Q.-Q. Jin, and T.-Z. Ren, “Expanded graphite/pencil-lead as counter electrode for dye-sensitized solar cells”, *Solid-State Electronics*, vol. 63, pp. 76-82, Sep 2011.
- [14] M. Manca, F. Malara, L. Martiradonna, L. De Marco, R. Giannuzzi, R. Cingolani, Giuseppe Gigli, “Charge recombination reduction in dye-sensitized solar cells by means of an electron beam-deposited TiO₂ buffer layer between conductive glass and photoelectrode”, *Thin Solid Films*, vol. 518, pp. 7147-7151, Sep 30 2010.
- [15] Y. Liu, H. Shen, X. R. Huang, and Y. J. Deng, “A new improved structure of dye-sensitized solar cells with reflection film”, *Chinese Science Bulletin*, vol. 51, pp. 369-373, Feb 2006.

CHAPTER 5

TITANIUM NITRIDE/POLYIMIDE COATINGS FOR DYE-SENSITIZED SOLAR CELL APPLICATIONS

5.1 Introduction

In the previous chapter, it was observed that ECCS and non-conducting glass substrates (NCG) coated with 40 wt% graphite/polyimide coating performed reasonably well as DSC counter electrodes but not as working electrodes due to very high interfacial charge recombination at the working electrode/electrolyte interface. Although, carbon/polyimide coatings were thermally stable but high surface roughness of such coatings (specially the R_p values) increased the possibility of detrimental device short-circuiting. Therefore, it was concluded that carbon coatings are not suitable for DSC applications where the intention is to develop a coating that has the potential to act as both a working and counter electrode for dye-sensitised solar cells based on low cost substrates such as ECCS and non-conducting soda glass.

Therefore, an alternative material is required with physical properties similar to the carbon materials, including high electrical conductivity and excellent thermal stability. In addition to carbon, there are a few materials available such as tungsten carbide and titanium nitride, which are chemically inert, thermally stable and sufficiently conductive in nature. Titanium nitride (TiN) is one good candidate, which has a cubic crystal structure and is extremely hard in nature ^[1]. Titanium nitride is a chemically inert, ceramic material and is 50 times more conductive than elemental graphite ^[2,3]. Thus, TATA steel the industrial sponsor of this research was interested in the application of TiN in DSC technology.

Titanium nitride is a versatile material with a number of uses ranging from cutting tools to abrasion resistant coatings ^[4]. In addition, superior electrical conductivity of this material makes it ideal for various electronic applications including dye-sensitised solar cells. Titanium nitride based counter electrodes are being investigated in current DSC research. However, DSC working electrodes based on TiN are very rare to find in the research literature ^[5,6]. A detail description regarding the application of TiN in DSC technology can be found in section 1.9.8.

Therefore, this work involves development of a novel coating based on TiN and a polyimide system. The primary aim of this work is to address the roughness and charge recombination related issues that remained unsolved in the previous chapter

based on carbon coatings. Thus, success of this work could offer a reliable low cost alternative to the expensive titanium metal and the FTO glass electrodes [7-11].

5.2 Experimental

This chapter deals with the roughness related issues more carefully by studying surface characteristics of doctor bladed TiN/PI coatings prepared on non-conductive glass (NCG) substrates according to the method already described in section 2.3.2. TiN/PI coated NCG substrates were dried at 150°C for 150 seconds followed by curing at 350°C for 5 minutes.

Coating characteristics such as R_a (average roughness) and R_p (average peak height) of cured TiN/PI coatings were measured simultaneously using a stylus profilometer (see section 2.4.2). The same measurements were repeated after high temperature heat treatment of cured TiN/PI coatings at 450°C for 30 minutes to assess the variation in R_a and R_p values after the high temperature heating process. In addition, coating sheet resistance was also measured after curing and during the high temperature heat treatment process at 450°C for 30 minutes. Based on complete surface and electrical characterization, the best composition with optimized properties was then selected for DSC applications.

Finally, a complete photovoltaic analysis is presented based on the best performing TiN/PI coated substrates (ECCS and NCG) as working and counter electrodes in reverse and forward illuminated DSCs respectively.

5.3 Results and Discussion

5.3.1 Characterization of TiN/PI coatings

TiN/PI coatings on NCG substrates were cured according to the method already explained in sections 2.3.2 and 5.2 followed by sheet resistance measurements using four-point probe technique. Since it has already been observed in section 4.3 that conductive coatings on ECCS substrates can only give indistinctive Z-axis resistance values, these substrates were not initially introduced at this stage as the primary driving force for this initial experiment was to identify the composition with lowest sheet resistance value (see sections 4.1 and 4.3). However, ECCS substrates will be used later to compare R_a and R_p values of the best performing TiN/PI composition on ECCS and NCG substrates after consecutive heating steps. Sheet resistance values of cured TiN/PI coatings with different TiN concentrations are given in Figure 5.1. It is evident from this figure that the electrical sheet resistance (R_s) of cured TiN/PI coatings decreases with increasing titanium nitride concentration in the polyimide matrix.

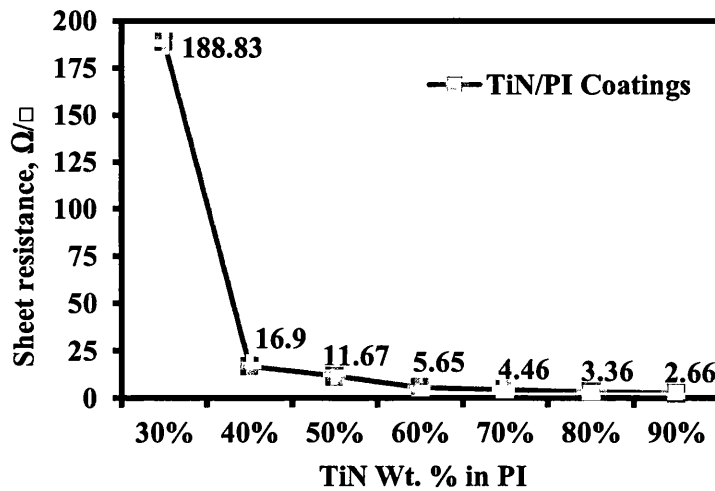


FIGURE 5.1: Sheet resistance vs. wt% TiN in PI at 350°C.

A gradual decrease in sheet resistance (Figure 5.1) was observed as the amount of titanium nitride in the polyimide matrix was increased from 30-90 wt%. It is obvious in Figure 5.1 that 30 wt% TiN/PI displayed highest sheet resistance value, which decreased dramatically when the amount of TiN was increased to 40 wt% in the polymer matrix. This is because at 40 wt %, TiN/PI successfully overcomes the percolation threshold and becomes more conductive when the amount of TiN was

further increased in the polymer matrix. At this point it suggests that the interconnections between TiN particles were successfully achieved providing a continuous pathway for conduction in the cured polymeric structure. Further additions of TiN improve particle interconnectivity in the polymer matrix and thereby increase the number of conductive pathways for the electrons to move freely in the coatings ^[12]. Thus, 90 wt% TiN/PI has the maximum number of conductive pathways than others as it demonstrates the lowest sheet resistance value amongst all samples.

R_a and R_p on the other hand (Table 5.1) displayed no significant variation and stayed relatively consistent in all cases. Unlike carbon-based coatings, R_a and R_p values obtained in this case were significantly low indicating a smooth and even surface of the cured TiN/PI coatings with TiN particle size < 3 μm .

TABLE 5.1: R_a and R_p values of cured TiN/ PI coatings at 350°C for 5 minutes.

<i>TiN wt. % in PI</i>	$R_a, \mu\text{m}$	$R_p, \mu\text{m}$
30%	0.58 (±0.07)	2.30 (±0.94)
40%	0.58 (±0.02)	1.92 (±0.05)
50%	0.61 (±0.04)	2.10 (±0.26)
60%	0.62 (±0.05)	2.09 (±0.12)
70%	0.66 (±0.03)	2.76 (±0.56)
80%	0.72 (±0.13)	2.25 (±0.24)
90%	0.67 (±0.04)	2.46 (±0.57)

It can be seen from Table 5.1 that cured samples with TiN/PI coatings demonstrate R_a values between 0.5 – 0.7 μm whereas, the average peak height (R_p) values varied between 2-3 μm .

Cured TiN/PI coatings were then further heat-treated up to the limit of TiO_2 sintering temperature, at 450°C for 30 minutes to investigate the impact of elevated temperature on the electrical as well as surface properties of the developed coatings. In addition, TiN is known to lose its electrical conductivity when heated to higher

temperatures ^[13]. It was observed that compositions containing 30 wt%, 40 wt% and 50 wt% TiN coatings display extremely high sheet resistance (R_s) values ranging from 48,000 – 285 Ω/\square after heat-treatment at 450°C for 30 minutes. Hence, such coatings are less important in this study as coatings with low sheet resistance values are more important in this case. Therefore, coatings with extremely high R_s values were not investigated further. Increases in sheet resistance were also observed in high TiN wt% coatings above 60 wt% TiN in PI (Figure 5.2). However, the rate of increase in sheet resistance in these coatings was comparatively slower than others with low TiN concentrations.

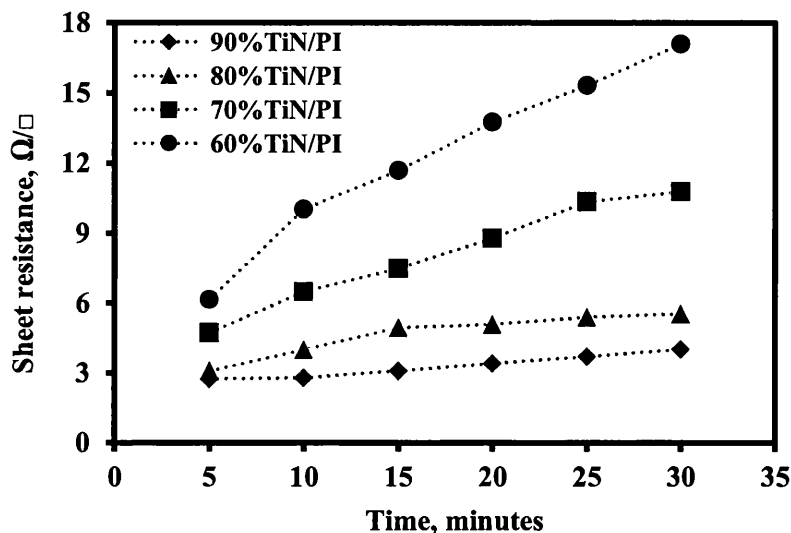


FIGURE 5.2: TiN/PI coatings: sheet resistance vs. time at 450°C between 0 and 30 minutes.

Figure 5.2 shows a relationship between the heat-treatment time and the change in electrical sheet resistance to visualize the increase in the resistance of selected TiN/PI coatings during the heat treatment process. It can be seen in Figure 5.2 that the coatings with less TiN loading tend to show a sharp increase in the sheet resistance with time during their heat treatment at 450°C for 30 minutes. Thus, 60 wt% TiN added PI shows a dramatic increase in the resistance whilst the increment was very slow in the case of 90 wt% TiN coating. High temperature oxidation of TiN particles in the oxidative environment could be the reason behind rapid loss in the electrical conductivity of all coatings ^[13-15]. Saha et al. reported that when TiN is heated up to 450°C, it starts growing an oxide layer, which continues to grow with heat-treatment time. The group also observed phase transformation in the oxide

layer, which was based on amorphous TiO_2 in the beginning but later transformed into a thick crystalline TiO_2 layer after heat-treatment for 16 hours [15]. However, the rate of oxidation of highly pigmented coatings was relatively slow which could be due to the presence of excess TiN particles in the matrix preventing faster oxidation. In addition, according to percolation theory, it can be elucidated that the coatings with high TiN concentrations contain greater number of percolation pathways, which are capable of preserving the electrical conductivity of such coatings even after high-temperature heat treatment in oxygen containing air atmosphere. Due to this reason, a heat-treated (450°C for 30 minutes) coating with low TiN loadings e.g. 60 wt% TiN/PI, shows approximately 200% increase in sheet resistance whereas, the 90 wt% TiN/PI coating demonstrated approximately 51% increase in the sheet resistance over the entire heat treatment time of 30 minutes (Figure 5.3).

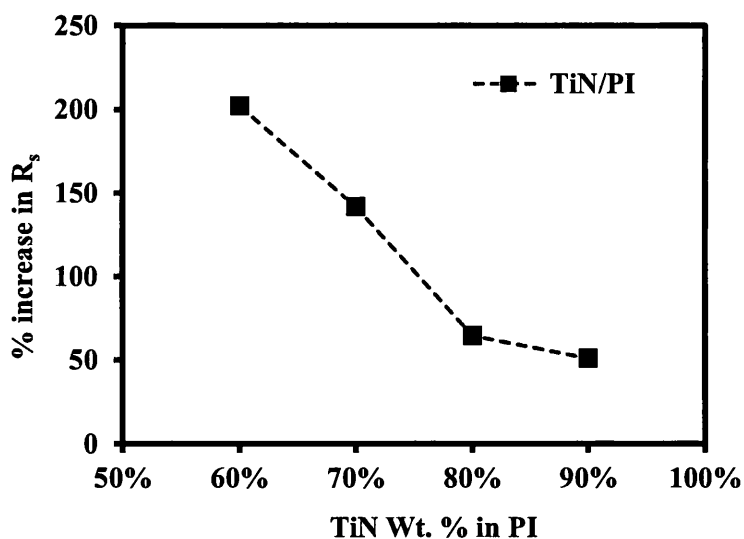


FIGURE 5.3: Percentage increase in sheet resistance of TiN/PI coatings after heat-treatment at 450°C for 30 minutes.

In addition to the sheet resistance measurements, surface characteristics of TiN/PI coatings were also studied after high temperature heat treatment at 450°C for 30 minutes. The average roughness (R_a) and the average peak height (R_p) are very important factors in this case (see sections 4.1 and 4.3) that influence DSC manufacturing. If the coatings are too rough then the fabricated DSCs could suffer from short-circuiting after their assembly with the counter electrodes. Hence, R_a and R_p values of TiN/PI coatings were monitored after the high temperature heating process at 450°C for 30 minutes. It can be seen from Figure 5.4 (a) that there is an

insignificant variation (compared to the carbon/PI coatings, section 4.3) in the average roughness values of the developed coatings during the high temperature heat treatment stage. It is evident that the average roughness (R_a) values in this case demonstrate an increasing trend with TiN wt%, nevertheless R_a values of highly pigmented coatings (70%, 80% and 90%) remind $\sim 0.7 \mu\text{m}$ (after high temperature heat treatment at 450°C for 30 minutes), which is acceptable for DSC application. Furthermore, this suggests that the roughness of such coatings is not significantly affected by the high temperature heat treatment, as it remains at a reasonable level even after 30 minutes at 450°C .

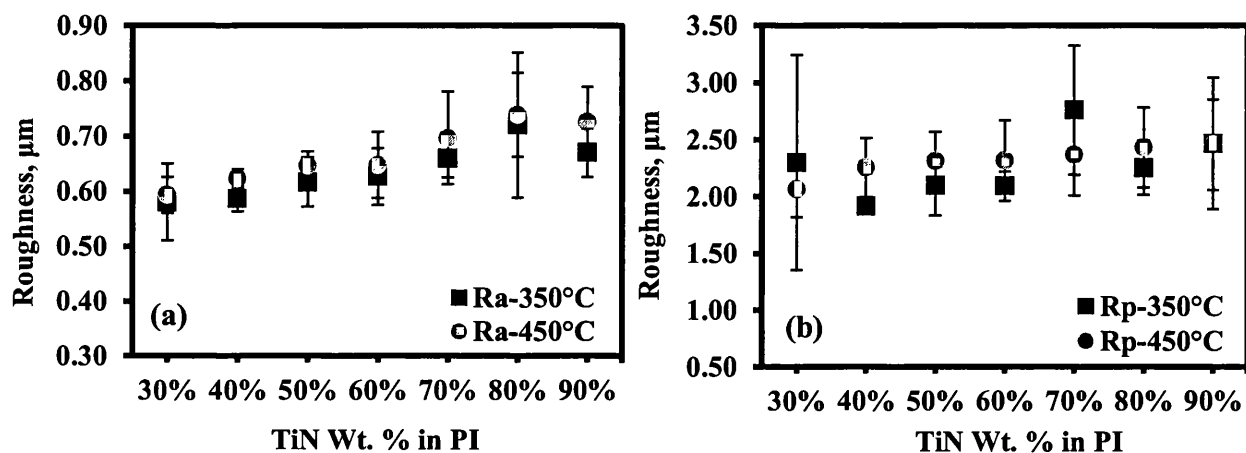


FIGURE 5.4: R_a and R_p values of TiN/PI coatings after curing at 350°C and heat treatment at 450°C for 30 minutes.

Besides the average roughness (R_a), determination of average peak height (R_p) in the roughness profile is also very important in this case. Presences of few bigger particles or some agglomerates (as in case of carbon/PI coatings, section 4.3) give rise to such peaks higher than the coating's general R_a value. Identifying the prevalence of the agglomerates at the surface is important in order to ensure continuous coating. Their presence can lead to short-circuiting if used to manufacture DSCs. Therefore, a lower peak height means a less chance of DSC short-circuiting. Figure 5.4 (b) reveals that most of the R_p values in this case of TiN/PI coatings are below $3 \mu\text{m}$ which is favourable for DSC application. However, in few instances, R_p values close to $3 \mu\text{m}$ were also observed (e.g. 70 wt% TiN, $R_p = 2.76 \mu\text{m}$). Nevertheless, such values are lower than those obtained in the case of carbon/PI based coatings and thus are suitable for device manufacturing. In addition,

variation in the R_p values between 350°C and 450°C (Figure 5.4, b) is slightly higher than in case of R_a values, which could be due to the presence of slightly bigger particles in the coatings or agglomerates detected during surface profilometry.

5.3.2 Selection of the best TiN/polyimide composition for DSC application

Developed TiN added polyimide coatings are high-temperature resistant and electrically conductive with significantly low R_a values. However, most of them are unable to maintain low electrical sheet resistance after high temperature heat treatment at 450°C for 30 minutes as shown in section 5.3.1. This could be due to the partial oxidation of TiN particles at higher temperatures, which results in a substantial decrease in the sheet resistance values of the developed coatings. The effect of oxygen on TiN properties will be investigated later using X-ray photoelectron spectroscopy studies. The 90 wt% TiN added polyimide coating displayed optimum characteristics in this test regime because the sheet resistance of this coating remained comparable to the standard FTO coated glass and the average roughness was also lower than the carbon based coatings developed in the previous chapter (see section 4.3). At this point in the study, ECCS substrates were introduced to identify the impact of applying the 90 wt% TiN/PI coating to ensure whether there is any abnormality in R_a and R_p values due the presence of micro-roughness ($R_a = 0.96 \mu\text{m}$) on the ECCS substrates. ECCS substrates coated with 90 wt% TiN/PI were sequentially heat-treated at 350°C (5 minutes) and 450°C (for 30 minutes) respectively and their R_a and R_p values were compared after each heating step. Figure 5.5 and Table 5.2 suggest that the average roughness of 90 wt% TiN/PI at different temperatures was not affected by the micro-roughness present on the ECCS surface. It can be seen that the 90 wt% TiN/PI coating is sufficiently thick to cover-up all the asperities present on the ECCS surface, which minimizes the chances of cell shorting ($R_a = 0.61 \mu\text{m}$ at 350°C and $0.67 \mu\text{m}$ at 450°C) and makes these coated metallic substrates useful for DSC application. The TiN/PI coating has small planarizing effect on the ECCS surface reducing the R_a from $0.96 \mu\text{m}$ down to $0.67 \mu\text{m}$. Hence, considering these facts, 90 wt% TiN added PI coating was selected as the best candidate for DSC application and further used to coat ECCS and NCG substrates for device fabrication.

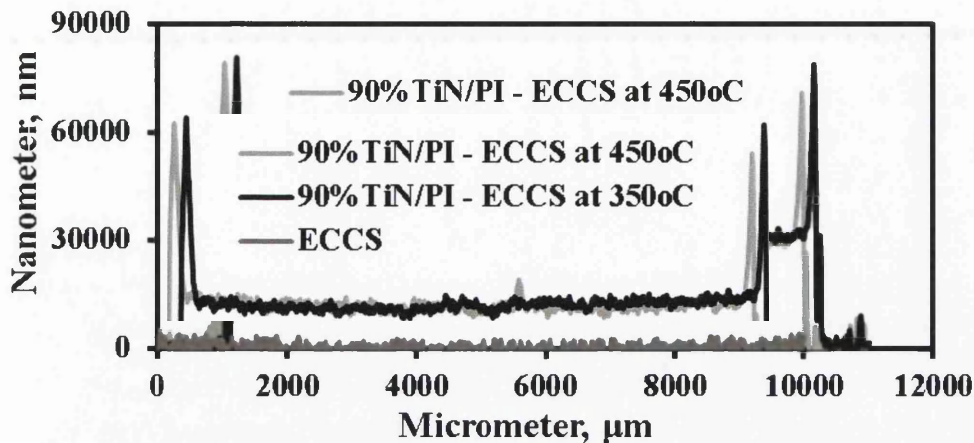


FIGURE 5.5 (a): 90 wt% TiN/PI on ECCS substrates heat treated at 350°C and 450°C.

TABLE 5.2: 90 wt% TiN/PI on ECCS substrates: at 350°C and at 450°C.

90% TiN/PI coatings on ECCS: at 350°C for 5 minutes & 450°C for 30 minutes				
350°C				
<i>TiN% wt in PI</i>	<i>Average roughness (Ra), μm</i>	<i>Average peak height (Rp), μm</i>	<i>Average thickness, μm</i>	<i>Sheet resistance, Ω/□</i>
90%	0.61	2.41	26.93	Z-axis
450°C				
90%	0.67	2.64	27.50	Z-axis
ECCS Baseline				
Uncoated ECCS	0.96	3.15	NA	Z-axis



FIGURE 5.5 (b): One year old ECCS based DSC substrate coated with 90% TiN/PI coating shows no significant signs of corrosion (Right) Uncoated ECCS substrate exposed to DSC electrolyte (Left).

In addition, Figure 5.5 (b) shows that 90% TiN/PI coated ECCS substrates display better corrosion protection against the DSC electrolyte compared to the uncoated metal. It was already clear from the beginning that both TiN and PI are chemically inert therefore they should protect the underlying ECCS metal substrates from the aggressive DSC electrolyte containing I^-/I_3^- redox couple. However, devices based on 90%TiN/PI coated ECCS were fabricated and kept for a year to check whether there is any corrosion of the underlying substrates taking place by the electrolyte present in the cells. After a year when the cells were dismantled and the coating was removed no signs of significant corrosion was observed on the ECCS substrates that were exposed to the DSC electrolyte for a year. The image on the right hand side of Figure 5.5 (b) shows a dismantled device that was preserved for a year. In contrast, the image on the right hand side of Figure 5.5 (b) shows an uncoated ECCS substrate that was exposed selectively to the DSC electrolyte only for a week. It can be seen in this image that the uncoated ECCS substrate demonstrated signs of severe corrosion where it was exposed to the electrolyte. This proves that 90%TiN/PI offers excellent corrosion protection against the DSC electrolyte, which makes it a suitable candidate for DSC application.

5.3.3 SEM analysis of 90 wt% TiN/PI coating

Figure 5.6 shows SEM images of 90 wt% TiN/PI coating after curing at 350°C for 5 minutes (Figure 5.6, a) and heat-treatment at 450°C for 30 minutes (Figure 5.6, b). Both the figures show no significant changes in the overall surface morphology of 90 wt% TiN/PI composition after its high temperature heat treatment at 450°C for 30 minutes. It is clearly visible from the SEM images that the 90 wt% TiN/PI coating is densely packed with evenly distributed TiN particles throughout the polymer matrix, which results in an electrically conductive and heat resistant composite coating with low sheet resistance value. Moreover, SEM images show the presence of some bigger TiN particles in the polyimide matrix, which was probably the reason for higher R_p values of the coatings including the 90 wt% TiN/PI. It is needless to mention that the 90 wt% TiN/PI samples for the SEM analysis were prepared on NCG substrates.

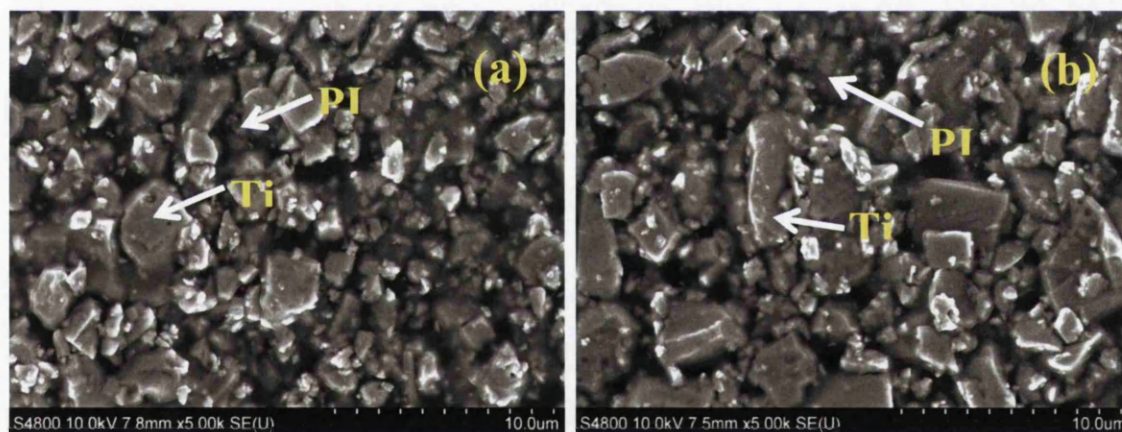


FIGURE 5.6: SEM images 90 wt% TiN/PI coating: (a) cured at 350°C for 5 minutes and (b) heat-treated at 450°C for 30 minutes.

5.3.4 X-ray photoelectron spectroscopy (XPS) of heat-treated 90 wt% TiN/PI coating

The effect of high temperature heat-treatment on the surface of the 90 wt% TiN/PI coating was studied using X-ray photoelectron spectroscopy. This is a very useful technique to study the elements present on the surface of a thin coating followed by their precise quantification. XPS was used to investigate the effect of oxygen on the 90 wt% TiN/PI coating during the high temperature heating steps. It is understood

from existing literature ^[13, 14] that TiN undergoes surface oxidation when heated in an oxygen rich environment. Nevertheless, it was important to study the surface characteristics of TiN/PI composite system to confirm this. A quantitative elemental analysis is presented in Figures 5.7 and 5.8, which describes ‘Atomic%’ concentration of each element present on the surface of the 90 wt% TiN/PI coating after curing at 350°C for 5 minutes and heating at 450°C for 10 and 30 minutes respectively.

In each case (Figure 5.8) peaks due to carbon (C 1s, 284.8 eV), oxygen (O 1s, 533.3 eV), titanium (Ti 2p 3/2, 458.9 eV) and nitrogen (N 1s, 400.3 eV) are observed. It can be seen from Figure 5.7 that the amount of oxygen has significantly increased whilst the amount of nitrogen has decreased after the heat-treatment at 450°C for 10 and 30 minutes. In addition, the amount of carbon has also slightly decreased due to polymer decomposition. Increase in the oxygen concentration could be due to formation of oxides and oxynitrides on the surface of the 90 wt% TiN/PI coating. The oxides and oxynitrides could possibly be TiO₂ and TiN_xO_y as reported previously. The small titanium 2p 3/2 peak at 458.9 eV (Figure 5.8, b) is consistent with titanium in the +4 oxidation state, suggesting TiO₂ formation ^[13-15], after the 30 minute heat treatment a small side peak (Figure 5.8, c) is observed in the oxygen 1s envelope at 530.2 eV, which is consistent with the appearance of a metal oxide. Such oxygen containing compounds can dramatically increase the sheet resistance of TiN/PI coatings as they are highly insulating in nature.

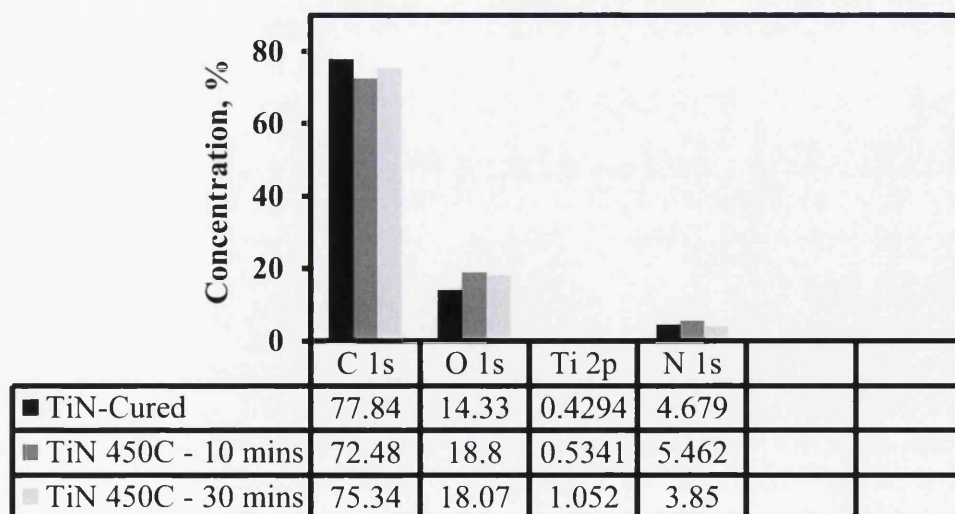


FIGURE 5.7: Quantification of elements present in the heat-treated 90 wt% TiN/PI coating.

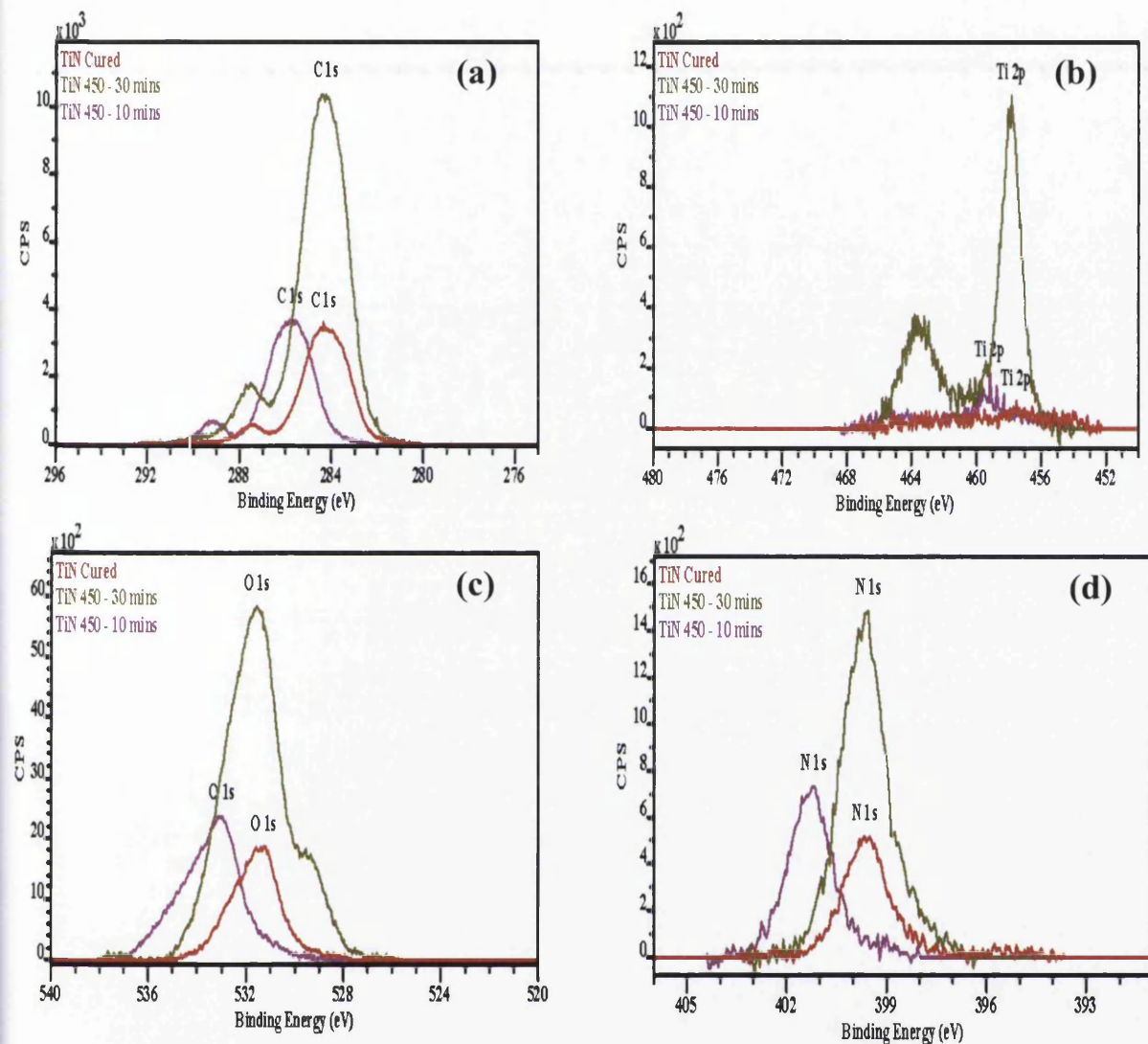


FIGURE 5.8: XPS analysis of heat-treated 90 wt% TiN Coating: (a) Carbon 1s, (b) Titanium 2p, (c) Oxygen 1s and (d) Nitrogen 1s.

5.3.5 J-V characteristics of 90 wt% TiN/PI working electrodes

90 wt% TiN/PI coated NCG and ECCS substrates were used in this experiment to study the photovoltaic performance of this best performing TiN/PI coating. In Figure 5.9, the current-voltage characteristics of reverse illuminated dye-sensitized solar cells based on 90 wt% TiN/PI coated ECCS and non-conducting glass working electrodes was very impressive compared to the graphite/PI based DSCs in the previous chapter.

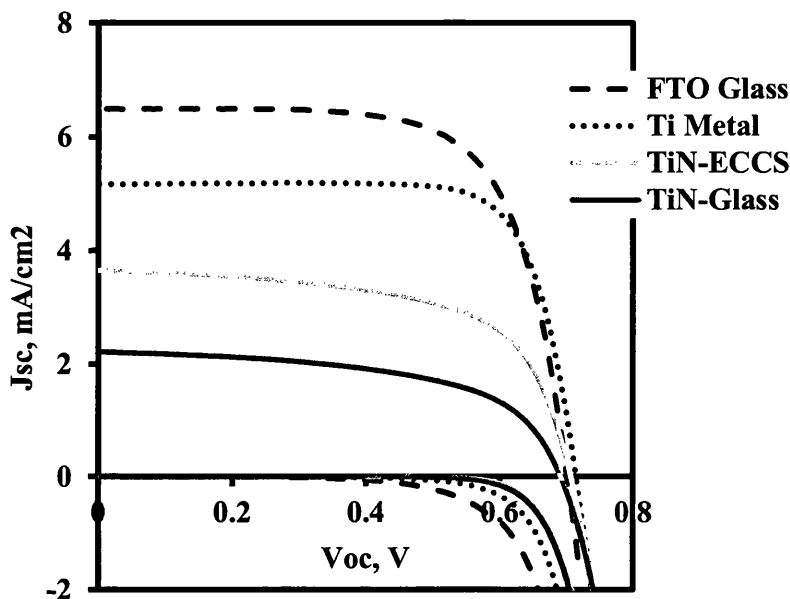


FIGURE 5.9: Average J-V curves of 90 wt% TiN/PI coated ECCS and non-conducting glass based DSCs and their comparison with standard FTO glass and titanium metal cells.

This study shows that the PV performance of DSCs based on 90 wt% TiN/PI coated ECCS working electrodes was better than the coated non-conducting glass based cells. The average photoconversion efficiency of 90 wt% TiN/PI coated ECCS based devices was around 1.63% (± 0.25) whereas, coated non-conducting glass based devices could only achieve up to 0.85% (± 0.17) in terms of its average photoconversion efficiency.

Coated ECCS based cells also demonstrated higher average J_{sc} value than their NCG based counterparts. However, both the coated ECCS and non-conducting glass based devices demonstrated significantly low average J_{sc} values than the standard FTO glass based devices in reverse illumination mode (Table 5.3). It was initially believed

that the variation in TiO₂ film thickness (as the photoanodes were prepared according to the method described in section 2.5.1) might be responsible for lowering the J_{sc} values. It is also obvious from Table 5.3 that there was a difference in the average TiO₂ film thickness values of the TiN/PI coated substrates and the standard FTO glass based cells. It has been reported in some studies that a difference of 4 μm in the TiO₂ film thickness may result in approximately 20% increment in the J_{sc} values of the FTO based DSCs [16, 17]. However, in this case standard FTO based devices exhibited over 70% increase in the average J_{sc} value compared to the 90 wt% TiN/PI coated ECCS cells whilst the difference in the TiO₂ thickness was approximately 3 μm. Same trend was observed in case of 90 wt% TiN/PI coated NCG cells with a TiO₂ thickness difference even less than 2 μm. Thus, it appears that the difference in the TiO₂ film thickness may not be the primary reason behind lowering the J_{sc} values of TiN/PI coated cells to a significant amount.

TABLE 5.3: DSCs based on 90 wt% TiN/PI coated working electrodes and their comparison with FTO glass and Ti-metal based devices.

Average Data Based on Total 22 Devices							
<i>Cells</i>	<i>V_{oc}, (V)</i>	<i>J_{sc}, (mA/cm²)</i>	<i>FF, %</i>	<i>η, %</i>	<i>R_s, Ω</i>	<i>R_{sh} Ω</i>	<i>TiO₂ thickness, μm</i>
TiN/PI-ECCS	0.70 ±0.00	3.68 ±0.43	62.26 ±2.60	1.63 ±0.25	20.44 ±3.63	2.60 x 10 ³ ±1296.84	7.60 ±1.44
TiN/PI-Glass	0.68 ±0.00	2.20 ±0.42	56.47 ±1.13	0.85 ±0.17	38.66 ±8.61	2.56 x 10 ³ ±610.49	9.06 ±2.94
Titanium Metal	0.71 ±0.00	5.16 ±0.30	76.60 ±1.95	2.82 ±0.06	10.90 ±0.96	1.64 x 10 ³ ±9907.86	8.86 ±1.90
FTO Glass	0.70 ±0.00	6.50 ±0.32	69.56 ±0.09	3.17 ±0.15	11.43 ±0.49	1.99 x 10 ⁴ ±7566.22	10.80 ±2.66

Therefore, low photocurrent obtained in the 90 wt% TiN/PI based cells could be due to the faster interfacial charge recombination at the substrate/electrolyte and TiO₂/electrolyte interfaces as the shunt resistance values (R_{sh}) in TiN/PI based cells were substantially lower than the FTO glass based devices. However, high V_{oc} values in all cases suggest slower interfacial charge recombination in all fabricated devices.

This will be investigated in detail using EIS and optoelectronic transient studies later in this section.

The fill factor of a device is normally governed by the parasitic resistance (shunt and series) of a cell. High series and extremely low shunt resistances can decrease the fill factor of a cell to a significant amount and this can be seen occurring in case of TiN/PI coated non-conducting glass based cells. It can be seen in Table 5.3 that the average fill factor demonstrated by the TiN/PI coated NCG cells was lowest amongst all due to high series and low shunt resistance values that may have resulted from the non-conducting nature of NCG substrates. In contrast, the average fill factor of TiN/PI coated ECCS based cells was comparable to the FTO glass based device because the average series resistance was relatively low along with the considerably high average shunt resistance.

It is clear from this experiment that 90 wt% TiN/PI coated ECCS based DSCs were less efficient compared to the FTO glass cells but demonstrated comparable V_{oc} and fill factor values. Now a comparison is required between 90 wt% TiN/PI coated ECCS and titanium metal-based cells to identify the best candidate for low cost DSC fabrication on a commercial basis.

Table 5.3 and Figure 5.9 show the comparison between 90 wt% TiN/PI based ECCS and Ti metal cells where it can be easily seen that both coated ECCS and titanium metal cells are comparable to each other in terms their V_{oc} , J_{sc} and fill factor values. Even the average photoconversion efficiencies of both the cells were not too far from each other.

Thus, PV performance demonstrated by the coated ECCS working electrodes was very promising, with a possibility of further efficiency enhancement by applying traditional $TiCl_4$ treatment to the TiO_2 photoanode ^[18]. However, mesoporous TiO_2 on 90 wt% TiN/PI coated ECCS substrates becomes very unstable and begins to delaminate immediately upon immersion in the aqueous $TiCl_4$: THF solution (Figure 5.10). Therefore, efficiency enhancement by $TiCl_4$ treatment was unfortunately not possible in this case.

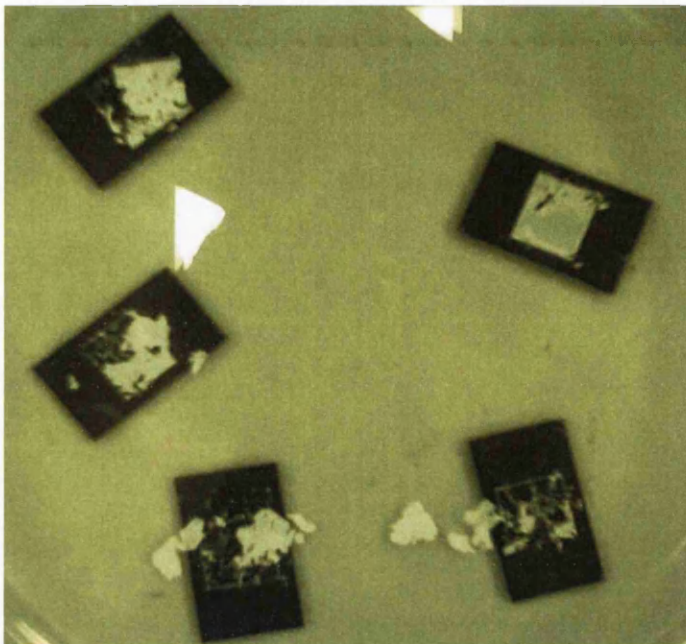


FIGURE 5.10: Delaminated TiO₂ on 90 wt% TiN/PI during its TiCl₄ treatment.

5.3.6 EIS of 90 wt% TiN/PI working electrodes

Electrochemical impedance spectroscopy (EIS) can be used to investigate interfacial charge recombination kinetics at the substrate/electrolyte and the mesoporous TiO₂/electrolyte interfaces in a dye-sensitised solar cell. An increase in interfacial charge recombination can reduce the PV performance of a DSC by reducing the V_{oc} . Thus; a faster rate of interfacial charge recombination is often responsible for low V_{oc} in a device. It has been observed that recombination at lower potentials (< 0.4 V) is dominated by that at the substrate/electrolyte interface as the TiO₂ is effectively an insulator. Recombination via the TiO₂/electrolyte interface is more dominant at higher potentials as the TiO₂ film becomes more conductive due to filling of the conduction band) ^[19-20]. Figure 5.11 illustrates recombination resistance vs. voltage in DSCs based on coated ECCS and non-conducting glass working electrodes and their comparison with standard FTO glass and titanium metal based cells. At the highest applied potentials FTO glass devices exhibit the highest R_{rc} , indicating slower recombination compared to the other devices. The reason for this might relate to how the substrate affects TiO₂ sintering, binder burn-off and resultant film morphology.

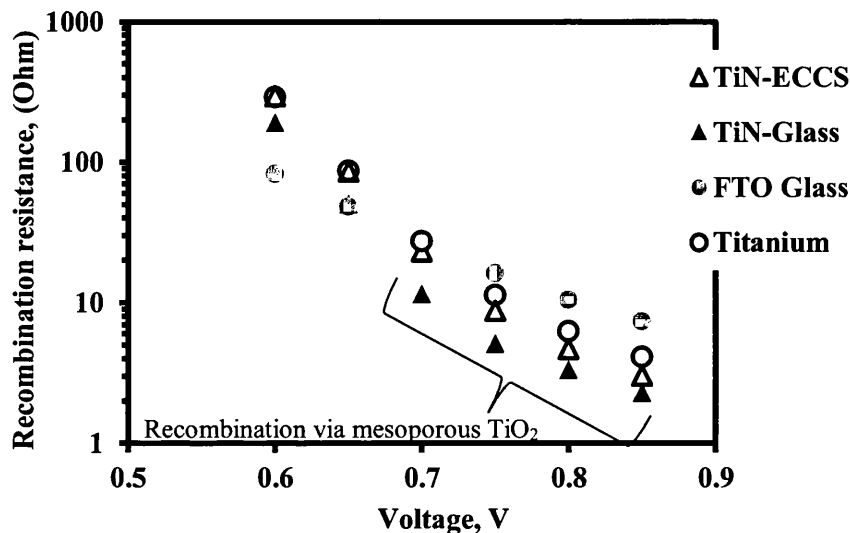


FIGURE 5.11: Average charge transfer resistance in the coated ECCS, coated NCG, FTO glass and titanium metal working electrodes based cells: average data based on 12 best devices.

One might expect that this difference would be more pronounced when comparing metal *vs* .glass-based devices, as metal substrates would heat up more quickly, presumably influencing binder burn-off and sintering. At the lowest potentials applied during impedance measurements, the FTO glass devices exhibit lower R_{rc} than the other devices. Even though it would be expected, that TiO_2 /electrolyte recombination would still dominate at these potentials (~ 0.6 V), the difference in R_{rc} , between devices, at these lower applied potentials may indicate some contribution of recombination *via* the substrate/electrolyte interface, meaning that the reason for higher R_{rc} in some of the metal based devices, may be due to the formation of metal oxide layers (TiO_2 in the case of TiN), that exhibit electron selective behaviour and so minimise recombination *via* the substrate in much the same way as a deliberately deposited compact TiO_2 “blocking layer”^[22] would. For example, in a solid state DSC.

Electron lifetime (τ_n) in the TiO_2 film can be calculated from the Bode plots obtained at a given potential. In this case we have chosen the bode plot at an applied potential close to the V_{oc} achieved at 1 sun. The longer the electron lifetime in the TiO_2 film the slower the rate of back reaction at the TiO_2 /electrolyte interface and more electrons have a chance to be extracted into the external circuit. Electron lifetime can

be calculated from equation [1]. Where, f_{max} is the characteristic frequency corresponding to the apex of the peaks in the lower frequency region (Figure 5.12).

$$\text{Electron lifetime } (\tau_n) \text{ at } V_{oc} \text{ (of the cells, } 0.70\text{V at } 1\text{Sun}) = 1/2\pi f_{max} \quad [1]$$

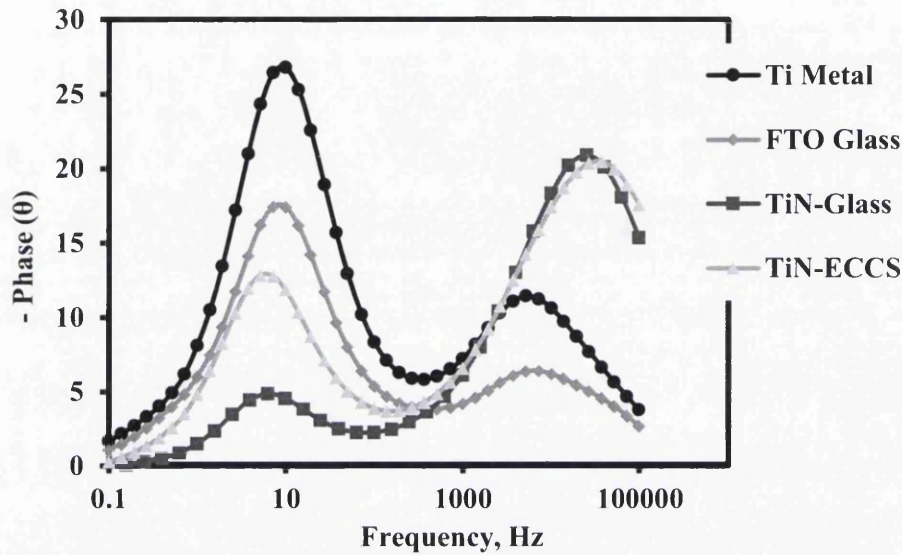


FIGURE 5.12: Average Bode plots of DSCs based on 90 wt% TiN/PI coated ECCS and glass cells and their comparison with FTO glass, Ti metal cells and uncoated ECCS cells at an applied potential of 0.7V: average data based on 12 best devices.

The average electron lifetimes calculated from equation [1] show in Table 5.4 that both 90 wt% TiN/PI coated ECCS and non-conducting glass based working electrodes have comparable electron lifetimes in the mesoporous TiO_2 film. It was also discovered that electron lifetimes of 90 wt% TiN/PI coated substrates were slightly higher than the τ_n of titanium metal mounted cell but remained comparable to the FTO glass based devices.

TABLE 5.4: Electron lifetimes of DSCs based on 90 wt% TiN/PI coated working electrodes and their comparison with FTO and titanium metal based cells: average data based on 12 best cells.

DSCs	Characteristic frequency, Hz	Lifetime (τ_n), ms
TiN/PI-ECCS	5.20	30
TiN/PI-Glass	6.31	25
FTO Glass	7.23	22
Ti Metal	9.93	16

5.3.7 Transient measurements of 90 wt% TiN/PI working electrodes

Optoelectronic transient studies can give valuable information about charge density, electron transport and recombination within a DSC. An optoelectronic transient signal either in the form of voltage or current is obtained by optically perturbing a DSC at various light intensities. This study however does not provide any information about the charge transfer process at the counter electrode of a device, as there is no photosensitive material present, which can be perturbed by the visible light [21].

5.3.7.1 Photovoltage decay measurements

The rate of electron recombination at the working electrode/electrolyte interface can be estimated by photovoltage decay measurements. In this technique, photovoltage in a DSC is first generated by bias light, which is then turned off and the voltage is measured over time.

In absence of the bias light, charge carriers recombine at the working electrode causing photovoltage to decay with time. Faster decays could indicate faster charge recombination at the working electrode/electrolyte interface. In Figure 5.13, it can be seen that the photovoltage decay rate in the FTO glass based devices is very rapid which results from a faster back reaction at the FTO/electrolyte interface. In contrast, 90 wt% TiN/PI coated ECCS and non-conducting glass based working electrodes display remarkably slower photovoltage decay rates similar to the substrates based on titanium metal. It was believed that the formation of a thin compact TiO₂ layer on 90 wt% TiN/PI coating during its high temperature treatment at 450°C (see sections 5.3.1 and 5.3.4) was responsible for the slower photovoltage decay. This thin layer of TiO₂ might act as an electron selective “blocking layer” as reported by Cameron *et al.* in their paper describing the role of TiO₂ based blocking layers deposited using spray pyrolysis technique in reducing the photovoltage decay rate, which would slow recombination at substrate/electrolyte interface. Thus, the presence of a blocking layer can significantly increase the overall PV performance of a device [22].

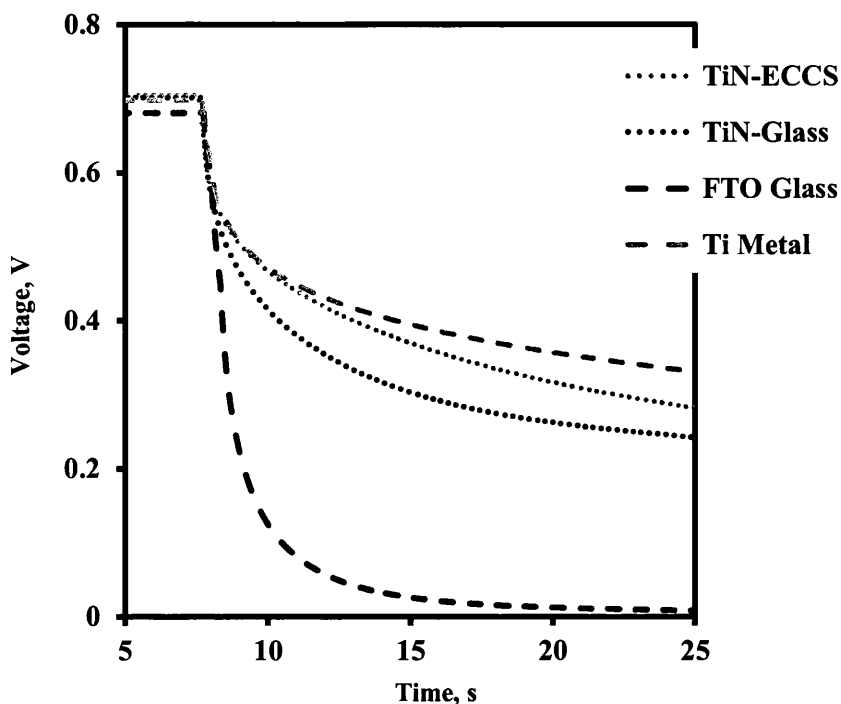


FIGURE 5.13: Average photovoltage decay measurements of 90 wt% TiN/PI coated working electrodes and their comparison with FTO and Ti based cells: average data based on 12 best devices.

Therefore, it appears from the PV decay analysis that the formation of a TiO_2 compact layer on 90 wt% TiN/PI as in case of Ti metal mounted cells, can substantially reduce the rate of back reaction via the substrate in such devices.

5.3.7.2 Electron lifetime measurements

The transient photovoltage decay lifetime in a dye-sensitized solar cell gives an idea regarding electron lifetime in the mesoporous TiO_2 film, at open circuit. In this case, the electron lifetime was measured by applying small optical perturbation to a dye-sensitized solar cell, which results in an increase in photogenerated charge carriers in the device, establishing a transient increase in potential difference across the cell, which then decays back to the steady state. A first order exponential decay function is then used to fit the transient photovoltage decay and the decay time constant is calculated to give the average electron lifetime at a given voltage. Figure 5.14 illustrates average electron lifetimes in ECCS and non-conducting glass working electrodes coated with 90 wt% TiN/PI coating and their comparison with standard FTO and Ti metal based cells.

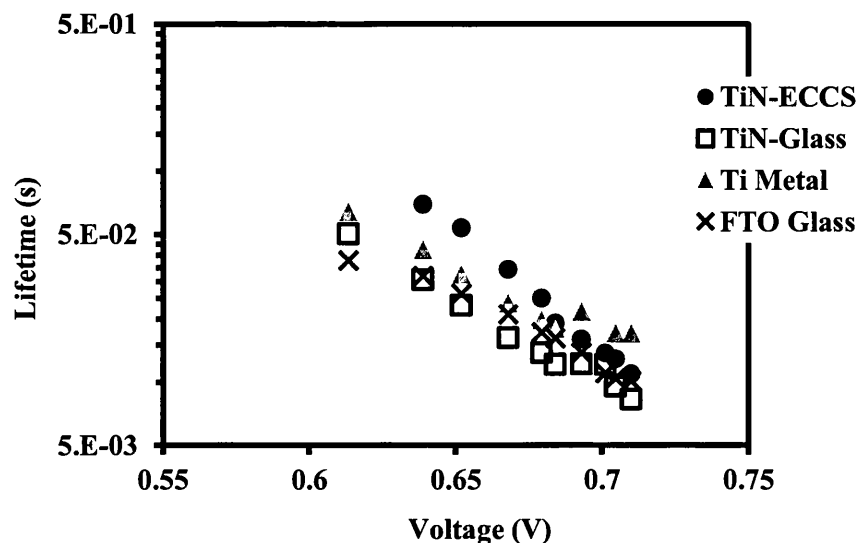


FIGURE 5.14: Average transient electron lifetime vs. voltage in 90 wt% TiN/PI coated substrates and their comparison with FTO and Ti based cells: average data based on 12 best devices.

It can be seen in this case that the FTO based device has the longest electron lifetime amongst all at around 0.6 V. This could be due to the absence of compact TiO₂ layer on the FTO working electrode and might indicate the onset of recombination at the substrate/electrolyte influencing electron lifetimes in these devices. Whereas, all other cells including titanium metal based substrate demonstrate comparatively higher electron lifetimes in the mesoporous TiO₂ at 0.6 V, due to the formation of a thin compact TiO₂ based layers during their high temperature heat treatment.

It is also evident from the figure that the electron lifetimes of the fabricated cells tend to decrease when the voltage shifts from 0.6 V to 0.7 V this could be due to the fact that at higher potentials the mesoporous TiO₂ film becomes sufficiently conductive allowing electrons to escape at faster rates from the porous TiO₂ film [19-20].

5.3.7.3 Charge density measurements

Charge densities of individual devices were measured *via* charge extraction, which involves illuminating the device at a certain light level, then switching of the light and short-circuiting the device simultaneously. By integrating the subsequent current extracted from the device, total charge can be calculated for the device, in its condition immediately before switching off the bias light.

It can be seen from Figure 5.15 that charge density in the Ti metal mounted DSC was highest of all devices. This may be due to the Ti metal substrate heating up more quickly than the glass/FTO based substrates, resulting in greater trap densities because of more crystal defects in the TiO₂.

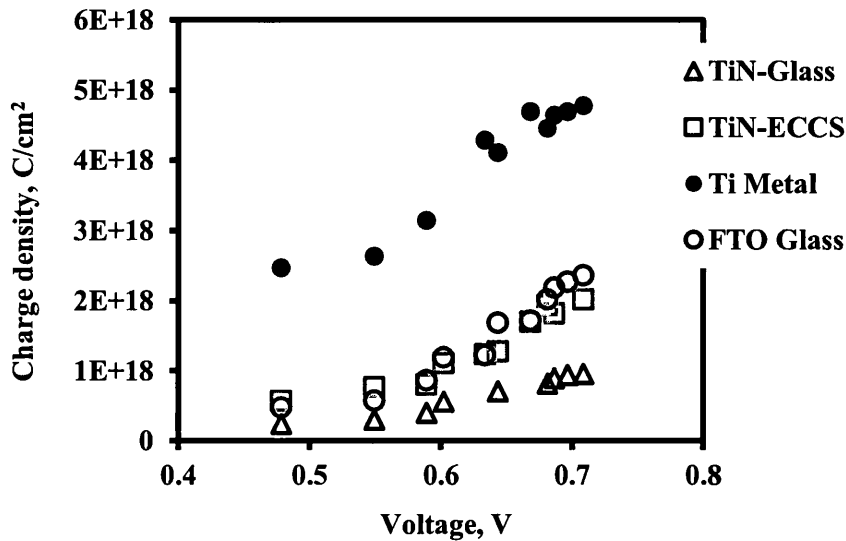


FIGURE 5.15: Average charge density vs. voltage in 90 wt% TiN/PI coated substrates and their comparison with FTO and Ti based cells: average data based on 12 best devices.

In contrast, 90 wt% TiN/PI coated non-conducting glass (NCG) cells exhibited lowest charge density within the device, which could be due to the slower heating rate of TiN/PI coated NCG without the FTO layer as the cells with FTO coated glass appear to have higher charge densities in this case. This was probably the reason of sub-standard PV performance observed in 90 wt% TiN/PI coated NCG cells.

On the other hand, the average charge density obtained in 90 wt% TiN/PI coated ECCS cells was almost similar to the FTO glass based devices. Although, ECCS would heat-up rapidly as Ti metal but the presence of TiN/PI coating may have altered the heating rate of ECCS in this case making it comparable to the FTO glass based substrates.

5.3.8. Reflectance measurements of the 90 wt% TiN/PI and FTO glass

As shown in Chapter 4, a reflective substrate can significantly increase DSC efficiency [23]. A UV-Vis spectrophotometer was used to record the percentage reflectance of the 90 wt% TiN/PI coating during heat treatment at 450°C at 10 minutes, 20 minutes, and 30 minutes intervals, during the heat treatment period. The obtained reflectance values were then compared with 15 Ω/\square FTO coated glass and shown in Figure 5.16.

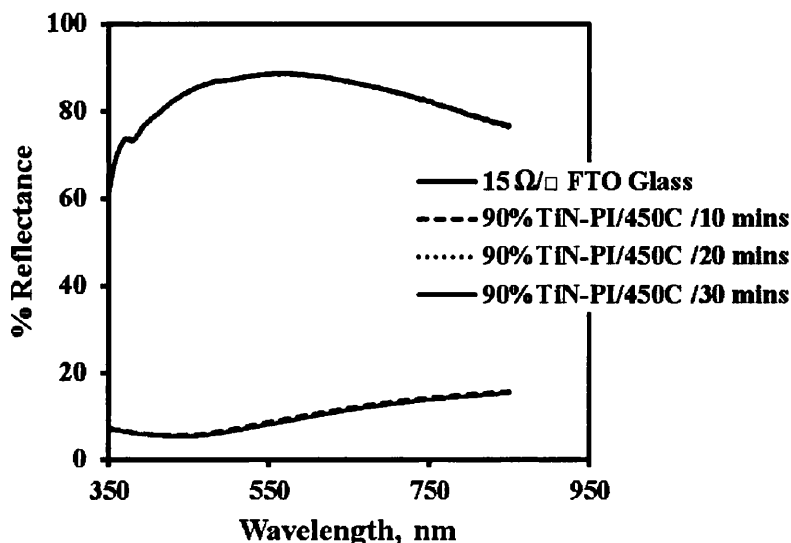


FIGURE 5.16: % Reflectance vs. wavelength of FTO glass and 90 wt% TiN/PI at 450°C.

Figure 5.16 shows that the 90 wt% TiN/PI coating is less reflective than FTO glass, which has a thin layer of fluorine, doped tin oxide. The deep brown colour of the 90 wt% TiN/PI coating is responsible for the non-reflective nature, due to maximum absorption of the visible light which may in turn interrupt the light absorption process by the photosensitive dye resulting in low photocurrent outputs from the cells.

5.3.9 J-V characteristics of 90 wt% TiN/PI coated counter electrodes

In this section, the 90 wt% TiN/PI coated ECCS and non-conducting glass substrates were used as DSC counter electrodes in devices with standard FTO glass working electrodes. Both coated ECCS and non-conducting glass based substrates were initially platinized using a conventional thermal platinization technique (see section 2.5.3).

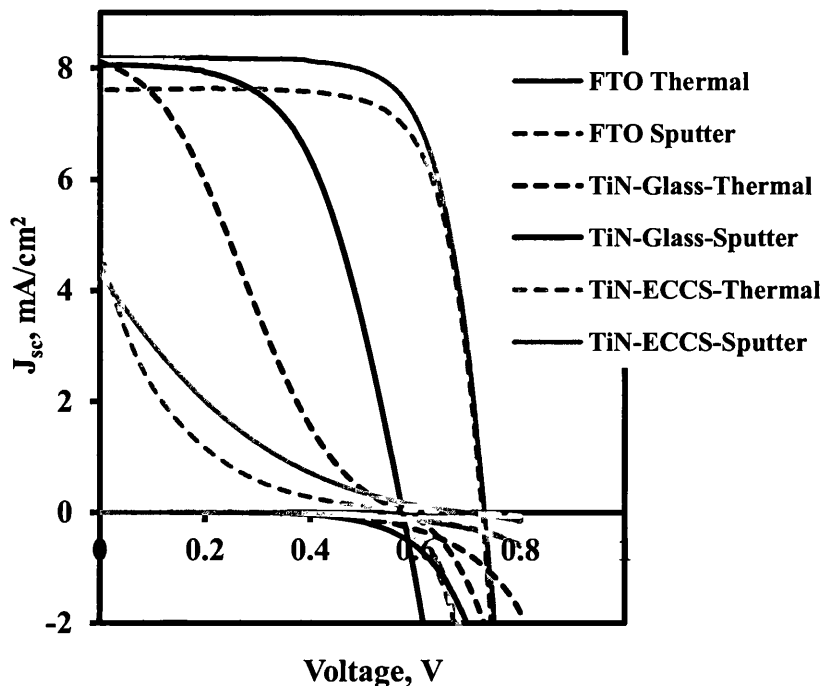


FIGURE 5.17: Average J-V characteristics of 90 wt% TiN/PI coated counter electrodes with thermally decomposed and sputter platinum vs. typical FTO cells with thermally deposited and sputter platinum: average data based on 24 devices.

The average PV performance of DSCs based on 90 wt% TiN/PI coated counter electrodes with thermally decomposed platinum is given in Figure 5.17 and Table 5.5. It is clearly visible from the table that none of the cells performed well in terms of their photoconversion efficiencies. The combined effect of high series and low shunt resistances resulted in losses in the average fill factor of the cells based on platinised 90 wt% TiN/PI on ECCS. Non-conducting glass based cells with thermally platinized 90 wt% TiN/PI also demonstrated poor average fill factors. Significant loss in fill factors in both cases was attributed to the poor catalytic activity of platinum onto 90 wt% TiN/PI coating. This could be due to the absorption of chloroplatinic acid by the oxide and oxynitride species (see sections 5.3.1 and 5.3.5) present on the 90 wt% TiN/PI coating, which in turn reduces the catalytic activity of the platinum catalyst. This is applicable for ECCS, and non-conducting glass based counter electrodes as poor fill factors due to parasitic losses were observed in the J-V curves in both cases (Figure 5.17). In order to avoid the interaction between TiN/PI and the chloroplatinic acid, a sputtering technique was

introduced to deposit elemental platinum (2 nm thick) using a Quorum 150T sputter coater, onto the 90 wt% TiN/PI coated ECCS and non-conducting glass substrates.

TABLE 5.5: Average J-V data of 90 wt% TiN/PI coated counter electrodes (with thermally deposited and sputter platinum) and their comparison with FTO glass based typical devices.

Average Data Based on 24 Devices						
<i>Cells</i>	<i>V_{oc}, (V)</i>	<i>J_{sc}, (mA/cm²)</i>	<i>FF, %</i>	<i>η, %</i>	<i>R_s, Ω</i>	<i>R_{sh} Ω</i>
TiN/PI ECCS Thermal Pt	0.69 ±0.02	4.74 ±0.87	7.33 ±0.87	0.24 ±0.07	2197.07 ±1370.95	30.02 ±1.33
TiN/PI Glass Thermal Pt	0.72 ±0.00	8.10 ±0.34	27.78 ±5.26	1.63 ±0.30	270.93 ±121.81	438.40 ±122.43
TiN/PI ECCS Sputter Pt	0.69 ±0.01	4.31 ±0.89	13.39 ±0.52	0.40 ±0.09	784.25 ±169.88	74.28 ±11.49
TiN/PI Glass Sputter Pt	0.72 ±0.01	8.05 ±0.17	55.92 ±1.26	3.27 ±0.15	25.31 ±1.46	6317.02 ±2094.01
FTO Glass Thermal Pt	0.73 ±0.00	8.20 ±0.16	71.69 ±1.20	4.30 ±0.15	10.20 ±1.16	24393.37 ±18427.15
FTO Glass Sputter Pt	0.72 ±0.01	7.61 ±0.40	72.62 ±0.90	4.02 ±0.29	9.39 ±0.66	17376.14 ±15779.15

Since the platinum catalyst was deposited in elemental form without any heat treatment, it did not seem to interact substantially with the TiN/PI coating. Table 5.5 and Figure 5.16 represent photovoltaic characteristics of 90 wt% TiN/PI coated ECCS and NCG counter electrodes with sputtered platinum. Coated non-conducting glass substrates with sputtered platinum perform relatively well in terms of their photoconversion efficiencies with an average value of 3.27%, which was comparable to the FTO counter electrode based device fabricated in the same manner. Moreover, the average J_{sc} value of these cells was significantly higher than the standard FTO counter electrode based devices with sputtered platinum.

However, the average fill factor of the coated glass counter electrode based cells was remarkably lower than the standard FTO cell with sputtered platinum. Lower fill factor in this case was due to the combined effect of high series and the low shunt resistances in such devices. It could also be attributed to the poor catalytic activity of the platinum catalyst, which will later be investigated using impedance spectroscopy.

The 90 wt% TiN/PI coated ECCS counter electrodes with sputtered platinum showed extremely poor PV performance (Table 5.5, Figure 5.17). Very high series resistance and extremely low shunt resistance were responsible for slow electron transfer at the counter electrodes of these devices. High series resistance in this case could be due to the high contact resistance between the ECCS metal and the 90 wt% TiN/PI coating, which resulted in slow electron transfer from the ECCS metal to the 90 wt% TiN/PI coating. Thus, high series resistance is generated between these two dissimilar entities resulting in substandard PV performance.

5.3.10 EIS of 90 wt% TiN/PI counter electrodes

Electron transfer kinetics at the counter-electrode/electrolyte interface of a DSC can be determined by the electrochemical impedance spectroscopy. The ease of electron transfer at the counter electrode in the presence of the platinum catalyst can be estimated from the charge transfer resistance values obtained from the impedance spectroscopy. The lower the charge transfer resistance at the counter-electrode/electrolyte interface, the higher the electron transfer rate from the platinised counter electrode to the I^-/I_3^- redox electrolyte leading to faster reduction of the triiodide species.

Slow electron transfer at the counter electrode is often observed due to poor catalytic performance of the platinum catalyst, which can result in poor PV performance. Hence, the platinum catalyst plays a pivotal role in the electron transfer process at the counter electrode/electrolyte interface and even a slight abnormality in the catalyst can cause remarkable variation in the PV performance of the cell.

Figure 5.18 shows the charge transfer resistance (R_{ce}), as a function of applied potential, of the 90 wt% TiN/PI coated ECCS and NCG counter electrodes coated with thermally decomposed and sputtered platinum. The R_{ce} values of the coated counter electrodes was also compared with standard FTO glass counter electrodes with thermally decomposed and sputtered platinum. The charge transfer resistances of 90 wt% TiN/PI coated ECCS counter electrodes with thermally decomposed and sputtered platinum were found to be high in this case due to the poor catalytic activity and very high contact resistance between ECCS and the TiN/PI coating.

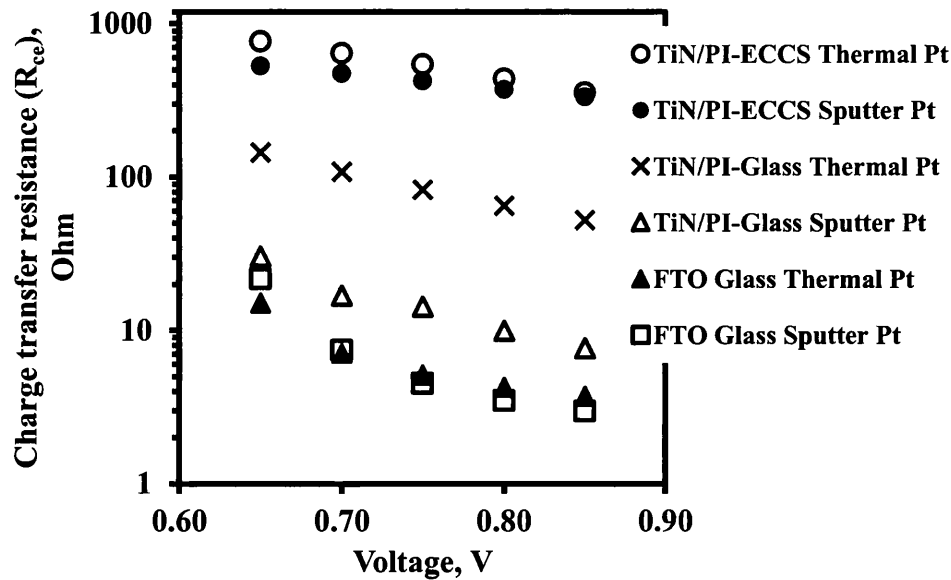


FIGURE 5.18: Average charge transfer resistance at the counter electrodes of the 90 wt% TiN/PI coated ECCS and non-conducting glass electrodes and FTO based cells (with thermally deposited and sputter platinum): average data based on 18 devices.

As a result, both type of cells demonstrated very poor PV performance as already represented in Table 5.5 and Figure 5.17. The 90 wt% TiN/PI coated, non-conducting glass counter electrodes with thermally decomposed platinum exhibited lower charge transfer resistance than the ECCS based cells which may be due to the presence of only coating's internal resistance rather than the contact resistance arising from the two dissimilar materials in contact. However, the interaction between TiN/PI and the chloroplatinic acid substantially reduced the catalytic activity of the platinum catalyst leading to poor photoconversion efficiency of only 1.63% (± 0.30)

In contrast, the charge transfer resistance of the 90 wt% TiN/PI coated non-conducting glass counter electrode with sputtered platinum was lower than all other coated counter electrodes. This could be due to the fact that the elemental platinum deposited in the sputtering technique did not react largely with the TiN/PI coating. Moreover, the sputtering technique does not require a high temperature heat treatment therefore coating's internal resistance also remained low resulting in overall improvement in the PV performance of the cells (Table 5.5). As might be expected, both the FTO glass based cells with thermally deposited and sputtered platinum, demonstrated the lowest charge transfer resistances at the counter-

electrode/electrolyte interface resulting in faster electron transfer to the redox electrolyte. This resulted in superior PV performance by the FTO counter electrode based cells, which was comparable to the 90 wt% TiN/PI coated glass counter electrode cells with sputtered platinum. The electrical double layer capacitance (C_{dl}) at the counter-electrode/electrolyte interface of the 90 wt% TiN/PI based counter electrodes also depends upon the catalytic activity and the surface area of the platinized counter electrodes. The C_{dl} is normally proportional to the surface area and the catalytic activity of the platinum catalyst, which means higher C_{dl} values result in greater catalytic activity and faster triiodide reduction at the counter electrode/electrolyte interface of a device [24]. It can be seen from Figure 5.19 that the C_{dl} of 90 wt% TiN/PI coated non-conducting glass counter electrode based cells with sputtered platinum was significantly higher than all other coted counter electrode based cells. Higher catalytic activity on such a counter electrode results in greater amount of charge accumulation on the rough TiN/PI surface followed by faster charge transfer to the redox couple. The C_{dl} of the 90 wt% TiN/PI with sputtered platinum was also closely comparable to the FTO glass based cells with thermally decomposed and sputtered platinum (Figure 5.19). This implies that 90 wt% TiN/PI coated non-conducting glass counter electrodes with sputtered platinum may demonstrate comparable PV performance to the FTO glass based cell.

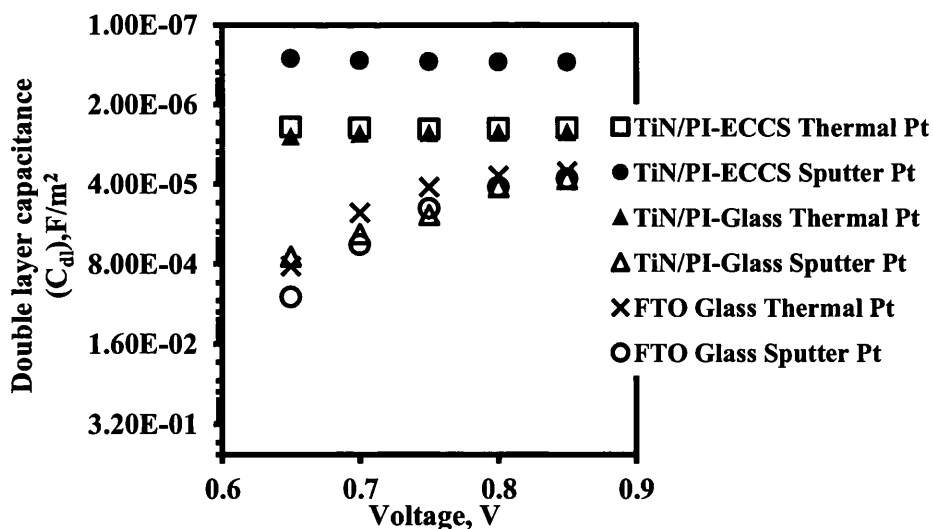


FIGURE 5.19: Average electrical double layer capacitance in platinized counter electrodes/electrolyte interface of 90 wt% TiN/PI coated ECCS and non-conducting glass electrodes and FTO based cells (with thermally deposited and sputter platinum): average data based on 18 devices.

5.4 Conclusions

Based on all experimental results obtained in this chapter, it can be concluded that, titanium nitride containing polyimide coatings are electrically conductive and high temperature resistant in nature. The 90 wt% TiN added polyimide coating was chosen for application in dye-sensitized solar cells because of its extremely low sheet resistance and outstanding high temperature stability. In addition, the surface roughness of the 90 wt% TiN/PI coating was substantially lower than those based on carbon materials in the previous chapter. This indicates that the 90 wt% TiN/PI coating was the best candidate for DSC applications in this chapter.

The photovoltaic performance of DSCs based on 90 wt% TiN/PI coated ECCS working electrodes was slightly lower than the standard devices based on FTO glass and titanium metal. More importantly, the presence of an oxide layer on 90 wt% TiN/PI coated substrates displayed lower tendency of charge recombination compared to the typical FTO glass mounted devices. However, a significant amount of current loss was observed due to low shunt resistance and poor light reflectivity of 90 wt% TiN/PI coating. The photoconversion efficiency of 90 wt% TiN/PI based cells could not be improved further through TiCl_4 treatment as the mesoporous TiO_2 immediately delaminates upon its immersion into the TiCl_4 solution.

The PV performance of 90 wt% TiN/PI coated (ECCS and NCG) counter electrodes was found to be dependent upon the platinization techniques and the substrates used for device fabrication. It has been observed in this case that coated ECCS based counter electrodes failed to demonstrate desirable PV performance. However, counter electrodes based on 90 wt% TiN/PI coated NCG with sputtered platinum displayed comparable PV performance to the cells with FTO based counter electrodes.

In short, this study confirms that 90 wt% TiN/PI coating can be used as both working and counter electrode material for DSC applications. Moreover, the chemically inert nature of this coating protects the underlying low cost metallic substrate from the aggressive electrolyte, thereby presenting a low cost alternative to Ti metal used in DSCs.

5.5. References

- [1] J. William S. Rees, *CVD of Nonmetals*. U.S.A: John Wiley & Sons, 2008.
- [2] N. H. Ulrich Schubert, *Synthesis of Inorganic Materials*. Germany: John Wiley & Sons, 2012.
- [3] Osamu Tanaike, Hajime Kiyono, Shiro Shimada, Masahiro Toyoda and Tomoki Tsumura., "Ammonia-treated Titania as an Anode Material of Lithium-ion Battery with High-rate Capability", *ECS Trans*, volume 16, issue 29, 151-156, 2009.
- [4] J. A. Brown, *Modern Manufacturing Processes*, First ed. U.S.A: Industrial Press Inc., 1991.
- [5] H. Xu, X. Zhang, C. Zhang, Z. Liu, X. Zhou, S. Pang, Xiao Chen, Shanmu Dong, Zhongyi Zhang, Lixue Zhang, Pengxian Han, Xiaogang Wang, and Guanglei Cui., "Nanostructured Titanium Nitride/PEDOT:PSS Composite Films As Counter Electrodes of Dye-Sensitized Solar Cells", *ACS Applied Materials & Interfaces*, vol. 4, pp. 1087-1092, Feb 2012.
- [6] B. Yoo, K.-J. Kim, Y. H. Kim, K. Kim, M. J. Ko, W. M. Kim, Nam-Gyu Park, "Titanium nitride thin film as a novel charge collector in TCO-less dye-sensitized solar cell", *Journal of Materials Chemistry*, vol. 21, pp. 3077-3084, 2011.
- [7] S. Ito, N.-L.C. Ha, G. Rothenberger, P. Liska, P. Comte, S. M. Zakeeruddin, Péter Péchy, Mohammad Khaja Nazeeruddin and Michael Grätzel, "High-efficiency (7.2%) flexible dye-sensitized solar cells with Ti-metal substrate for nanocrystalline-TiO₂ photoanode", *Chemical Communications*, pp. 4004-4006, 2006.
- [8] T. M. Watson, I. Mabbett, H. Wang, L. Peter, and D. Worsley, "Ultrafast near infrared sintering of TiO₂ layers on metal substrates for dye-sensitized solar cells", *Progress in Photovoltaics*, vol. 19, pp. 482-486, Jun 2011.
- [9] M. J. Carnie, C. Charbonneau, P. R. F. Barnes, M. L. Davies, I. Mabbett, T. M. Watson, and D. Worsley, "Ultra-fast sintered TiO₂ films in dye-sensitized solar cells: phase variation, electron transport and recombination", *Journal of Materials Chemistry A*, vol. 1, pp. 2225-2230, 2013.
- [10] T. M. Watson, G. J. Reynolds, and D. A. Worsley, "Painted steel mounted dye sensitised solar cells: titanium metallisation using magnetron sputtering", *Ironmaking & Steelmaking*, vol. 38, pp. 168-172, Apr 2011.
- [11] D.-H. Kim, J.-H. Heo, D.-J. Kwak, and Y.-M. Sung, "Synthesis of TCO-free Dye-sensitized Solar Cells with Nanoporous Ti Electrodes Using RF Magnetron Sputtering Technology", *Journal of Electrical Engineering & Technology*, vol. 5, pp. 146-150, Mar, 2010.
- [12] J. K. W. Sandler, J. E. Kirk, I. A. Kinloch, M. S. P. Shaffer, and A. H. Windle, "Ultra-low electrical percolation threshold in carbon-nanotube-epoxy composites", *Polymer*, vol. 44, pp. 5893-5899, Sep 2003.
- [13] Y. Yin, L. Hang, S. Zhang, and X. L. Bui, "Thermal oxidation properties of titanium nitride and titanium-aluminum nitride materials - A perspective for high temperature air-stable solar selective absorber applications", *Thin Solid Films*, vol. 515, pp. 2829-2832, Jan 22 2007.
- [14] M. Wittmer, J. Noser, and H. Melchior, "Oxidation-Kinetics of TiN Thin-Films", *Journal of Applied Physics*, vol. 52, pp. 6659-6664, 1981.
- [15] N. C. Saha and H. G. Tompkins, "Titanium Nitride Oxidation Chemistry - An X-Ray Photoelectron-Spectroscopy Study", *Journal of Applied Physics*, vol.

- 72, pp. 3072-3079, Oct 1 1992.
- [16] V. Baglio, M. Girolamo, V. Antonucci, and A. S. Arico, "Influence of TiO₂ Film Thickness on the Electrochemical Behaviour of Dye-Sensitized Solar Cells", *International Journal of Electrochemical Science*, vol. 6, pp. 3375-3384, Aug 2011.
- [17] I. Shin, H. Seo, M.-K. Son, J.-K. Kim, K. Prabakar, and H.-J. Kim, "Analysis of TiO₂ thickness effect on characteristic of a dye-sensitized solar cell by using electrochemical impedance spectroscopy", *Current Applied Physics*, vol. 10, pp. S422-S424, May 2010.
- [18] P. M. Sommeling, B. C. O'Regan, R. R. Haswell, H. J. P. Smit, N. J. Bakker, J. J. T. Smits, J. M. Kroon, and J. A. M. van Roosmalen., "Influence of a TiCl₄ post-treatment on nanocrystalline TiO₂ films in dye-sensitized solar cells", *Journal of Physical Chemistry B*, vol. 110, pp. 19191-19197, Oct 5 2006.
- [19] F. Fabregat-Santiago, J. Bisquert, G. Garcia-Belmonte, G. Boschloo, and A. Hagfeldt, "Influence of electrolyte in transport and recombination in dye-sensitized solar cells studied by impedance spectroscopy", *Solar Energy Materials and Solar Cells*, vol. 87, pp. 117-131, May 2005.
- [20] I. Abayev, A. Zaban, F. Fabregat-Santiago, and J. Bisquert, "Electronic conductivity in nanostructured TiO₂ films permeated with electrolyte", *Physica Status Solidi a-Applied Research*, vol. 196, pp. R4-R6, Mar 2003.
- [21] P. R. F. Barnes, K. Miettunen, X. Li, A. Y. Anderson, T. Bessho, M. Grätzel, Brian C. O'Regan, "Interpretation of Optoelectronic Transient and Charge Extraction Measurements in Dye-Sensitized Solar Cells", *Advanced Materials*, vol. 25, pp. 1881-1922, Apr 4 2013.
- [22] P. J. Cameron and L. M. Peter, "Characterization of titanium dioxide blocking layers in dye-sensitized nanocrystalline solar cells", *Journal of Physical Chemistry B*, vol. 107, pp. 14394-14400, Dec 25 2003.
- [23] Y. Liu, H. Shen, X. R. Huang, and Y. J. Deng, "A new improved structure of dye-sensitized solar cells with reflection film", *Chinese Science Bulletin*, vol. 51, pp. 369-373, Feb 2006.
- [24] B. Zhao, H. Huang, P. Jiang, H. Zhao, X. Huang, P. Shen, Dingcai Wu, Ruowen Fu, and Songting Tan, "Flexible Counter Electrodes Based on Mesoporous Carbon Aerogel for High-Performance Dye-Sensitized Solar Cells", *Journal of Physical Chemistry C*, vol. 115, pp. 22615-22621, Nov 17 2011.

**HYBRID COATINGS FOR DYE-
SENSITIZED SOLAR CELL
APPLICATIONS**

6.1 Introduction

In previous experimental chapters, we have already discussed PV performance of graphite/PI and titanium nitride/PI coatings for dye-sensitized solar cell application. However, none of them could perform equally well as both DSC working and counter electrodes. For instance, 40 wt% graphite/PI coating is not suitable to be used in DSC working electrodes but it performs slightly well as a counter electrode material. Same is true for 90 wt% TiN/PI coating that is good for the working electrodes but not ideal for the counter electrodes (unless we use sputtered platinum). In addition, 90 wt% TiN/PI needs large TiN loading, which is economically not feasible. Therefore, we need such a coating, which will act consistently well as both working and counter electrode materials whilst exhibiting an optimum PV performance.

As we have already seen that graphite/PI coatings are slightly catalytic in nature thus demonstrate better performance as DSC counter electrodes whereas, micron sized TiN based PI coatings are non-catalytic (see section 1.9.8) hence suitable for working electrode application. Therefore, a hybrid of both may result in an optimized composition with a characteristic to function as DSC working as well as counter electrode material. However, the amounts of TiN and graphite have to be adjusted in such a way that an optimum composition with tailored properties is achieved. However, a trade-off between efficiency and consistent PV performance is expected whilst achieving this goal.

6.2 Experimental

Polyimide matrix based hybrid coatings of titanium nitride and graphite were developed in the same manner as described previously for graphite/PI and TiN/PI coatings (see sections 2.3.1 and 2.3.2). The mixture was first doctor bladed onto NCG substrates followed by drying and curing steps (drying at 150°C for 150 seconds and curing at 350°C for 5 minutes respectively). Special care was taken in controlling the amounts of graphite and TiN in the polyimide precursor. Similar to the previous chapters (Chapters 4 and 5), electrical sheet resistance of the developed coatings were systematically assessed after curing at 350°C (for 5 minutes) and high temperature heat treatment at 450°C (for 30 minutes) respectively. In addition, surface morphology of the coatings was monitored using a stylus profilometer (see section 2.4.2) and a scanning electron microscope (see section 2.4.5).

Finally, the hybrid coating with optimum performance was then selected to coat ECCS and non-conducting glass (NCG) substrates for their application as DSC working and counter electrodes. Fabricated DSCs were then characterized using solar simulation, EIS and optoelectronic transient techniques. More information on these techniques can be found in sections 2.6.1, 2.6.2 and 2.6.3 of the experimental chapter.

6.3 Results & Discussion

6.3.1 Characterization of hybrid coatings

As a rule of thumb, the amount of graphite in this case must be less than 40 wt% of the precursor matrix as this composition has already been used in Chapter 4 and the outcome was not impressive. Hence, the amount of graphite in the PI precursor was kept at 20 wt% in this case because at this point it crosses the percolation threshold limit (see section 4.3). On the other hand, 30 wt% TiN was initially mixed with 20 wt% graphite as TiN/PI coatings discussed in Chapter 5 became electrically conductive when the amount of TiN was increased to 30 wt% in the polymer precursor. Thus, the developed composition with 30 wt% TiN and 20 wt% graphite in the polyimide demonstrated intermediate average roughness values in Figure 6.2 but the electrical sheet resistance (Figure 6.1) of this composition on non-conducting glass (NCG) was significantly high after its curing and high temperature heat treatment at 350°C and 450°C respectively (Figure 6.1). This composition is labelled as “Hybrid-1” in Figure 6.1.

It can be seen from Figure 6.2 that the average surface roughness (R_a) and the average peak height (R_p) of hybrid-1 composition are significantly lower than the best performing carbon/PI coating (see section 4.3) and higher than the optimum TiN/PI coating (see section 5.3). Therefore, this composition (hybrid-1) may be suitable for DSC application; however, higher sheet resistance obtained (Figure 6.1) after curing (350°C for 5 minutes) and high temperature heat treatment (450°C for 30 minutes) makes the coating unfavourable for DSC application.

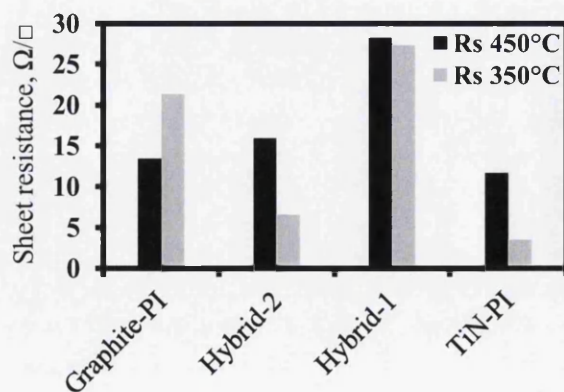


FIGURE 6.1: Hybrid coatings and their comparison with best performing graphite/PI and TiN/PI coatings on non-conductive glass substrate: sheet resistance vs. composition.

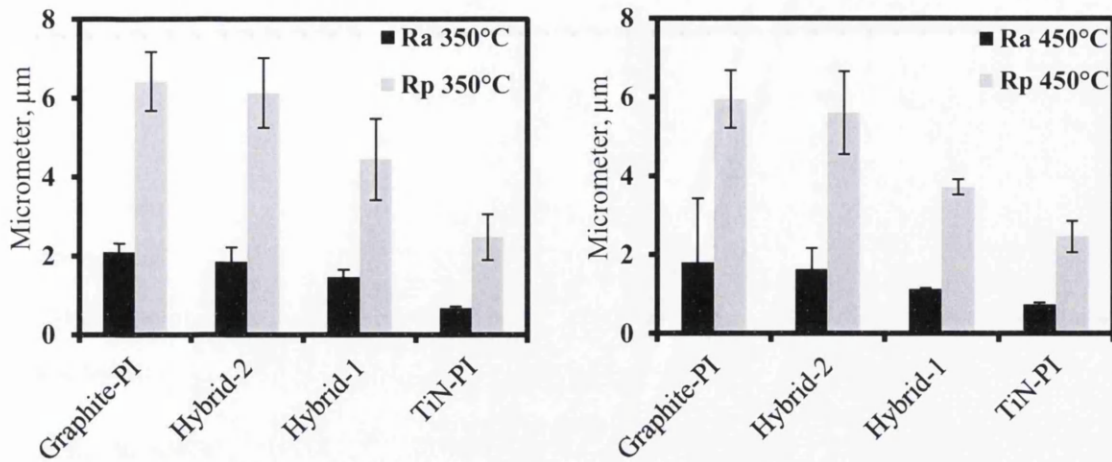


FIGURE 6.2: Hybrid coatings and their comparison with best performing graphite/PI and TiN/PI coatings on non-conductive glass substrate: R_a and R_p vs. composition.

Inadequate percolation between the particles (graphite and TiN) in the PI matrix is probably one of the most important factors responsible for such a high sheet resistance values [1]. In addition, partial oxidation of TiN particles could also be involved in reducing the electrical conductivity of this coating (see section 5.3). The number of percolation pathways in this coating can be increased either by increasing the amount of graphite particles or by adding more TiN into the matrix. Addition of excess graphite may increase the electrical conductivity but it could also make the coating catalytic (see section 4.3). Therefore, by keeping the graphite concentration constant, amount of TiN was increased up to 50 wt% in the developed formulation. It can be seen from Figure 6.1 that electrical sheet resistance values of this hybrid coating (50 wt% TiN and 20 wt% graphite named as “Hybrid-2”) are significantly low after curing (350°C for 5 minutes) and high temperature heat treatment at 450°C for 30 minutes. Furthermore, Figure 6.2 suggests that the R_a and R_p values of “Hybrid-2” are significantly higher than “Hybrid-1” but comparable to the best performing graphite/PI coating. In addition, such values were also substantially higher than the optimum TiN/PI coating discussed in the previous chapter. On the other hand, “Hybrid-2” coating on ECCS substrates displayed similar characteristics in terms of its surface morphology ($R_a < 1.6 \mu\text{m}$ and $R_p < 5.5 \mu\text{m}$) and high temperature stability but Z-axis conductivity was obtained in this case due to the conductive nature of the underlying metal.

It should also be mentioned that the hybrid coatings also demonstrated excellent thermal stability similar to other compositions discussed in this thesis. Hence, in terms of performance and particle loading, hybrid-2 composition could be suitable for DSC application as the main objective in this case was to obtain an optimum performance whilst keeping the amount of TiN as low as possible. Therefore, DSCs based on hybrid-2 composition were fabricated and their PV performance is discussed in this chapter. The name “Hybrid-2” is later replaced with “Hybrid” in all experimental results presented in this chapter.

6.3.2 Scanning electron microscopy

Surface morphology of the best performing hybrid coating (50 wt% TiN + 20 wt% Graphite) was studied using a scanning electron microscope. Figure 6.3 and 6.4 in this section show coating morphology after curing and high temperature heat treatment at 450°C respectively. It can be seen from Figure 6.3 that TiN and graphite particles are uniformly mixed together in the polymer matrix. Furthermore, effective close packing between TiN and graphite particles can be seen in this case which was responsible for the low sheet resistance of the coating. Interconnection between TiN and graphite particles was maintained even up to 450°C for 30 minutes without any significant variation in the coating morphology (Figure 6.4). This also suggests that high temperature stability of the hybrid coating helps preserve its electrical conductivity whilst maintaining the interconnection between TiN and the graphite particles. However, increase in the sheet resistance after high temperature heat treatment was observed that could be due to the partial oxidation of TiN particles in the coating [2].

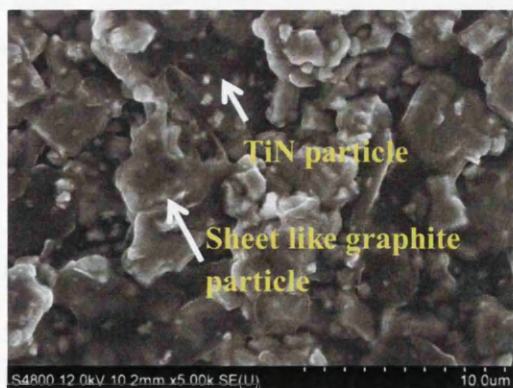


FIGURE 6.3: Hybrid coating cured at 350°C/5 mins.

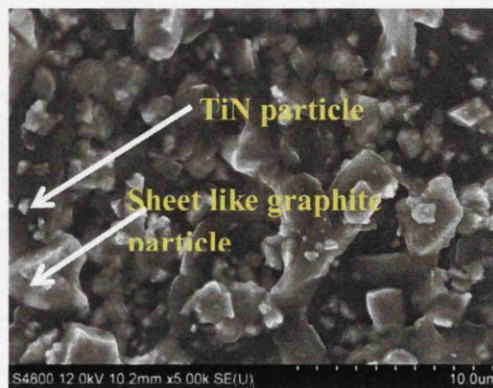


FIGURE 6.4: Hybrid coating heated at 450°C/30 mins.

6.3.3 Photovoltaic Characterization

6.3.3.1 J-V characteristics of hybrid working electrodes

Substrates for DSC applications were prepared by doctor blading the hybrid composition (50 wt% TiN + 20 wt% Graphite) onto NCG and ECCS substrates followed by device construction according to the method described section 2.5.

Figure 6.5 illustrates average J-V characteristics of reverse illuminated DSCs (coated working and thermally platinized FTO counter electrodes) based on the hybrid coating and their comparison with typical FTO glass based cells.

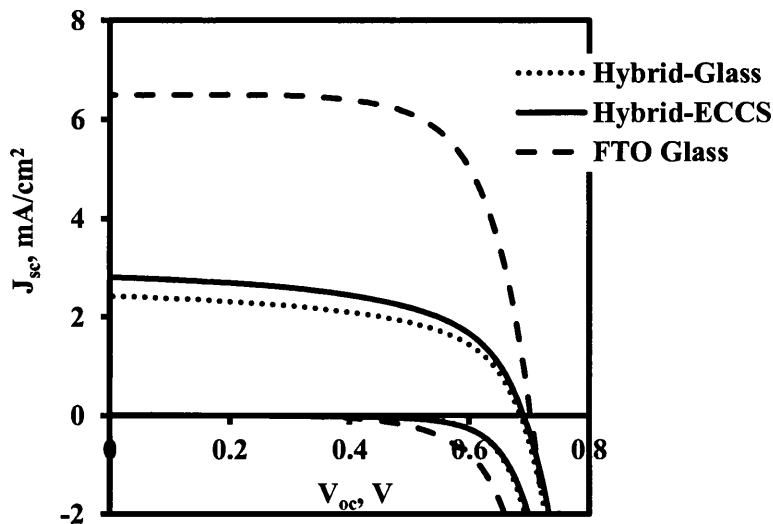


FIGURE 6.5: Average J-V curves of TiN-graphite hybrid coating based working electrodes and their comparison with standard FTO devices.

It is evident from the average J-V curves that both the ECCS and non-conducting glass (NCG) based working electrodes display identical current-voltage characteristics when coated with the 50 wt% TiN and 20 wt% graphite based hybrid coating. This is an unprecedented result where both the coated ECCS and NCG devices demonstrated closely comparable photovoltaic performances. It is clear from Figure 6.5 and Table 6.1 that quantities such as the average J_{sc} , fill factor and photoconversion efficiency values of ECCS and NCG devices are almost identical to each other. For example, the average J_{sc} value obtained from coated ECCS based devices was around 2.80 mA/cm^2 whereas, the average J_{sc} of NCG cells was around 2.40 mA/cm^2 . In addition, a comparative study shows in Figure 6.6 (“a” and “b”) that

cells with ECCS working electrodes coated with hybrid coating demonstrated intermediate average J_{sc} and photoconversion efficiency values that stay between graphite/PI and TiN/PI based devices based on the same working electrode.

TABLE 6.1: Average current-voltage characteristics of TiN-graphite hybrid coating based working electrodes.

Average Data Based on 11 Devices						
Cells	V_{oc} , (V)	J_{sc} , (mA/cm ²)	FF, %	η , %	R_s , Ω	R_{sh} Ω
Hybrid-Glass	0.68 ±0.00	2.40 ±0.27	57.54 ±0.64	0.94 ±0.12	31.77 ±3.69	2528.76 ±532.06
Hybrid-ECCS	0.68 ±0.01	2.80 ±0.22	56.97 ±1.45	1.09 ±0.09	30.78 ±2.09	1927.88 ±248.34
FTO Glass	0.70 ±0.00	6.50 ±0.32	69.56 ±0.09	3.17 ±0.15	11.43 ±0.49	19984.00 ±7566.22

On the other hand, devices based on NCG substrates coated with hybrid coating demonstrated highest J_{sc} and photoconversion efficiency values amongst all coated NCG based devices (Figure 6.6).

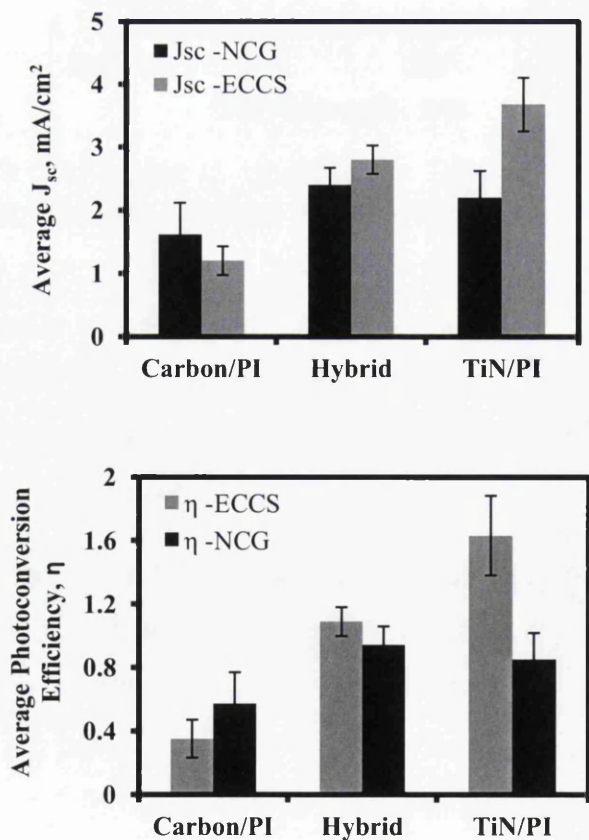


FIGURE 6.6: Average J_{sc} and η values: a comparison between graphite/PI, hybrid/PI and TiN/PI based devices.

This suggests that the hybrid coating of graphite and titanium nitride could perform equally well on both metallic and non-metallic substrates demonstrating an optimum photovoltaic performance. However, it was disappointing that the average J_{sc} values demonstrated by the hybrid coated working electrode based cells were substantially low compared to the standard FTO glass based devices [3]. Like other coatings described in Chapters 4 and 5, this was also due to the non-reflective property of the hybrid coating which was brown in colour. Reflectance measurements performed using a UV-Vis spectrophotometer shows this in Figure 6.7.

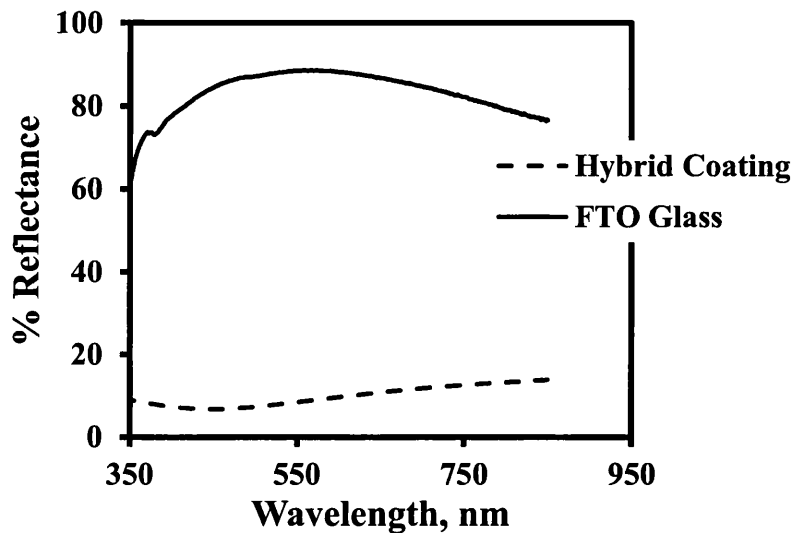


FIGURE 6.7: %reflectance vs. wavelength in TiN-graphite hybrid coating based working electrodes and their comparison with standard FTO coated substrate.

It was also remarkable in both cases that the average series resistance in hybrid coated ECCS and NCG based cells remained low and almost identical to each other. This in association with high average shunt resistance resulted in reasonably high average fill factors in both sets of cells.

Figure 6.5 also provides a hint from the dark current curves that the rate of interfacial recombination at the coated substrate/electrolyte interface could be slower than the FTO glass/electrolyte interface. This will be confirmed later by the EIS and PV decay studies.

6.3.3.2 EIS of hybrid working electrodes

Electrochemical impedance data show in Figure 6.8 that all devices based on hybrid coated working electrodes display similar recombination characteristics at the $\text{TiO}_2/\text{electrolyte}$ and substrate/electrolyte interfaces ^[4]. However, which type of recombination is predominantly happening is difficult to predict from EIS alone. It can be seen from Figure 6.8 that the average interfacial charge recombination resistance values (R_{rc}) of coated working electrodes were slightly higher at around 0.55 V suggesting that the recombination via the substrate is slower (compared to FTO based devices) at this potential. However, the average R_{rc} values of hybrid-based devices gradually decrease with increasing voltage and demonstrate faster recombination (via the TiO_2 and the surface oxide film similar to the TiN/PI coatings in Chapter 5) at around 0.85 V ^[5]. In contrast, FTO glass based standard cells on the other hand displayed comparatively slower interfacial recombination at higher applied potentials due the absence of an additional oxide layer as in case of coated substrates (Chapter 5). However, at potential close to the V_{oc} (of the cells at 1 sun), the rate of interfacial charge recombination was found comparable to each other in case of all devices.

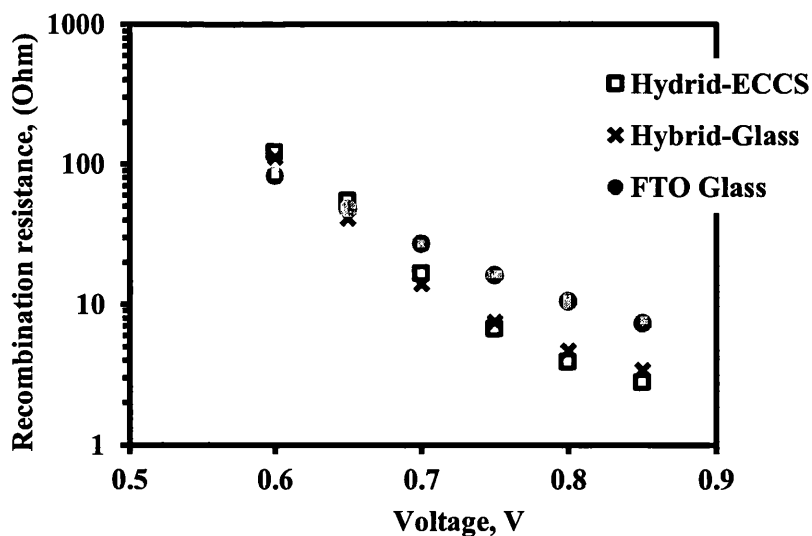


FIGURE 6.8: Average charge recombination resistance in hybrid coating based working electrodes and their comparison with standard FTO devices: average based on 9 best performing cells.

6.3.3.3 Photovoltage decay measurements

Photovoltage decay analysis in Figure 6.9 shows that ECCS and NCG based working electrodes coated with the hybrid coating demonstrate slower decay in the average photovoltage compared to the traditional FTO glass based devices, when the bias light was turned off. This indicates that the charge recombination at the coated substrate/electrolyte interface was relatively slower than at the FTO/electrolyte interface. Slower rate of PV decay has already been observed in TiN/PI based working electrodes due to the formation of a thin Ti-oxide based compact layer on the surface of the heat-treated TiN (see section 5.3) [6]. Therefore, presence of 50 wt% TiN in this hybrid coating could possibly result in similar phenomenon when heated at 450°C for the deposition of mesoporous TiO₂ film. However, the average PV decay in coated ECCS based cells was significantly slower than their non-conducting glass based counterparts.

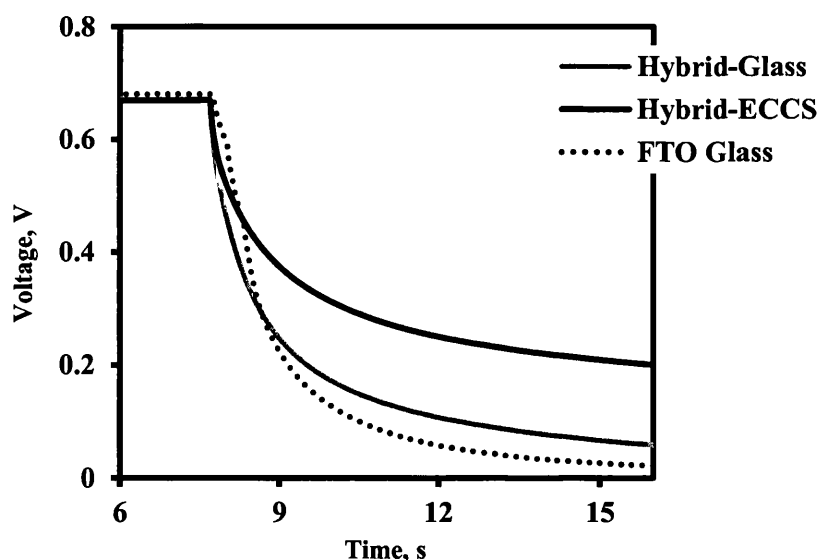


FIGURE 6.9: Average photovoltage decay curves of TiN-graphite hybrid coating based working electrodes and their comparison with standard FTO cells: average based on 9 best performing devices.

This could be due to higher oxide concentration on the surface of coated ECCS than the coated NCG substrates. Variation in the oxide concentrations on coated ECCS and NCG may have been caused by the differences in thermal conductivities of both the substrates, as ECCS could heat up more rapidly than NCG within a same time span forming excess oxides on the coated substrates.

6.3.3.4 Electron lifetime measurements

Average electron recombination lifetimes of the fabricated cells were estimated from the optoelectronic transient studies and plotted against the voltage in Figure 6.10. In general, higher electron recombination lifetime indicates slower interfacial charge recombination in a dye-sensitised solar cell. Thus, results obtained in Figure 6.10 are in agreement with the PV decay analysis, which has already been suggested slower recombination at the substrate/electrolyte interface of the fabricated cells. This study strongly suggests that the slower charge recombination in case of coated working electrodes could be due to the presence of a compact blocking layer on the surface of the hybrid coating, which extends the carrier lifetimes in the Fermi level of mesoporous TiO₂. Hence, the average electron lifetimes in coated ECCS and NCG based cells were significantly higher than the typical FTO glass based devices.

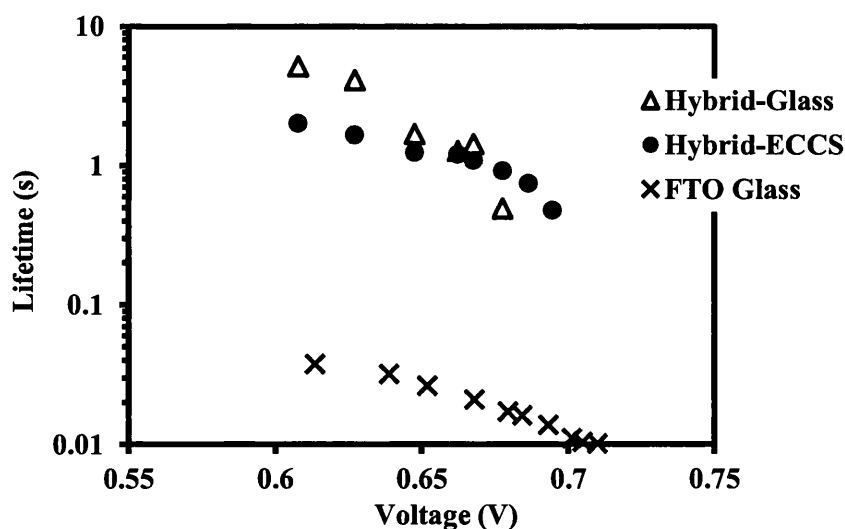


FIGURE 6.10: Average recombination lifetime vs. voltage in TiN-graphite hybrid coating based working electrodes and their comparison with standard FTO cells: average based on 9 best performing devices.

6.3.3.5 J-V characteristics of hybrid counter electrodes

TiN and graphite based hybrid coating was used to coat NCG and ECCS substrates to manufacture coated counter electrodes (CE) for traditional FTO glass working electrode based DSCs. The purpose of this experiment was to develop flexible counter electrodes for forward illuminated glass-metal hybrid devices and to evaluate

the PV performance of TCO free glass substrates coated with this electrically conductive hybrid coating. It is need less to mention, thermal platinization technique was used in this case to platinize the coated counter electrodes.

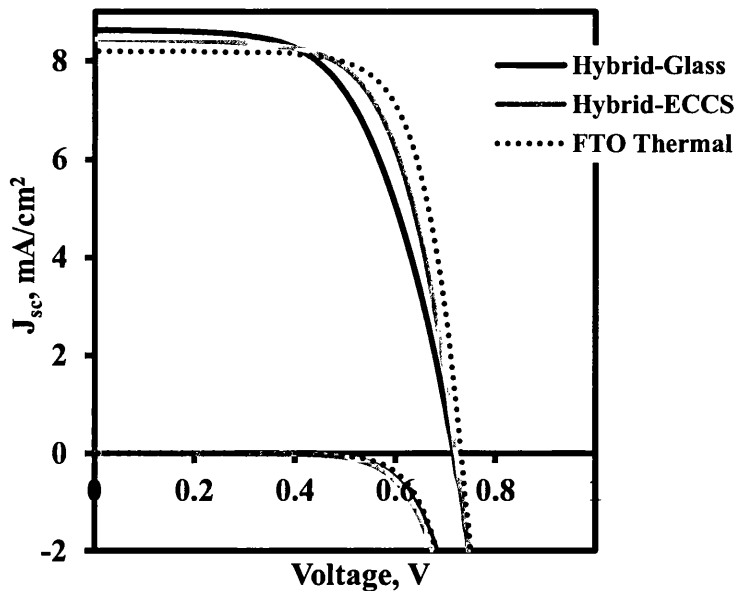


FIGURE 6.11: Average J-V characteristics of TiN-graphite hybrid coating based counter electrodes and their comparison with standard FTO cells: average based on 9 best performing devices.

It is clearly visible in Figure 6.11 that devices with coated counter electrodes demonstrate nearly the same average J_{sc} values as FTO counter electrode based devices. In addition, it can be seen from Table 6.2 that other quantities such as V_{oc} and the photoconversion efficiency were also very close to the standard devices based on FTO glass counter electrodes. However, it is evident from Table 6.2 that the average fill factors of the cells based on the hybrid coating were slightly lower than the one demonstrated by FTO glass CE based cells. This could be due to significantly low shunt and relatively high series resistance values exhibited by the devices with coated counter electrodes.

Devices with coated NCG counter electrodes displayed similar characteristics to their ECCS based counterparts but their average fill factor was slightly lower than the ECCS counter electrode based cells (Table 6.2).

TABLE 6.2: TiN-graphite hybrid coating based counter electrodes and their comparison with standard FTO cells.

Average Data Based on 12 Devices						
Cells	V_{oc} ,(V)	J_{sc} ,(mA/cm^2)	FF, %	η , %	R_s , Ω	R_{sh} Ω
Hybrid-Glass	0.71 ± 0.00	8.62 ± 0.09	59.88 ± 4.23	3.70 ± 0.26	18.47 ± 5.03	7214.8 ± 1986.97
Hybrid-ECCS	0.71 ± 0.00	8.43 ± 0.26	65.87 ± 0.96	4.00 ± 0.11	13.25 ± 0.98	5841.20 ± 568.31
FTO Glass	0.73 ± 0.00	8.20 ± 0.16	71.69 ± 1.20	4.30 ± 0.15	10.20 ± 1.16	24393.37 ± 18427.15

This could be due to high average series resistance demonstrated by the devices with coated NCG counter electrodes. High series resistance could also be responsible for lowering the average photoconversion efficiency of such devices.

It is clear from the J-V characteristics that all counter electrodes based on hybrid coating performs equally well as FTO glass based standard cells with a slight variations in the fill factor and photoconversion efficiency values. This could be attributed to slower charge transfer kinetics at the coated counter electrodes/electrolyte interface, which will be investigated later using electrochemical impedance spectroscopy.

6.3.3.6 EIS of hybrid counter electrodes

The charge transfer kinetics at the platinized coating/electrolyte interface was investigated using electrochemical impedance spectroscopy. Figure 6.12 clearly shows in this case that DSCs with coated ECCS based counter electrodes display similar charge transfer kinetics to the platinized FTO counter electrode based devices. As a result, $\sim 4\%$ average photoconversion efficiencies were obtained in both cases, which was due to low charge transfer resistances (R_{ce}) at the counter electrode/electrolyte interfaces of such cells (Figure 6.12). Low charge transfer resistances observed in both cases could be due to the low series resistance values demonstrated by the coated ECCS and FTO glass based counter electrodes. Coated NCG based counter electrodes also displayed comparable characteristics to the coated-ECCS and FTO counter electrodes based cells. However, it can be seen from Figure 6.12 that the average R_{ce} value obtained in this case was higher than the

coated-ECCS and FTO counter electrode based devices. This could possibly due to comparatively high average series resistance demonstrated by such cells.

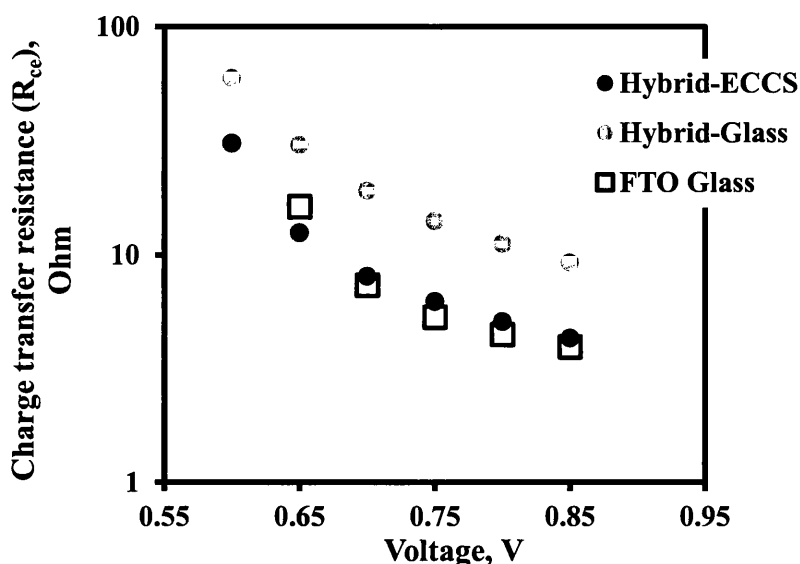


FIGURE 6.12: Average charge transfer resistance vs. voltage in TiN-graphite hybrid coating based counter electrodes and their comparison with standard FTO cells: average based on 9 best performing devices.

Capacitance between the platinized counter electrodes and the electrolyte is known as electrical double layer capacitance (C_{dl}) which depends on the catalytic nature and the surface area of the platinized counter electrode [7]. Double layer capacitance in a DSC normally increases with the surface area and catalytic activity of the catalyst. This leads to faster reduction of the redox couple at the counter electrode/electrolyte interface, which could also improve the overall PV performance of a device.

It can be seen from Figure 6.13 that the average C_{dl} values of all fabricated cells are closely comparable to each other. Enhanced C_{dl} values were observed in this case close to the V_{oc} of the cells at 1 sun. This suggests that the platinum catalyst present on the counter electrodes of such cells was in the right amount and efficiently catalysed the triiodide reduction at counter electrodes. There is a possibility, that the counter electrodes with hybrid coating may have been benefited from the rough surface, which could also enhance the C_{dl} values due to its high surface area.

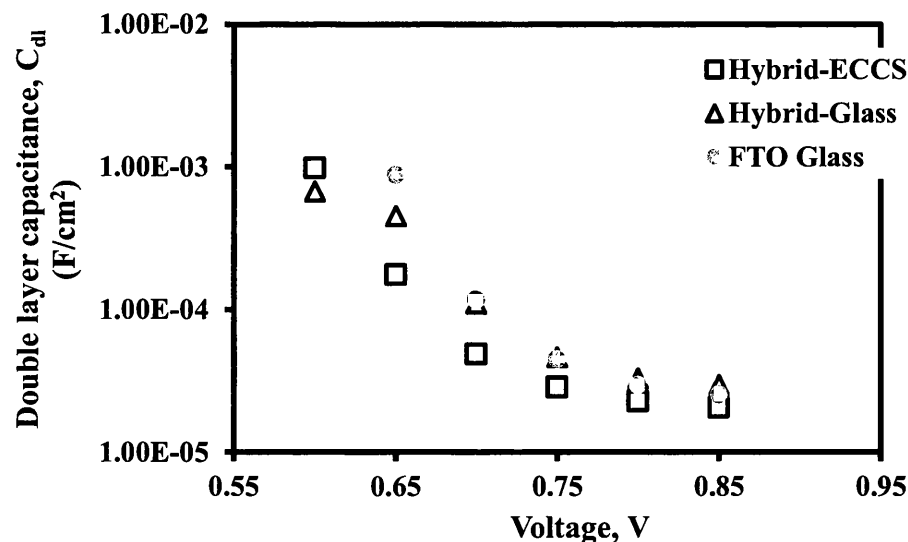


FIGURE 6.13: Average double layer capacitance vs. voltage in TiN-graphite hybrid coating based counter electrodes and their comparison with standard FTO cells: average based on 9 best performing devices.

6.4 Conclusions

The hybrid coating made of 20 wt% graphite and 50 wt% TiN requires less amount of graphite and TiN yet demonstrates optimum electrical and heat resistant properties. Hence, from the commercial point of view, this coating could be used to coat cheap metal substrates for roll-to-roll DSC production in a cost effective manner.

This hybrid coating could work equally well in both DSC working and counter electrodes. Devices based on coated non-conducting glass and ECCS working electrodes demonstrated identical PV performance. However, poor light reflectivity of this hybrid coating did reduce the average J_{sc} of the cells to a significant amount compared to the standard FTO glass based devices. Nevertheless, DSCs based on coated counter electrodes (NCG and ECCS) displayed identical PV performance to the FTO glass counter electrode based standard devices. Unlike the scenario observed in previous chapter, titanium nitride present in this hybrid coating did not react with the platinum catalyst during the thermal platinisation technique, which gives high efficiency cells without requiring the use of sputtering technique for Pt-deposition.

Considering the results obtained from this experiment, it can be concluded that the hybrid coating based on TiN and graphite is better than the 40 wt% graphite/PI and 90 wt% TiN/PI coatings in terms of its overall PV performance.

6.5 References

- [1] Y. Sun, "Silver nanowires - unique templates for functional nanostructures" *Nanoscale*, vol. 2, pp. 1626-1642, 2010.
- [2] N. C. Saha and H. G. Tompkins, "Titanium Nitride Oxidation Chemistry - An X-Ray Photoelectron-Spectroscopy Study", *Journal of Applied Physics*, vol. 72, pp. 3072-3079, 1992.
- [3] Y. Liu, H. Shen, X. R. Huang, and Y. J. Deng, "A new improved structure of dye-sensitized solar cells with reflection film", *Chinese Science Bulletin*, vol. 51, pp. 369- 373, 2006.
- [4] M. Manca, F. Malara, L. Martiradonna, L. De Marco, R. Giannuzzi, R. Cingolani, Giuseppe Gigli, "Charge recombination reduction in dye-sensitized solar cells by means of an electron beam-deposited TiO₂ buffer layer between conductive glass and photoelectrode", *Thin Solid Films*, vol. 518, pp. 7147-7151, 2010.
- [5] F. Fabregat-Santiago, J. Bisquert, G. Garcia-Belmonte, G. Boschloo, and A. Hagfeldt, "Influence of electrolyte in transport and recombination in dye-sensitized solar cells studied by impedance spectroscopy", *Solar Energy Materials and Solar Cells*, vol. 87, pp. 117-131, 2005.
- [6] A. Glaser, S. Surnev, F. P. Netzer, N. Fateh, G. A. Fontalvo, and C. Mitterer, "Oxidation of vanadium nitride and titanium nitride coatings", *Surface Science*, vol. 601, pp. 1153-1159, 2007.
- [7] B. Zhao, H. Huang, P. Jiang, H. Zhao, X. Huang, P. Shen, D. Wu, R. Fu, S. Tan, "Flexible Counter Electrodes Based on Mesoporous Carbon Aerogel for High-Performance Dye-Sensitized Solar Cells", *Journal of Physical Chemistry C*, vol. 115, pp. 22615-22621, 2011.

CHAPTER 7

CONCLUSIONS AND FUTURE WORK

7.1 Conclusions

This research has successfully proven that low cost steel substrates such as ECCS can be used to manufacture DSCs if coated with a polyimide based conductive coatings. Such coatings appear to demonstrate some chemical inertness that protects the underlying metal from the attack of aggressive I^-/I_3^- DSC electrolyte. In addition, high temperature stability (up to 450°C) and low electrical resistivity are the two very important properties of the coatings, which enables high temperature processing of the coated metallic substrates without compromising the electrical conductivity of the underlying metal. These coatings can also be utilised to coat non-metallic substrates such as a plain soda-lime glass as FTO free substrate for DSC application. However, PV performance of DSCs varies significantly depending upon the nature of the conductive fillers used to develop such coatings.

It is evident from Chapter 4 of this thesis that carbon/polyimide coatings as working electrodes were not ideal for DSC application. Coatings based on MWCNTs/polyimide demonstrated substantially high R_a and R_p values. In addition, developed coatings exhibited high sheet resistance values, which were unfavourable for DSC application. Although, graphite/PI coatings seemed to be promising in the beginning due to comparatively low R_a , R_p and sheet resistance values but remarkably low J_{sc} values were obtained from 40 wt% graphite/PI based devices. This was due to the black colour of the coating, which displayed poor reflection properties responsible for significant reduction in the J_{sc} . Moreover, graphite/PI coating was slightly catalytic in nature, which initiated interfacial charge recombination in such devices contributing towards the overall loss in J_{sc} . On the other hand, platinised (thermally) counter electrodes based on 40 wt% graphite/PI coating performed remarkably well with PV performance comparable to the FTO counter electrode based devices. This suggests that 40 wt% graphite/PI coating is not suitable for DSC working electrodes but it could be useful as counter electrode material for low cost DSC manufacturing.

As a possible solution to the problems encountered in Chapter 4, fifth chapter was therefore dedicated to titanium nitride/polyimide coatings. TiN/PI coatings were also high temperature resistant with attractive sheet resistance values. However, high temperature oxidation of TiN particles was responsible for reduction in the sheet

resistance of such coatings. Therefore, highly concentrated TiN/PI coatings (with TiN up to 90 wt%) were developed to maintain low sheet resistance even after a few high temperature heat treatment steps. Thus, 90 wt% TiN/PI coating was chosen for DSC application due to its remarkably low R_a , R_p and sheet resistance values. It was observed from the current-voltage characteristics that 90 wt% TiN/PI based DSCs demonstrated comparable performance to the FTO glass based standard devices in terms of their V_{oc} and fill factor values. However, the photoconversion efficiencies obtained from such devices were lower than the standard FTO based devices. Nevertheless, the cells based on 90 wt% TiN/PI coated ECCS was comparable to the titanium metal mounted cells in terms of their overall PV performance. It was also realised that a blocking layer of TiO_2 is being formed during the high temperature heat treatment of the 90 wt% TiN/PI coating, which prevents back reaction in such devices. However, brown colour of this coating could not improve its light reflection property, which caused J_{sc} reduction to some extent. Counter electrodes based on 90 wt% TiN/PI with thermally deposited platinum failed to exhibit desired PV performance due to the oxide growth on the TiN/PI surface. However, the same coating displays comparatively better PV performance as a counter electrode material when the platinum was deposited using the sputtering technique. This is obviously not suitable for the low cost DSC manufacturing therefore, it can be concluded in this case that the TiN/PI coating could be used as a working electrode material but not suitable for counter electrode application.

It was evident in this case that none of the developed coatings could perform equally well as both working and counter electrode materials. Therefore, in order to address this issue hybrid coatings were developed for DSC application. Developed hybrid coatings were based on graphite and titanium nitride added together in the polyimide matrix in order to obtain optimized physical properties. Similar to the coatings discussed earlier, hybrid coatings displayed excellent heat stability and high electrical conductivity whilst using optimum amounts of each filler. It was found that only 20 wt% graphite and 50 wt% TiN in the polyimide can form an ideal composition for DSC application. Devices fabricated using such a coating (20 wt% graphite- 50 wt% TiN/PI) demonstrated improved PV performance, which was comparable to the standard FTO glass based devices. Unfortunately, low reflectivity of this coating did reduce the average J_{sc} and the photoconversion efficiency in this case but it does provide an option for the future that by improving its reflectivity,

device performance can also be improved to a significant amount. On the other hand, counter electrodes based this hybrid coating (20 wt% graphite- 50 wt% TiN/PI) performed undoubtedly well with thermally decomposed platinum. Photoconversion efficiencies obtained in this case were almost equal to the FTO counter electrode based cells, which implies that graphite-TiN added hybrid coating could be a low cost counter electrode material for DSC application and could act as an alternative to the FTO coated substrates.

7.2 Future Work

Coating reflectivity could be improved by incorporating white pigments. Conductive oxides (e.g., fluorine doped tin oxide) are white in colour so can be used to enhance coating reflectivity without compromising the electrical conductivity. In this manner, current output from a dye-sensitized solar cell could be increased followed by an improved device performance. In addition, white coloured fillers with small particle sizes may also produce smooth surface suitable for device fabrication.

It may be possible to functionalize MWCNT in order to obtain better dispersion in the PI matrix, which could effectively reduce the roughness of the MWCNT/PI coatings. However, the functionalization process may also have some detrimental effects on the electrical conductivity of MWCNT. Thus, it would be an interesting experiment in the future to optimize the MWCNT functionalization process without sacrificing its electrical conductivity. Different types of materials could be used for the functionalization process to obtain optimum performance.

Development of graphene- TiN hybrid coating could also result in significant improvement in the PV performance of the existing hybrid coating. Graphene is an excellent conductor of electricity with many attractive physical properties therefore this experiment may yield some promising results in the future.

These types of conductive coatings can also be used for heat release application (Joule heating). Preliminary experiments have already provided promising results in this area with a possibility of large-scale production. This type of heat release coatings could be used for domestic application replacing the traditional hot water based heat exchangers. However, some simulation experiments are required the future to calculate the efficiency of such coatings.

In future industrial trials in a roll-to-roll production facility would be useful for this research.

Coating durability assessment will be an essential piece of information to strengthen this research in the future. Especially determination of corrosion behaviour of the coatings and the substrate using SVET (scanning vibrating electrode technique) will be an interesting study to perform.

List of Publications & Presentations

1. Vyas N, Charbonneau C, Carnie M, Watson T, Worsley D. Development of a novel corrosion resistant and electrically conducting functional coating for metal mounted dye-sensitized solar cell. 9th Photovoltaic Science, Applications and Technology Conference PVSAT-9, Conference Proceedings 2013. Published by the Solar Energy Society ISBN: 0 904963 79 9
2. “An Inorganic/Organic Hybrid Coating for Low Cost Metal Mounted Dye Sensitized Solar Cells”, Niladri Vyas, Cecile Charbonneau, Matthew Carnie, Trystan Watson, David Worsley, *ECS Trans*, Volume 53, Issue 24, 29-37, 2013, doi:10.1149/05324.0029ecst
3. “Low-cost TCO Less Counter Electrodes for Dye-sensitized Solar Cell Application”, Niladri Vyas, David Wragg, Cecile Charbonneau, Matthew Carnie, David Worsley, Trystan Watson, *ECS Trans*, Volume 53, Issue 24, 39-46, 2013, doi: 1149/05324.0039ecst
4. Titanium Nitride/Polyimide Based Corrosion Resistant and Electrically Conducting Composite Coating for Metal Mounted Dye-Sensitized Solar Cells”, 11th International Conference on Materials Chemistry (MC11), Royal Society of Chemistry, University of Warwick, UK, July 2013 (poster)
5. “Titanium Nitride/Polyimide Based Corrosion Resistant and Electrically Conducting Composite Coating for Metal Mounted Dye-Sensitized Solar Cells” Niladri Vyas, Matthew Carnie, Trystan Watson, David Worsley, ISE Satellite Student Regional Symposium: Great Western Photoelectrochemistry Meeting, University of Bath, UK, 10th June 2013 (Oral)
6. “Low-cost TCO Less Counter Electrodes for Dye-sensitized Solar Cell Application”, Niladri Vyas, David Wragg, Cecile Charbonneau, Matthew Carnie, David Worsley, Trystan Watson, 223rd ECS Meeting Toronto, May, 2013 (Oral)
7. “An Inorganic/Organic Hybrid Coating for Low Cost Metal Mounted Dye Sensitized Solar Cells”, Niladri Vyas, Cecile Charbonneau, Matthew Carnie, Trystan Watson, David Worsley, 223rd ECS Meeting Toronto, 2013 (Oral)
8. “Development of a Novel Corrosion Resistant and Electrically Conducting Functional Coating for Metal Mounted Dye-Sensitized Solar Cells” Niladri Vyas, Cecile Charbonneau, Matthew Carnie, Trystan Watson, David Worsley, 9th Photovoltaic Science Application and Technology (PVSAT – 9) , Swansea University, April 2013 (Poster)